

AD-A146 226

BASIC STUDY OF BLADED DISK STRUCTURAL RESPONSE(U)  
UNITED TECHNOLOGIES RESEARCH CENTER EAST HARTFORD CT  
A V SRINIVASAN ET AL. NOV 83 R83-914806-48

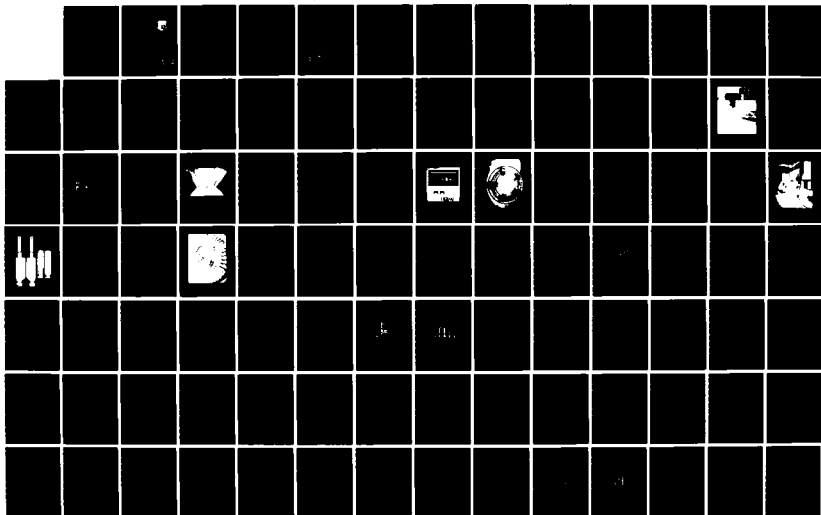
1/3

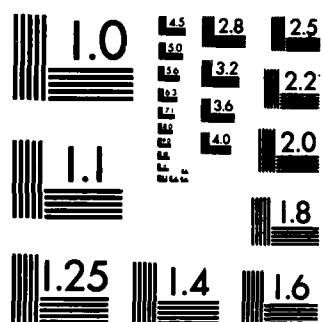
UNCLASSIFIED

AFWAL-TR-83-2075 F33615-79-C-2054

F/G 1/3

NL





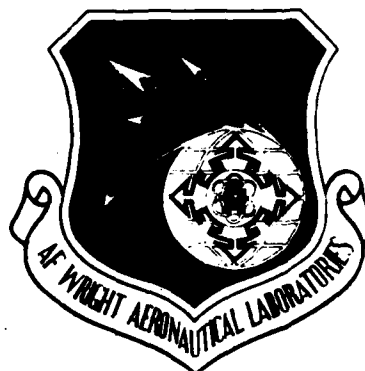
MICROCOPY RESOLUTION TEST CHART  
NATIONAL BUREAU OF STANDARDS-1963-A

12

AFWAL-TR-83-2075

## BASIC STUDY OF BLADED DISK STRUCTURAL RESPONSE

A.V. Srinivasan  
D.G. Cutts



UNITED TECHNOLOGIES RESEARCH CENTER  
East Hartford, Conn. 06108

November 1983

Final Report for Period September 1979 — January 1984

Approved for public release; distribution unlimited.

AERO PROPULSION LABORATORY  
AIR FORCE WRIGHT AERONAUTICAL LABORATORIES  
AIR FORCE SYSTEMS COMMAND  
Wright-Patterson Air Force Base, Ohio 45433

DTIC  
ELECTE  
OCT 2 1984  
S B

AD-A146 226

DTIC FILE COPY

84 09 27 023

NOTICE

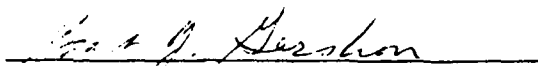
When Government drawings, specifications, or other data are used for any purpose other than in connection with a definitely related Government procurement operation, the United States Government thereby incurs no responsibility nor any obligation whatsoever; and the fact that the government may have formulated, furnished, or in any way supplied the said drawings, specifications, or other data, is not to be regarded by implication or otherwise as in any manner licensing the holder or any other person or corporation, or conveying any rights or permission to manufacture use, or sell any patented invention that may in any way be related thereto.

This report has been reviewed by the Office of Public Affairs (ASD/PA) and is releasable to the National Technical Information Service (NTIS). At NTIS, it will be available to the general public, including foreign nations.

This technical report has been reviewed and is approved for publication.



Project Engineer  
Engine Assessment Branch  
Turbine Engine Division  
Aero Propulsion Laboratory



Actg Branch Chief  
Engine Assessment Branch  
Turbine Engine Division  
Aero Propulsion Laboratory

FOR THE COMMANDER



Director  
Turbine Engine Division  
Aero Propulsion Laboratory

"If your address has changed, if you wish to be removed from our mailing list, or if the addressee is no longer employed by your organization please notify AFWAL/POTA, W-PAFB, OH 45433 to help us maintain a current mailing list".

Copies of this report should not be returned unless return is required by security considerations, contractual obligations, or notice on a specific document.



Unclassified

SECURITY CLASSIFICATION OF THIS PAGE (When Data Entered)

REPORT DOCUMENTATION PAGE		READ INSTRUCTIONS BEFORE COMPLETING FORM																					
1. REPORT NUMBER AFWAL-TR-83-2075	2. GOVT ACCESSION NO.	3. RECIPIENT'S CATALOG NUMBER																					
4. TITLE (and Subtitle)  BASIC STUDY OF BLADED DISK STRUCTURAL RESPONSE		5. TYPE OF REPORT & PERIOD COVERED Final Report September 1979-January 1984																					
		6. PERFORMING ORG. REPORT NUMBER R83-914806-48																					
7. AUTHOR(s)  A. V. Srinivasan  D. G. Cutts		8. CONTRACT OR GRANT NUMBER(s)  F33615-79-C-2054																					
9. PERFORMING ORGANIZATION NAME AND ADDRESS United Technologies Research Center East Hartford CN 06108		10. PROGRAM ELEMENT, PROJECT, TASK AREA & WORK UNIT NUMBERS  2307S206																					
11. CONTROLLING OFFICE NAME AND ADDRESS Aero Propulsion Laboratory (AFWAL/POTA) Air Force Wright Aeronautical Labs (AFSC) Wright-Patterson Air Force Base, Ohio 45433		12. REPORT DATE November 1983																					
		13. NUMBER OF PAGES 250																					
14. MONITORING AGENCY NAME & ADDRESS (if different from Controlling Office)		15. SECURITY CLASS. (of this report)  Unclassified																					
		15a. DECLASSIFICATION/DOWNGRADING SCHEDULE																					
16. DISTRIBUTION STATEMENT (of this Report)  Approved for public release; distribution unlimited																							
17. DISTRIBUTION STATEMENT (of the abstract entered in Block 20, if different from Report)																							
18. SUPPLEMENTARY NOTES																							
19. KEY WORDS (Continue on reverse side if necessary and identify by block number)																							
<table border="0"> <tbody> <tr> <td>Shrouded fan</td> <td>Exit guide vanes</td> <td>Optical measurement</td> </tr> <tr> <td>Bladed disk</td> <td>Distortion screen</td> <td>Evacuated</td> </tr> <tr> <td>Structural response</td> <td>Traveling waves</td> <td>Mistuning</td> </tr> <tr> <td>Frequency response</td> <td>Standing waves</td> <td>Twin modes</td> </tr> <tr> <td>Piezoelectric crystal-excitation</td> <td>Strain response</td> <td>Twin mode analysis</td> </tr> <tr> <td>Aerodynamic excitation</td> <td>Shroud motion measurement</td> <td>Damping</td> </tr> <tr> <td></td> <td></td> <td>Forced vibration</td> </tr> </tbody> </table>			Shrouded fan	Exit guide vanes	Optical measurement	Bladed disk	Distortion screen	Evacuated	Structural response	Traveling waves	Mistuning	Frequency response	Standing waves	Twin modes	Piezoelectric crystal-excitation	Strain response	Twin mode analysis	Aerodynamic excitation	Shroud motion measurement	Damping			Forced vibration
Shrouded fan	Exit guide vanes	Optical measurement																					
Bladed disk	Distortion screen	Evacuated																					
Structural response	Traveling waves	Mistuning																					
Frequency response	Standing waves	Twin modes																					
Piezoelectric crystal-excitation	Strain response	Twin mode analysis																					
Aerodynamic excitation	Shroud motion measurement	Damping																					
		Forced vibration																					
20. ABSTRACT (Continue on reverse side if necessary and identify by block number)																							
<p>1. imp. The dynamic response of a shrouded fan was characterized over a range of speeds by subjecting the assembly to forced vibration in vacuum in a spin rig and to distortion induced vibration in an aerodynamic rig. The characterization was established by analysis of blade strain response data obtained when the assembly was driven by predetermined standing or traveling wave forcing through piezoelectric crystal drive elements attached to the blades, by means of an aerodynamic distortion screen and by exit guide vanes. Both tuned and mistuned configurations of the assembly were tested. In addition, the relative motion at shroud interfaces was measured using optical sensors for various input conditions. The vibratory motions were of a microslip type with no evidence of stick-slip type of motion.</p>																							

DD FORM 1 JAN 73 1473

EDITION OF 1 NOV 65 IS OBSOLETE  
S/N 0102-014-6601

Unclassified

SECURITY CLASSIFICATION OF THIS PAGE (When Data Entered)

## FOREWORD

The research program comprising the forced vibration testing of a part-span shrouded fan in vacuum as well as in an aerodynamic environment was sponsored by the U.S. Air Force Aero Propulsion Laboratory at the Wright-Patterson Air Force Base under Contract No. F33615-79-C-2054. The Air Force project managers were James MacBain and William Stange.

Principal United Technologies Research Center (UTRC) participants in the contract activity were A. V. Srinivasan and D. G. Cutts. Very significant support was provided by Robert Thornton (design and fabrication of the excitation system) and Larry Hardin (strain gage modules and the entire phase of aerodynamic testing). Additionally, it is a pleasure to acknowledge the contributions made by Robin Ford in the area of twin mode analysis. Discussions held among all the participants and the project managers throughout the program were informative and constructive and resulted in a new body of knowledge contained in this document.

This report is the final documentation of all the efforts in regard to mechanical and aeromechanical characterization of a part-span shrouded fan.

**DTIC**  
**ELECTE**  
**S** OCT 2 1984 **D**  
**B**



Accession For	
NTIS GRA&I	<input checked="checked" type="checkbox"/>
DTIC TAB	<input type="checkbox"/>
Unannounced	<input type="checkbox"/>
By _____	
Distribution/	
Availability Codes	
Dist	Avail and/or Special
A-1	

# TABLE OF CONTENTS

	<u>Page</u>
I. INTRODUCTION . . . . .	1
II. PROGRAM OBJECTIVES . . . . .	4
III. TEST RIGS . . . . .	5
1. Test Rigs Used in the Program . . . . .	5
a. The Rotating Test Facility: Rig A. . . . .	5
b. The Aerodynamic Test Facility: Rig B . . . . .	5
IV. THE TEST COMPONENT . . . . .	11
V. MECHANISMS OF EXCITATION OF THE ASSEMBLY . . . . .	13
1. Development of Piezoceramic Driven Elements . . . . .	14
2. Blade Drive Control System. . . . .	15
3. Drive Modules . . . . .	18
4. System Development. . . . .	18
VI. BLADE STRAIN MEASUREMENT SYSTEM . . . . .	20
VII. RIG ASSEMBLY AND SHAKEDOWN TESTS IN RIG A . . . . .	25
VIII. PRELIMINARY TESTS TO DETERMINE THE R-80 RESPONSE FEATURES . .	27
IX. MECHANICAL CHARACTERIZATION OF THE R-80 FAN ASSEMBLY . . . . .	48
1. Initially Tuned Condition . . . . .	48
2. Discussion of Results . . . . .	48
3. Mistuned Assembly . . . . .	72
4. Discussion of Results . . . . .	77

# TABLE OF CONTENTS (Cont'd)

	<u>Page</u>
X. MEASUREMENT OF MOTION AT SHROUD INTERFACES . . . . .	100
1. System Design and Fabrication . . . . .	100
2. System Calibration. . . . .	104
3. Data Acquisition and Reduction. . . . .	108
4. Testing . . . . .	112
5. Noise Levels. . . . .	115
6. Presentation of Results . . . . .	115
7. Discussion of Results . . . . .	132
XI. TWIN MODE ANALYSIS OF MISTUNED SYSTEMS . . . . .	159
XII. AEROMECHANICAL CHARACTERIZATION OF THE R-80 FAN ASSEMBLY . . .	169
1. Instrumentation and Calibration in Rig B. . . . .	169
2. Aerodynamic Distortion Screen Design. . . . .	175
3. Screen Evaluation and Distortion Measurement. . . . .	183
4. Integral Order Resonance. . . . .	186
5. Nonintegral Order Vibration through the Piezoelectric Crystals . . . . .	191
6. Discussion of Results . . . . .	207
7. Correlation Between Measured Strain and Aerodynamic Stimulus . . . . .	215
8. Dynamic Response Due to Blade/Vane Interaction. . . . .	219
9. Discussion of Results . . . . .	222
10. System Damping Variation on the Constant Speed Line . . . .	222
XIII. GENERAL SUMMARY AND CONCLUSIONS . . . . .	229
XIV. REFERENCES . . . . .	233

# LIST OF TABLES

<u>Number</u>	<u>Title</u>	<u>Page</u>
1	Blade Alone First Bending Mode Frequencies For Coupled and Uncoupled Conditions. . . . .	29
2	Second Family Modal Frequencies and Dual Mode Separation. . . . .	31
3	First Family Modal Frequencies and Dual Mode Separation for the Experimentally Tuned and Intentionally Mistuned Conditions. . . . .	32
4	Resonant Frequencies and Loss Factors For Individual Blades in "Initially Tuned" Condition (Uncoupled Configuration). . . . .	42
5	Summary of Tests Performed on Fan Assembly (Initial Tuned Condition) in Rig. A. . . . .	49
6	Summary of Modal Characteristics for Initially Tuned System in Rig A. . . . .	71
7	Tip Mass Change and Resulting "Blade Alone" Modal Frequencies for Modified Blades in Mistuned Assembly. . .	73
8	Summary of Tests Performed on Fan Assembly (Mistuned Condition) in Rig A). . . . .	76
9	Summary of Modal Characteristics for Mistuned System in Rig A. . . . .	88
10	Maximum Values of Response Wave Ratio and Corresponding Frequencies For All Test Conditions For Tuned and Mistuned Assembly Excited With Traveling Waves. . . . .	98
11	Loss Factors and Frequencies of Maximum Individual Blade Response for the Mistuned System With 2nd and 4th Traveling Wave Excitation. . . . .	99
12	Summary of Measurement System Pre-Test Static Calibration Results. . . . .	105

# LIST OF TABLES (Cont'd)

<u>Number</u>	<u>Title</u>	<u>Page</u>
13	Summary of Shroud Motion Measurement Tests Performed on Mistuned Fan Assembly. . . . .	109
14	Data Reduction and Analysis Plan . . . . .	110
15	Comparison of Individual Blade Modal Frequencies and Dampings Before and After Sensor Installation. . . . .	113
16	Data Sample Identification . . . . .	119
17	Summary of Tests Performed on Fan Assembly (Mistuned Condition) in Rig B . . . . .	170
18	Summary of Tests Performed on Fan Assembly ("Tuned" Condition) in Rig B. . . . .	171
19	Resonant Frequencies for Individual Blades in Uncoupled Configuration as Measured in Rig B . . . . .	172
20	Identification and Location of Pressure Instrumentation. .	176
21	Summary of Peak Response Characteristics for the Mistuned Assembly in Rig B. . . . .	208
22	Summary of Peak Response Characteristics for Tuned Assembly in Rig B. . . . .	209
23	Maximum Values of Response Wave Ratio and Corresponding Frequencies For All Test Conditions for Tuned and Mistuned Assembly. Excited With Traveling Waves in Rig B . . . . .	210

# LIST OF ILLUSTRATIONS

<u>Figure</u>	<u>Title</u>	<u>Page</u>
1	Rotating Test Facility: Rig A . . . . .	6
2	Rotating Test Facility: An Overview . . . . .	7
3	The Aerodynamic Rig: Rig B . . . . .	8
4	Details of the Test Section: Rig B . . . . .	10
5	The R-80 Fan During Assembly . . . . .	12
6	Blade Drive Control Module . . . . .	16
7	Rotating Control Hardware and Amplifier Units (Ready for Potting). . . . .	17
8A	Data Acquisition System Schematic. . . . .	21
8B	Data Acquisition System. . . . .	22
9	Strain Gage Amplifier. . . . .	23
10	Data Reduction Flow Chart. . . . .	24
11	The Instrumented R-80 Fan . . . . .	26
12	Preliminary Tests of R-80 Fan: Multiplicity of Modes . .	28
13	Method of Modifying Tip Mass . . . . .	33
14	Stick Plots of Assembly First Family Resonant Response when Excited by a 2ND Stationary Wave . . . .	34
15	4ND Twin Modes Obtained After Partial Tuning . . . . .	36
16A	Polar Plot of Forced Response for Blade #16 . . . . .	38
16B	Polar Plot of Forced Response for Blade #16 . . . . .	38
16C	Polar Plot of Forced Response for Blade #16 . . . . .	39
17A	Polar Plot of Forced Response for Blade #39 . . . . .	40
17B	Polar Plot of Forced Response for Blade #39 . . . . .	40
17C	Polar Plot of Forced Response for Blade #39 . . . . .	41
17D	Polar Plot of Forced Response for Blade #39 . . . . .	41
18	Histogram of Blade First Bending Mode Frequencies . . . .	43
19	Histogram of Blade First Torsion Mode After Tuning . . . .	44
20	Schematic of Second Family 2ND Twin Modes . . . . .	46
21	Schematic of Second Family 3ND Mode Shape at 263.4 Hz . . . . .	47
22	Variation of Maximum Strain Response with Excitation Frequency for the Tuned Assembly Excited with a 4ND Forward Traveling Wave in Evacuated Conditions at Zero Speed . . . . .	50
23	Variation of Maximum Strain Response with Excitation Frequency for the Tuned Assembly Excited with a 4ND Backward Traveling Wave in Evacuated Conditions at Zero Speed . . . . .	51

# LIST OF ILLUSTRATIONS (Cont'd)

<u>Figure</u>	<u>Title</u>	<u>Page</u>
24	Polar Plot of Blade #27 Strain Response with 2ND Backward Traveling Wave Excitation of the Tuned Assembly in Evacuated Conditions at Zero Speed . . . . .	52
25	Response of the Tuned Assembly to 4ND Backward Traveling Wave Excitation at 65.57 Hz in Evacuated Conditions at Zero Speed . . . . .	54
26	Response of the Tuned Assembly to 4ND Backward Traveling Wave Excitation at 65.18 Hz in Evacuated Conditions at Zero Speed . . . . .	55
27	Response of the Tuned Assembly to 4ND Backward Traveling Wave Excitation at 65.47 Hz in Evacuated Conditions at Zero Speed . . . . .	56
28	Variation of Maximum Strain Response with Excitation Frequency for the Tuned Assembly Excited with a 4ND Backward Traveling Wave in Evacuated Conditions at 1163 rpm . . . . .	57
29	Response of the Tuned Assembly to 4ND Backward Traveling Wave Excitation at 77.48 Hz in Evacuated Conditions at 1163 rpm . . . . .	59
30	Response of the Tuned Assembly to 4ND Backward Traveling Wave Excitation at 77.61 Hz in Evacuated Conditions at 1163 rpm . . . . .	60
31	Response of the Tuned Assembly to 4ND Backward Traveling Wave Excitation at 77.05 Hz in Evacuated Conditions at 1163 rpm . . . . .	61
32	Response of the Tuned Assembly to 2ND Stationary Wave Excitation at 189.38 Hz in Evacuated Conditions at Zero Speed . . . . .	62
33	Response of the Tuned Assembly to 2ND Stationary Wave Excitation at 189.08 Hz in Evacuated Conditions at Zero Speed . . . . .	63
34	Response of the Tuned Assembly to 2ND Stationary Wave Excitation at 188.68 Hz in Evacuated Conditions at Zero Speed . . . . .	64
35	Response of the Tuned Assembly to 2ND Stationary Wave Excitation (shifted 45°) at 180.68 Hz in Evacuated Conditions at Zero Speed . . . . .	65



# LIST OF ILLUSTRATIONS (Cont'd)

<u>Figure</u>	<u>Title</u>	<u>Page</u>
36	Response of the Tuned Assembly to 3ND Stationary Wave Excitation at 265.57 Hz in Evacuated Conditions at Zero Speed . . . . .	66
37	Response of the Tuned Assembly to 3ND Stationary Wave Excitation at 265.04 Hz in Evacuated Conditions at Zero Speed . . . . .	67
38	Response of the Tuned Assembly to 4ND Stationary Wave Excitation at 280.28 Hz in Evacuated Conditions at Zero Speed . . . . .	68
39	Response of the Tuned Assembly to 4ND Stationary Wave Excitation at 278.61 Hz in Evacuated Conditions at Zero Speed . . . . .	69
40	Histogram of "Blade Alone" First Bending Mode Frequencies After Mistuning . . . . .	74
41	Histogram of "Blade Alone" First Torsion Mode Frequencies After Mistuning . . . . .	75
42	Variation of Maximum Strain Response Excitation Frequency for the Mistuned Assembly Excited with 4ND Backward Traveling Wave in Evacuated Conditions at Zero Speed . . . . .	78
43	Response of the Mistuned Assembly to 4ND Backward Traveling Wave Excitation at 65.58 Hz in Evacuated Conditions at Zero Speed . . . . .	79
44	Polar Plot of Blade #18 Strain Response with 4ND Backward Traveling Wave Excitation of the Mistuned Assembly in Evacuated Conditions at Zero Speed . . . . .	80
45	Blade Strain Response and Special Harmonic Distribution at 65.25 Hz for 4ND Backward Traveling Wave Excitation of the Mistuned Assembly in Evacuated Conditions at Zero Speed . . . . .	81
46	Variation of Maximum Strain Response with Excitation Frequency for the Mistuned Assembly Excited with a 4ND Backward Traveling Wave in Evacuated Conditions at 1163 rpm . . . . .	82
47	2ND Mode Shape of the Mistuned Assembly at 190.13 Hz in Evacuated Conditions at Zero Speed . . . . .	84
48	2ND Mode Shape of the Mistuned Assembly at 188.38 Hz in Evacuated Conditions at Zero Speed . . . . .	85

# LIST OF ILLUSTRATIONS (Cont'd)

<u>Figure</u>	<u>Title</u>	<u>Page</u>
49	3ND Mode Shape of the Mistuned Assembly at 265.03 Hz in Evacuated Conditions at Zero Speed . . . . .	86
50	3ND Mode Shape of the Mistuned Assembly at 264.90 Hz in Evacuated Conditions at Zero Speed . . . . .	87
51	4ND Mode Shape of the Mistuned Assembly at 282.54 Hz in Evacuated Conditions at Zero Speed . . . . .	89
52	4ND Mode Shape of the Mistuned Assembly at 278.61 Hz in Evacuated Conditions at Zero Speed . . . . .	90
53	Assembly Response to Excitation of Blade #28 at 70.50 Hz in Evacuated Conditions at 1200 rpm . . . . .	91
54	Assembly Response to Excitation of Blade #28 at 279.44 Hz in Evacuated Conditions at 1200 rpm . . . . .	92
55	Strain Response of the Mistuned Assembly to a 2ND Forward Traveling Wave Input at 187.7 Hz in Evacuated Conditions at Zero Speed . . . . .	93
56	Strain Response of the Mistuned Assembly to a 2ND Forward Traveling Wave Input at 188.68 Hz in Evacuated Conditions at Zero Speed . . . . .	94
57	Variation of Response Wave Ratio and Contributing Harmonics with Frequency for Tuned and Mistuned Assemblies with Excitation Frequency (2ND Forward Traveling Wave Excitation in Evacuated Conditions at Zero Speed) . . . . .	96
58	Shroud Motion Measurement Device . . . . .	101
59	Motion Sensor Housing Design . . . . .	102
60	Motion Measurement System Block Diagram . . . . .	103
61	Fully Instrumented R-80 Fan Assembly . . . . .	106
62	Shroud Geometry and Location of Motion Sensors at Interface . . . . .	107
63	Definition of Shroud Displacement Axis System . . . . .	111
64	Variation of Averaged Values of Static Shroud Relative Displacements ( $\bar{X}$ , $\bar{Y}$ & $\theta$ ) with Rotational Speed Squared . . . . .	116
65	Spacial Variation of Averaged Values of Static Shroud Relative Displacements ( $\bar{X}$ , $\bar{Y}$ & $\theta$ ) at Various Speeds and Individual Blade First Bending Modal Frequencies for Blades 24 through 34 . . . . .	117

# LIST OF ILLUSTRATIONS (Cont'd)

<u>Figure</u>	<u>Title</u>	<u>Page</u>
66	Strain Response for Instrumented Blades for Data Sample #1 . . . . .	120
67	Blade Strain Response and Spacial Harmonic Distribution for Condition Corresponding to Data Sample #1 . . . . .	121
68	Strain Response for Instrumented Blades for Data Sample #2 . . . . .	122
69	Blade Strain Response and Spacial Harmonic Distribution for Condition Corresponding to Data Sample #2 . . . . .	123
70	Strain Response for Instrumented Blades for Data Sample #3 . . . . .	124
71	Blade Strain Response and Spacial Harmonic Distribution for Condition Corresponding to Data Sample #3 . . . . .	126
72	Strain Response for Instrumented Blades for Data Sample #4 . . . . .	126
73	Blade Strain Response and Spacial Harmonic Distribution for Condition Corresponding to Data Sample #4 . . . . .	127
74	Strain Response for Instrumented Blades for Data Sample #5 . . . . .	128
75	Blade Strain Response and Spacial Harmonic Distribution for Condition Corresponding to Data Sample #5 . . . . .	129
76	Strain Response for Instrumented Blades for Data Sample #6 . . . . .	130
77	Blade Strain Response and Spacial Harmonic Distribution for Condition Corresponding to Data Sample #6 . . . . .	131
78	Modulus and Phase Plots of the Measured Response Parameters for Blades #25 through #34 with Backward Traveling Wave Excitation - Data Sample #1 (X - Axis Components of Shroud Motion) . . . . .	134
79	Modulus and Phase Plots of the Measured Response Parameters for Blades #25 through #34 with Backward Traveling Wave Excitation - Data Sample #1 (Y - Axis Components of Shroud Motion) . . . . .	135
80	Time History of Relative Displacements at Shroud Interface #30-31 for Data Sample #1 . . . . .	136
81	Relative Motion at Two Points on Shroud Interface #30-31 for Data Sample #1 . . . . .	137

# LIST OF ILLUSTRATIONS (Cont'd)

<u>Figure</u>	<u>Title</u>	<u>Page</u>
82	Modulus and Phase Plots of the Measured Response Parameters for Blades #25 through #34 with Backward Traveling Wave Excitation - Data Sample #2 (X - Axis Components of Shroud Motion) . . . . .	138
83	Modulus and Phase Plots of the Measured Response Parameters for Blades #25 through #34 with Backward Traveling Wave Excitation - Data Sample #2 (Y - Axis Components of Shroud Motion) . . . . .	139
84	Time History of Relative Displacements at Shroud Interface #26-27 for Data Sample #2 . . . . .	140
85	Relative Motion at Two Points on Shroud Interface #26-27 for Data Sample #2 . . . . .	141
86	Modulus and Phase Plots of the Measured Response Parameters for Blades #25 through #34 with Backward Traveling Wave Excitation - Data Sample #3 (X - Axis Components of Shroud Motion) . . . . .	142
87	Modulus and Phase Plots of the Measured Response Parameters for Blades #25 through #34 with Backward Traveling Wave Excitation - Data Sample #3 (Y - Axis Components of Shroud Motion) . . . . .	143
88	Time History of Relative Displacements at Shroud Interface #27-28 for Data Sample #3 . . . . .	144
89	Relative Motion at Two Points on Shroud Interface #27-28 for Data Sample #3 . . . . .	145
90	Modulus and Phase Plots of the Measured Response Parameters for Blades #25 through #34 with Backward Traveling Wave Excitation - Data Sample #4 (X - Axis Components of Shroud Motion) . . . . .	146
91	Modulus and Phase Plots of the Measured Response Parameters for Blades #25 through #34 with Backward Traveling Wave Excitation - Data Sample #4 (Y - Axis Components of Shroud Motion) . . . . .	147
92	Time History of Relative Displacements at Shroud Interface #27-28 for Data Sample #4 . . . . .	148
93	Relative Motion at Two Points on Shroud Interface #27-28 for Data Sample #4 . . . . .	149

# LIST OF ILLUSTRATIONS (Cont'd)

<u>Figure</u>	<u>Title</u>	<u>Page</u>
94	Modulus and Phase Plots of the Measured Response Parameters for Blades #25 through #34 with Backward Traveling Wave Excitation - Data Sample #5 (X - Axis Components of Shroud Motion) . . . . .	150
95	Modulus and Phase Plots of the Measured Response Parameters for Blades #25 through #34 with Backward Traveling Wave Excitation - Data Sample #5 (Y - Axis Components of Shroud Motion) . . . . .	151
96	Time History of Relative Displacements at Shroud Interface #27-28 for Data Sample #5 . . . . .	152
97	Relative Motion at Two Points on Shroud Interface #27-28 for Data Sample #5 . . . . .	153
98	Modulus and Phase Plots of the Measured Response Parameters for Blades #25 through #34 with Backward Traveling Wave Excitation - Data Sample #6 (X - Axis Components of Shroud Motion) . . . . .	154
99	Modulus and Phase Plots of the Measured Response Parameters for Blades #25 through #34 with Backward Traveling Wave Excitation - Data Sample #6 (Y - Axis Components of Shroud Motion) . . . . .	155
100	Time History of Relative Displacements at Shroud Interface #27-28 for Data Sample #6 . . . . .	156
101	Relative Motion at Two Points on Shroud Interface #27-28 for Data Sample #6 . . . . .	157
102	Polar Plots of Response of Blade #29 (Tuned Assembly) to a Forward Traveling Wave Excitation; Comparison of Theory With Test . . . . .	163
103	Polar Plots of Response of Blade #30 (Tuned Assembly) to a Forward Traveling Wave Excitation; Comparison of Theory With Test . . . . .	164
104	Polar Plots of Response of Blade #36 (Tuned Assembly) to a Forward Traveling Wave Excitation; Comparison of Theory With Test . . . . .	165
105	Polar Plots of Response of Blade #29 (Mistuned Assembly) to a Forward Traveling Wave Excitation; Comparison of Theory With Test . . . . .	166
106	Polar Plots of Response of Blade #30 (Mistuned Assembly) to a Forward Traveling Wave Excitation; Comparison of Theory With Test . . . . .	167

# LIST OF ILLUSTRATIONS (Cont'd)

<u>Figure</u>	<u>Title</u>	<u>Page</u>
107	Polar Plots of Response of Blade #36 (Mistuned Assembly) to a Forward Traveling Wave Excitation; Comparison of Theory With Test . . . . .	168
108	Histograms of "Blade Alone" Modal Frequencies for the "Tuned" and Mistuned Assembly in Rig. B. . . . .	169
109	Pressure Instrumentation in Test Section of Rig B. . . . .	174
110	Setup for Measuring "Blade Alone" Modal Frequencies in Rig B . . . . .	177
111	R80 Fan Clean Inlet Speed Line: Comparison of Measured Values iwth Design Points . . . . .	178
112	Theoretical Variation of Resistance Coefficient and Corresponding Overlay Segment Characteristics for a Quadrant of the Four Cycle Distortion Screen. . . . .	180
113	The Four Lobe Aerodynamic Distortion Screen. . . . .	181
114	Distortion Screen Mounted in Rig B . . . . .	182
115	Computational Flow Chart to Obtain the Harmonic Content of the Circumferential Variation of Flow Coefficients. . . . .	184
116	Variation of Average Flow Coefficient with Circumferential Angle at the Two Measuring Stations Downstream of the Distortion Screen . . . . .	185
117	Variation of System "Total" 4E Response and Blade Maximum Strain Amplitude of Mistuned Assembly Due to a Four Lobed Distortion in the Airstream with Excitation Frequency. . . . .	187
118	Response of the Mistuned Assembly to the Four Lobed Distortion in the Airstream at an Excitation Frequency of 77.04 Hz (1156 RPM): Peak System "Total" Response and Maximum Blade Strain . . . . .	188
119	Response of the Mistuned Assembly to the Four Lobed Distortion in the Airstream at an Excitation Frequency of 66.36 Hz (995.4 RPM). Peak Resonse of Blade #28. . . . .	189
120	Polar Plots of Fourth Harmonic of Blade Response $R_4(t)$ in Mistuned Assembly with 4ND Aerodynamic Excitation. . Responses shown for Blades #11, #30 and #32 . . . . .	190
121	Variation of System "Total" 4E Response and Blade Maximum Strain Amplitude of Tuned Assembly Due to a Four Lobed Distortion in the Airstream with Excitation Frequency. . . . .	192

# LIST OF ILLUSTRATIONS (Cont'd)

<u>Figure</u>	<u>Title</u>	<u>Page</u>
122	Response of Tuned Assembly to the Four Lobed Distortion in the Airstream at an Excitation Frequency of 76.64 Hz (1150 RPM); Peak System "Total" Response and Maximum Blade Strain. . . . .	193
123	Polar Plots of Fourth Harmonic of Blade Response $R_4(t)$ In Tuned Assembly With 4ND Aerodynamic Excitation. Responses shown for Blades #11, #27 and #28 . . . . .	194
124	Responses of the Mistuned Assembly to a 2ND Backward Traveling Wave Excitation (Crystal) at 191.61 Hz at Zero Speed in Rig B. . . . .	195
125	Response of the Mistuned Assembly to a 2ND Backward Traveling Wave Excitation (Crystal) at 190.48 Hz at Zero Speed in Rig B. . . . .	196
126	Response of the Mistuned Assembly to a 2ND Backward Traveling Wave Excitation (Crystal) at 197.14 Hz at 1200 RPM in Rig B. . . . .	197
127	Response of the Mistuned Assembly to a 2ND Backward Traveling Wave Excitation (Crystal) at 195.47 Hz at 1200 RPM in Rig B. . . . .	198
128	Response of the Mistuned Assembly to a 2ND Backward Traveling Wave Excitation (Crystal) at 197.2 Hz at 1200 RPM in Rig B. . . . .	199
129	Response of the Mistuned Assembly to a 2ND Backward Traveling Wave Excitation (Crystal) at 196.07 Hz at 1200 RPM in Rig B. . . . .	200
130	Response of the Mistuned Assembly to a 3ND Backward Traveling Wave Excitation (Crystal) at 268.79 Hz at 1200 RPM in Rig B. . . . .	201
131	Response of the Mistuned Assembly to a 4ND Backward Traveling Wave Excitation (Crystal) at 283.4 Hz at 1200 RPM in Rig B. . . . .	202
132	Tuned Assembly "System Total" Response Variation With Frequency for 2ND Backward Traveling Wave Excitation at Speed in Rig. B . . . . .	203
133	Mistuned Assembly "System Total" Response Variation With Frequency for 2ND Backward and Forward Traveling Wave Excitation at Speed in Rig. B. . . . .	204

# LIST OF ILLUSTRATIONS (Cont'd)

<u>Figure</u>	<u>Title</u>	<u>Page</u>
134	Tuned and Mistuned Assembly "System Total" Response Variation with Frequency for 3ND Backward Traveling Wave Excitation at Speed in Rig B . . . . .	205
135	Tuned and Mistuned Assembly "System Total" Response Variation with Frequency for 4ND Backward Traveling Wave Excitation at Speed in Rig B . . . . .	206
136	Comparison of Mistuned Assembly System "Total" 2ND Response in Rig A and Rig B . . . . .	212
137A	Campbell Diagram Showing First Family Response Frequencies from Theoretical Calculations and Test.	213
137B	Campbell Diagram Showing Second Family Response Frequencies from the Theoretical and Test . . . . .	214
138	Spatial Positions of 4ND Flow Coefficient and Tuned Assembly Strain Response Distributions (One Quadrant) . . . . .	216
139	Correlation Between Principal Componentes of Flow Distortion and Tuned Assembly System Strain Responses . . . . .	218
140	Variation of Blade Strain Amplitude and Component Wave Ratio (Stationary/Traveling) in the 6ND Modal Response due to Exit Guide Vane Excitation with Rotational Speed . . . . .	221
141	Response of the Tuned Assembly to Exit Guide Vane Excitation at 379.7 RPM in Rig B. . . . .	223
142	Polar Plots of Blade Strain Response in the 6ND Mode due to Exit Guide Vane Excitation for Blades #28 and #36. . . . .	224
143	Time Domain Analysis of 2ND Mode Decay at 1200 RPM of the Mistuned Fan . . . . .	226
144	Time Domain Analysis of 2ND Mode Decay at 560 RPM of the Mistuned Fan . . . . .	227
145	Time Domain Analysis of 2ND Mode Decay at 560 RPM of the Tuned Fan . . . . .	228



## I. INTRODUCTION

Vibration induced fatigue failure of rotor blades is of continuing concern to the designer of aircraft engines. The emphasis on improved engine performance under the necessary constraints of minimum weight and satisfactory life requires that vibration levels in all rotor blades be kept low. Further, certain important design considerations of rotor blades require a thorough understanding of the aeromechanical characteristics of bladed disk assemblies. These design considerations include (i) blade life prediction which uses vibration amplitudes in its calculations, (ii) setting allowable frequency margins which need to be justified on the basis of the intensity of resonant stresses at integral order speeds, and (iii) prediction of susceptibility of the component to aeroelastic instabilities. Clearly, a successful design process depends on the reliability of the analyses that serve as the basis of design systems. Such reliability can be established only through a data base obtained through tests of components conducted under controlled environments. 261473

An assembly of light and flexible blades with or without shrouds is prone to vibration in an operating environment. Periodically varying pressure fields from guide vanes, flow distortion due to struts or other upstream obstructions and unbalance of the rotor system are some of the principal sources of excitation that result in blade vibration response. Limiting the vibratory stresses to acceptable levels in a given design requires that the designer be able to calculate the dynamic characteristics of the assembly.

The calculation of vibratory characteristics of an assembly of blades usually relies on an important assumption; i.e., any one blade on the rotor is assumed to be identical in all respects to any other blade on the same rotor. Based on this assumption, the frequency response characteristics of a bladed disk assembly are computed. The results are used by designers to set resonant speed margins of rotors and also to determine blade flutter susceptibility. However, minor differences in individual blade characteristics are inevitable, severe requirements on manufacturing tolerances notwithstanding. A phenomenon known as mistuning arises from scatter of vibrational characteristics such as, for example, a scatter in frequencies of individual blades mounted on the periphery of a rotor disk. Even a rotor with essentially no scatter in its blade frequencies develops some scatter due to nonuniform normal wear during service. Therefore, it is only the degree of mistuning that differs from one rotor to another.

For a "tuned" rotor, the distribution of vibratory amplitudes remains harmonic and the vibratory mode shape of the bladed-disk assembly can be described in the familiar nodal diameter/nodal circle pattern. The modes of a mistuned assembly may not exhibit such ordered patterns. The circumferential variation of vibratory amplitudes in a mistuned rotor may not bear any resemblance to a sinusoidal wave. The extent of change from an ideal, well-ordered set of modes to an arbitrary, irregular set of vibratory patterns depends upon a host of parameters, such as (i) extent of scatter in individual blade frequencies, (ii) blade location around periphery of the rotor, (iii) degree of mechanical and/or aerodynamic coupling, and (iv) mechanical damping present in the system and the nature of its distribution around the rotor due, for example, to nonuniform rubbing at shroud interfaces.

→ Some comments in regard to the last item are in order. In the area of turbomachinery structural dynamics, an aspect that has eluded both analysis and experimentation pertains to relative motion at shroud interfaces of a bladed-disk assembly. The practice of designing a part-span shroud on fan blades has been in vogue for a number of years following the practice of using lacing wires in steam turbines. The difficulties associated with analysis of an assembly of blades with shrouds lie in the uncertainties of the nature of boundary conditions at these interfaces. Although the primary motivation to design shrouds on fans continues to be governed by rotor stiffness requirements, the contributions to damping due to rubbing at the interfaces are acknowledged. The extent of these contributions to vibration damping, however, has not been accurately established. Careful measurements made on a typical advanced fan blade made of titanium alloy (8-1-1) show (see Ref. 1) that (1) material hysteresis damping is negligibly small and (2) damping at dove-tail root interfaces tends to diminish rapidly as the centrifugal pull on the blade increases. Therefore, the structural integrity of a titanium alloy fan during resonant vibration or flutter must depend upon dry friction damping at shrouds and aerodynamic damping. Therefore, there is clearly a need to develop a body of data from a vibrating fan so that the nature and extent of the complex motions at shroud interfaces can be understood. It is only through such a data base that one can attempt to define the scope of analytical modeling needed. A successful development of properly calibrated analytical models will influence the blade designer to consider including damping as an additional criterion in his design.

The vibratory response characteristics of bladed-disk assemblies with part span shrouds can be quite complex in view of blade to blade nonuniformities in frequencies as well as damping at shroud interfaces. Some of the principal issues that need clarification are: (i) what is the extent of

coupling provided by the shrouds and how does it vary over a range of speeds and frequencies? (ii) How significant are twin modes and how does damping influence the twin mode responses? (iii) What is the extent of influence of a severe aerodynamic environment on the basic modal characteristics of the assembly of blades? (iv) What relationship exists between aerodynamic stimulus and blade strain? (v) What is the nature of shroud motion at the interfaces? (vi) What levels of nonaerodynamic and aerodynamic damping can be expected in a vibrating assembly? The answers to these and other questions will undoubtedly enhance our understanding of the behavior of bladed-disk systems and lead to improvements in prediction methods.

The Air Force Aero Propulsion Laboratory at the Wright-Patterson Air Force Base sponsored a research effort at UTRC under Contract #F33615-79-C-2054 to address some of the issues mentioned above. This report discusses these issues further and presents the results obtained from forced vibration tests conducted on a part-span shrouded fan assembly in vacuum as well as in an aerodynamic environment.

## II. PROGRAM OBJECTIVES

The primary objective of this research effort is to characterize a shrouded fan, i.e., understand its dynamic response characteristics over a range of speeds when it is subjected to forced vibration in vacuum in a spin rig and to distortion induced vibration in an aerodynamic rig. Such a characterization is to be established by analysis of strain response data obtained when the assembly is driven by predetermined standing or traveling wave forcing in a vacuum rig and an aerodynamic rig. Both tuned and mistuned conditions are to be considered. Further, in order to complete the process of understanding the behavior of the system, the motion at shroud interfaces is to be recorded from spin rig tests and analyzed. A distortion screen is to be used in inducing a selected mode of vibration and a comparison is to be made between responses in the tuned and mistuned conditions. In order to relate the response to the aerodynamic stimulus, data is to be taken to determine the velocity defects in the flow at several predetermined radial, circumferential and axial locations between the screen and the rotor. Vibration measurements are to be made both at "clean" and distorted flow conditions. To the extent possible, similar modes are to be observed in the non-aerodynamic and aerodynamic environment so that an assessment of contributions to damping from these two different sources can be made. Finally, the influence of exit guide vanes on the response characteristics of the fan is to be measured.

With these objectives in mind, an experimental research effort was outlined taking into consideration (a) test rigs available to conduct this program, (b) calculated vibration characteristics of the test component selected for use in this program, and (c) important features in regard to the state-of-the-art techniques in vibration excitation, data acquisition and processing techniques developed at the Research Center.

### III. TEST RIGS

The important features of the test plan will be presented in this section. Additional details, as necessary, in regard to each aspect of the plan, will be presented in subsequent sections of this report.

#### 1. Test Rigs Used in the Program

Two rigs were used to conduct tests called for in the research program. The salient features of both the rigs designated A and B are described below. Rig A was used for all nonaerodynamic tests, and Rig B was used in all aerodynamic test conditions.

##### a. The Rotating Test Facility: Rig A

The schematic of the rotating test facility is shown in Fig. 1 and the photograph (Fig. 2) shows an overview of the rig. The facility had been designed to spin components of up to five feet in diameter rotating at speeds up to 3000 rpm. This diameter and rotational speed results in a force field of the order of 10,000 g's. The rotational speed of the test specimen is controlled by a 15 hp variable speed electric motor whose speed is regulated to less than 1 percent variation by a tachometer feedback control. The 6' diameter chamber can be evacuated to a pressure of approximately 5 torr. The facility had been designed such that the top half of the chamber can be removed for inspection and replacement of models. A 40 channel slip ring unit provides the capability to acquire data from the spinning test component.

##### b. The Aerodynamic Test Facility: Rig B

The overall arrangement of the aerodynamic rig is shown in Fig. 3. Air enters the facility through a twelve foot diameter inlet with aluminum honeycomb inset into the face to remove cross-flow effects. The inlet contracts, passing the flow through a series of fine mesh screens to reduce the turbulence level. A further contraction achieves the five feet outer diameter of the test section. A distortion-generating section may be installed upstream of the test section. Provision is made for installing spacers to locate the distortion generator at various upstream positions relative to the test section. The test section itself consists of an axial series of constant diameter casings enclosing the rotor assembly and any necessary inlet and/or exit guide vanes. The rotor is mounted on a drive shaft cantilevered from two downstream bearings providing a clean flow path

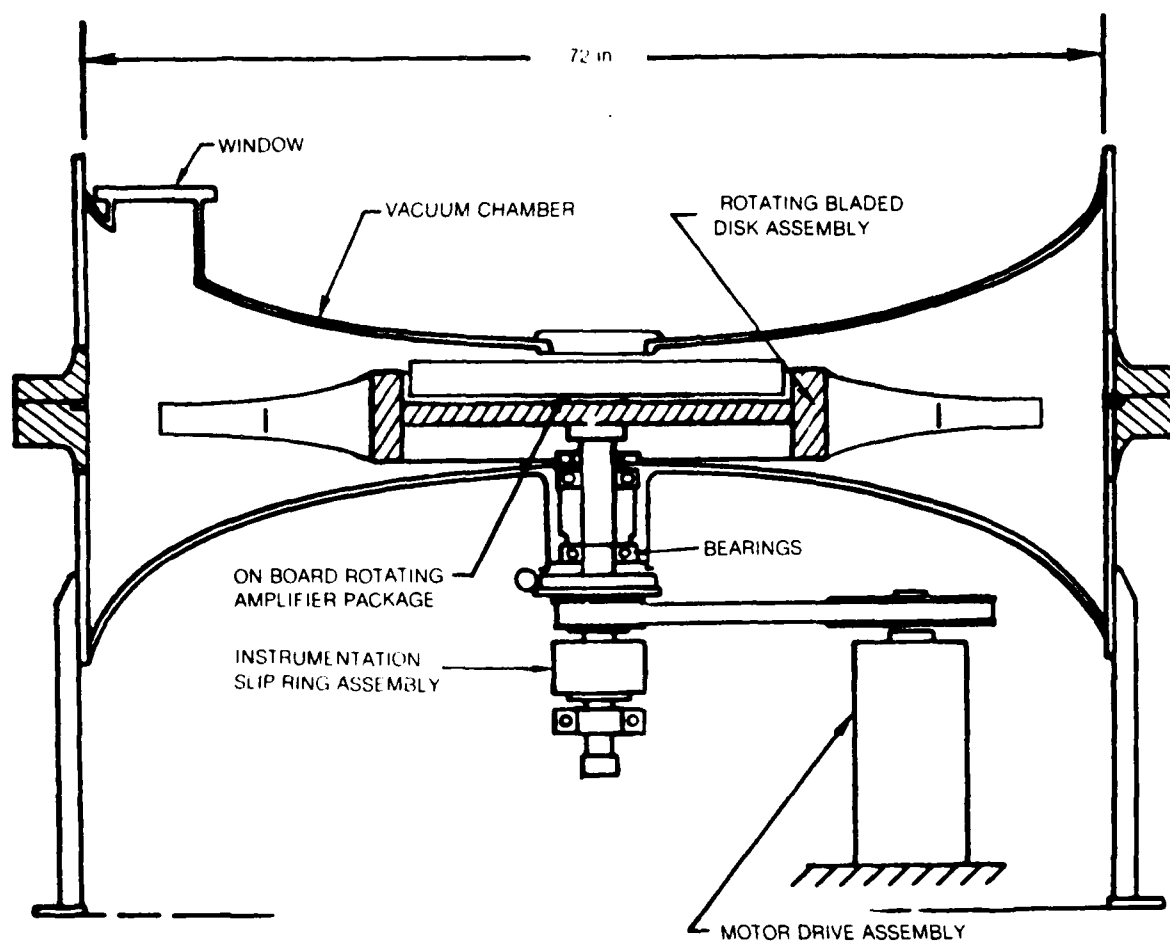


Figure 1 Rotating Test Facility: Rig A

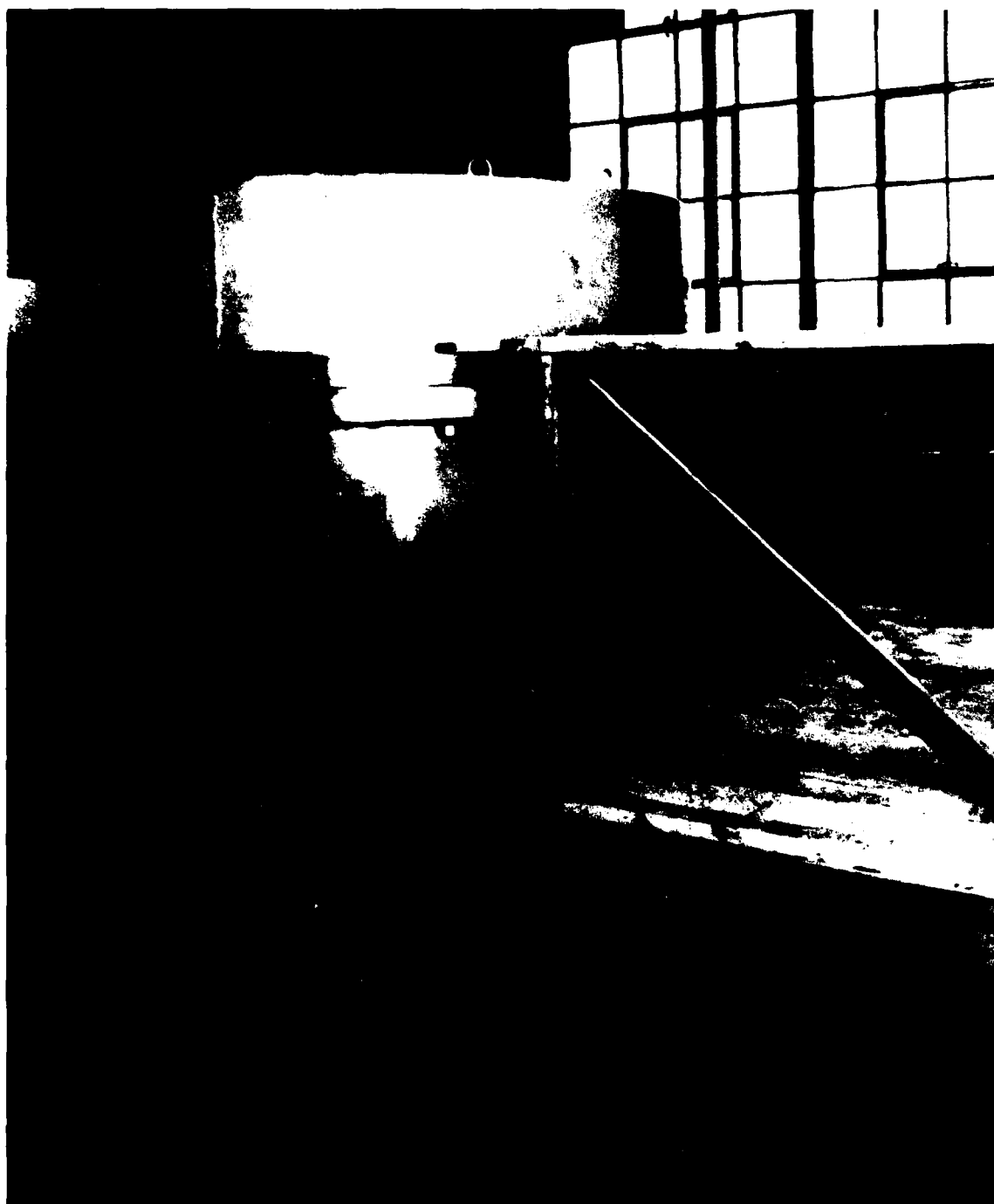


Figure 2 Rotating Test Facility: An Overview

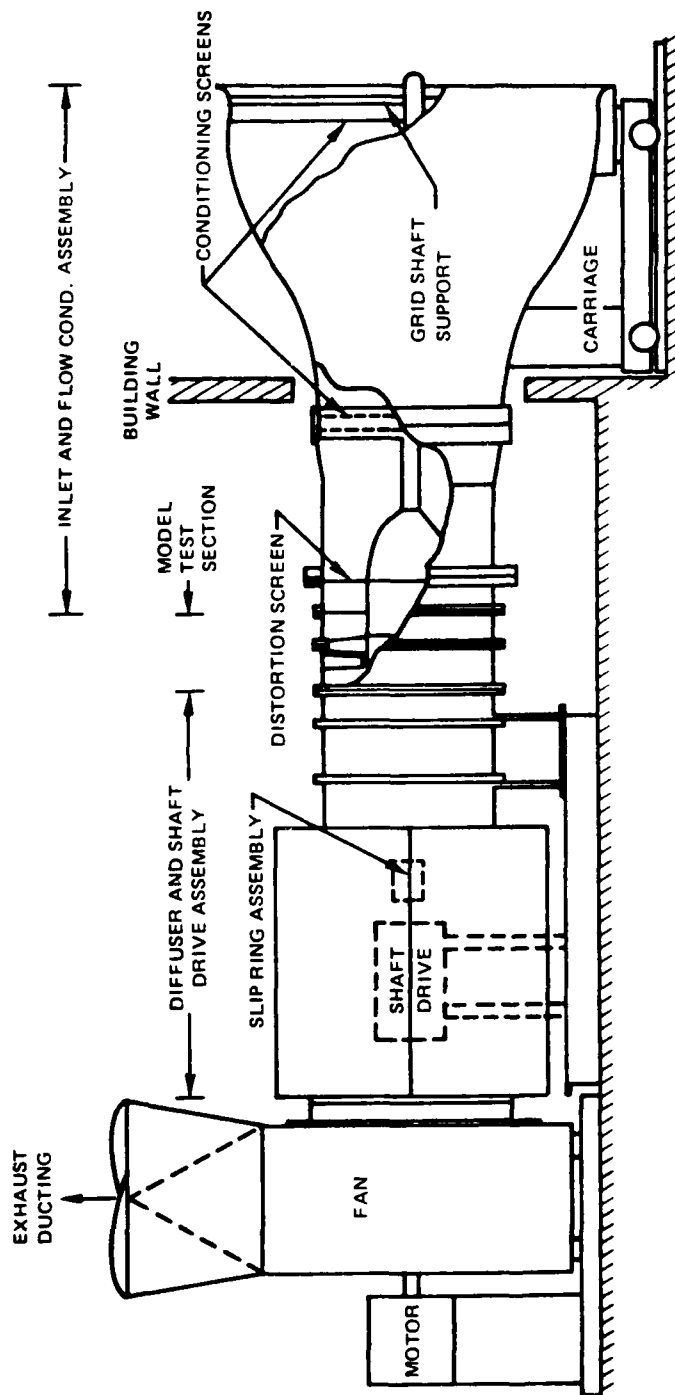
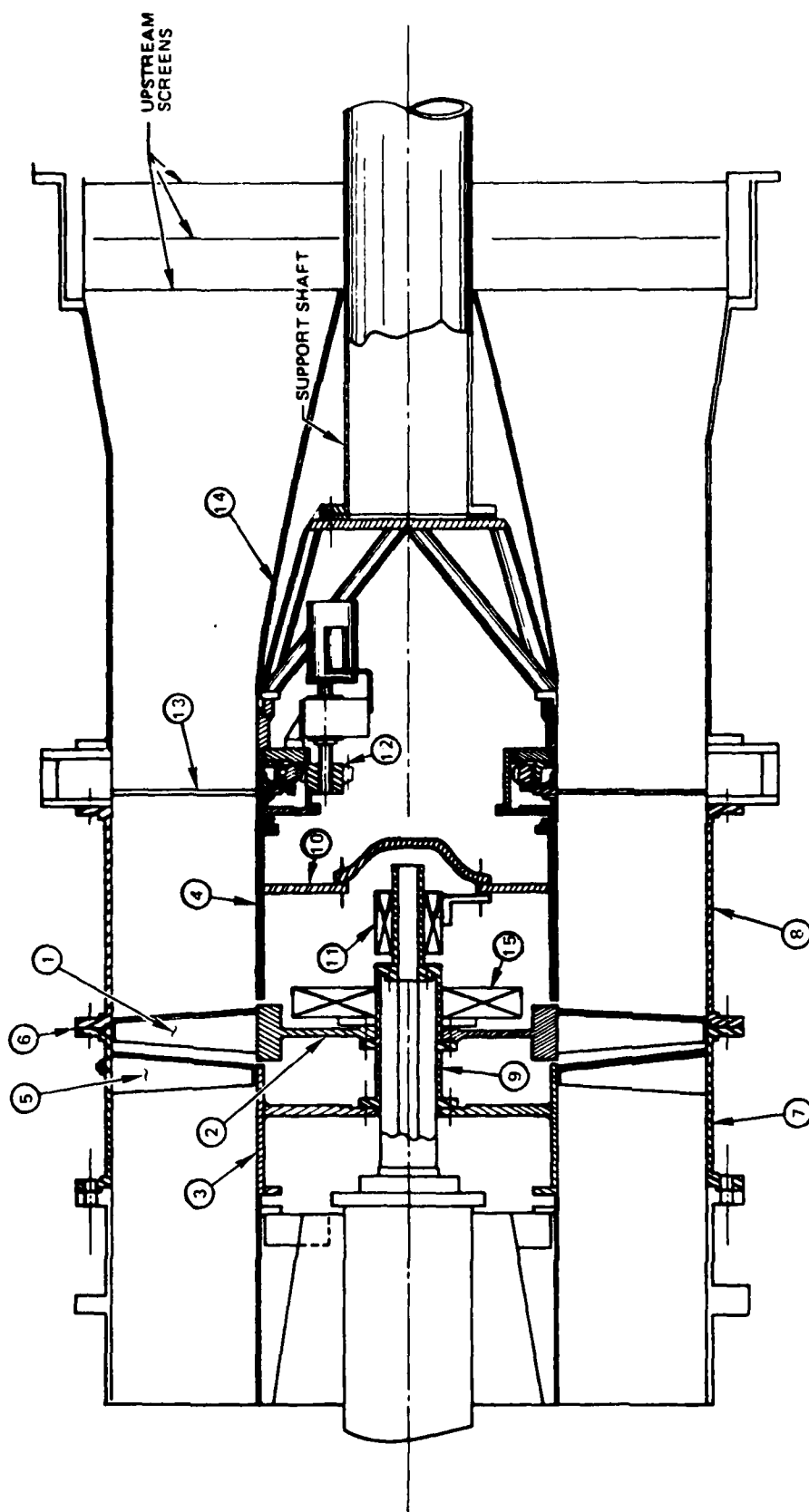


Figure 3 The Aerodynamic Rig: Rig B



to the model blading. The shaft is driven by a 200 hp D.C. motor with a maximum speed of 1200 rpm and 0.1 percent accuracy on speed regulation. Downstream of the test section, the flow is decelerated by means of a dump diffuser before entering the inlet of a centrifugal fan which exhausts the air through the building roof. The fan is capable of a maximum static pressure rise of 25 inches of water and has a vortex valve mounted in its inlet face to control the axial flow rate. Axial velocities between 50 and 300 ft/sec are possible with typical fan and compressor models. The rotating frame instrumentation is interfaced to stationary frame equipment through a 100-channel slipring package mounted on the aft end of the rotor shaft. Details of the test section are shown in Fig. 4.



- LEGEND.
- |                                    |   |
|------------------------------------|---|
| 1. MODEL FAN BLADE                 | 9. SHAFT ADAPTER                            |
| 2. MODEL DISK                      | 10. STATIONARY DIAPHRAGM SEAL               |
| 3. ROTATING AFT HUB CASING         | 11. ADDITIONAL SLIP RING PACKAGE            |
| 4. NON ROTATING FORWARD HUB CASING | 12. SCREEN ROTATING MECHANISM               |
| 5. EXIT GUIDE VANE                 | 13. DISTORTION SCREEN                       |
| 6. CONTAINMENT RING                | 14. INLET FAIRING AND HUB SUPPORT STRUCTURE |
| 7. AFT OUTER CASING                | 15. INSTRUMENTATION PACKAGE                 |
| 8. FORWARD OUTER CASING            |   |

Figure 4 Details of the Test Section: Rig B

#### IV. THE TEST COMPONENT

The capabilities of the available rigs dictated the design goals for the bladed-disk assembly. Operating at 1200 rpm, the fan must develop a moderate to small pressure rise--less than 1%, and must have, in the speed range, modes of vibration in the first and second families that can respond under forced vibration. The final design resulted in a 60" diameter fan consisting of 40 blades. Each blade made of aluminum (AL6061T6) is 15" long with an aspect ratio of 2.5 (tip) - 3.0 (root) with a part span shroud located at 47% span. The maximum thickness of the airfoil increases linearly towards the tip in order to bring the frequencies low enough to be excited within the speed range. The root attachment is a bolted dovetail arrangement with matching slots in a disk of 30" diameter. To provide realistic loading at shroud and root interfaces, at 1200 rpm, a pretwist of 1° was built into the design so that on assembly, the shrouds would be loaded with about 180 lbs. and the root was tightened using two axial bolts through the disk. A photograph of the assembly designated as the R-80 fan is shown in Fig. 5.



Figure 5 The R-80 Fan During Assembly

## V. MECHANISMS OF EXCITATION OF THE ASSEMBLY

In the effort pertaining to the mechanical characterization of the fan in an evacuated spin rig, a method to impose a forcing function was needed. The conventional method of shooting air jets at blades was not preferred, not only because of considerable modifications needed to be made on the rig, but also of additional uncertainties accompanying any measurement of damping. The techniques required for the excitation of a bladed disk assembly must permit control of the level, frequency and phase of excitation of individual blades. In this way, the modal parameters (frequency, mode shape and damping) can be completely defined.

Three techniques were chosen to excite the model fan: (i) preliminary characterization through the use of instrumented hammer in the nonrotating condition, (ii) piezoelectric crystal forcing element for use in both rotating and nonrotating conditions and (iii) distortion screens for aerodynamic excitation.

The instrumented hammer is generally used to excite a structure transiently for use in modal analysis systems which employ the FFT techniques to determine modal parameters. This impulsive force technique utilizes short transient force inputs (with corresponding broad-band spectra) to excite all the modes in the structure simultaneously. A force transducer is mounted on the hammer and an accelerometer is located on the structure at a fixed location. The structure is excited at a multiplicity of predetermined locations using the hammer and the response is picked up by the accelerometer. The two transient time histories, i.e., force and response, are automatically digitized and then Fourier transformed by a minicomputer to yield input and output spectra.

The piezoelectric crystal, which was used in both rotating and non-rotating tests, by virtue of its unique electromechanical properties, is ideally suited for exciting structures with minimum modification of the structural mass and stiffness properties. Piezoelectric crystals have been successfully used as structural exciters in the areas of material damping measurement (Ref. 1) and bladed disk forced vibrations (Ref. 2). Excitation by crystals can be effected by using an elongated crystal wafer bonded to the surface of the structure such that when a voltage is applied to the crystal, a longitudinal strain is imparted to the surface which in turn produces a local bending moment about the neutral axis and so bends the structure. This method is best suited to plate-like structures. UTRC has successfully developed a crystal excitation system that has proven to be a reliable method of imposing standing and traveling wave modes of forcing as described below.

## 1. Development of Piezoceramic Driven Elements

Preliminary research into the feasibility of using piezoceramic elements for use in exciting a structural component followed by a demonstration program conducted in two phases and described below served as the basis for the design, development, fabrication and installation of a unique excitation system that was used as the principal source of excitation during mechanical characterization of the fan.

The first phase of demonstration consisted of simple tests conducted on flat plates. Crystal drive capability at resonance was demonstrated on two flat cantilevered aluminum alloy plates with dimensions 15 x 5 x 0.125 and 7.5 x 2.5 x 0.05 (inch units). Each plate was driven by a single crystal (1 x 0.25 x 0.02) glued to the surface at the fixed end. The largest plate required 400 volts (pk-pk) to generate a  $\pm 0.05$  inch tip displacement at the resonant frequency of 17 Hz.

In the second phase, tests were conducted on a table model of a "bladed disk." A 13 inch diameter eight "bladed disk" was cut from flat aluminum alloy sheet 0.05 inch thick. Each "blade" is rectangular (5 inches long and 1.1 inches wide) and is instrumented near the root with a driver crystal on one surface and a responsive crystal (sensor) on the other at the same/spanwise/chordwise location. The eight bladed flat plate disk model was characterized using a Frequency Response Analyzer. Both Bode and Nyquist response plots were generated for a) each individual blade (with the others clamped) and b) the assembly (excited using a crystal on a single blade). The individual "blades" were found to be mistuned by up to 5% of the average value of the first blade bending mode frequencies. Four significant modal responses of the assembly were measured between 50 and 80 Hz. These results formed the basis for the evaluation of techniques and voltage requirements needed to excite the blades in a required stationary mode or at a given constant inter-blade phase angle. Preliminary results indicated that the degree of mistuning plays an important part in the power requirements of the drive system.

Prior to the final design of the Excitation System, the feasibility of using bender element type piezoceramic crystals to excite the test blades was established by full scale testing. The test pieces used were an aluminum flat plate and an aluminum curved plate having similar dimensions to those of the above-shroud portion of the test blade (span = 7.9 inches). The plate was clamped at its root station. Excitation was provided by two lead zirconate titanate crystals mounted and connected in parallel on the plate near the root. The crystal dimensions were; length 1.3 inches, thickness 0.0075 inch, and width 0.9 inch and 0.75 inch, respectively. The adhesive used was DEVCON 5 Minute Epoxy. It was found that for a given applied signal, the blade

response was approximately proportional to crystal width. For an applied voltage of 100 volts rms, maximum root stress in the first mode (59 Hz), obtained using both crystals, was approximately 1600 psi with a tip deflection of 0.11 inch DA. A strain gage mounted on the crystal indicated no phase shift in strain between the plate and the crystal. Excitation for extended periods of time and other physical tests proved the ruggedness of the mounted crystals.

For application to the curved surface of the test blade, a configuration consisting of three crystal elements each 0.5 inch wide closely mounted in parallel directly on the blade surface was being considered. Three closely spaced drive crystals from samples of Gulton Industries' G1278 material (each 1.33" x 0.59" x 0.0075") were mounted just above the shroud on the curved aluminum sheet test piece. Power requirements for measurable response in the first flap and torsion modes were confirmed to be 100 volts rms/40-50m A rms.

Information received from Gulton Industries indicated that G1356 lead zirconate titanate crystals were better suited to the present application than the G1278 crystals used in development because of their greater tolerance to high voltages. Samples of the material were received and tested on the test plate. The performance of the new crystals was found to be superior to that of the earlier selection, and the final configuration chosen for the test blade comprised only two G1356 crystals each 1.00" x 0.5" x 0.01" mounted on the suction surface just above the shroud.

The aerodynamic effects of the crystals were minimized by covering and contouring the surface with epoxy. The connecting wires were made from flat copper ribbon wire attached to the blade with Scotch Brand Transparent Tape which was also used to insulate the wire from the blade. A small patch of silver epoxy was put on the underside of the crystal to provide the electrical contact (return path) between the crystal electrode and the blade.

## 2. Blade Drive Control System

The Blade Drive System was designed to excite standing wave or traveling wave patterns of vibration in a forty bladed disc assembly by synchronously energizing the crystal drivers mounted on each blade. The electronic system consists of an operator control chassis (see Fig. 6) and rotating control hardware (see Fig. 7) including 40 high voltage amplifiers. The rotating control hardware can be programmed manually via switches on the operator control chassis. Synchronized reference signals are generated by the control hardware and routed to the blades as designated by operator selection for each blade.





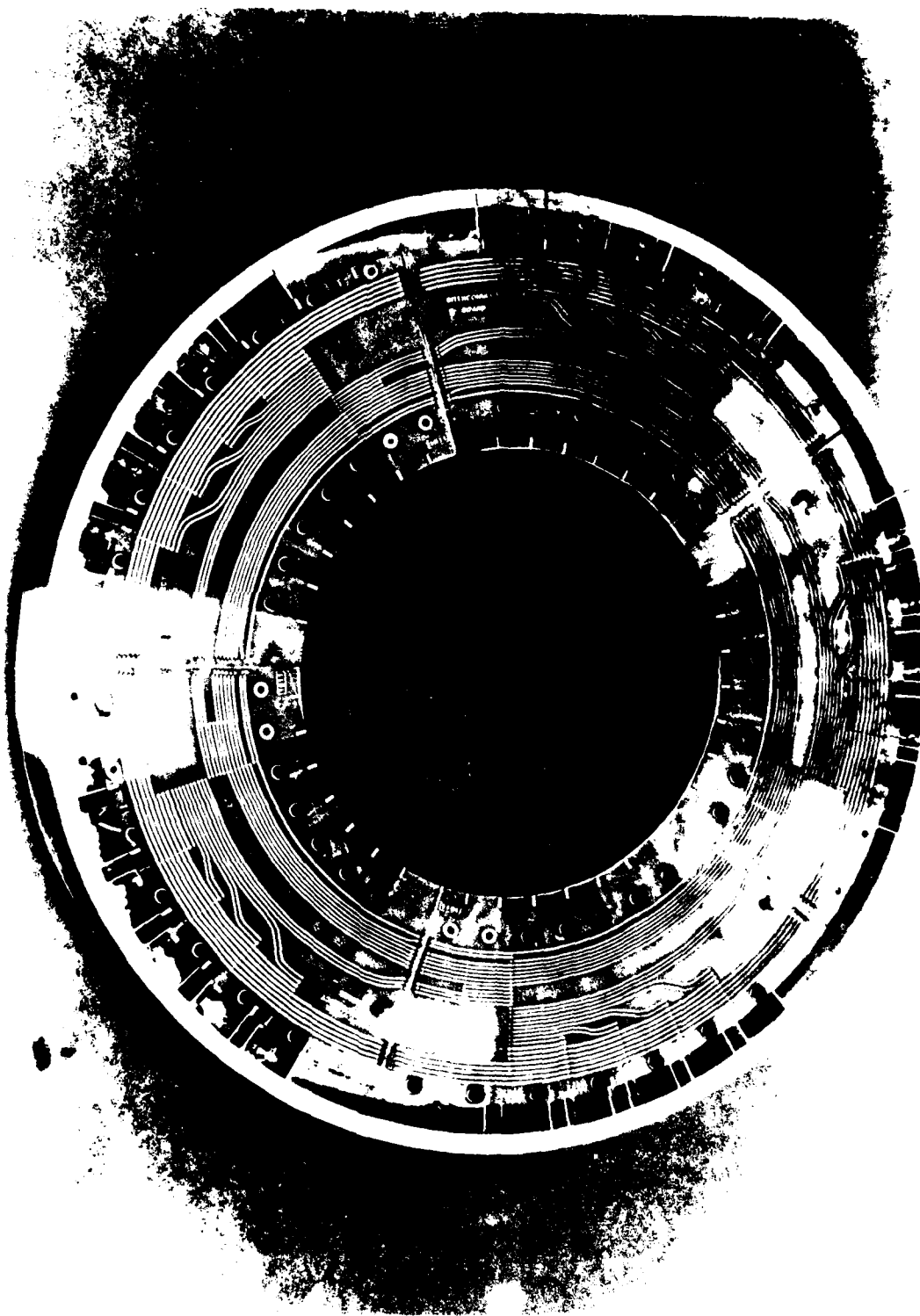


Figure 7 Rotating Control Hardware and Amplifier Units  
(Ready for Potting)

The control system consists of an operator control panel and rotating microprocessor-based control hardware, linked via 15 control signal slip rings and four power slip rings. The operator control panel provides a drive amplitude control, a select switch for traveling wave nodal diameters and switches used in combination to program the mode of operation for each blade as described above. A matrix of indicator lights display the selected mode for each blade. A programmed standing wave pattern (see Fig. 6) may be rotated around the disc in one blade increments. Up to 10 nodal diameter patterns may be generated over an input frequency range of 40 to 400 Hz. Phase control accuracy is  $\pm 1$  deg. The system may be operated over a temperature range of 0-70°C and with steady accelerations of up to 600g.

### 3. Drive Modules

A drive module is provided for each of the forty blades. A remote control static selector on the modules determines the control reference signal to which the blade drive will respond. This selection is determined by the operator in order to generate the desired assembly response. Selections are:

- 1) in phase with control frequency
  - 2) 180 deg. delay from control frequency
  - 3) no excitation
- or 4) incremental phase from control frequency

A low distortion digital to sine wave converter is incorporated. A power amplifier provides up to  $\pm 140$  volts DC excitation to the crystal. Excitation amplitude is manually variable from 0 to full scale via a single operator control which varies excitation to all blade drives. No feedback of blade position is utilized.

### 4. System Development

Breadboard testing of design concepts demonstrated satisfactory operation for input frequencies within the range of 40 to 400 Hz. A digital to sine wave converter was demonstrated. A two channel drive unit was breadboarded to confirm the selection of the main components and provide a

demonstration of interblade phase control. Refinements made to the system included the improvement of the resolution of the digital to sine wave converter with the resultant reduction of harmonic content to better than -50dB.

Mechanical and electrical design of the system incorporated potted printed circuit board concepts for the rotating hardware. Installation of the drive module on the rotor was simplified by limiting the connections to one plug-type slip ring connection and one soldered-wire connection to each blade crystal. The total system was bench tested using simulated drive crystals and demonstrated compliance with the design specifications. The system was operated extensively and marginal components were identified and replaced prior to potting. A final bench test was made after the potting operation.

## VI. BLADE STRAIN MEASUREMENT SYSTEM

The basic response of the assembly was measured using strain information from a single location on each of the 40 blades. This location was selected on the basis of a calculated high stress region on the blade just above the leading edge of the shroud (mid span, 20% chord). In order to obtain more detailed blade modal data, one blade was instrumented at two additional locations, one at mid-span (80% chord) and the other at the root (50% chord). With so many channels of data, a multiplex system was designed to allow 20 channels of data to be acquired simultaneously. A schematic of the Data Acquisition System is shown in Fig. 8A and a photograph of the entire system is shown in Fig. 8B. The data acquisition system ATLAS (Aeromechanics Transient Logging and Analysis) can be clearly seen in the photograph and was used in all phases of this program. To increase the signal-to-noise ratio of the strain data, two 350 $\Omega$  gages were mounted, one on each surface of the blade, and connected, in a half-bridge network, to on-board signal amplifiers. 20 multiplexed 7-channel strain gage amplifiers (with nominal gain of 500) were designed and built. The microelectronic circuits were mounted on flexible PC board and potted to form cigar-shaped modules about 4 1/2 inches long and 1 inch wide as shown in Fig. 9. Twenty of these modules were mounted in the disk just inside of the rim and connected to the strain gages using 24-gage enamel coated wire glued to the surface of the blade. Power, switching and signal wires were routed along the disk to the slip rings. The switching was arranged such that the responses from blades in all 20 odd-numbered slots could be acquired simultaneously and similarly for the 20 blades in the even-numbered slots. All data were digitized and stored on magnetic tape for subsequent analysis.

The digitized time series from all the gages were harmonically analyzed to determine the response mode shape (strain) around the rotor. These lead to stickplots at an instant of time and a quarter period later as will be displayed subsequently. Further data reduction involved the calculation of the strength of contributing harmonics. The flow chart shown in Fig. 10 shows the step-by-step procedure in data reduction.

On-line observation of strain responses for taking preliminary readings and setting test conditions was possible with use of a patch board, a rotary switching system and a dual channel oscilloscope. This enabled any selected blade response to be compared with any of the others very conveniently.

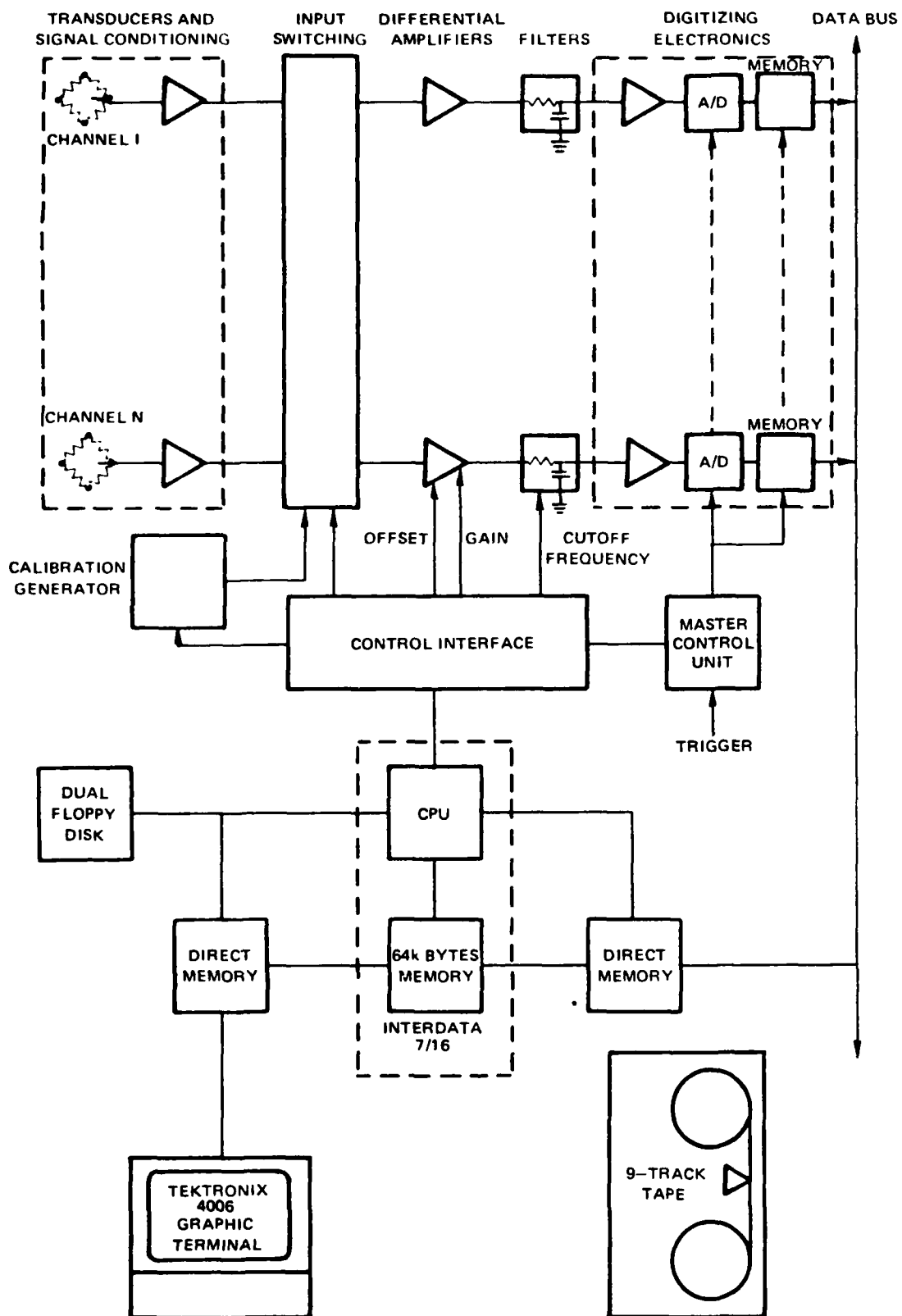


Figure 8A Data Acquisition System Schematic



Figure 8B Data Acquisition System

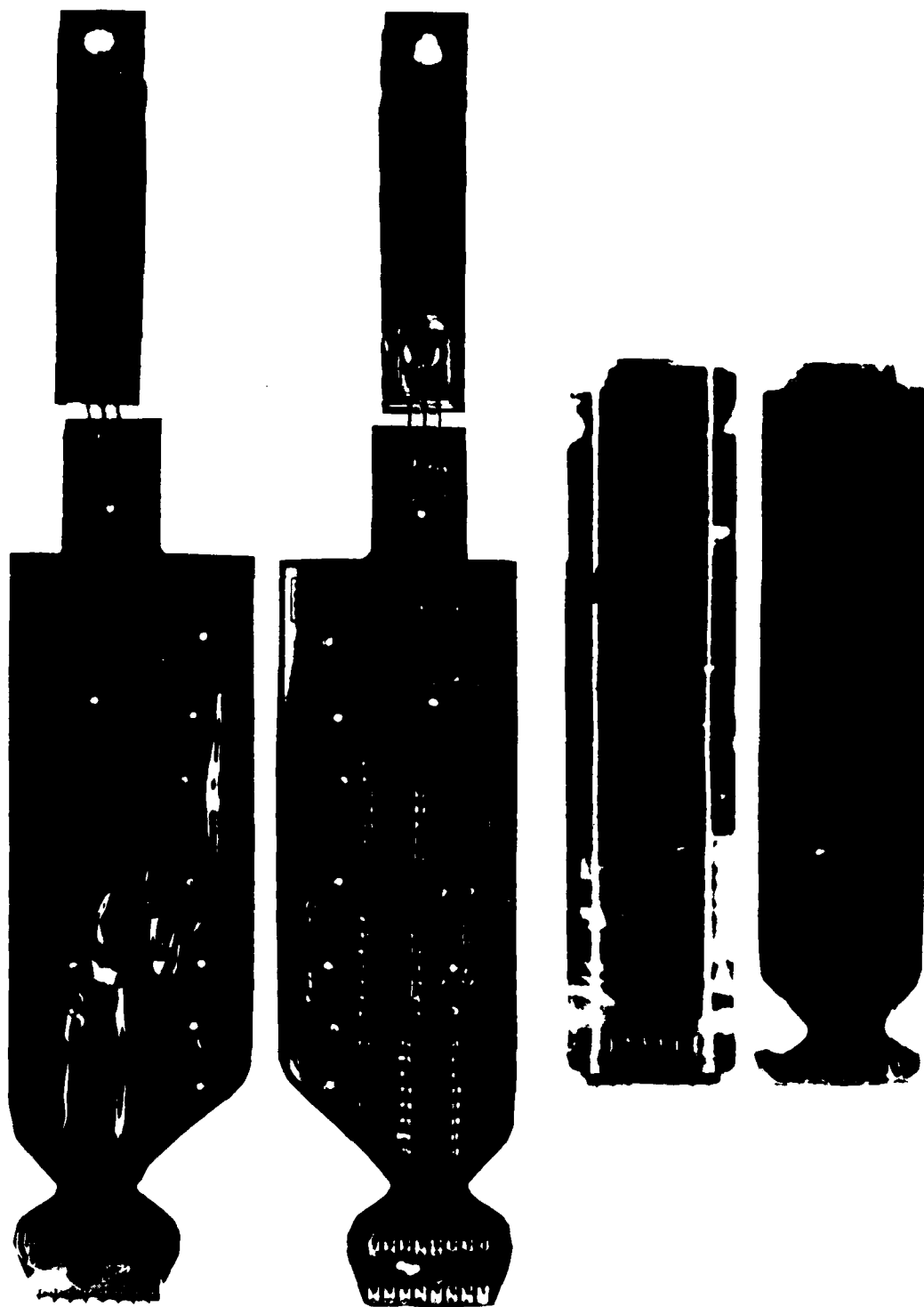
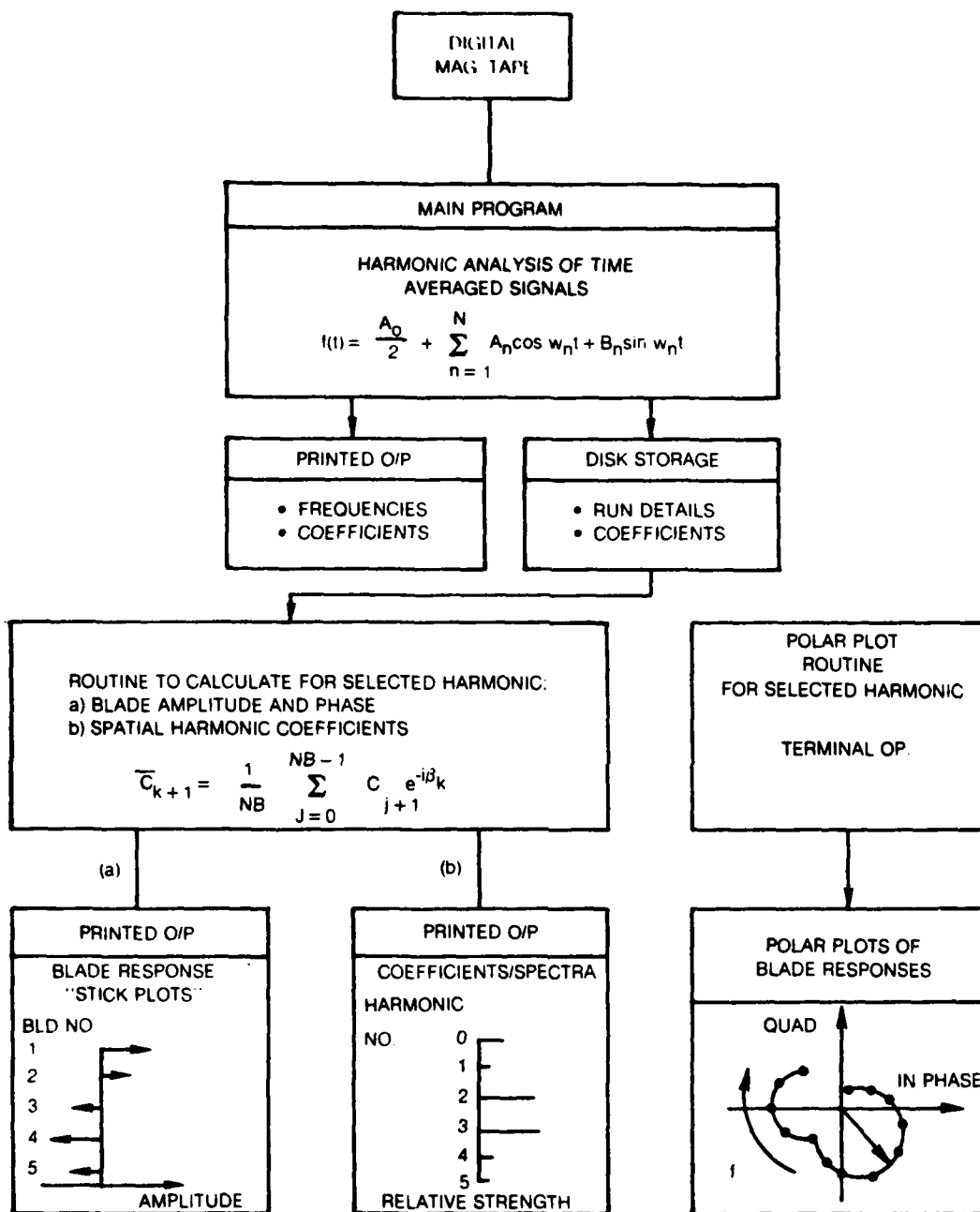


Figure 9 Strain Gage Amplifier





## VII. RIG ASSEMBLY AND SHAKEDOWN TESTS IN RIG A

The instrumented bladed disk assembly (see Fig. 11) was mounted on the vertical 2 1/2" diameter shaft of the spin rig using an aluminum flanged hub shaft adapter. The excitation system module was mounted using an adapter which was also bolted through the disk onto the flanged hub. Electrical connections were made via connectors at the top of the shaft. A wiring harness was then passed down a 1" diameter hole bored through the center of the shaft. Connections were made to the slip ring units (50 rings).

The strain-gage output lines were connected to the on line monitoring system with output observed on a dual channel oscilloscope and a digital voltmeter. The excitation system power supplies and control console were connected. After initial system checks which showed satisfactory operation of the excitation system and strain acquisition system, blade tip amplitudes of 0.1 in were obtained at an input power supply of only 40%. Final check out of the system at 0 rpm indicated a noise level of less than 2 mv and resonant response levels exceeding 250 mV. The rotating assembly was balanced in place using velocity pickups mounted on the bearings. The rig was run up to 1200 rpm and rough running regions were noted. Analysis of these data indicated that possible regions for low rig vibration runs were: <360, 550-750, 830-880, and 1050-1200 rpm. Strainage system noise levels were 1.5 mV at 0 rpm, and 15 mV at 1200 rpm. This was high frequency noise which was easily removed using low pass filter of 1000 Hz. It was confirmed that the excitation system was capable of imposing all the required forcing functions and that measurable blade responses would be obtained.

Vibratory characteristics of the fan at different speeds were recorded using (a) the frequency response method in which any individual blade or the assembly is excited at gradually incremented frequencies over a chosen resonant response, and (b) the transient response method in which the stimulus causing a resonant response is suddenly removed and the resulting decay analyzed. The stimuli used included (a) crystal excitation imposing stationary and traveling wave (forward and backward) forcing functions on the spinning component in evacuated conditions.

The nature of the response was determined from strain-gages on all of the blades and an optical instrumentation system was used to measure shroud motion at ten consecutive shroud interfaces as will be described in a later section of this report.



Figure 11 The Instrumented R-80 Fan

#### VIII. PRELIMINARY TESTS TO DETERMINE THE R-80 RESPONSE FEATURES

The purpose of this phase of testing was to determine (a) how well the assembly responds to excitation, (b) the nature and level of mistuning actually present in the assembled system, and (c) to develop test techniques using the excitation and instrumentation systems discussed in the previous section. As it turned out, this phase was quite essential and useful in setting the direction of the entire program.

These preliminary investigations at zero speed consisted of attempting to excite system modes of the fan assembly by (a) individual blade excitation, (b) standing wave and (c) traveling waves. A patch board and rotary switch arrangement was developed so that the phase of the response could be quickly scanned to ascertain if a mode had been excited. Difficulty was experienced initially in locating any of the system modes. In order to assist in locating system resonances, a limited modal analysis test was performed on the assembly in air using an instrumented hammer. Each blade was impacted at its tip and a miniature accelerometer was used to measure the response at a location mid way between the tip and the shroud of one blade. Both direct and cross frequency response functions were obtained for each blade. The test results indicated a multiplicity of modes contained within two narrow frequency bands centered on 65 Hz and 290 Hz (See Fig. 12). The first family modes, characterized by blade motion involving only above-shroud bending, were found to be contained in a band between 60-69 Hz. By careful examination of the frequency response plots, certain frequencies were identified at which, response peaks were noted on a number of blades. These frequencies were 61.3, 62.2, 63.4, 64.7, 65.5, 66.1, and 67.4 Hz. Various excitation patterns were subsequently used to induce modal responses at or near these frequencies. Although resonant conditions were obtained, the nodal patterns around the rotor were generally of a complex nature containing a mixture of several harmonics. Blades displaying peak response in the vicinity of 60.4 and 68.2 Hz tended to respond as though uncoupled.

The response with many peaks in the 60-69 Hz bandwidth were further examined by performing "blade alone" tests. In these tests, all blades but the one being tested were effectively decoupled by means of wedges of plastic placed between them. The test blade was then excited using its crystal and its resonant frequency in the first bending (1B) mode was determined. The resulting frequencies for all the blades compared with the frequency of the highest peak on the direct frequency response plot for each blade is shown in Table 1.

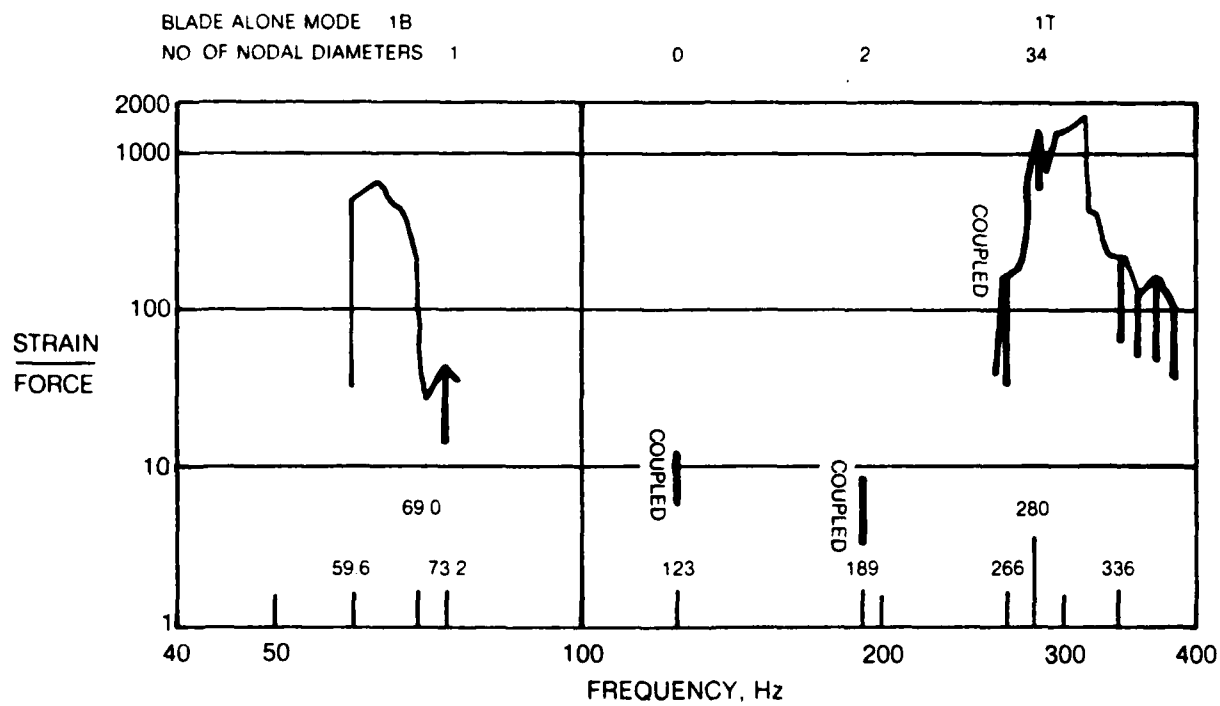


Figure 12 Preliminary Tests of R-80 Fan: Multiplicity of Modes

TABLE 1

BLADE ALONE FIRST BENDING MODE  
FREQUENCIES FOR COUPLED & UNCOUPLED CONDITIONS

BLADE #	RESPONSE FREQUENCY, Hz		BLADE #	RESPONSE FREQUENCY, Hz	
	Coupled	U/C Blade Alone		Coupled	U/C Blade Alone
1	67.73	67.88	21	65.81	65.24
2	60.72	61.33	22	60.72	62.26
3	62.67	63.15	23	62.67	62.52
4	64.87	64.28	24	65.81	65.53
5	66.57	66.34	25	63.76	65.04
6	62.85	63.68	26	66.77	66.68
7	65.62	65.82	27	66.77	66.81
8	61.95	62.27	28	59.68	60.00
9	65.62	64.96	29	67.73	67.05
10	64.50	64.88	30	64.69	65.42
11	66.77	66.37	31	66.96	66.69
12	62.67	13.60	32	66.77	67.10
13	66.77	66.03	33	64.69	65.28
14	64.69	64.73	34	63.95	65.05
15	66.96	66.07	35	63.95	64.02
16	63.76	64.59	36	62.67	62.87
17	65.62	64.91	37	65.81	65.12
18	67.73	67.44	38	66.96	67.59
19	65.62	65.41	39	65.62	68.88
20	62.67	63.20	40	62.67	62.90

Average      64.90

The second family of modes, characterized by blade motions in bending and torsion could be excited in one, two, three and four nodal diameter patterns and were found to display dual modal characteristics with frequencies as shown in Table 2.

These preliminary tests indicated that the wide spread (13%) in the individual blade first bending frequencies could be the main contributing factor to the inability to obtain regular and well ordered modes on the rotor. The subsequent phase of activity focused on developing methods to tune the individual blades. The only practical method of tuning these blades was by the modification of the tip mass using holes drilled spanwise into the blade tips. Mass could be increased by inserting lead plugs into the holes. (See Fig. 13). Successive levels of tuning were attempted as described below to bring the assembly as close to a tuned system as is practical for a shrouded fan.

After some preliminary investigation into suitable methods of tuning, the blades were tuned individually to a frequency of 60 Hz, which was the lowest individual blade frequency measured previously. The method involved damping out all blades but the one being tuned by inserting a large piece of plasticene between adjacent blades and exciting the free blade at 60 Hz. Plasticene was added to the tip of the blade until the maximum response was obtained. The average mass added to each blade was 15.71 gms. With tuning completed, frequency response functions, both direct and cross terms, were obtained for six sample blades. The bandwidth of the first family responses was found to have been reduced from 8 Hz to approximately 3 Hz (58.3 to 61.3 Hz). In this tuned condition, five first family modes with recognizable nodal diameter patterns were excited and for three of these, dual modes were also obtained. The results are shown in Table 3 and a typical circumferential mode shape plot for the two nodal diameter pattern is shown in Figure 14. There is some doubt about the validity of the 5 and 6ND modes since their frequencies are lower than that of the 4ND mode.

A preliminary investigation into the effectiveness of deliberate mistuning by adding tip masses to split specific modes was performed. The masses were added symmetrically at the antinodes of one of the dual modes. The results for the 2ND mode using twelve blade mistuning (average mass per blade added was 16.6 gms.) are also shown in Table 3. Eight blade mistuning (average mass 9.08 gms) was attempted on the 4ND mode but no dual mode could be found with this configuration.

The second family of modes was excited and frequencies noted for the tuned assembly. The results are given in Table 2 and compared with as-built condition results. No major change in characteristics occurred with tuning except that the 1ND mode split was reduced.

TABLE 2

## SECOND FAMILY MODAL FREQUENCIES AND DUAL MODE SEPARATION

No. of Nodal Diameters	As-Built Condition		Experimentally Tuned Condition	
	Frequency Hz	Split %	Frequency Hz	Split %
1	73.67 72.49	1.6	68.54 68.26	0.4
0	123.4 *		119.0 **	
2	189.9 189.2	0.4	186.0 185.0	0.5
3	266.7 265.1	0.6	260.8 259.6	0.5
4	280.4 279.4	0.4	~ 273	
5			280.9	

\* Nodal circle not located.

\*\* Nodal circle at 66% above-shroud-span

TABLE 3

FIRST FAMILY MODAL FREQUENCIES AND DUAL MODE SEPARATION  
FOR THE EXPERIMENTALLY TUNED AND INTENTIONALLY MISTUNED CONDITIONS

No. of Nodal Diameters	<u>Tuned Condition</u>		<u>Twelve Blade Mistuning</u>		<u>Eight Blade Mistuning</u>
	Frequency Hz	Split %	Frequency Hz	Split %	Frequency Hz
2	59.57 59.37	0.3	59.57 56.50	5.4	
3	60.71				
4	61.27 61.15	0.2			61.22
5	60.81 61.12	0.5			
6	60.57				



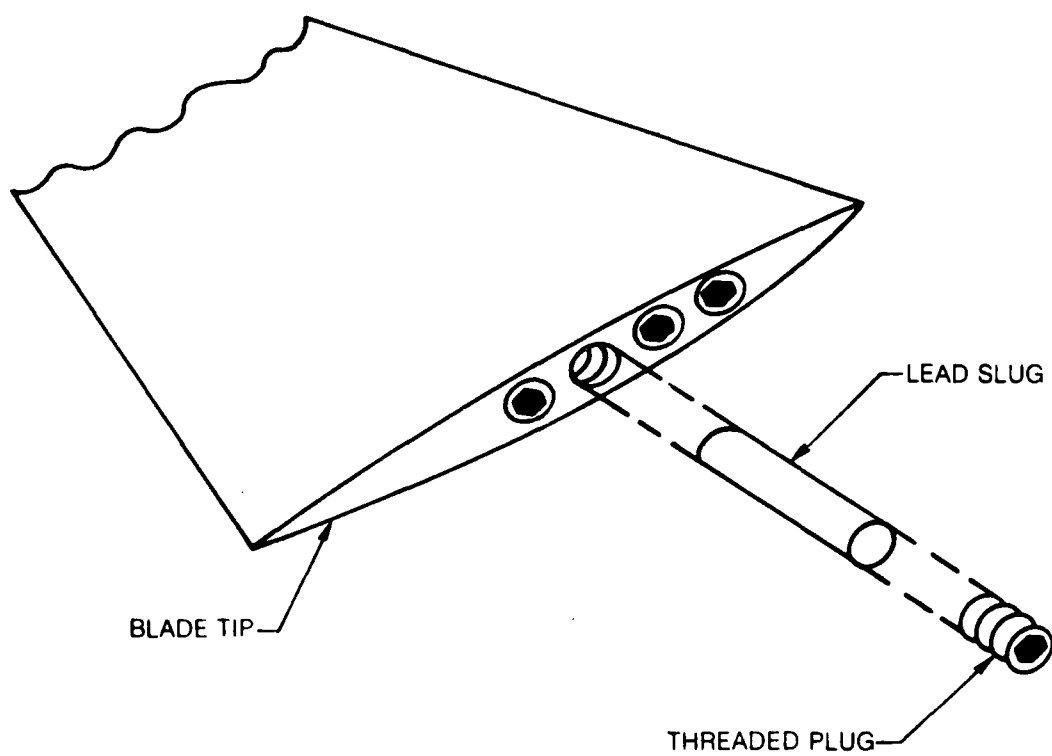


Figure 13 Method of Modifying Tip Mass

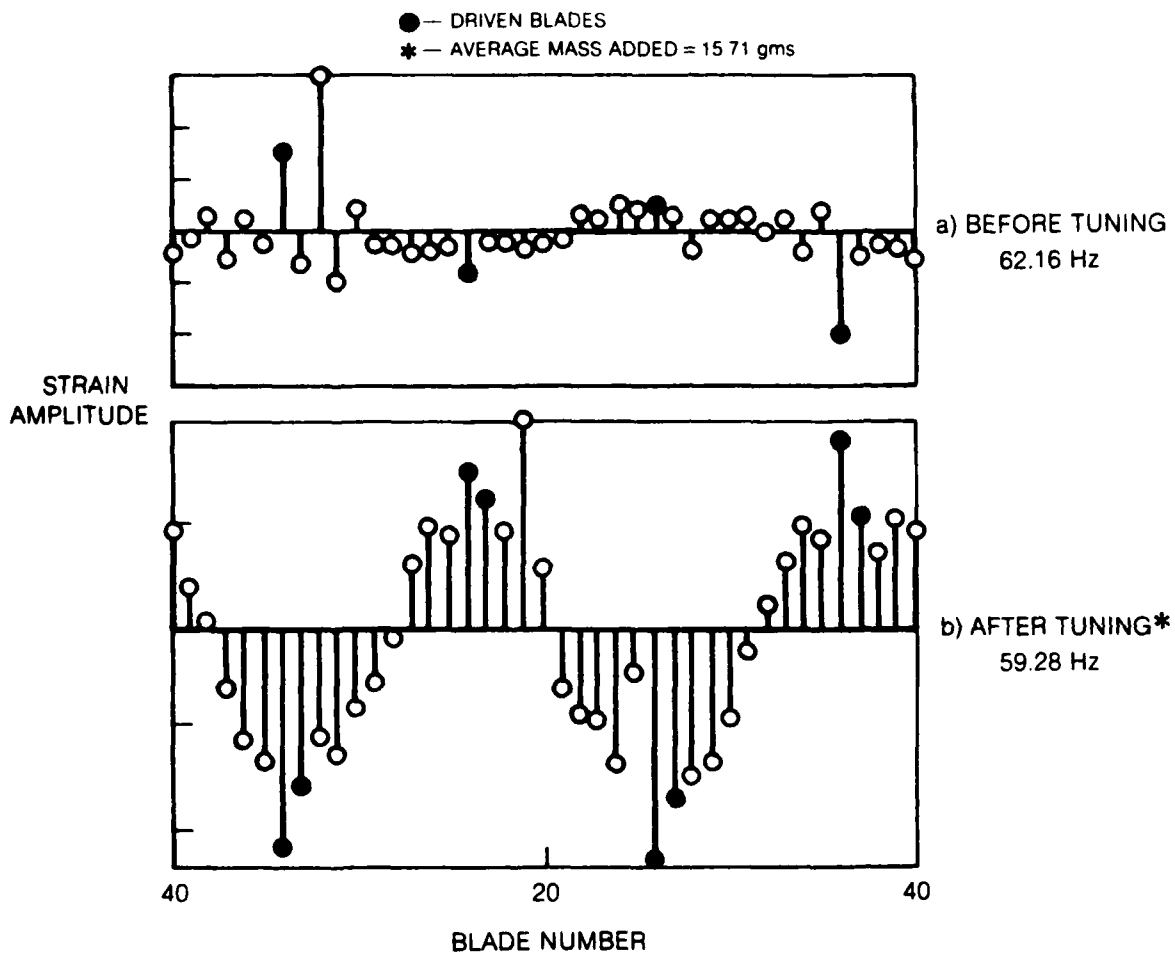


Figure 14 Stick Plots of Assembly First Family Resonant Response when Excited by a 2ND Stationary Wave

The results from this study indicated that tip mass tuning was effective and "regular" first family dual modes could be excited. On this basis, preparations were made to permanently tune the assembly. A test was performed to measure the rate of change of blade resonant frequency with added tip mass. This quantity was found to be 0.26 Hz/gm in the frequency range of interest. Based on this and on the number and size of the holes which could be drilled in the blades, a target frequency of 63 Hz was chosen. A drilling rig was specially designed and fabricated to facilitate the drilling operation. The two blades with frequencies of less than 62 Hz were modified by having up to eight holes drilled resulting in frequencies of 62.6 Hz (from 60.0 Hz) and 63.45 Hz (from 61.50 Hz). The blade having the highest frequency (67.88 Hz) had 6 holes drilled and filled with lead resulting in a blade frequency of 63.78 Hz. It was thus shown that the chosen method was effective and feasible for use in tuning the whole assembly.

A second level of tuning process was attempted and it was determined that the blade frequencies could be reduced to between 62.5 Hz and 66 Hz without having to add excessive amounts of tip mass affecting blade structure or assembly balance. Furthermore, 50 percent of the blades would have frequencies in the 63 to 64 Hz range. This 2nd level blade tuning was performed requiring the drilling of 94 holes, 1.2 inches long and .161 inch in diameter in the tips of the blades, and the insertion of 77 lead pellets and set screws. The resulting individual blade frequency distribution was as follows:

62 - 63 Hz	3 blades
63 - 64 Hz	20 blades
64 - 65 Hz	12 blades
65 - 66 Hz	5 blades

These frequencies were obtained by loading down the blades, except the test blade, with lead weights near the tips and below the shroud. The individual blade was then excited using its crystal and the peak amplitude frequency was recorded.

Using a 4ND standing wave forcing function, a 4ND mode and a possible twin were located after much difficulty at 65.17 Hz and 65.76 Hz. The mode shapes are given in Figure 15. Modes with 5 and 6 nodal diameters could also be excited using the appropriate forcing function. However, the waveforms of the mode shapes found were not very uniform and an investigation was performed into the possibility of shaping the modes by adding small amounts of mass to the tips of selected blades. It was found that the amplitude and phase of individual blades could be altered to some extent in this manner without altering the basic mode shape or frequency.

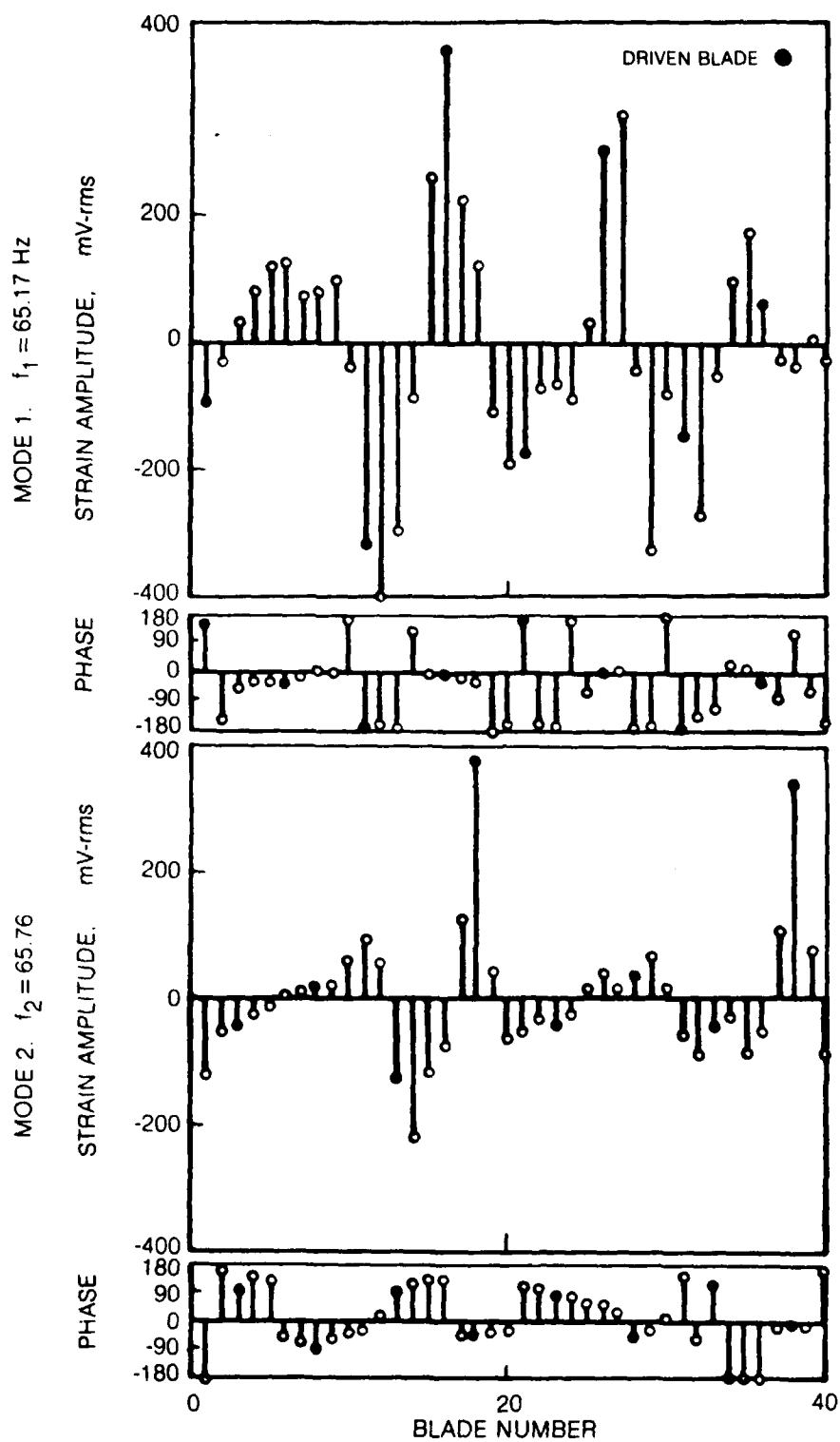


Figure 15 4ND Twin Modes Obtained After Partial Tuning

Because of the difficulty of obtaining clearly defined vibration modes, the resonant behavior of the assembly was investigated over the entire frequency range of the first family. A single blade was excited at a constant level and the amplitude and phase of that blade was measured at intervals of approximately 0.04 Hz. This technique was applied to blades #16 and #39 and the results were plotted in polar form as shown in Figs. 16 and 17. The following conclusions were drawn:

1. No resonances in this family were detected outside the range 61.5 Hz to 66 Hz.
2. Within that range, there are many resonances which are so close in frequency that the responses overlap and it is difficult to discriminate one from another, even with the help of the polar plot.
3. About 14 to 18 resonances can be deduced (with some difficulty because of the overlap) from each test sequence.
4. The 4ND patterns noted above correspond to resonances in the high frequency end of the range.

Thus, it would appear that the 4ND modes which can be excited using standing or travelling waves may not represent pure modes of the system.

In a further attempt to improve the first family mode shapes, a third level of tuning the fan assembly was performed. The objectives were to reduce the largest individual blade frequencies to less than 65 Hz and to increase the lowest frequencies to greater than 62.5 Hz. Eleven more holes had to be drilled into the tips of the blades and lead pellets inserted. Tests were performed to measure the individual blade frequencies in the first bending (1B) and first torsion (1T) modes in air. These frequencies were obtained by loading down the blades, except the test blade, with lead weights near the tips and below the shroud. The individual blade was then excited using its crystal and the peak amplitude frequency was recorded. The loss factor in each mode, for each blade, was also measured by obtaining decay response curves resulting from sudden cut-off of the excitation stimulus. Table 4 lists the measured frequencies and loss factors for each blade. The resulting individual blade frequency distributions shown as histograms in Figs. 18 and 19 are as follows:

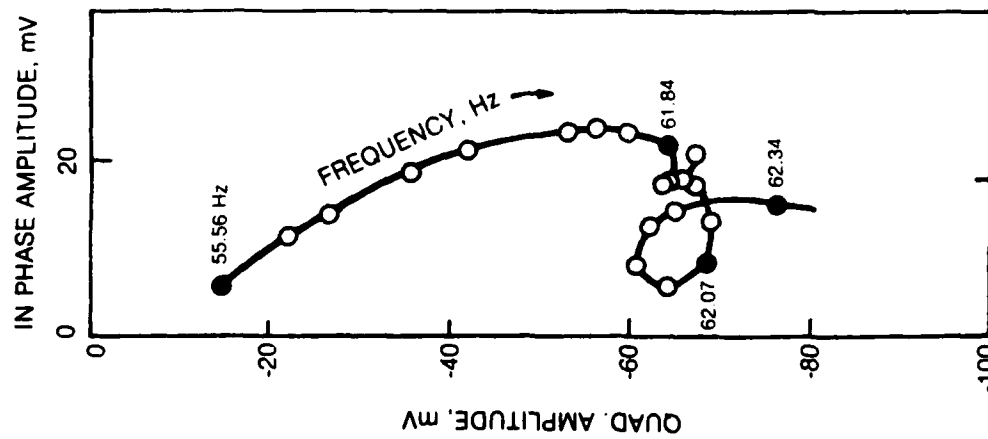


Figure 16A. Polar Plot of Forced Response for Blade #16

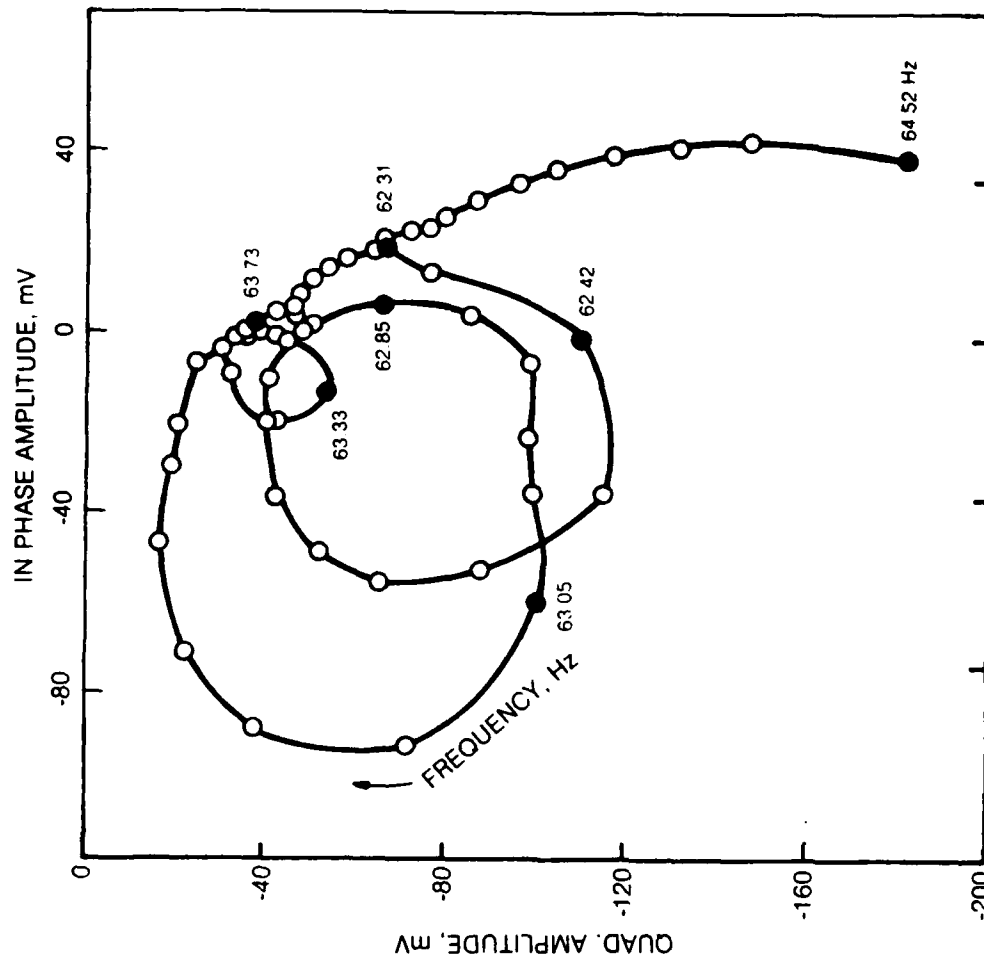


Figure 16B Polar Plot of Forced Response for Blade #16

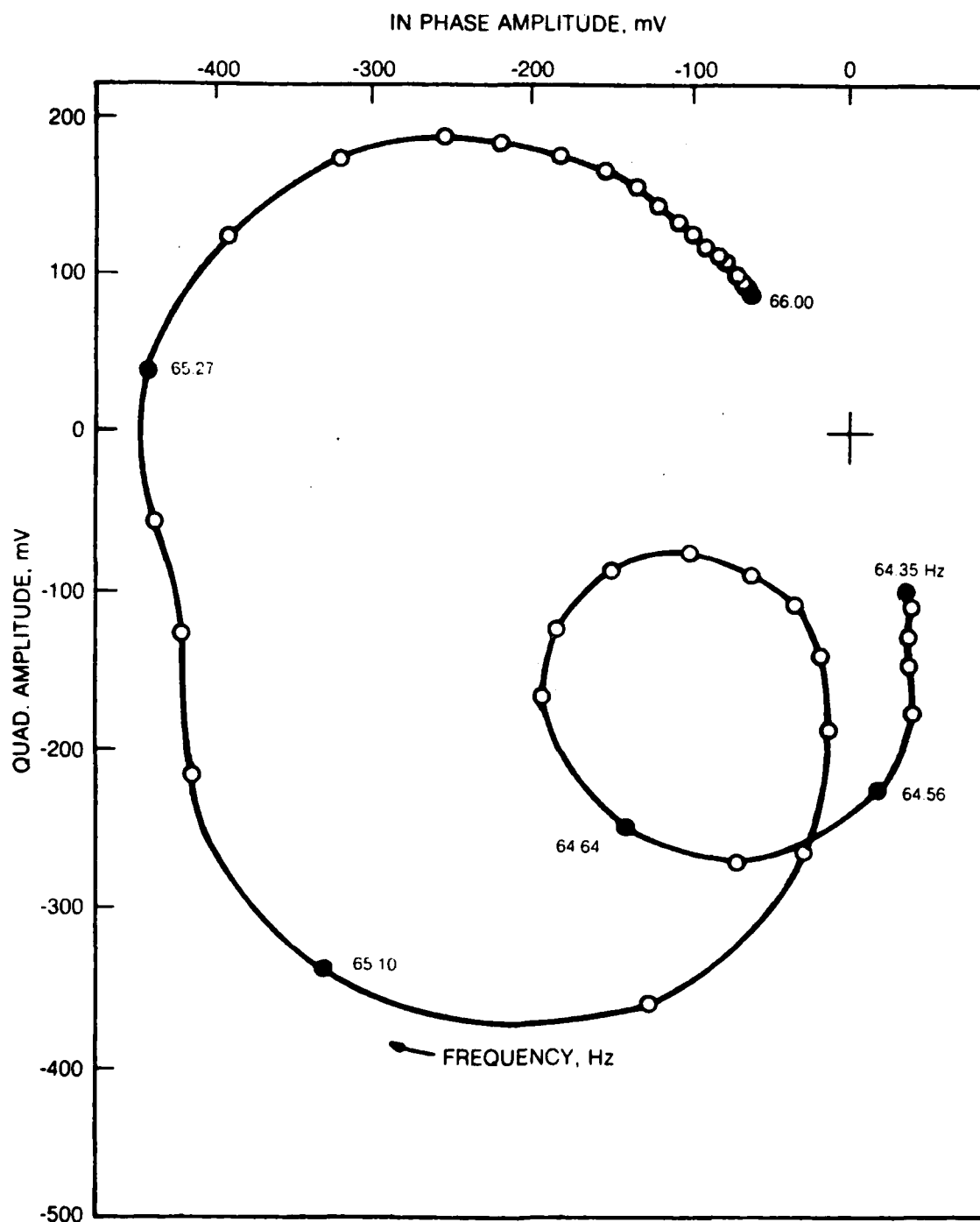


FIGURE 16c. Polar Plot of Forced Response for Blade #16.

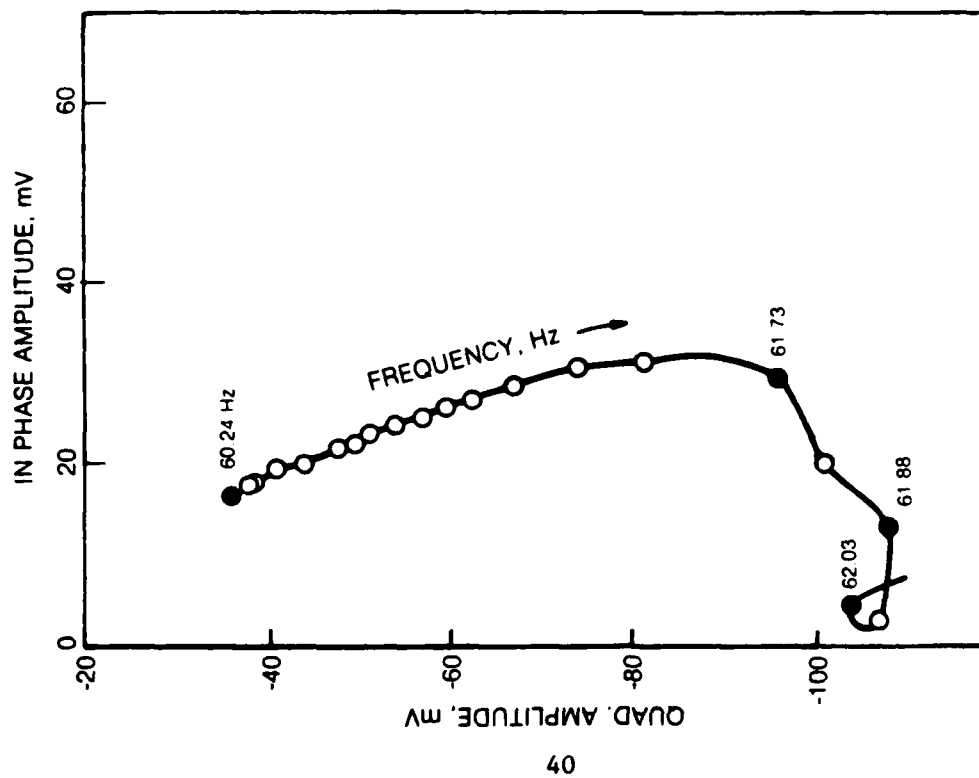


Figure 17A Polar Plot of Forced Response for Blade #39

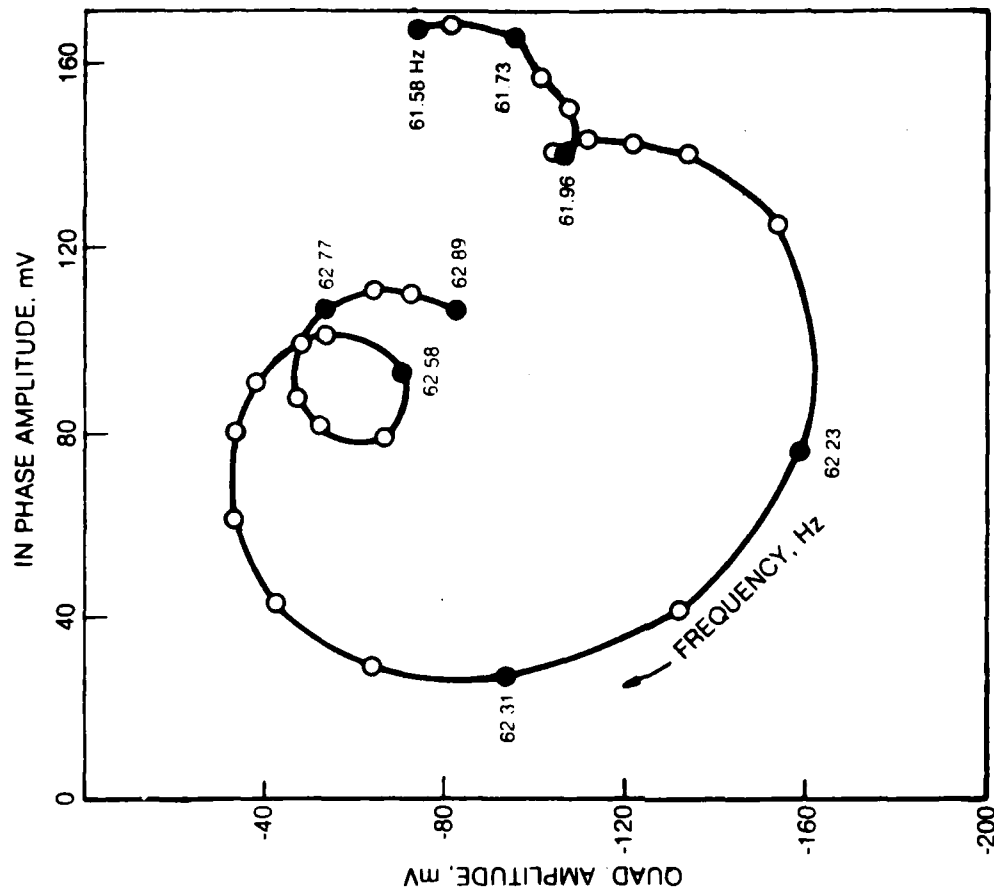


Figure 17B Polar Plot of Forced Response for Blade #39



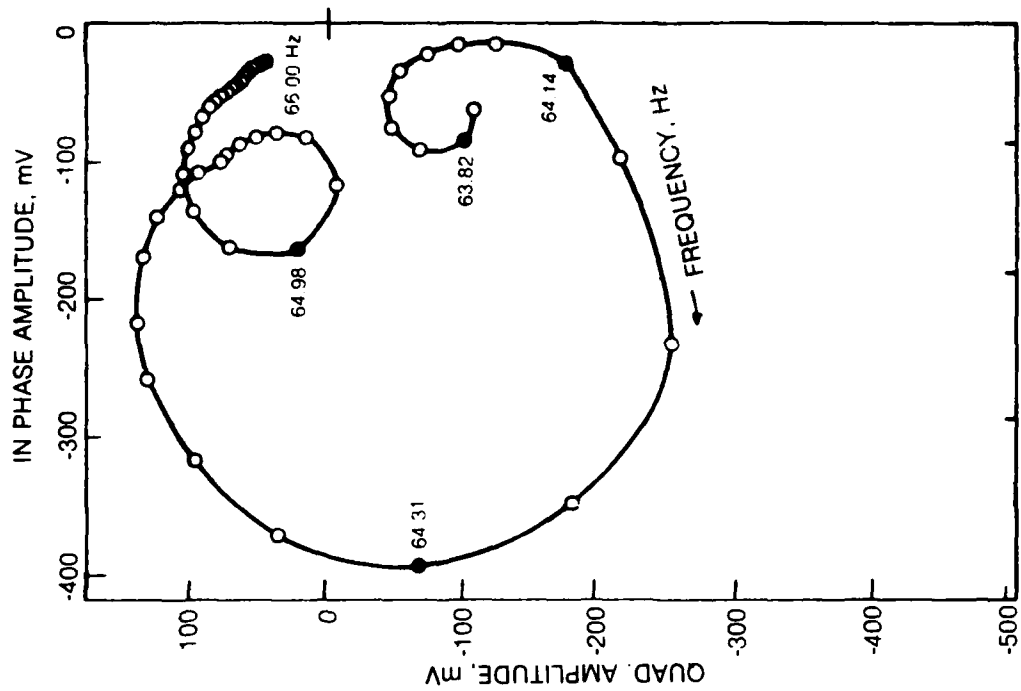


Figure 17C Polar Plot of  
Forced Response for Blade #39

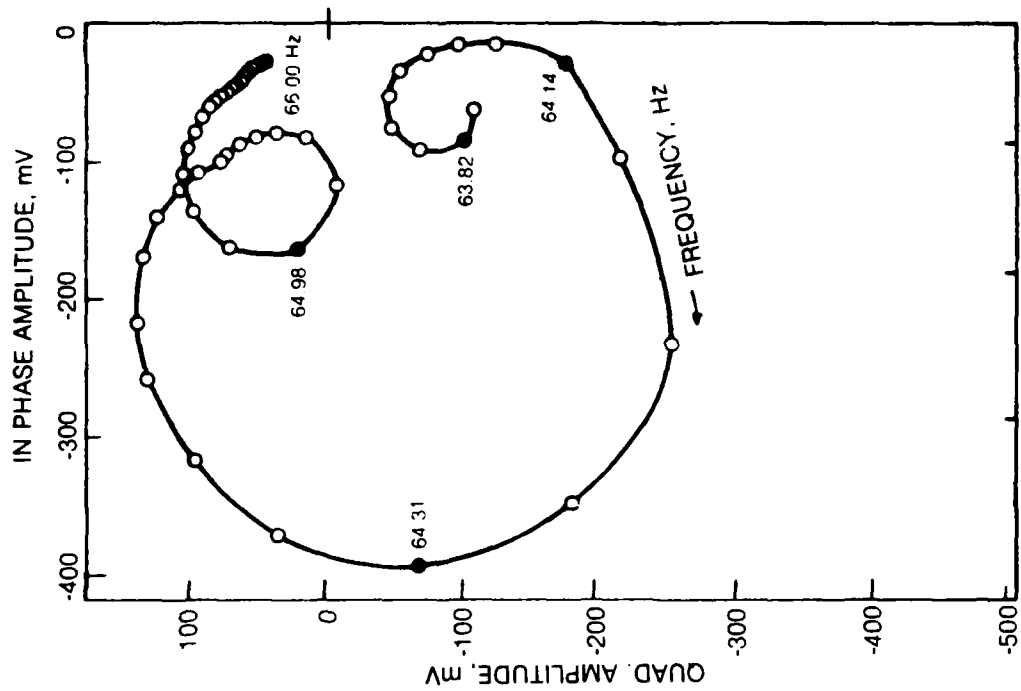


Figure 17D Polar Plot of  
Forced Response for Blade #39

TABLE 4  
 RESONANT FREQUENCIES AND LOSS FACTORS FOR INDIVIDUAL BLADES IN "INITIALLY  
 TUNED" CONDITION (UNCOUPLED CONFIGURATION)

BLADE NUMBER	1B MODE		1T MODE	
	FREQUENCY, Hz	LOSS FACTOR	FREQUENCY, Hz	LOSS FACTOR
1	64.70	0.0087	316.3	0.0170
2	63.44	0.0076	319.2	0.0164
3	63.15	0.0079	311.2	0.0261
4	62.60	0.0103	314.5	0.0212
5	63.14	0.0084	310.7	0.0147
6	63.79	0.0083	309.4	0.0131
7	63.91	0.0078	311.8	0.0168
8	62.81	0.0073	304.4	0.0166
9	63.02	0.0065	309.4	0.0135
10	63.57	0.0077	315.6	0.0310
11	64.36	0.0076	309.8	0.0103
12	63.69	0.0073	308.5	0.0237
13	64.00	0.0062	322.8	0.0284
14	64.11	0.0082	305.5	0.0171
15	63.97	0.0075	314.1	0.0133
16	64.19	0.0068	311.1	0.0200
17	63.64	0.0060	315.7	0.0273
18	63.98	0.0058	306.1	0.0252
19	63.22	0.0059	307.4	0.0122
20	63.21	0.0072	No Data	No Data
21	63.15	0.0071	305.9	0.0266
22	62.91	0.0100	302.5	0.0193
23	62.87	0.0060	302.8	0.0142
24	63.24	0.0065	314.5	0.0290
25	63.14	0.0056	308.4	0.0100
26	64.77	0.0061	317.9	0.0118
27	64.75	0.0055	313.8	0.0161
28	62.81	0.0069	296.9	0.0224
29	64.83	0.0069	316.3	0.0244
30	63.38	0.0067	312.8	0.0195
31	64.80	0.0070	314.6	0.0233
32	64.30	0.0066	316.5	0.0309
33	63.35	0.0066	309.9	0.0215
34	63.12	0.0065	312.0	0.0127
35	64.30	0.0073	306.0	0.0141
36	63.00	0.0074	305.0	0.0150
37	63.69	0.0081	306.6	0.0260
38	64.30	0.0077	311.2	0.0098
39	63.87	0.0086	316.3	0.0257
40	63.09	0.0073	307.6	0.0150

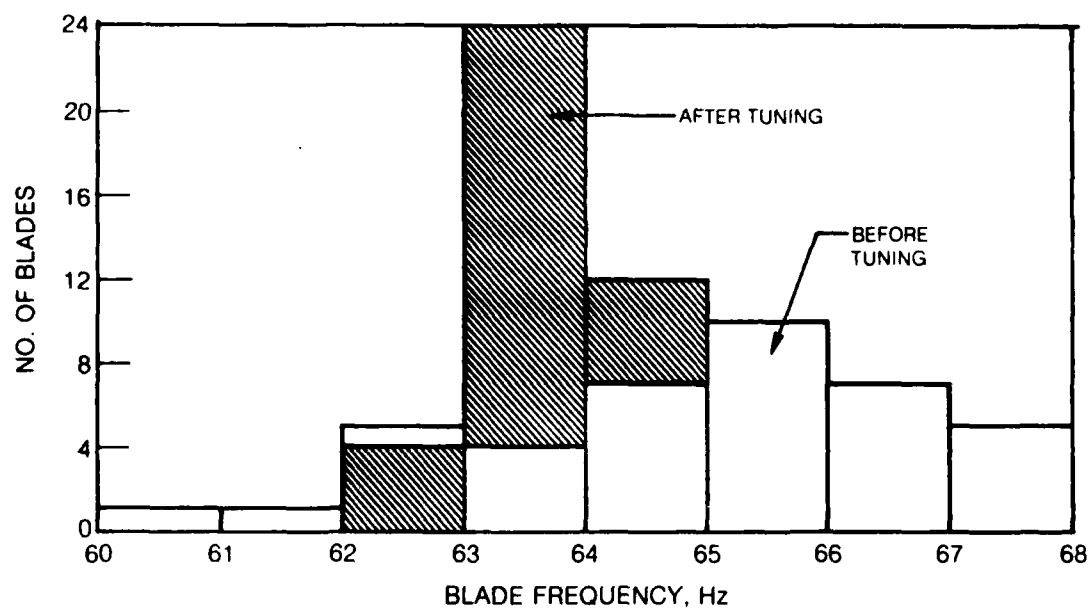


Figure 18 Histogram of Blade First Bending Mode Frequencies

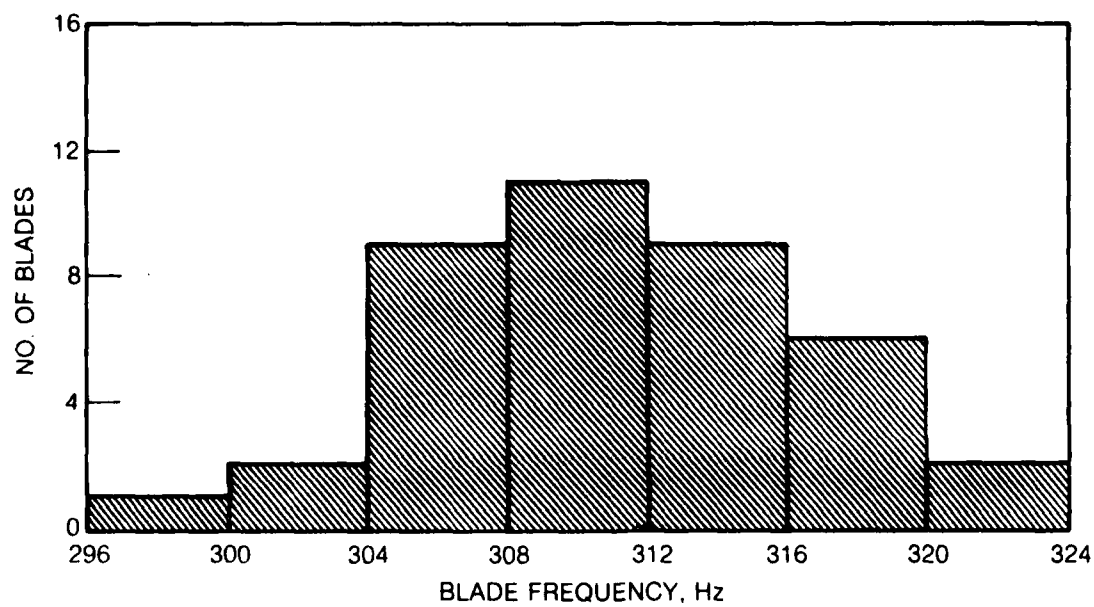


Figure 19 Histogram of Blade First Torsion Mode Frequencies After Tuning

<u>First Bending Mode (Hz)</u>			<u>First Torsion Mode (Hz)</u>			
62.6	-	63	4 blades	296.9	- 300	1 blade
63	-	64	24 blades	300	- 304	2 blades
64	-	64.8	12 blades	304	- 308	9 blades
				308	- 316	20 blades
				316	- 322.8	7 blades

The measured loss factors ranged from .005 to .010 for the 1B mode and from 0.01 to .03 for the 1T mode.

The second family of modes was investigated with the assembly in air at zero speed. 2ND and 3ND mode pairs were excited using a single blade excitation and the nodal lines mapped out using a roving accelerometer. Typical results are shown in Figs. 20 and 21. The 4ND mode proved to be difficult to locate using single blade excitation because of the close proximity of higher modes. However, two 4ND modes were excited using a traveling wave input.

A mistuning study was conducted in an attempt to split the 2ND twin modes using the available holes drilled in the blade tips. It was determined that by adding 25 g to blade #28 and 5.5 g to blade #8, the originally coincident twin modes could be split by 1.1 Hz (188.7 and 187.5 Hz). Further separation is possible (of the same order) by removing lead pellets from four antinodal blades.

Although the objectives of narrowing the frequency range were met, the characterization of the first family modes proved to be difficult, as before, indicating that the small degree of mistuning still present along with any nonuniformities at the shroud interfaces were sufficient to cause overlapping of the desired mode. Further tuning was deemed impractical and the current configuration of the assembly was accepted as the assembly representing the "initial tuned fan" that will serve to measure the dynamic characteristics in vacuum as well as under aerodynamically excited conditions.

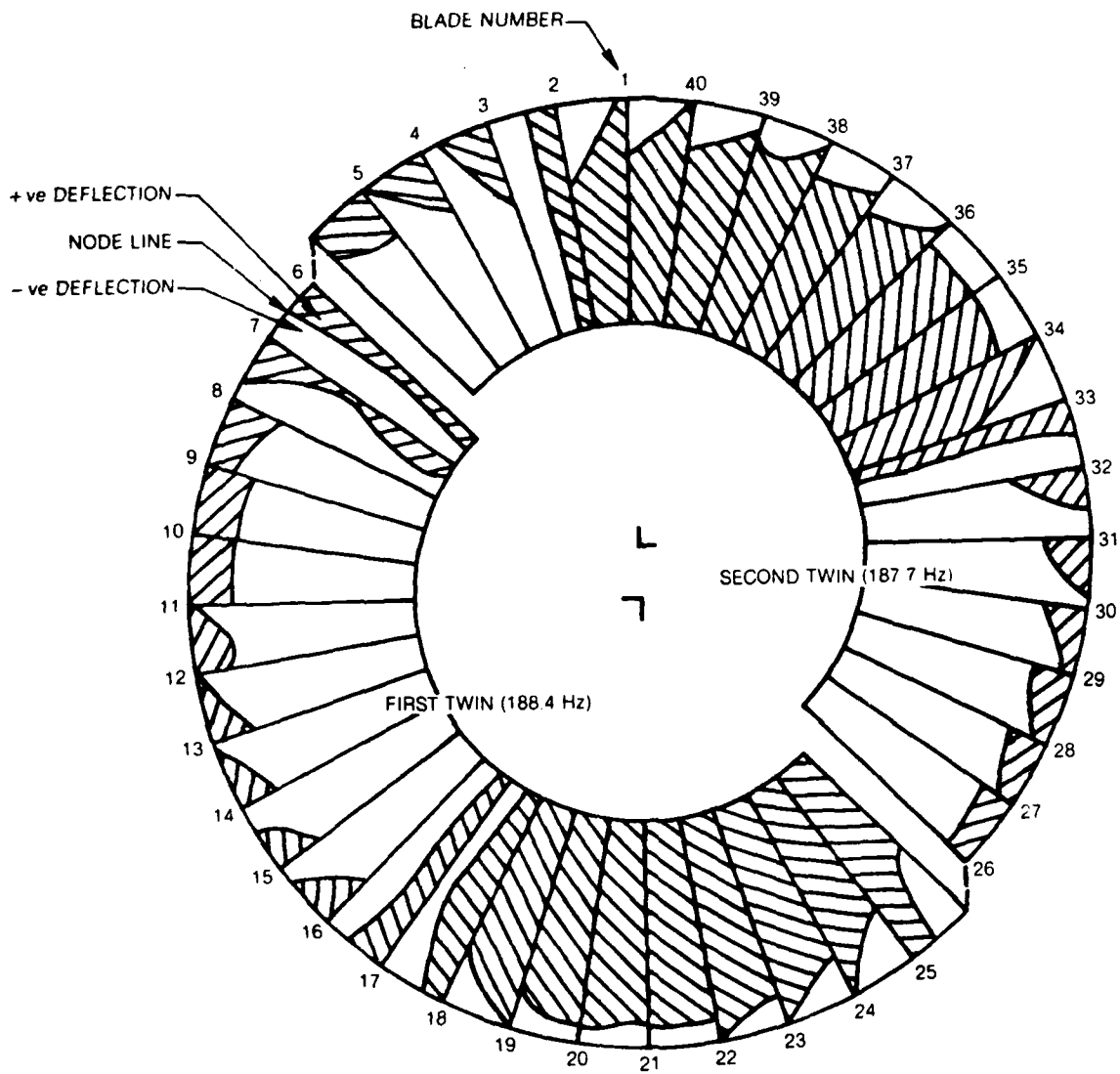


Figure 20 Schematic of Second Family 2ND Twin Modes

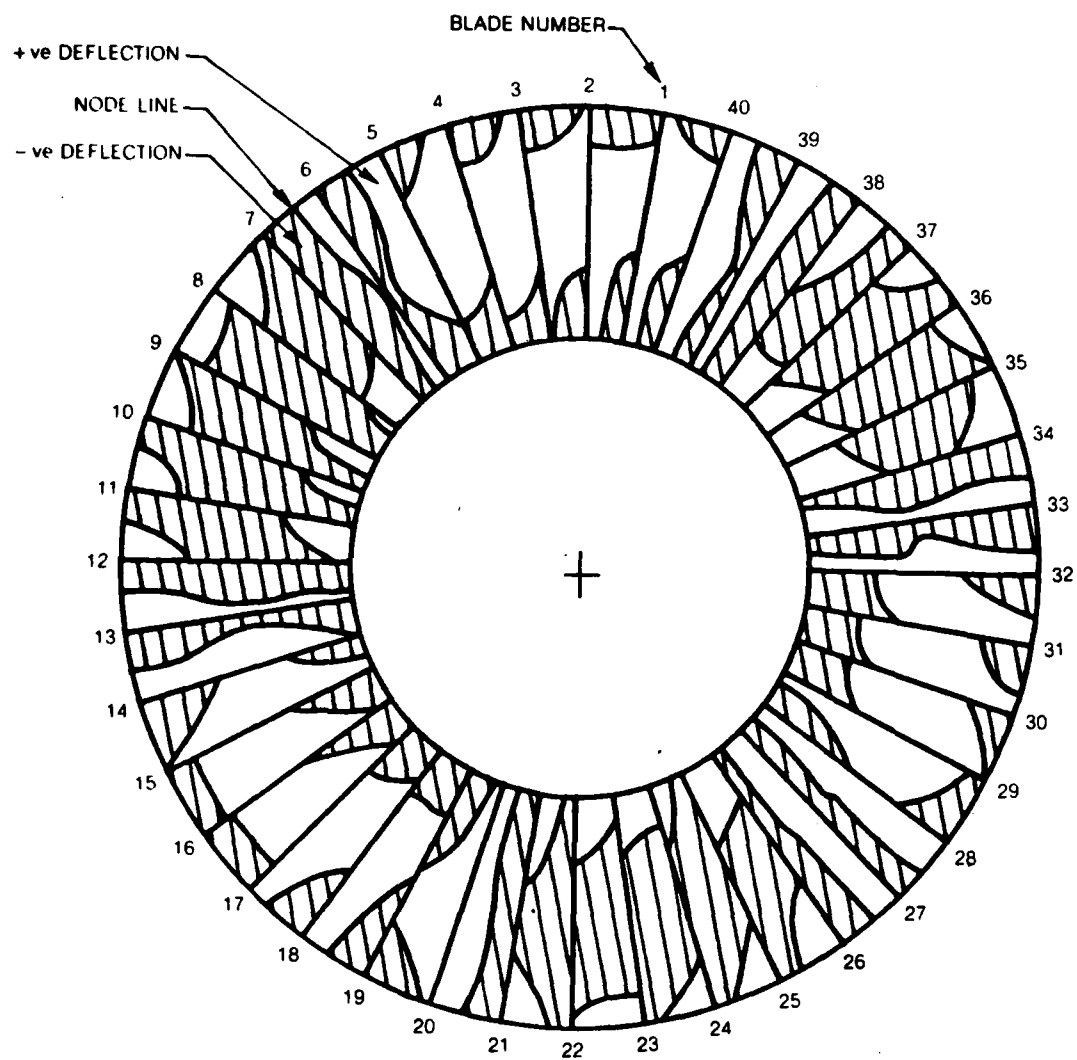


Figure 21 Schematic of Second Family 3ND Mode Shape at 263.4 Hz

## IX. MECHANICAL CHARACTERIZATION OF THE R-80 FAN ASSEMBLY

### 1. Initially Tuned Condition

With the assembly in the "tuned" configuration, a series of tests were performed to measure its dynamic characteristics in the first two families of modes. Table 5 lists in detail the tests performed with the associated run numbers and test conditions. The principal goals were to identify the extent and influence of asymmetry that characterized the assembly in its "tuned" condition; in particular (a) the generally irregular responses in the first family (b) its split modes in the second family, and (c) modal damping. Over 70 test runs were conducted in which the system response of each blade was recorded as the input frequency varied in discrete increments over the resonance being investigated. All data from these tests were digitized and recorded on magnetic tape.

### 2. Discussion of Results

At zero speed, the assembly was subjected to forward and backward traveling wave excitations in a four nodal diameter pattern (Run #76). The excitation frequencies were varied in steps of approximately 0.1 Hz in the range of 66.5 Hz to 62 Hz to observe the assembly response in the first family modes. The maximum strain measured at each frequency is plotted in Figs. 22 and 23, along with the blade number at which the maximum was observed. The general response characteristics are not different for the two waves, although blade 16 appears to be most responsive to the forward wave excitation. Blade 27 is responsive, experiencing essentially the same strain for excitations from each wave. The generally similar characteristics in response tend to confirm the usual assumption that the direction of the forcing wave has little or no influence on a mechanically coupled system (unlike an aerodynamically coupled system). It is likely that a shroudless fan assembly would exhibit a more exact similarity in responses to forward and backward traveling forcing functions.

Response of blade #27 is plotted in polar form (amplitude and phase) over the frequency range of 62.1 Hz to 66.6 Hz and is shown in Figure 24. The many loops that are evident in the polar plots are indicative of the participation of blade #27 in many modes of the system present in this range. Polar plots of other blades show similar multi-loop characteristics.

The number of peaks occurring in the response diagrams (Figs. 22 and 23) is also indicative of the proximity of diametral modes of the assembly in this frequency range. In the small range of 2 Hz, i.e. between 64 and 66 Hz, blade #'s 6, 39, 27, 20 and 16, reach peak strains at different frequencies-



TABLE 5. SUMMARY OF TESTS PERFORMED ON FAN ASSEMBLY (INITIAL TUNED CONDITION) IN RIG A

FORCING		TESTS PERFORMED															
CONFIGURATION	NODAL DIAM.	TEST CONDITIONS: - SPEED (RPM) PRESSURE (TORR)															
		0/760		0/22		570/22		1050/22		1163*/22		1200/22					
** BLADE ALONE (All others detuned)	-	1	2														
		x	x														
SINGLE BLADE EXCITATION	-	3	4	3	4	3	4	3	4	3	4	3	4	3	4		
		64	47	75	51	72	54	69	58	68					61		
		63	48	74	52	71	53	70	59	67(68					60		
FIRST FAMILY OF MODES	4	5		5	6							5	6				
		65		76	76							66*** 73	77				
SECOND FAMILY OF MODES	2	5	6	7	8	5	6	7	8	5	6	7	8	5	6	7	8
		46		44	45	11		9	10	12	13	15	18	16	17	21	19
	3	26		24	25	27		29	30	31	31	40	39	38	34		
	4	49				50				55	56		57			62	

KEY TO TEST:

- 1 = INDIVIDUAL BLADE EXCITATION. 1st BENDING MODE FREQUENCY AND DAMPING DECAY (40 BLADES)
- 2 = INDIVIDUAL BLADE EXCITATION. 1st TORSION MODE FREQUENCY AND DAMPING DECAY (40 BLADES)
- 3 = SINGLE BLADE FREQUENCY RESPONSE, 1st BENDING MODE (2 BLADES #29 AND #28)
- 4 = SINGLE BLADE FREQUENCY RESPONSE, 1st TORSION MODE (2 BLADES #13 AND #28)
- 5 = FORWARD TRAVELING WAVE - FREQUENCY RESPONSE
- 6 = BACKWARD TRAVELING WAVE - FREQUENCY RESPONSE
- 7, 8 = STATIONARY WAVE EXCITATION OF TWIN MODES - FREQUENCY RESPONSE.

NOTES: \* INTEGRAL ORDER SPEED FOR FIRST FAMILY 4ND MODE.

\*\* NOT RECORDED ON TAPE

\*\*\* RESULTS OBTAINED FOR TWO LEVELS OF INPUT

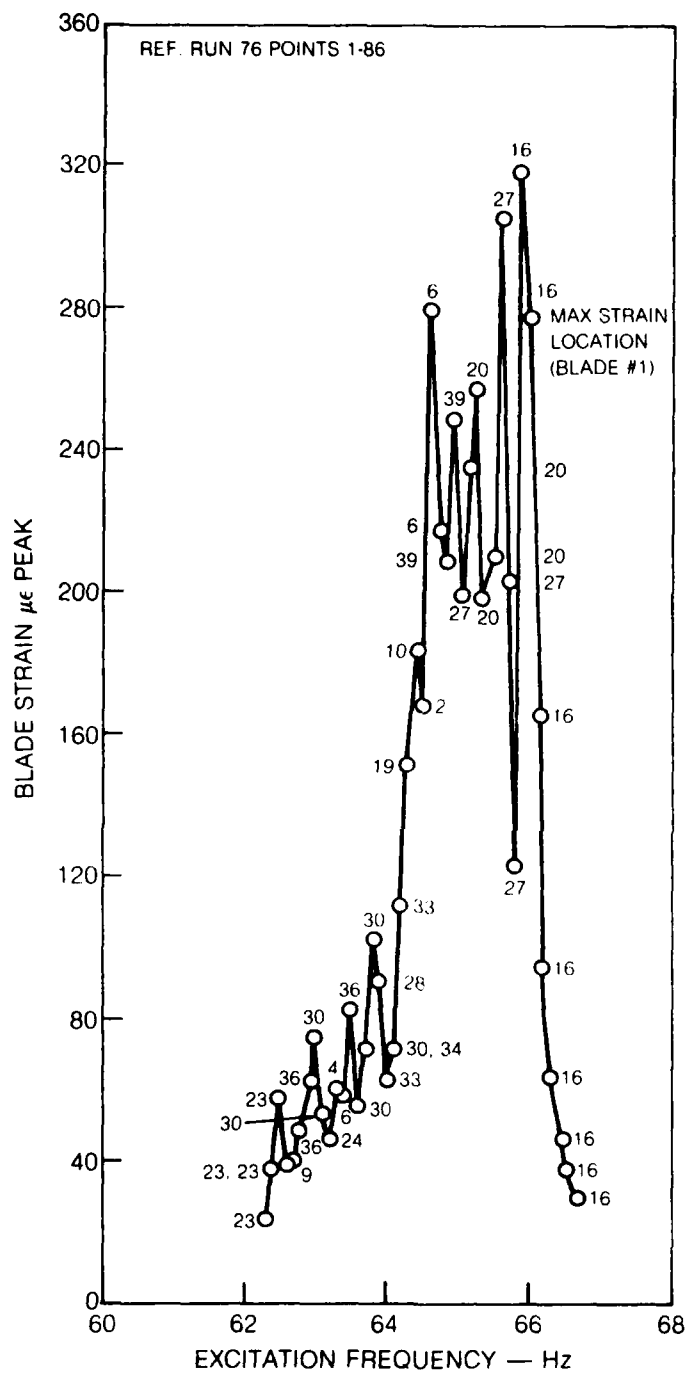


Figure 22 Variation of Maximum Strain Response with Excitation Frequency for the Tuned Assembly Excited with a 4ND Forward Traveling Wave in Evacuated Conditions at Zero Speed

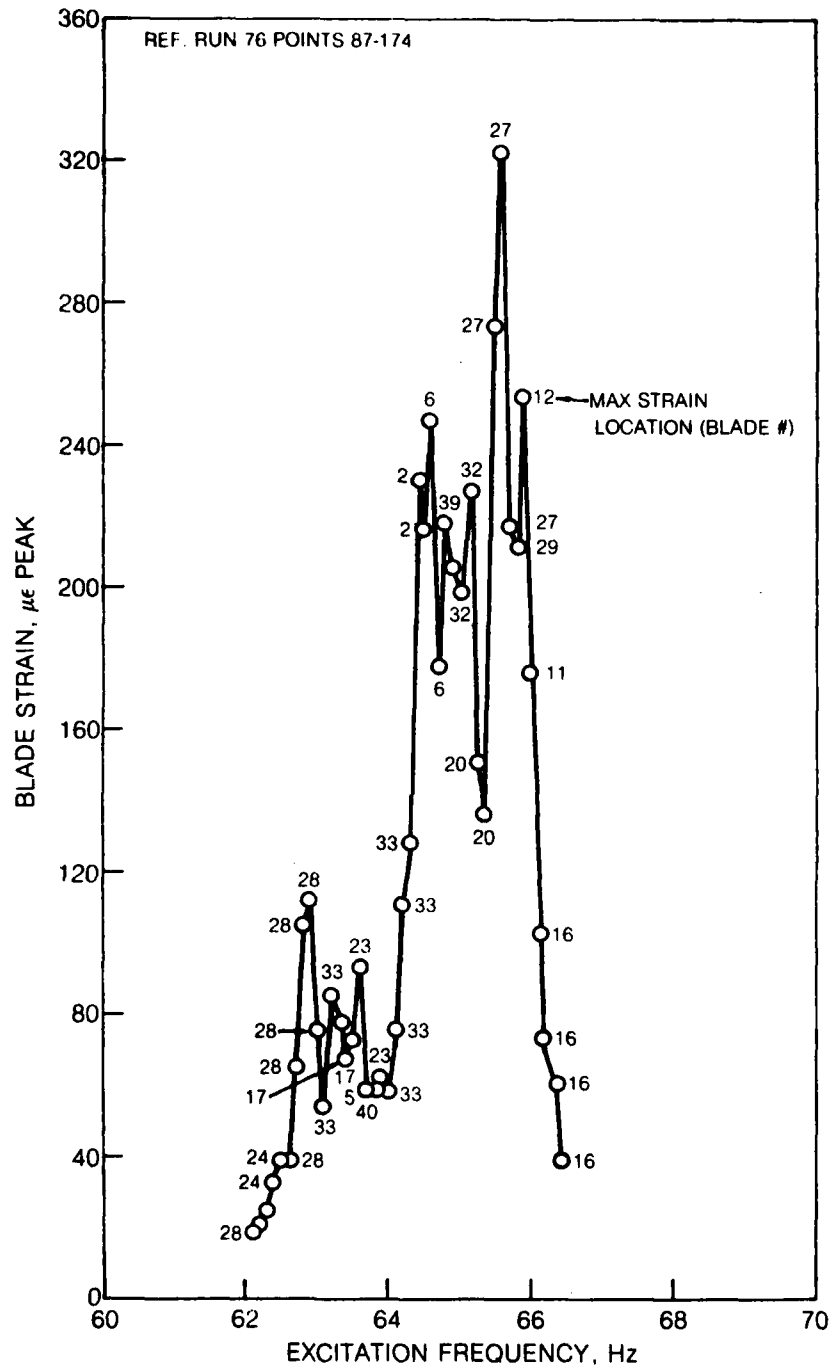


Figure 23 Variation of Maximum Strain Response with Excitation Frequency for the Tuned Assembly Excited with a 4ND Backward Traveling Wave in Evacuated Conditions at Zero Speed

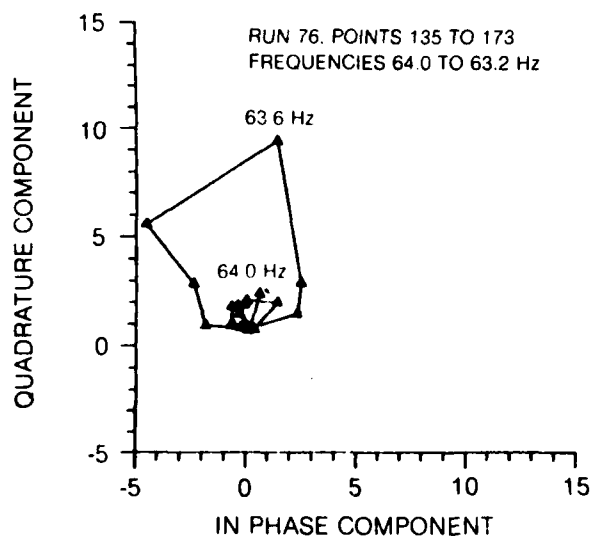
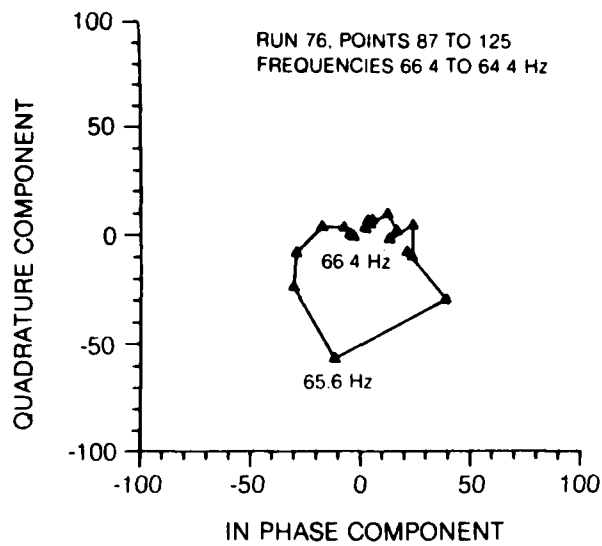


Figure 24 Polar Plot of Blade #27 Strain Response with 2ND Backward Traveling Wave Excitation of the Tuned Assembly in Evacuated Conditions at Zero Speed

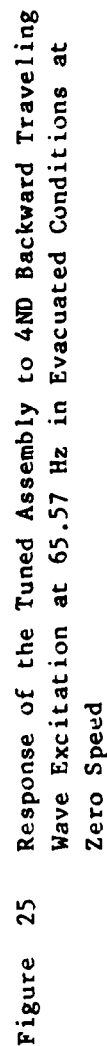
the latter depending upon the frequency of the blade in question in the coupled system. The response of the system is a sum of contributions from all the modes in the vicinity and, therefore, a Fourier analysis of the strain pattern at an instant of time shows the strength of the contributing harmonics. Figure 25 shows an example of such a response where blade #27 strain is peaking. Note that this response is shown in the polar plot for blade #27 in Fig. 24 at 65.6 Hz. The largest backward wave component also occurs at this frequency.

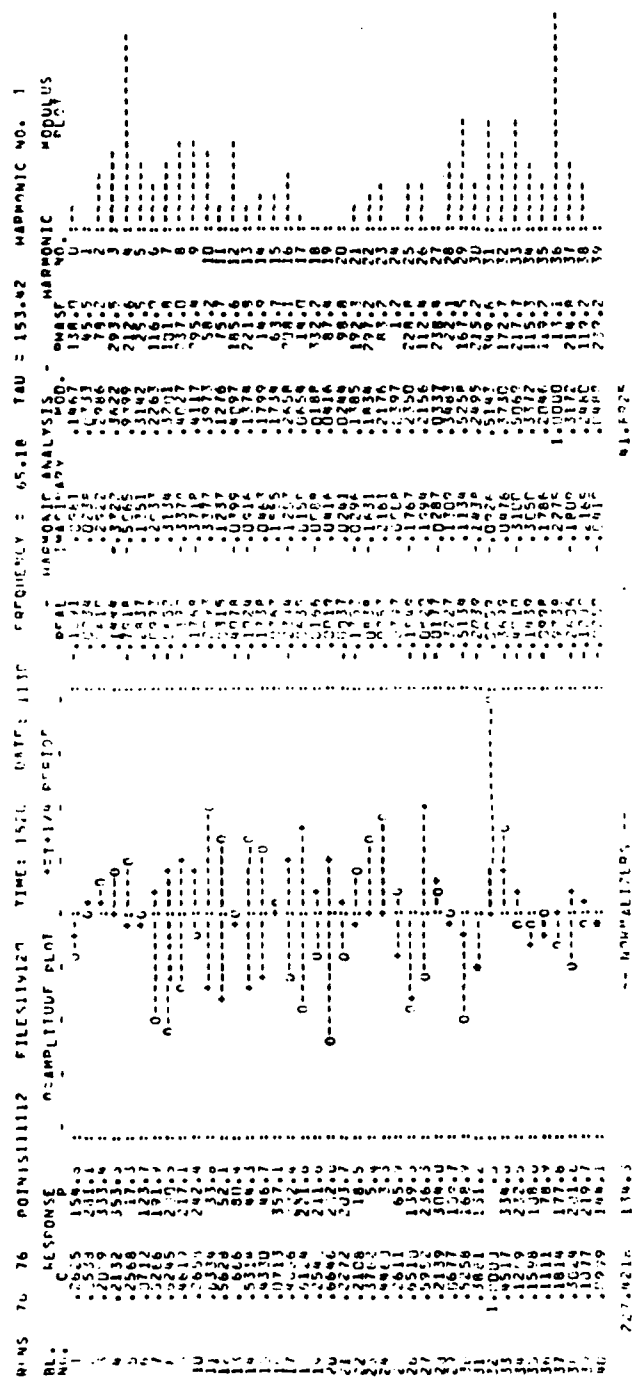
Although the response in this family has been found to be irregular, when the assembly was excited by a four nodal diameter travelling wave using the crystal excitation, two stationary modes in a four nodal diameter pattern were evidenced in the spatial harmonic plots at frequencies of 65.18 and 65.47 Hz. This feature is shown in Figs. 26 and 27. The angle between the antinodes of the modes was found to be  $17.4^\circ$ . This is close to the  $22.5^\circ$  angle required for regular 4ND dual modes. Each of these modes, however, show a large response of a single blade at nearly six times the amplitude of the fundamental. This characteristic causes an increase in the harmonic contents as indicated on the plots.

In order to excite the assembly at a speed that would correspond to an integral order speed, several tests were performed over a speed range. It was noted, on the basis of earlier testing, that the level of mistuning that was still present in the shrouded assembly in its "tuned" state would not permit a clear identification of an integral order speed. However, it was also known that all system modes in the first family occurred within a narrow band of frequencies. Measurement of this band of frequencies over selected speeds led to the calculation of a mean frequency ( $f_m$ ) at each speed. The "integral order" speed corresponding to the 4E speed was identified by noting the intersection of  $f_m$  with the 4E line and was found to be 1163 rpm.

Both forward and backward traveling wave excitations were applied to the rotor at 1163 rpm. The frequency of vibration was varied in the range of 78.7 Hz to 75.2 Hz. The response diagram shown in Fig. 28 for 1163 rpm with backward traveling wave excitation has a peak occurring at 77.6 Hz which corresponds to the integral order frequency chosen as explained above. The response diagram appears to be somewhat more regular within the narrow range of 76.5 Hz and 78.5 Hz, although there are still about 6 different peaks. It is likely that the increase in shroud tightness may have had the effect of bringing about more uniformity to the shroud boundary conditions.

Four nodal stationary waves were also evidenced at this speed in the harmonic plots for the assembly response at frequencies 77.35 to 77.82 Hz. Again the responses were characterized by an additional large single blade response. Two modes are indicated, one where blade #8 has a maximum response





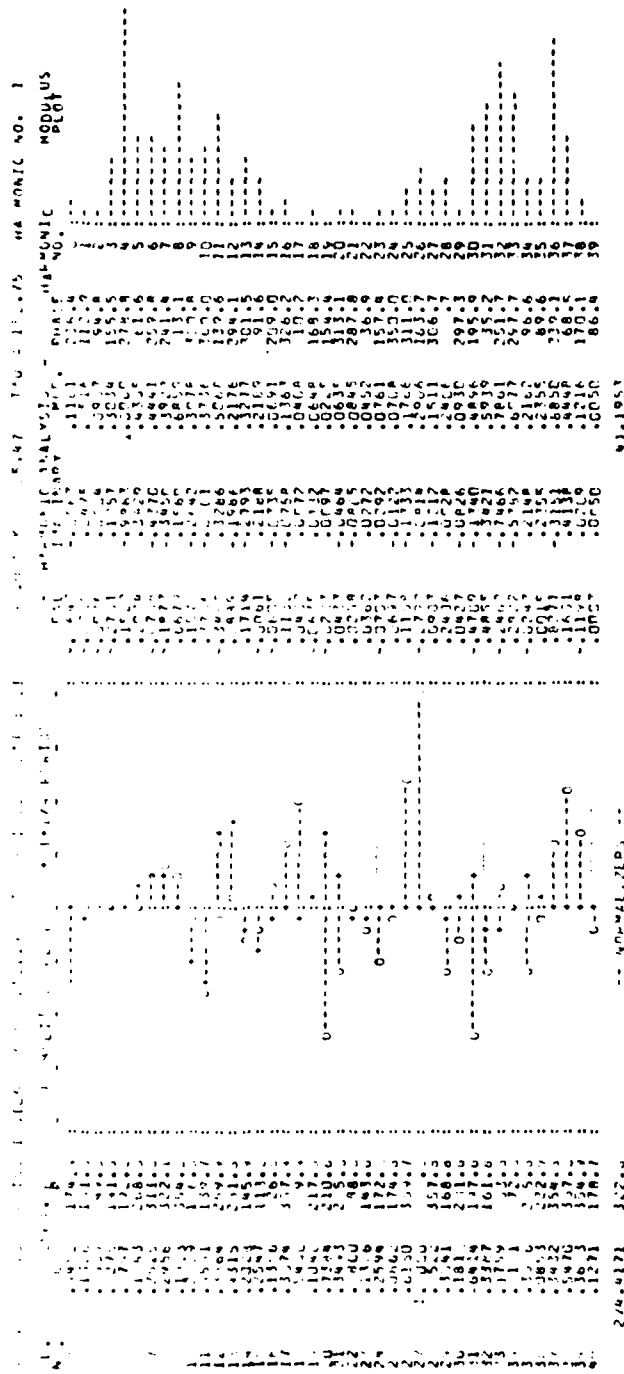


Figure 27 Response of the Tuned Assembly to 4th Backward Traveling Wave Excitation at 65.47 Hz in Evacuated Conditions at Zero Speed



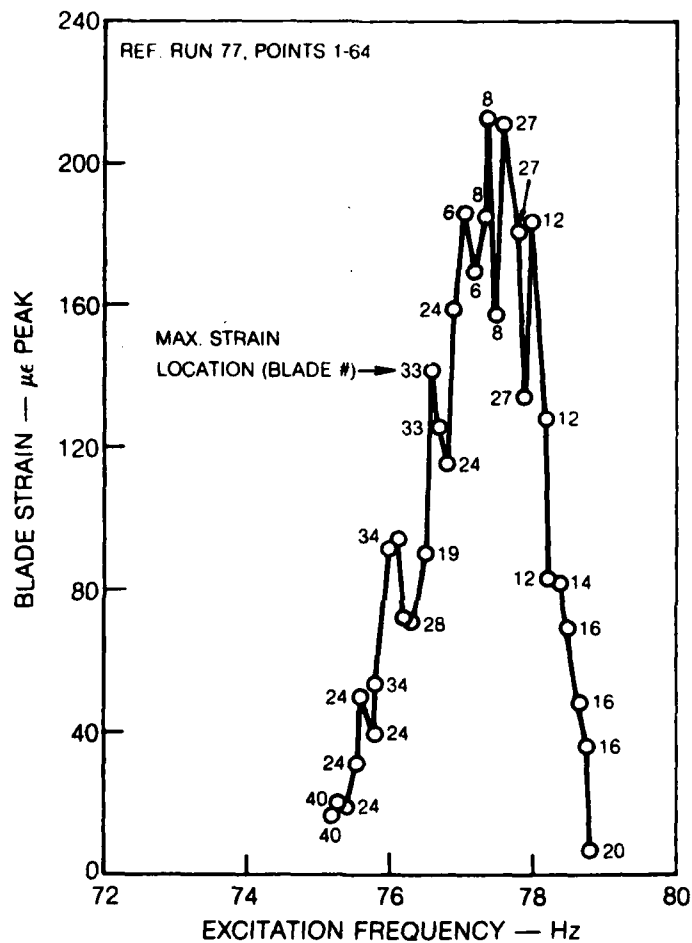


Figure 28 Variation of Maximum Strain Response with Excitation Frequency for the Tuned Assembly Excited with a 4ND Backward Traveling Wave in Evacuated Conditions at 1163 rpm

and the other where blade #27 has a maximum. Figures 29 and 30 show the two types of modes at 77.48 and 77.61 Hz having the largest stationary wave content. These do not appear to be regular twin modes. The largest backward travelling wave component occurs at 77.05 Hz. This response is shown in Fig. 31.

In exploring the second family of modes of the assembly over the range of speeds, the data were examined to identify twin modes. The reduced data, that display stick plots of the mode shape around the rotor and the strength of the contributing harmonics, should generally be adequate for this purpose. However, a close examination of the data from the R-80 fan raised some interesting questions in regard to the criteria for identification of twin modes. These questions are relevant for systems where the asymmetry has no regular pattern. Sample stickplots given in Figs. 32, 33 and 34 show the response of the rotor at three successive frequencies. For a two nodal diameter standing wave forcing function, the responses over a frequency range do indeed have a corresponding predominant harmonic. Upon closer examination of these figures, it is noted that the stick plots show essentially the same response patterns with slightly varying amounts of traveling waves present. The location of maximum strain and the amplitude of the standing wave vary. Selection of the data point closest to the twin mode sought must be based on consideration of (a) the degree of regularity, i.e. percentage of traveling wave component, (b) the amplification of the response (is it at a peak?) and (c) the degree of orthogonality between the twin modes.

The selection of the point at which the percentage of traveling wave content is a minimum generally does not seem to result in responses with peak amplitudes or orthogonal modes. Maximum strain in a blade can be misleading because in a mistuned system the location of the maximum response changes from one blade to another across the resonance of the assembly or an individual blade response may be many times greater than the fundamental response amplitude. The amplitude of the standing wave, along with some or all of the above considerations, appears to serve as a useful criterion. Applying this criterion to the responses shown in Figs. 32, 33 and 34, results in the response at 189.08 Hz as the desired twin mode. On this basis, the data points closest to the frequencies of the regular twin modes of the system were selected for all the other test conditions. The mode shapes at zero speed in evacuated conditions, thus selected, are given in Figs. 33 and 35 through 39.

Polar plots of the modulus and phase (relative to the input signal) of the response of individual blades were made for all test conditions in order to obtain better estimates of the resonant frequencies between the data

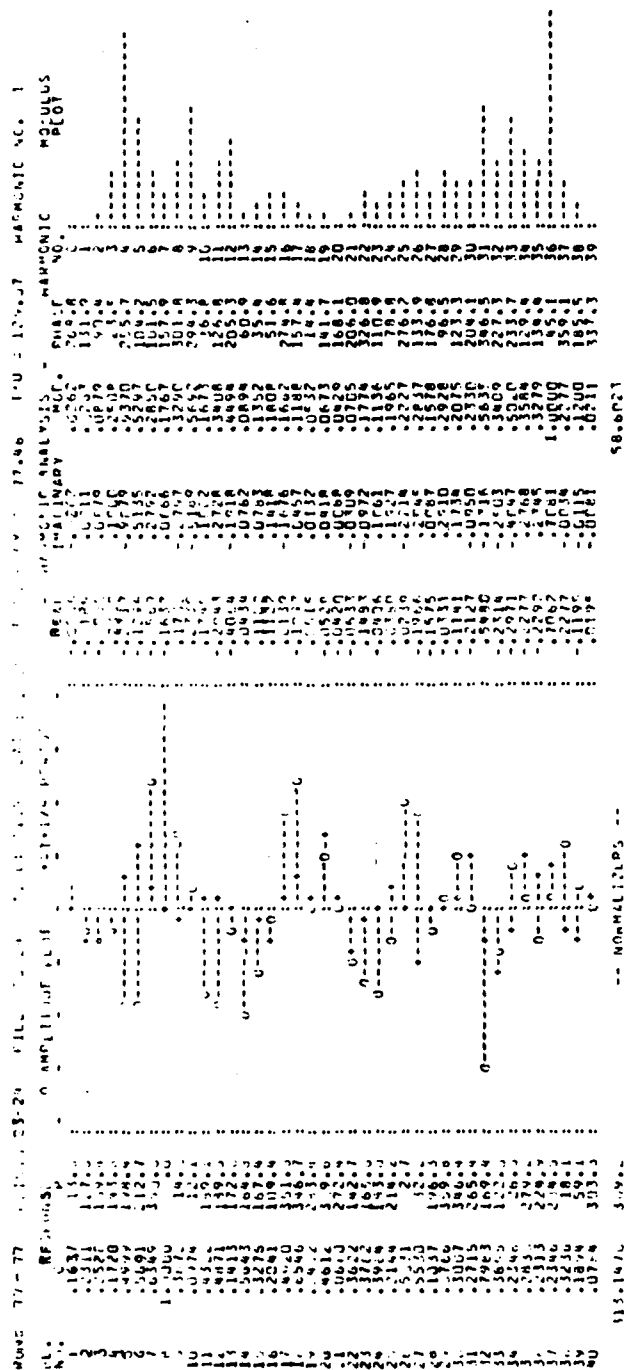
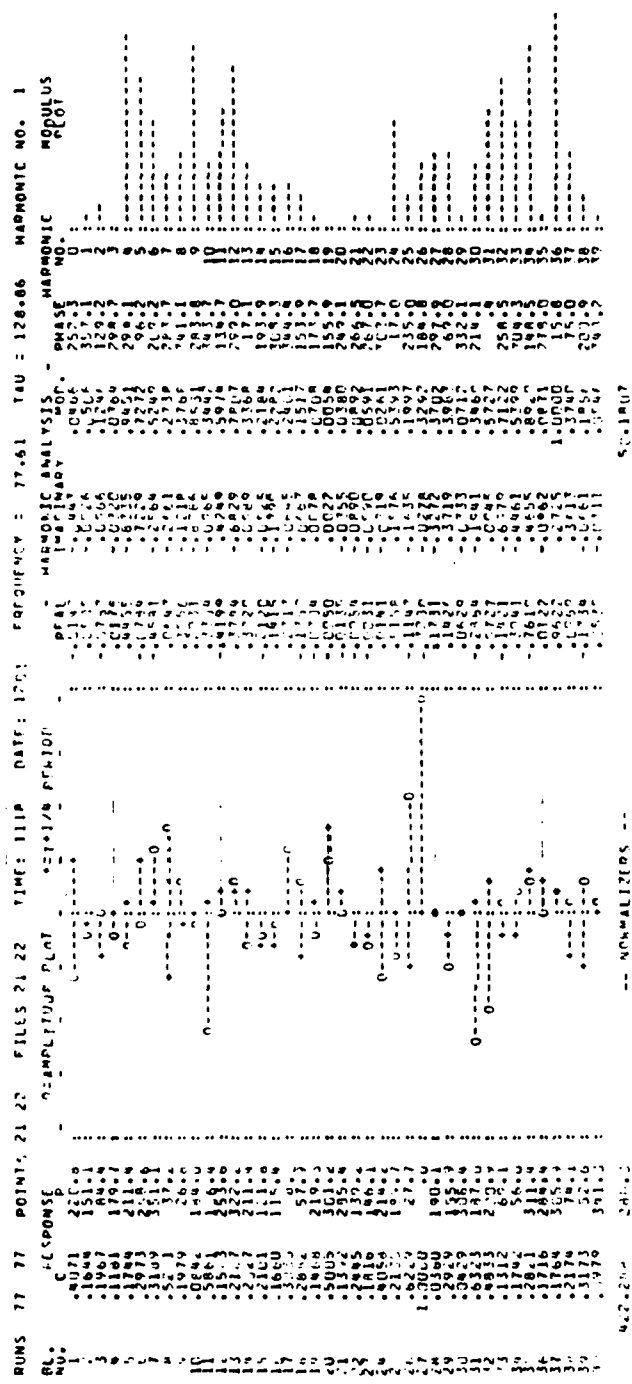


Figure 29 Response of the Tuned Assembly to 4ND Backward Traveling Wave Excitation at 77.48 Hz in Evacuated Conditions at 1163 rpm



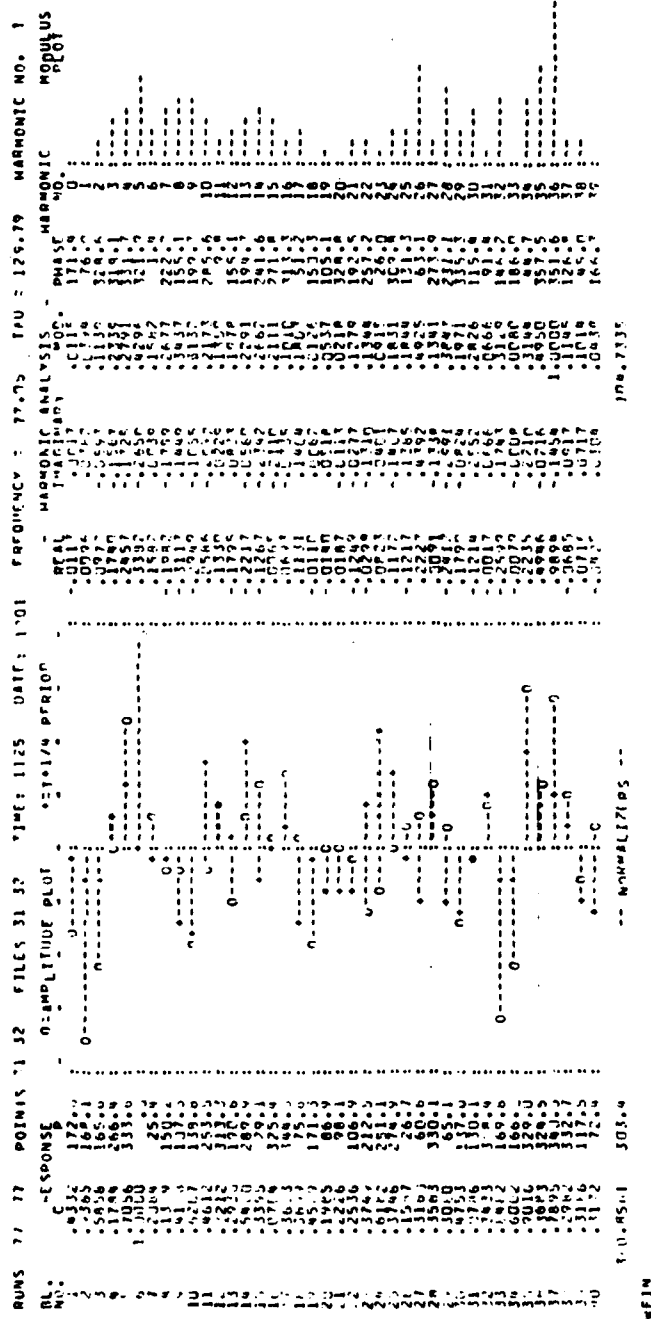


Figure 31 Response of the Tuned Assembly to 4ND Backward Traveling Wave Excitation at 77.05 Hz in Evacuated Conditions at 1163 rpm

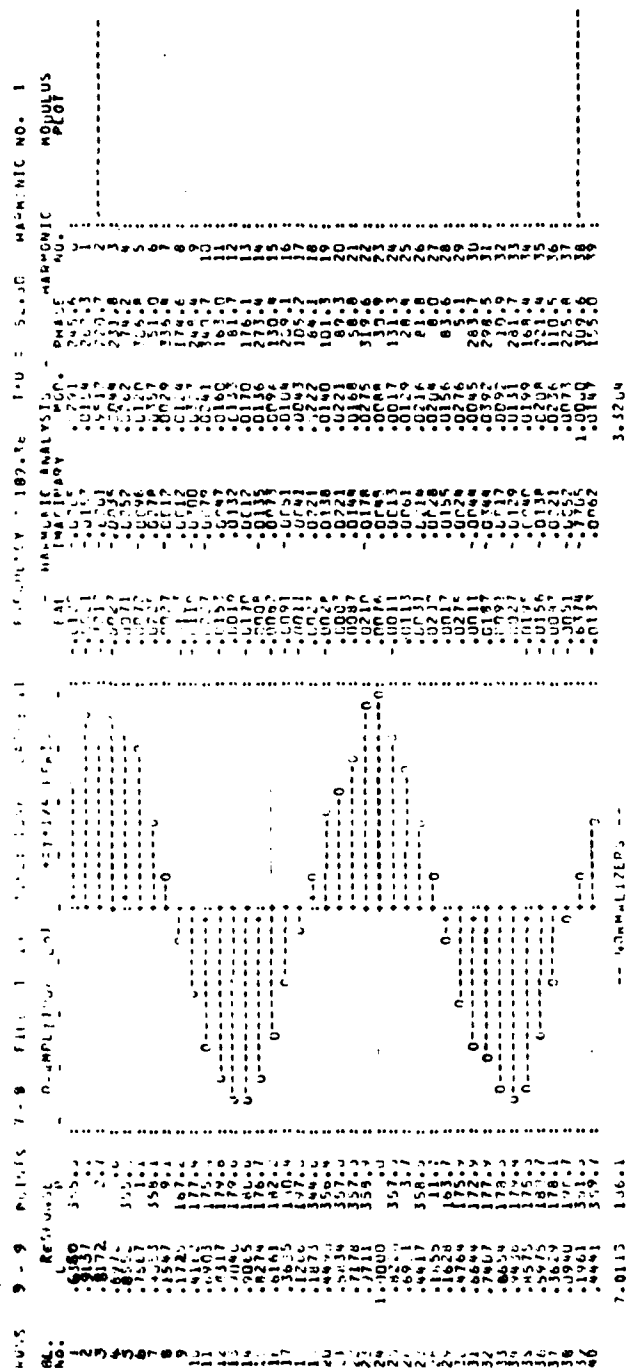
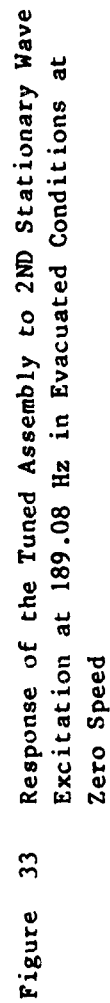


Figure 32 Response of the Tuned Assembly to 2ND Stationary Wave  
Excitation at 189.38 Hz in Evacuated Conditions at  
Zero Speed



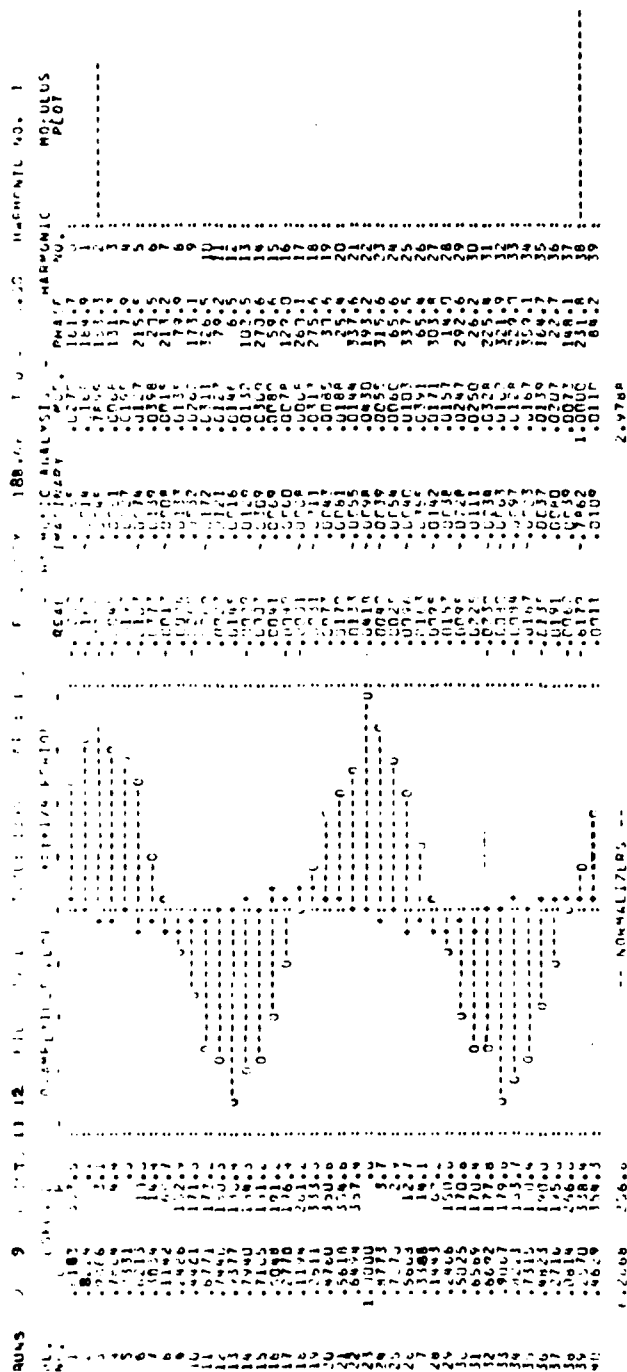
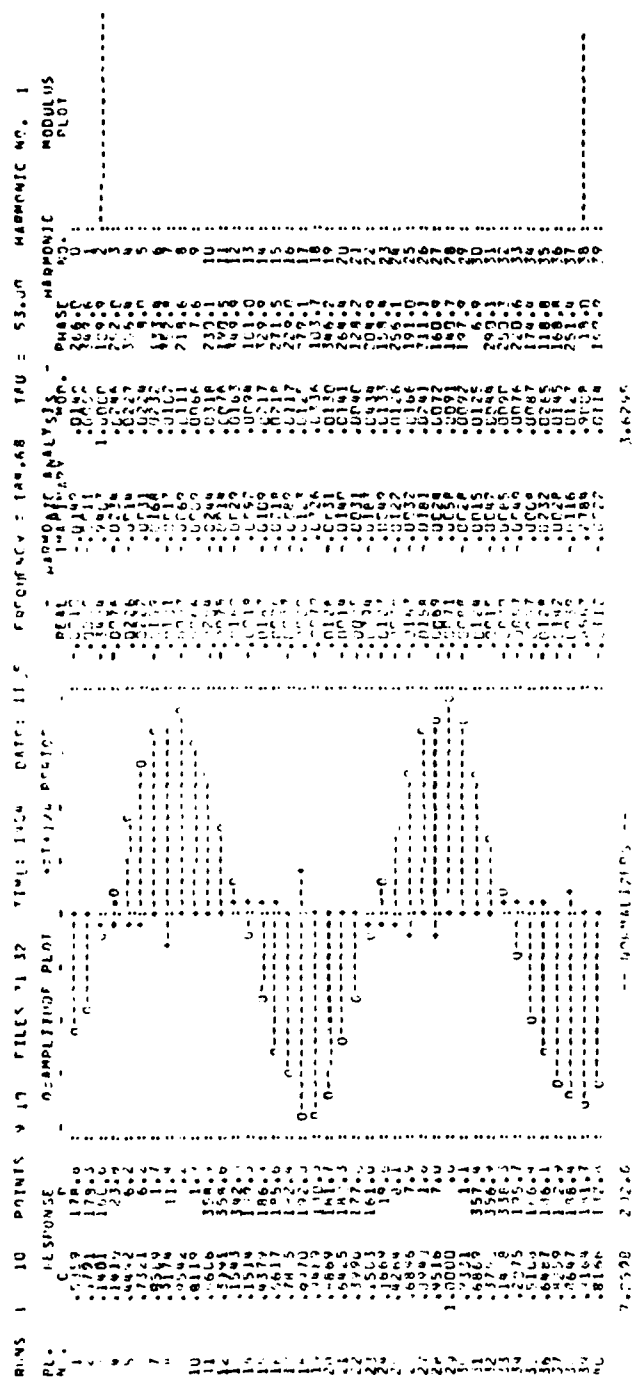


Figure 34 Response of the Tuned Assembly to 2ND Stationary Wave  
Excitation at 188.68 Hz in Evacuated Conditions at  
Zero Speed





**Figure 35 Response of the Tuned Assembly to 2ND Stationary Wave Excitation (shifted 45°) at 188.68 Hz in Evacuated Conditions at Zero Speed**

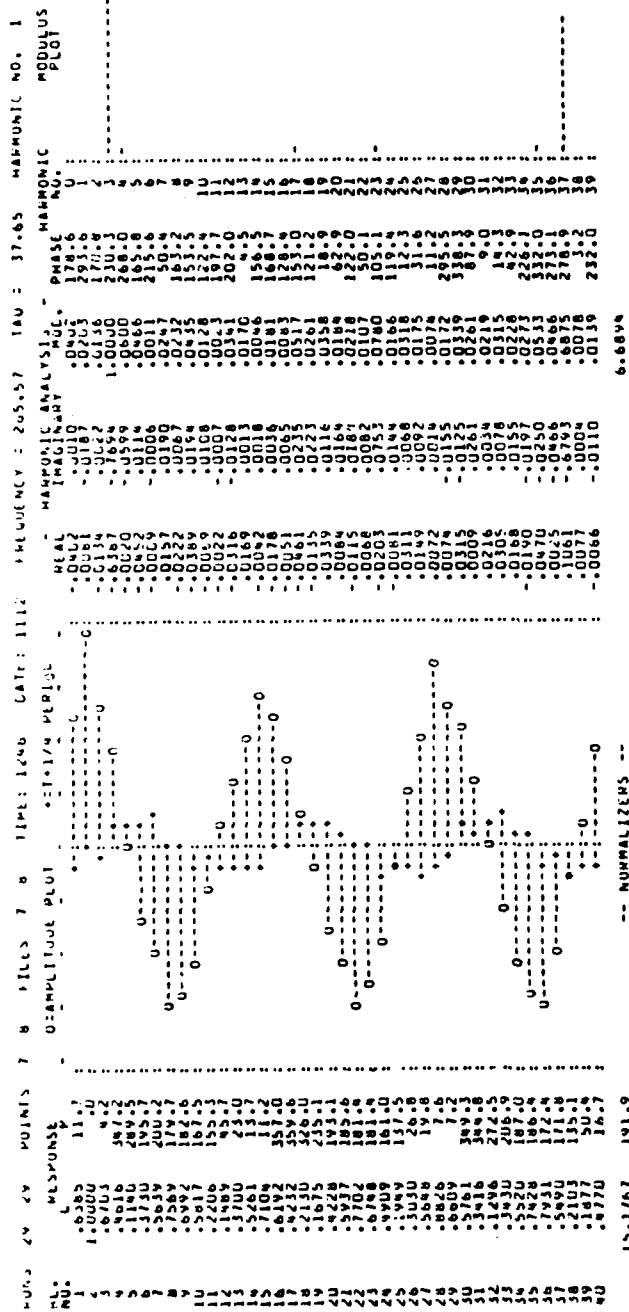


Figure 36 Response of the Tuned Assembly to 3ND Stationary Wave  
 Excitation at 265.57 Hz in Evacuated Conditions at  
 Zero Speed

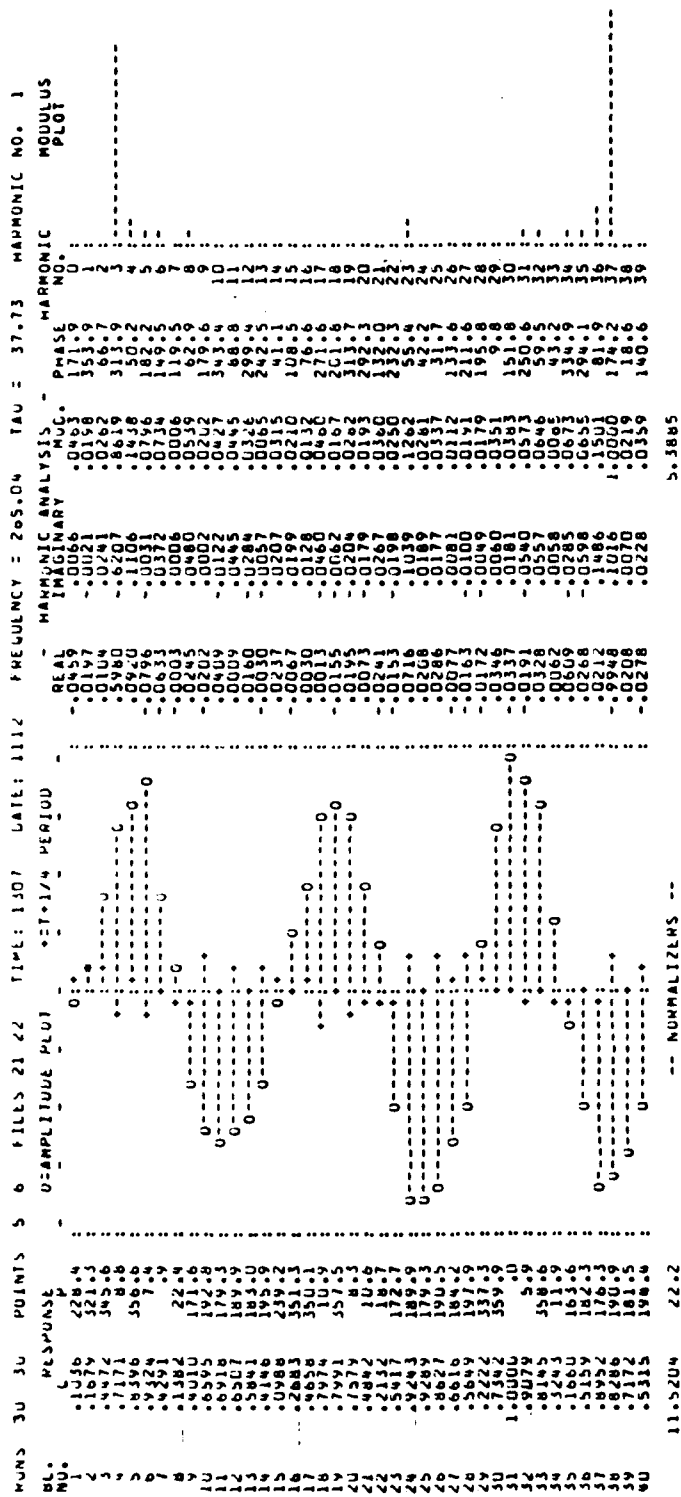


Figure 37 Response of the Tuned Assembly to 3ND Stationary Wave  
Excitation at 265.04 Hz in Evacuated Conditions at  
Zero Speed

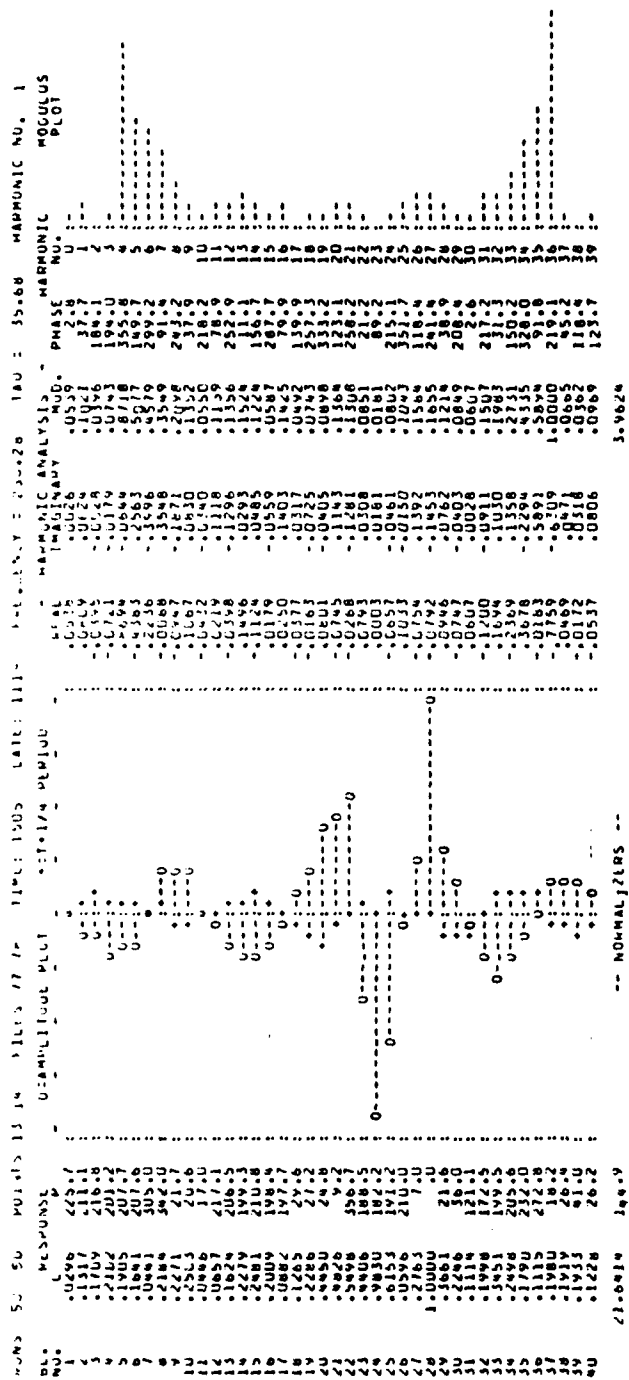
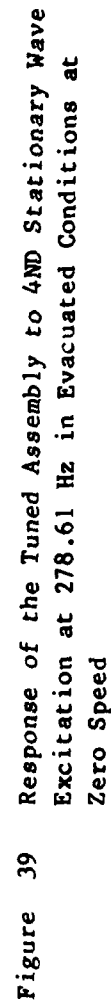


Figure 38 Response of the Tuned Assembly to 4ND Stationary Wave Excitation at 280.28 Hz in Evacuated Conditions at Zero Speed



points and to obtain estimates of modal damping. From the harmonic analysis, the positions (orientations from blade slot #1) of the standing waves representing the twin modes were determined and the amount of traveling wave as a percentage of the standing wave in the modal response were evaluated. The modal frequencies, locations, traveling wave percentages, loss factors and blade locations of maximum response are given in Table 6. It should be noted that the modal characteristics given in Table 6 for the two and three nodal diameter modes were obtained using stationary wave excitation where each twin was selectively (in excitation pattern and frequency) excited. In the case of the four nodal diameter mode, the results were obtained using a forward traveling wave. This technique seemed much simpler than the stationary wave method in that the excitation pattern and its orientation did not have to be determined before the test. However, for a mistuned system, the resonant frequencies of the twin modes excited by a traveling wave do not correspond exactly to those obtained using stationary wave excitation. This phenomenon will be discussed in some detail in the section pertaining to the mistuned assembly. In order to obtain results which can subsequently be compared with corresponding data from the aerodynamic rig, the twin resonant frequencies and the loss factors were determined using the criterion discussed above and are shown in Table 6.

The results obtained by exciting a single blade (blade #28) and recording its peak response in the first bending and first torsion mode are also shown in Table 6. Many of the values for resonant frequency and damping are approximate (frequency  $\pm 0.5$  Hz, damping  $\pm 50\%$ ) because of the closeness of other system modes obscuring the required resonances in the polar plots. Comparing the results with those from "blade alone" tests, the change in the frequencies for the blade is negligible but the damping levels are about 50% lower in the bending mode and an order of magnitude lower for the torsion mode. With reference to Table 6, the damping measured for the system modes is low and of the same order as the damping in the 1T mode referred to above. Contributions from material damping being identical in each of these tests (at essentially same strain levels), the higher damping in the 1B mode for the case of single blade excitation must mean more rubbing action as a result of restraining adjacent blades. The system modes contain contributions from both bending and torsion and the rubbing action at the interfaces appears to be much less. This observation regarding the rubbing action variation and the presence of system modes suggest caution in drawing conclusions in regard to damping from single blade excitation tests on a shrouded assembly.

Other important observations from Table 6 include (i) measurable changes in damping obtained under 760 Torr and 22 Torr, (ii) the generally low values of damping measured in the speed range and (iii), the closely spaced 2, 3, and 4ND twin modes.

TABLE 6. SUMMARY OF MODAL CHARACTERISTICS FOR INITIALLY TUNED SYSTEM IN RIG A

			MODAL CHARACTERISTICS				
			TEST CONDITIONS - RPM/PRESSURE (TORR)				
Excitation			0/760	0/22	570/22	1050/22	1200/22
Stationary	2ND Twin 1	Frequency (Hz)	188.4	189.0	189.9	193.5	194.3
		Position (°)	22.3	21.8	-53.2	-50.1	-51.9
		Trav comp (%)	1.3	6.0	5.1	67.1	21.6
		Damping (n)	0.0079	0.0053	0.0042	0.0055	0.0041
Stationary	2ND Twin 2	Frequency (Hz)	187.7	188.6	189.5	193.0	194.3
		Position (°)	-24.4	-22.9	-16.1	-0.95	-0.6
		Trav comp (%)	3.1	5.7	19.5	12.6	3.3
		Damping (n)	0.0079	0.0048	0.0044	0.0052	?
Stationary	3RD Twin 1	Frequency (Hz)	265.9	265.5	266.1	268.9	
		Position (°)	9.2	8.0	7.3	6.6	
		Trav comp (%)	3.7	23.2	75.5	67.5	
		Damping (n)	0.003	0.0019	?	0.0026	
Stationary	3RD Twin 2	Frequency (Hz)	265.3	265.0	265.6	267.8	
		Position (°)	-20.3	-23.4	-23.3	-20.6	
		Trav comp (%)	6.7	7.6	51.3	62.8	
		Damping (n)	0.003	0.0030	0.0023	0.0026	
Fed. Traveling	4ND Twin 1	Frequency (Hz)	279.2	280.3	281.7	282.5	284.1
		Position (°)	-19.2	-18.0	-16.9	-16.8	-14.6
		Trav comp (%)	11.6	8.7	2.1	2.4	11.9
		Damping (n)	?	?	0.001	0.002	0.002
Fed. Traveling	4ND Twin 2	Frequency (Hz)	277.8	278.6	280.3	281.3	282.5
		Position (°)	-35.2	10.0	-32.9	-35.1	-34.4
		Trav comp (%)	6.8	2.1	2.1	6.0	13.4
		Damping (n)	0.003	0.003	0.004	0.002	0.002
Single Blade (#28)	1R	Frequency (Hz)	62.7				
		(62.8)					
		Damping (n)	0.0035				
		(0.0069)					
Single Blade (#28)	1T	Frequency (Hz)	297	297		303	304
		(297)					
		Damping (n)	0.0013	0.0013		0.001	0.005
		(0.0224)					

NOTE: Values in parenthesis are from "blade alone" tests - for comparison.

\* @ 1163 RPM.

### 3. Mistuned Assembly

The results of testing the initially "tuned" assembly indicated that the mode of vibration that could be excited with considerable clarity belonged to the second family in a two dimensional pattern. The closely spaced split modes (less than 1 Hz) for this pattern could be excited individually in the "tuned" assembly. Therefore, one of the goals of mistuning this fan was to change the frequencies of some of the blades in such a way that would enhance the split in this mode. With this objective in mind and with the additional restriction that no additional holes could be drilled in the blade tips, the tip masses of nine blades were modified. The position of these blades, the change in mass on each blade, and the resulting "blade alone" 1B and 1T frequencies obtained by test, are given in Table 7. The resulting distribution of "blade alone" frequencies for the assembly of 40 blades for the 1B and 1T modes are shown as histograms in Figs. 40 and 41.

Preliminary testing of the assembly in air indicated that the 2, 3 and 4ND modes could be excited in what appeared to be their twin modes as shown below.

<u>MODE</u>	<u>FREQUENCY Hz</u>	<u>% SPLIT</u>
2 ND	188.3	1.0
	190.1	
3 ND	265.1	0.2
	265.6	
4 ND	278.4	1.3
	281.9	

With the assembly in this deliberately mistuned condition a series of tests was performed to measure its modified dynamic characteristics in the first two families of modes. Table 8 shows the Test Matrix listing in detail all the tests performed with the associated run numbers and test conditions. The principal goals were to identify the extent and influence of the mistuning on the system in relation to a) the first family response, b) the split modes in the second family, and c) modal damping. Fifty-five test runs were made in which frequency response measurements were recorded. The procedures followed were essentially the same as those employed for the tuned system. All data from these tests were digitized and recorded on magnetic tape.



TABLE 7. TIP MASS CHANGE AND RESULTING "BLADE ALONE"  
MODAL FREQUENCIES FOR MODIFIED BLADES  
IN MISTUNED ASSEMBLY.

BLADE #	POSITION *	MASS CHANGE	FREQUENCY Hz	
	Deg	gms	1B Mode	IT Mode
4	27	-7.49	~66	312.3
8	63	+6.14	61.52	300.5
13	108	-10.32	67.99	328.4
14	117	-3.49	66.09	313.8
24	207	-10.23	66.60	310.9
28	216	+26.57	56.22	294.6
32	279	-10.72	67.70	314.9
33	288	-10.00	66.86	313.9
34	297	-10.22	66.63	315.5

\* Orientation from blade slot #1 in direction of increasing blade number.

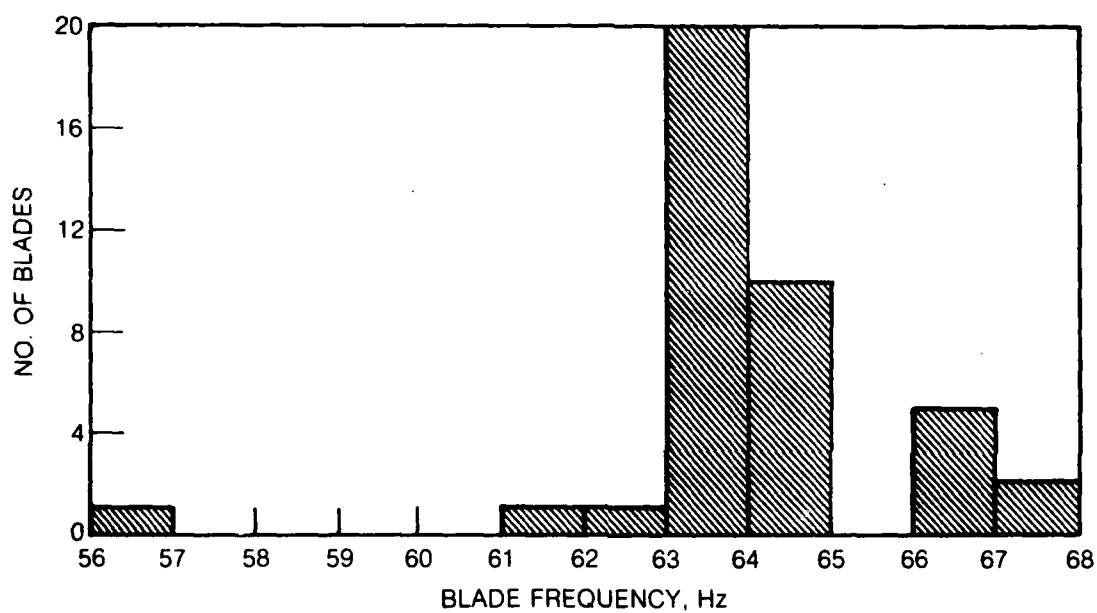


Figure 40 Histogram of "Blade Alone" First Bending Mode Frequencies After Mistuning

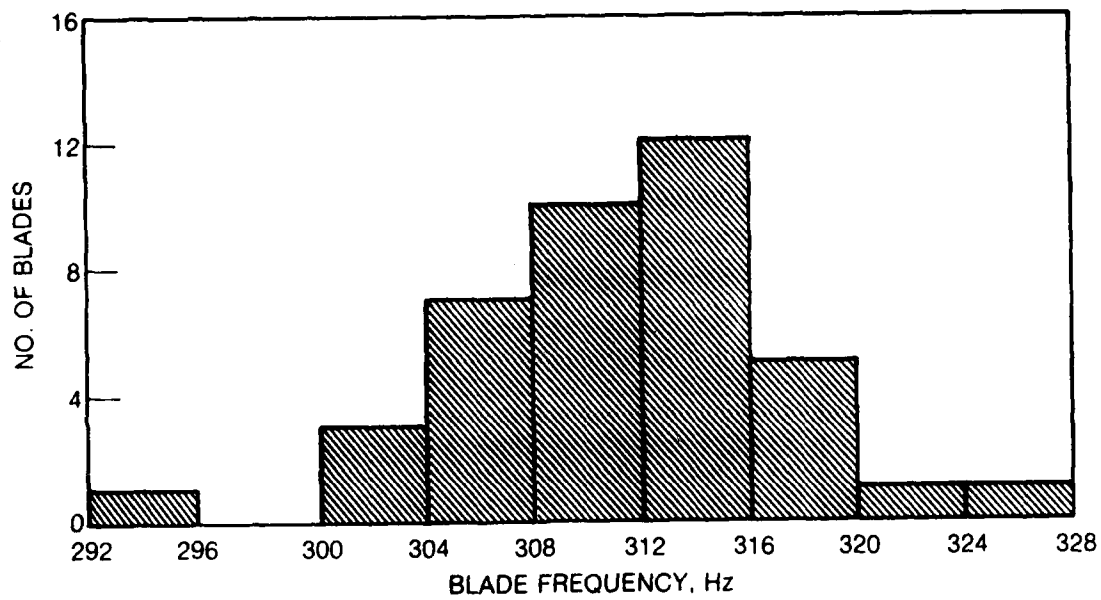


Figure 41 Histogram of "Blade Alone" First Torsion Mode Frequencies After Mistuning

TABLE 8. SUMMARY OF TESTS PERFORMED ON FAN ASSEMBLY (MISTUNED CONDITION) IN RIG A.

FORCING	NODAL DIAM.	TESTS PERFORMED RUN NUMBER											
		TEST CONDITIONS: - RPM/PRESSURE (TORR)											
		0/760			0/22			560/22			1050/22		
BLADE ALONE (All others detuned)	**	1	2									1163*/22	1200/22
		x	x										
SINGLE BLADE EXCITATION		3	4										
		101	102										
FIRST FAMILY OF MODES	4												
SECOND FAMILY OF MODES	2	5	6	7	8	5	6	7	8	5	6	7	8
		99	100	97	98	81	82	78	79	84	85	86	87
	3												
	4												

KEY TO TEST:

- 1 = INDIVIDUAL BLADE EXCITATION. 1st BENDING MODE FREQUENCY AND DAMPING DECAY (12 BLADES)
- 2 = INDIVIDUAL BLADE EXCITATION. 1st TORSION MODE FREQUENCY AND DAMPING DECAY (12 BLADES)
- 3 = SINGLE BLADE FREQUENCY RESPONSE, 1st BENDING MODE (BLADE #28)
- 4 = SINGLE BLADE FREQUENCY RESPONSE, 1st TORSION MODE (BLADE #28)
- 5 = FORWARD TRAVELING WAVE - FREQUENCY RESPONSE
- 6 = BACKWARD TRAVELING WAVE - FREQUENCY RESPONSE
- 7,8 = STATIONARY WAVE EXCITATION OF TWIN MODES - FREQUENCY RESPONSE

NOTES: \* INTEGRAL ORDER SPEED FOR FIRST FAMILY 4ND MODE

\*\* NOT RECORDED ON TAPE

\*\*\* RESULTS OBTAINED FOR TWO LEVELS OF INPUT

#### 4. Discussion of Results

At zero speed, the assembly was subjected to four nodal diameter backward traveling wave excitation (see Table 8 - Run 112). The excitation frequency was varied in steps of about 0.1 Hz from 71.4 to 55.4 Hz to observe the assembly response in the first family of modes. The maximum strain measured at each frequency is shown plotted in Fig. 42 along with the blade number at which the maximum was observed. Blade #28, which has the lowest 1B mode frequency, reaches a peak at that frequency (~ 56 Hz). Blade #13, which has the highest 1B mode frequency reaches a peak at that frequency (~ 68 Hz). Between 64.5 Hz and 67.2 Hz, different blades reach peak amplitudes, the highest level being attained by blade #18 at a frequency of 65.58 Hz. The corresponding system mode at this frequency is shown in Fig. 43 and contains a somewhat predominant 4ND backward traveling wave response and many other harmonics. It is interesting to note from Fig. 42 that blade #18 experiences another (smaller) maximum strain at its own "blade alone" frequency (~ 64 Hz). These two resonances are indicated on the polar plot of response for blade #18 shown in Fig. 44. The output plots (stick plots) were examined at each frequency for indications of four nodal diameter standing wave resonances. One such resonance was found at a frequency of 65.25 Hz. The mode shape and spatial harmonic content are given in Figure 45. As can be seen, it is certainly not regular and its characteristics are dominated by the large amplitudes experienced by blades #27 and #31. The maximum 4ND backward traveling wave component occurred at 65.58 Hz with blade #18 resonant as can be seen in Fig. 43.

The assembly was similarly excited at 1163 rpm i.e., the 4E integral order speed that was used for the tuned system. This speed was considered to be applicable in this case also since the speed still corresponds to the fourth order of the central frequency in the assembly peak response frequency band (excluding blade #28).

The response diagram shown in Fig. 46 for 1163 rpm indicates that blades #28 and #13 behave in an uncoupled manner as they did at zero speed. Their peak response frequencies were increased to 69.7 Hz and 79.8 Hz because of centrifugal loading. However, there are not as many peaks in the response compared with those at zero speed and the blade with the highest strain was blade #26 (at 77.5 Hz) rather than blade #18 previously noted. It is likely that some of these changes are due to unknown changes occurring at shroud interfaces and also to the discrete step variation in excitation.

The largest four nodal diameter stationary wave response occurred at 77.7 Hz. The mode shape was, as expected, irregular and dominated by large

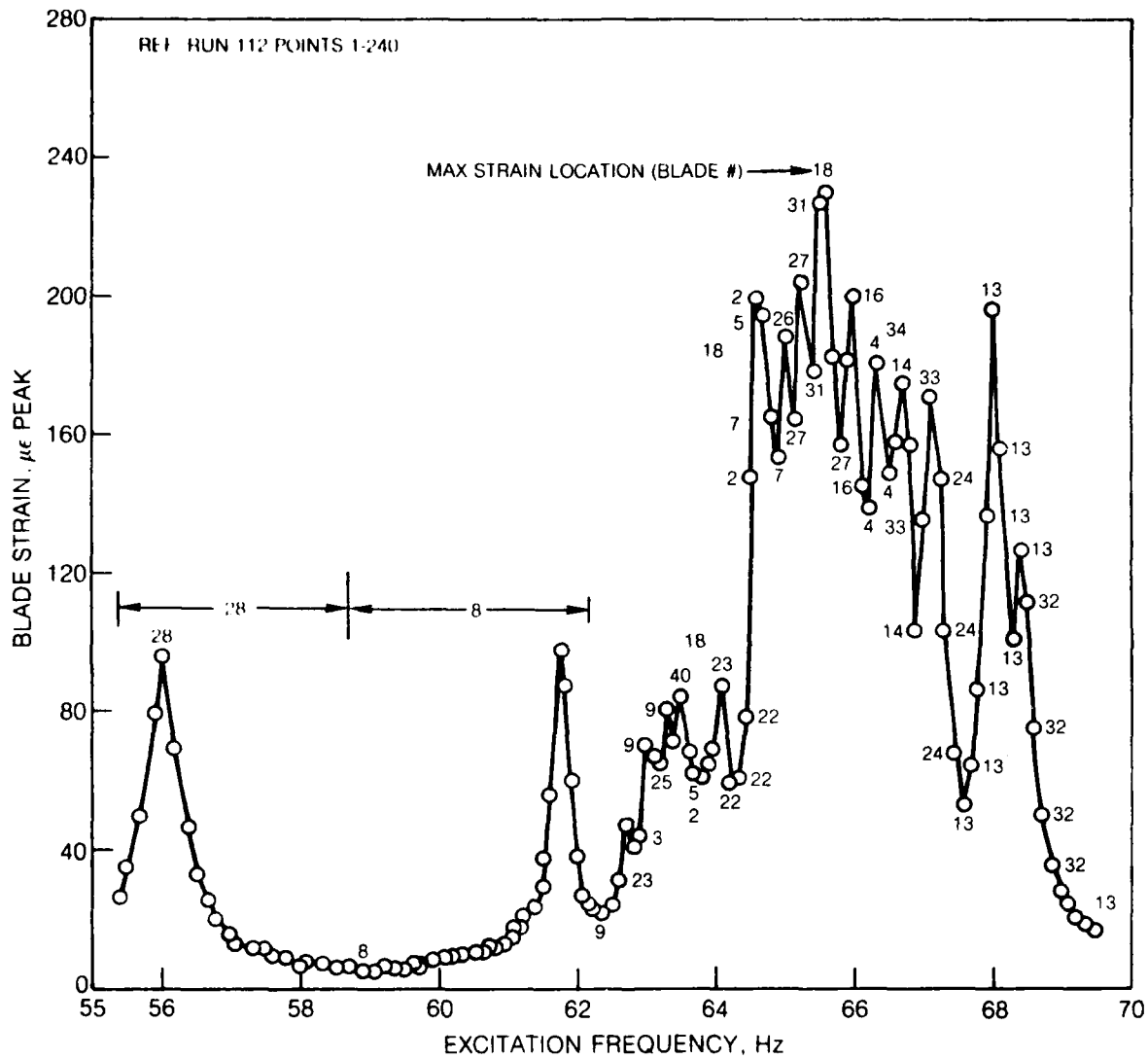


Figure 42 Variation of Maximum Strain Response Excitation Frequency for the Mistuned Assembly Excited with 4ND Backward Traveling Wave in Evacuated Conditions at Zero Speed

AD-A146 226

BASIC STUDY OF BLADED DISK STRUCTURAL RESPONSE(U)  
UNITED TECHNOLOGIES RESEARCH CENTER EAST HARTFORD CT  
A V SRINIVASAN ET AL. NOV 83 R83-914806-48

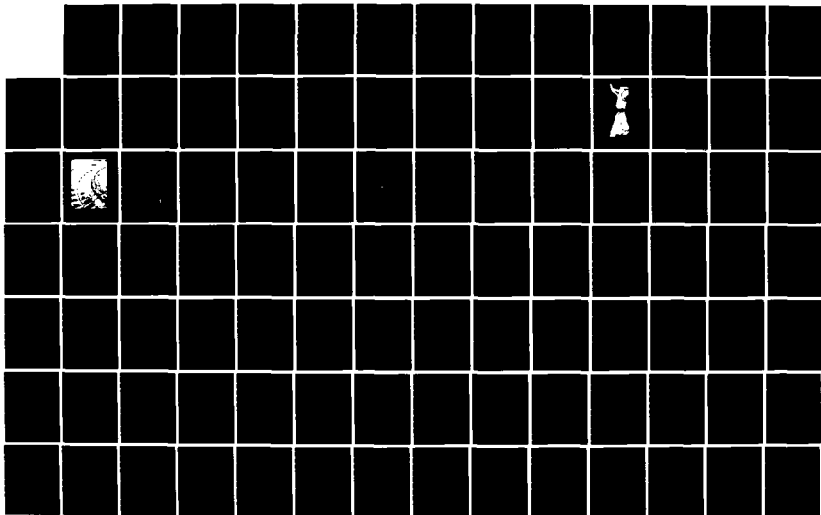
2/3

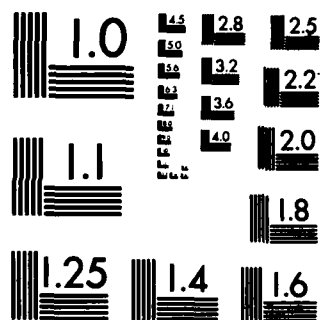
UNCLASSIFIED

AFWAL-TR-83-2075 F33615-79-C-2054

F/G 1/3

NL





MICROCOPY RESOLUTION TEST CHART  
NATIONAL BUREAU OF STANDARDS-1963-A



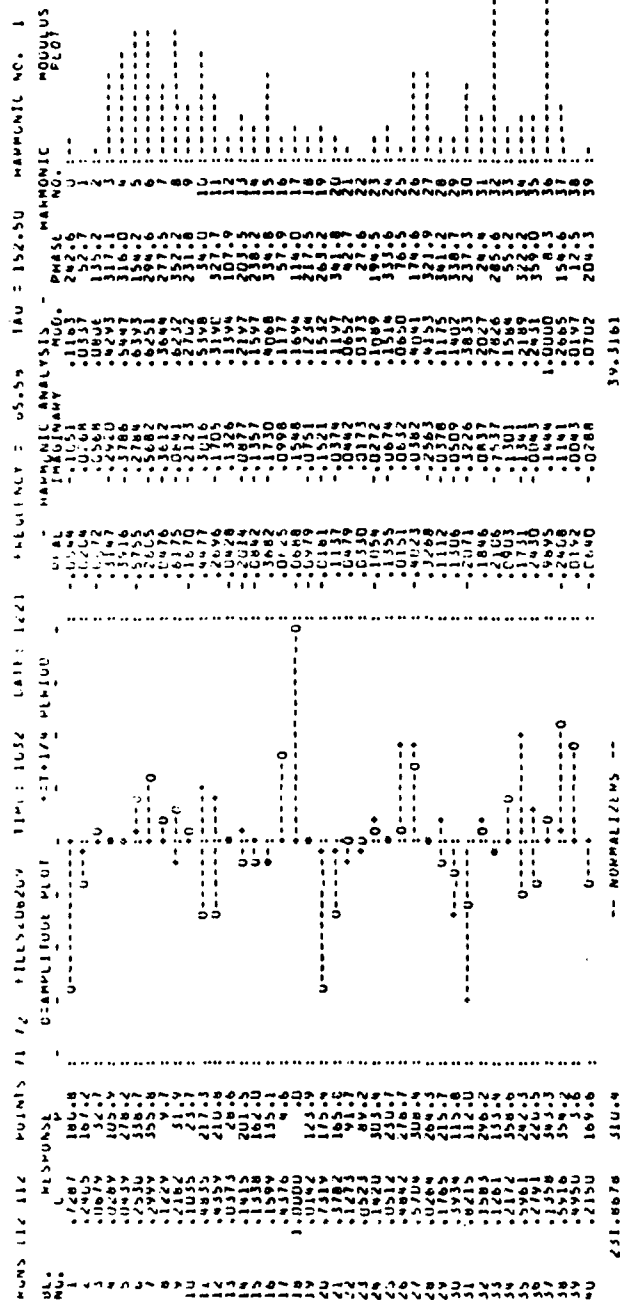


Figure 43 Response of the Mistuned Assembly to 4ND Backward  
 Traveling Wave Excitation at 65.58 Hz in  
 Evacuated Conditions at Zero Speed

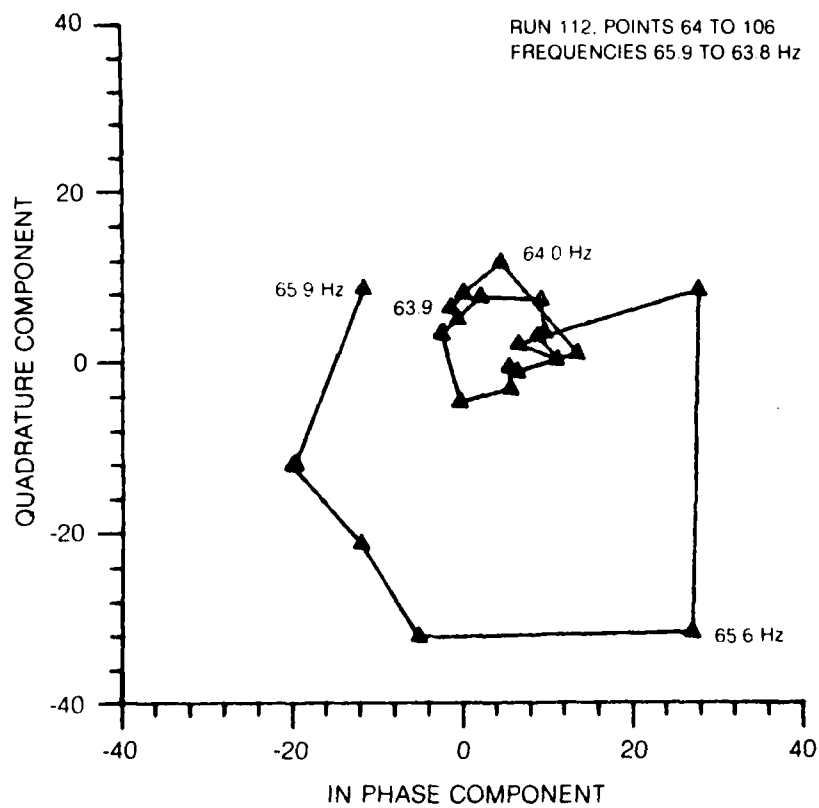
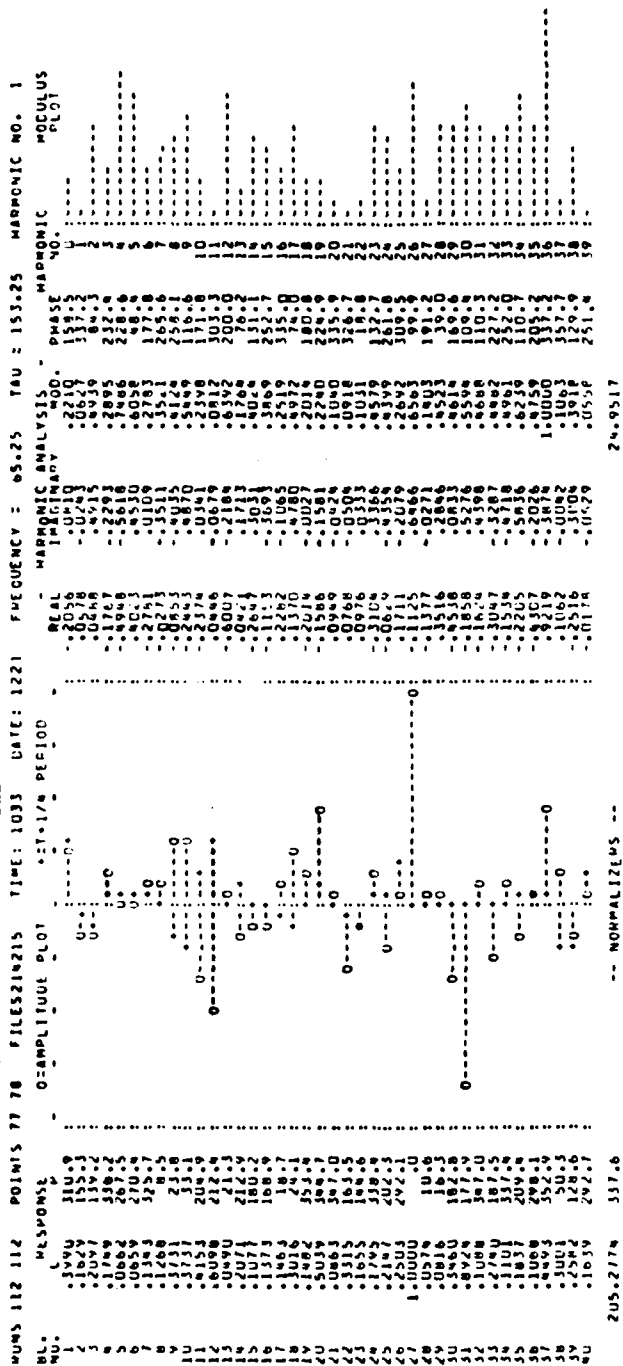


Figure 44 Polar Plot of Blade #18 Strain Response with 4ND Backward Traveling Wave Excitation of the Mistuned Assembly in Evacuated Conditions at Zero Speed



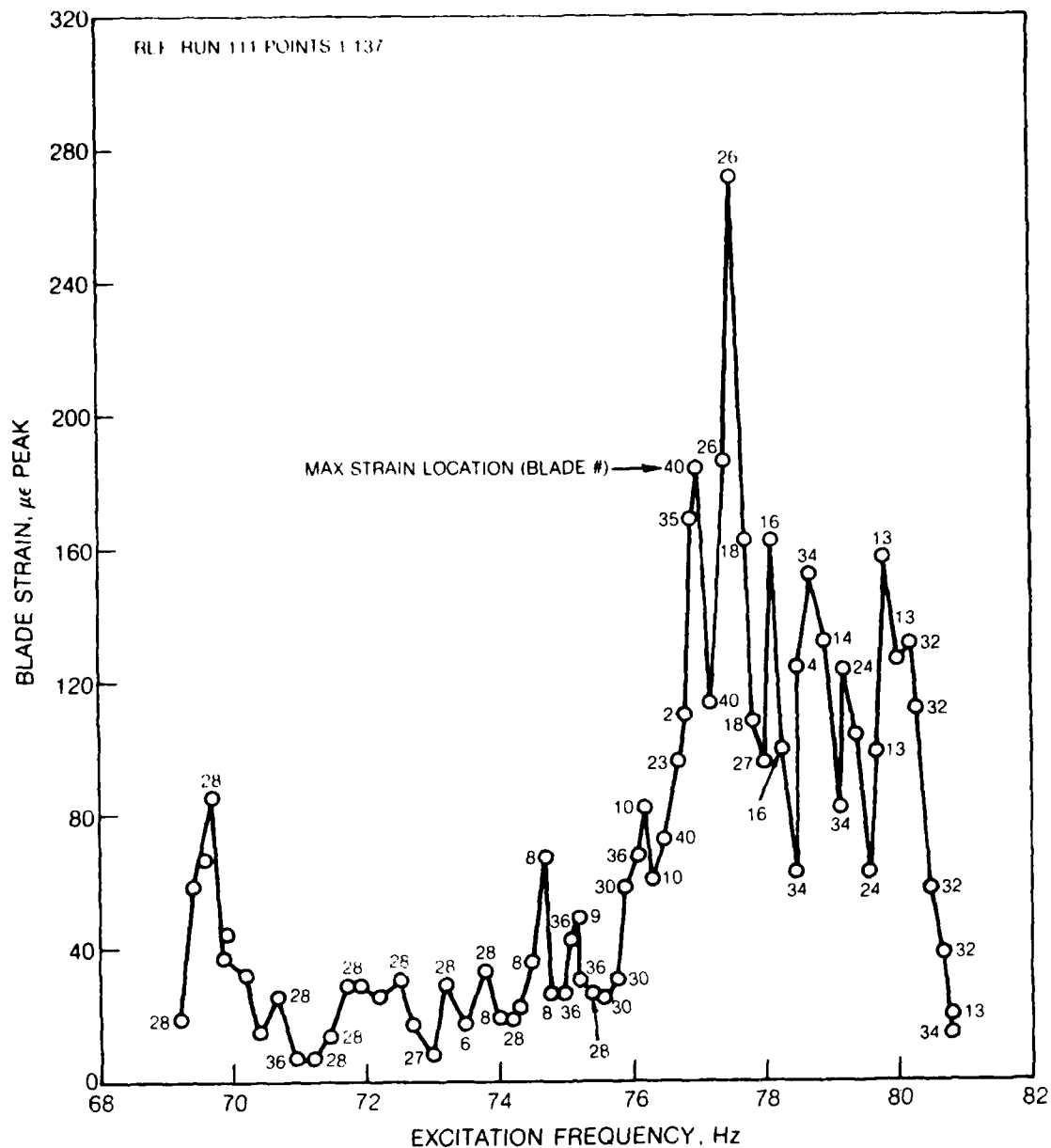


Figure 46 Variation of Maximum Strain Response with Excitation Frequency for the Mistuned Assembly Excited with a 4ND Backward Traveling Wave in Evacuated Conditions at 1163 rpm

response of a few blades, namely, blades #18, 20, 27, and 31. The maximum 4ND backward traveling wave component occurred at 77.5 Hz.

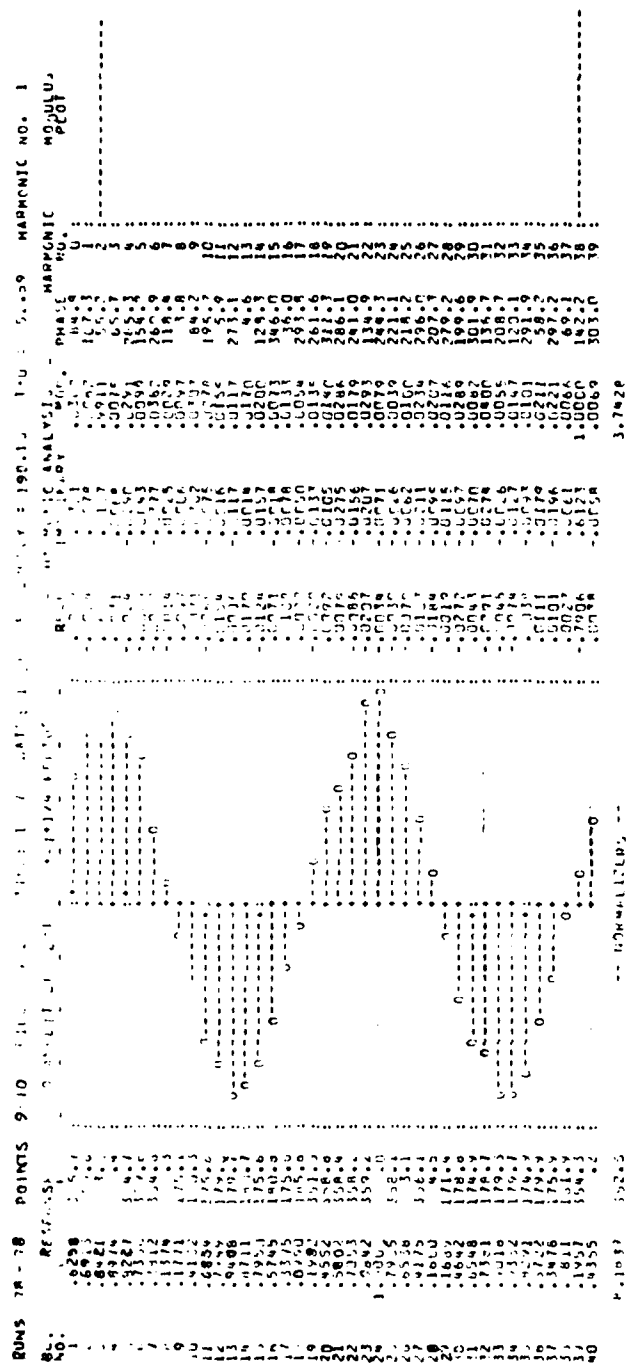
The data obtained from stationary wave excitation tests were examined to identify twin modes in the second family of system modes. The data points closest to the frequencies of the apparent twin modes of the system were selected for all test conditions using the criteria discussed earlier for the tuned assembly. The mode shapes thus selected at zero speed and in evacuated conditions are given in Figs. 47 through 52. Polar plots of the response (not shown) of individual blades were used to obtain better estimates of the resonant frequencies between the data points and to obtain estimates of modal damping. These frequencies are given in Table 9 together with mode positions, percentages of traveling wave, loss factors, and the serial number of the blade experiencing maximum strain.

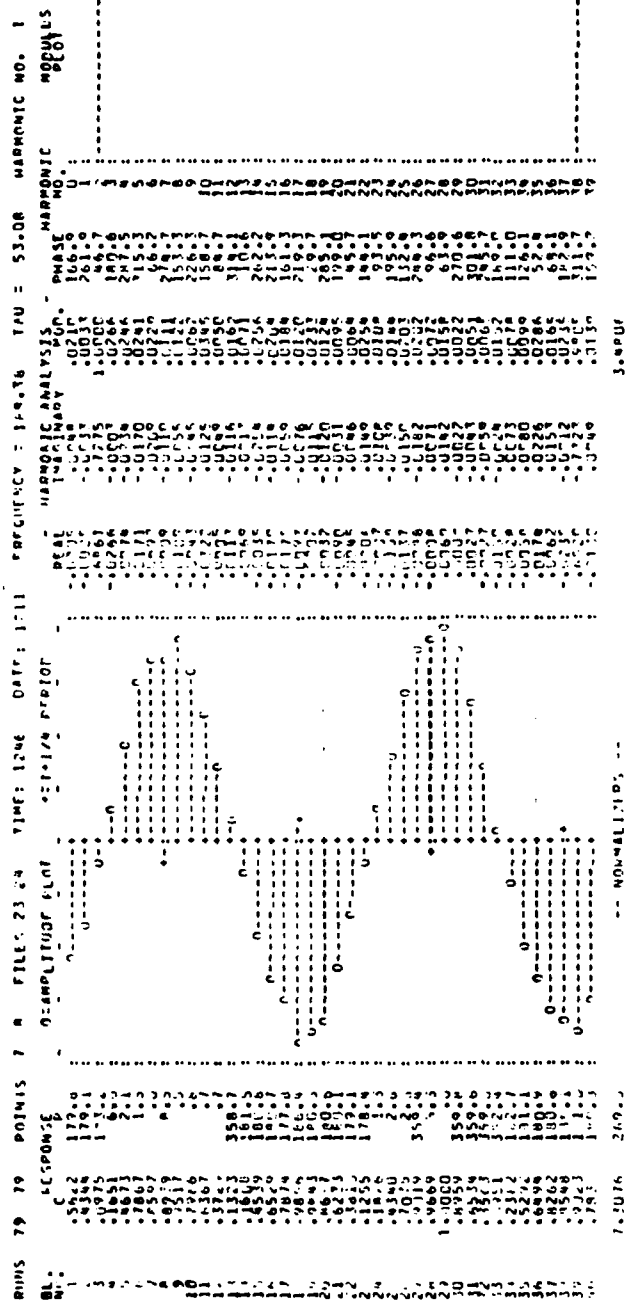
Examination of Table 9 indicates that only the 2ND modes have the correct spatial phasing between them. This is due, in part, to the dominance of individual blade responses in the higher order system modes.

The results obtained by exciting a single blade, namely blade #28, in its first bending and first torsion modes are also given in Table 9. These frequencies and corresponding estimates of damping were obtained from polar plots of response. Because of the wide separation between the "blade alone" frequency of blade #28 and those of all the others, the response of blade #28 may be considered as practically "blade alone" or uncoupled especially in the bending mode. This was confirmed in the stickplots of system response obtained from these tests, two samples of which taken at 1200 rpm are shown in Figs. 53 and 54. However, the damping values obtained from single blade excitation tests are considerably smaller than those from the "blade alone" tests.

The response of the mistuned fan to a traveling wave excitation is now examined. Stickplots and their associated spatial harmonic analyses are shown in Figs. 55 and 56 for two data points (at frequencies 187.70 and 188.68 Hz) from Run #81. Both of these are responses to a two nodal diameter forward traveling wave excitation at zero speed. The response at 187.7 Hz is essentially a standing wave with only 8.3% traveling wave content. In less than 1 Hz, the characteristic changes to one with 42.6% traveling wave.

An understanding of the behavior of a bladed disk assembly subjected to an  $n$  nodal diameter forcing function is enhanced by studying the strengths of the contributing harmonics  $A_n$  and  $A_{-n}$ . The sum  $A_n + A_{-n}$  can be considered as a "system total" response because it represents the total amplitude experienced, on the whole, by a blade at some instant of time as the  $A_n$  and  $A_{-n}$





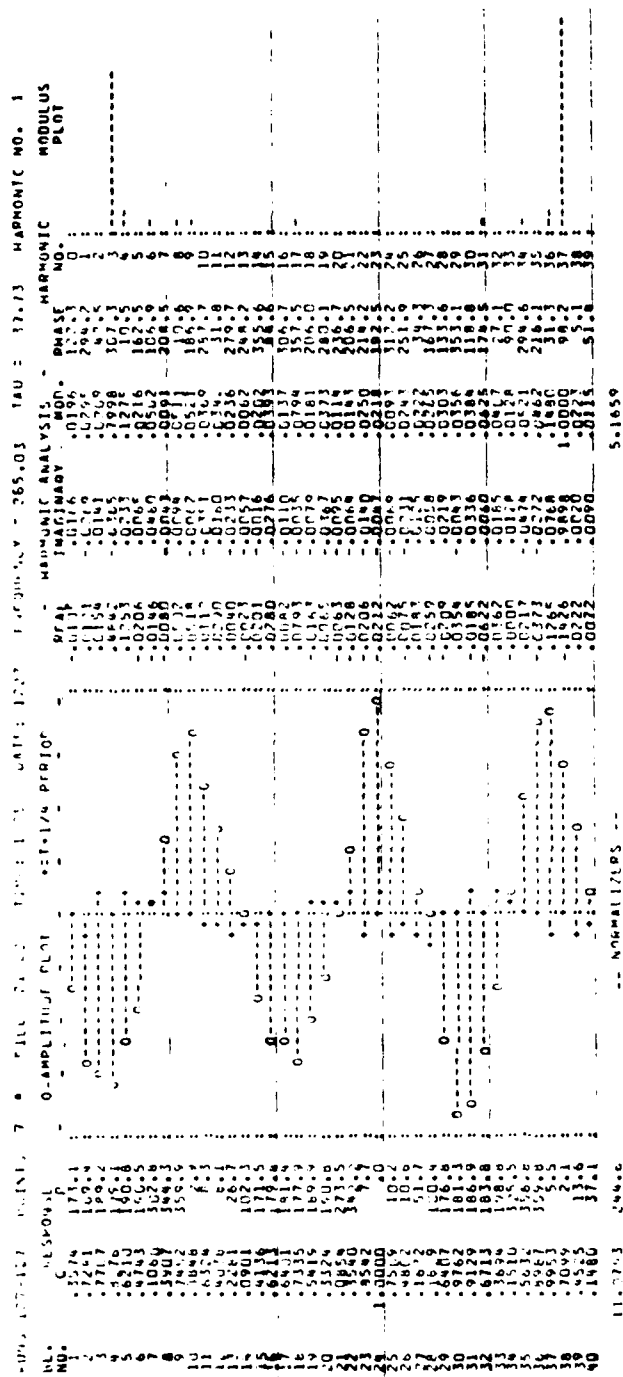


Figure 49 3ND Mode Shape of the Mistuned Assembly at 265.03 Hz in Evacuated Conditions at Zero Speed



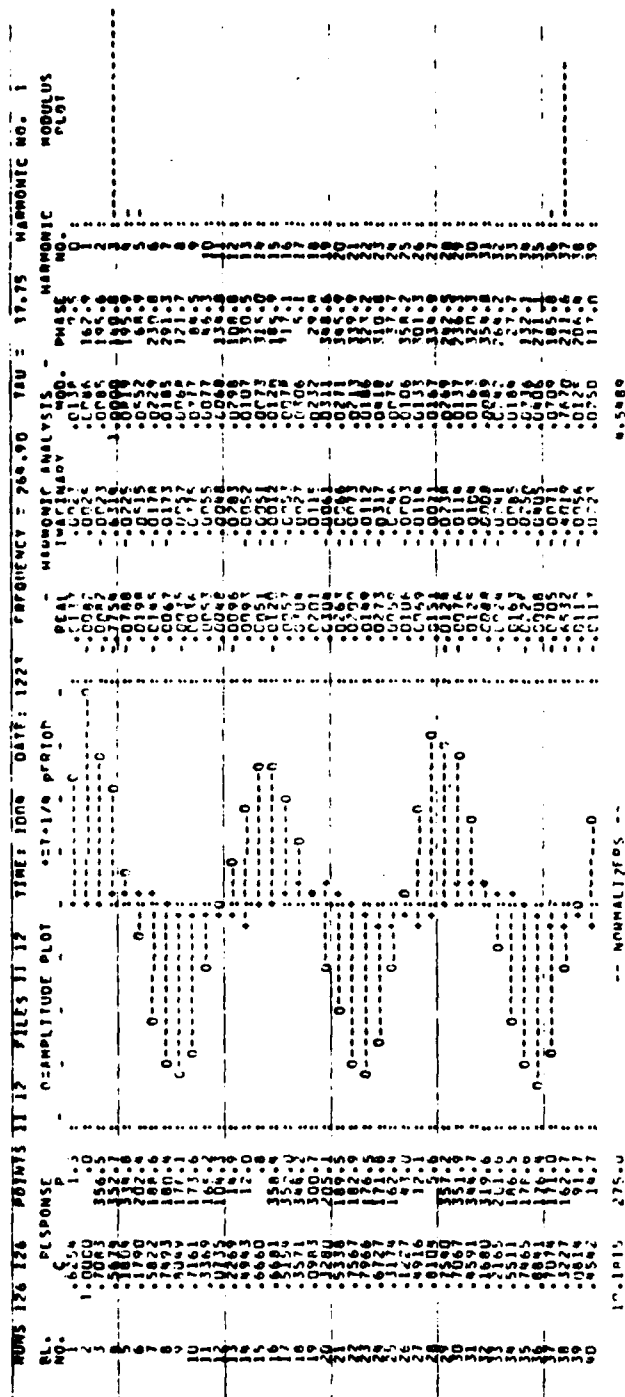


Figure 50 3ND Mode Shape of the Mistuned Assembly at 264.90 Hz in Evacuated Conditions at Zero Speed

TABLE 9

## SUMMARY OF MODAL CHARACTERISTICS FOR MISTUNED SYSTEM IN RIG A

			MODAL CHARACTERISTICS				
			TEST CONDITIONS - RPM/PRESSURE (Torr)				
EXCITATION			0/ 760	0/22	560/22	1050/22	1200/22
STATIONARY	2ND TWIN 1	Frequency (Hz)	189.2	190.1	190.6	194.3	195.4
		Position ( $\theta^{\circ}$ )	21.2	22.4	24.2	25.2	64.8
		Trav comp (%)	0.5	0.4	16.1	33.0	36.0
		Damping ( $\eta$ )	0.0063	0.0039	0.0052	0.0050	0.0051
		Blade $N^{\circ}$	23	24	23	24	24
STATIONARY	2ND TWIN 2	Frequency (Hz)	187.6	188.4	188.7	192.3	193.5
		Position ( $\theta^{\circ}$ )	65.9	65.5	67.4	69.8	-18.7
		Trav comp (%)	0.3	1.0	13.8	28.7	37.6
		Damping ( $\eta$ )	0.0064	0.0059	0.0053	0.0052	0.0052
		Blade $N^{\circ}$	29	29	29	18	29
STATIONARY	3RD TWIN 1	Frequency (Hz)		265.0	265.6		268.5
		Position ( $\theta^{\circ}$ )		-34.9	-13.0		51.0
		Trav comp (%)		12.5	2.4		5.7
		Damping ( $\eta$ )		?	0.002		0.0022
		Blade $N^{\circ}$		24	35		28
STATIONARY	3RD TWIN 2	Frequency (Hz)		264.9	265.4		267.8
		Position ( $\theta^{\circ}$ )		11.8	-30.9		-46.0
		Trav comp (%)		15.2	38.2		36.3
		Damping ( $\eta$ )		0.0030	0.004		0.0015
		Blade $N^{\circ}$		2	11		2
STATIONARY	4ND TWIN 1	Frequency (Hz)		282.5			285.3
		Position ( $\theta^{\circ}$ )		28.7			26.6
		Trav comp (%)		23.1			22.1
		Damping ( $\eta$ )		0.0021			0.0025
		Blade $N^{\circ}$		30			2
STATIONARY	4ND TWIN 2	Frequency (Hz)		278.6			284.3
		Position ( $\theta^{\circ}$ )		12.7			-1.0
		Trav comp (%)		3.2			46.0
		Damping ( $\eta$ )		0.0022			0.0025
		Blade $N^{\circ}$		28			22
SINGLE BLADE (#28)	"18"	Frequency (Hz)	55.9 (56.2)	55.9	59.5	67.4	70.5
		Damping ( $\eta$ )	0.0045 (0.0118)	0.0046	-	0.0059	0.0051
	"17"	Frequency (Hz)	277.8 (294.6)	278.4	278.8	277.5	279.4
		Damping ( $\eta$ )	0.0018 (0.0398)	0.0023		0.0043	0.0029

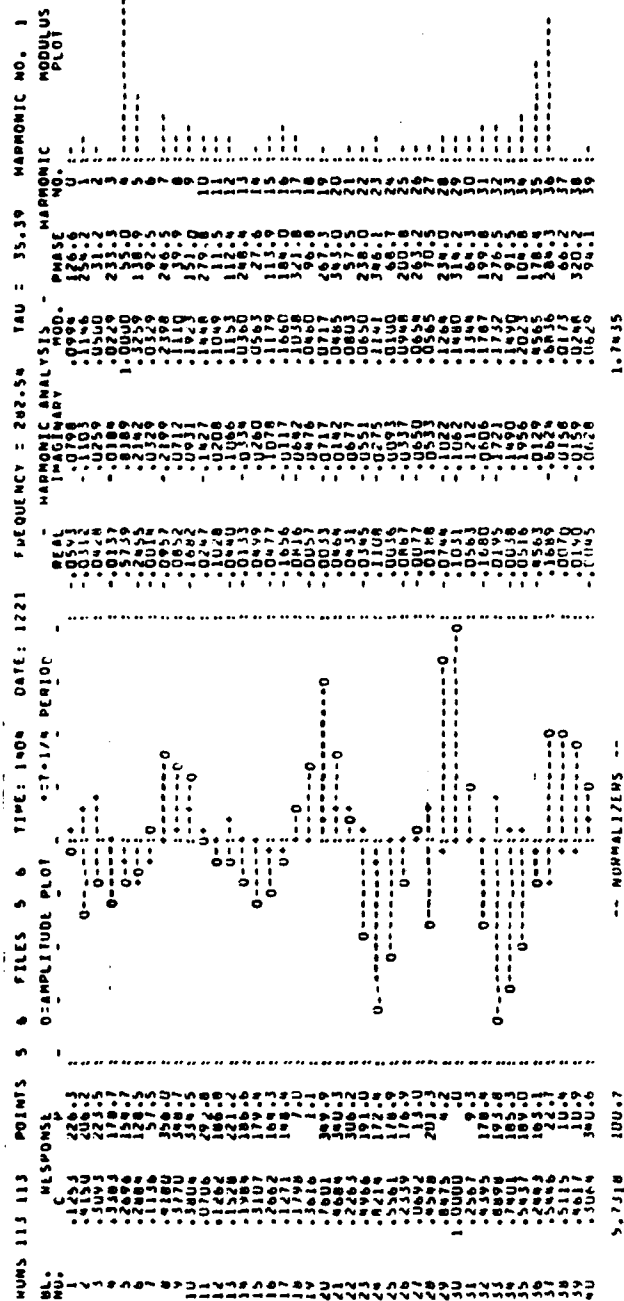


Figure 51 4ND Mode Shape of the Mistuned Assembly at 282.54 Hz in Evacuated Conditions at Zero Speed

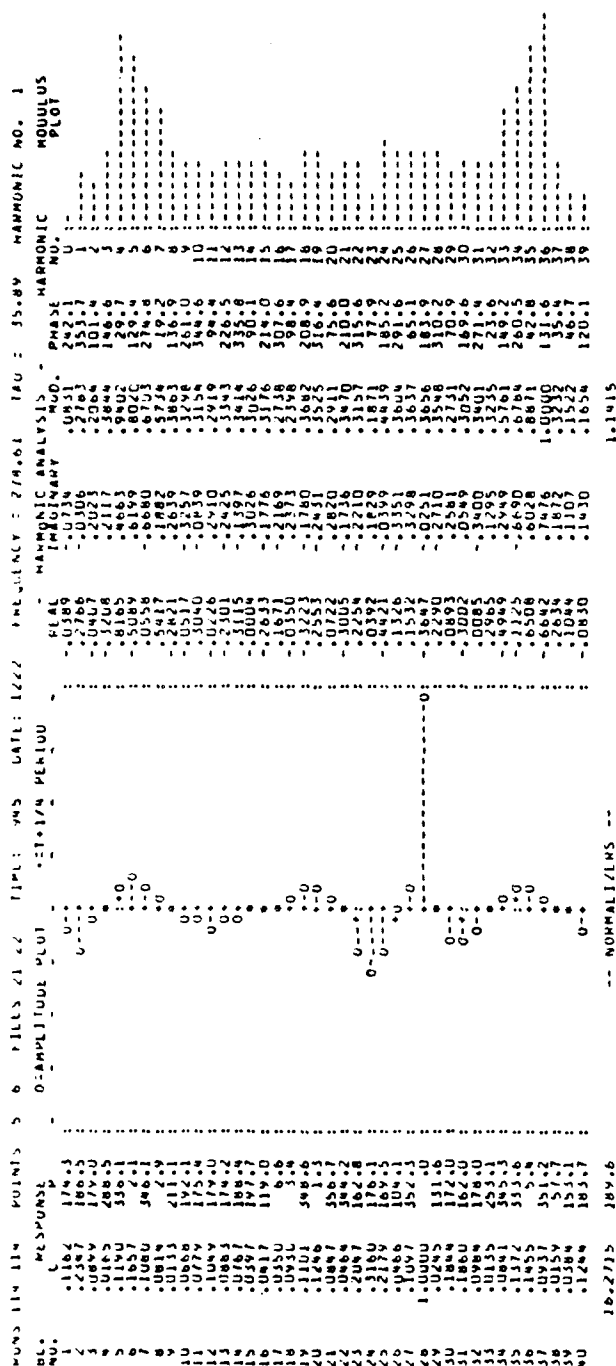


Figure 52 4ND Mode Shape of the Mistuned Assembly at 278.61 Hz in Evacuated Conditions at Zero Speed

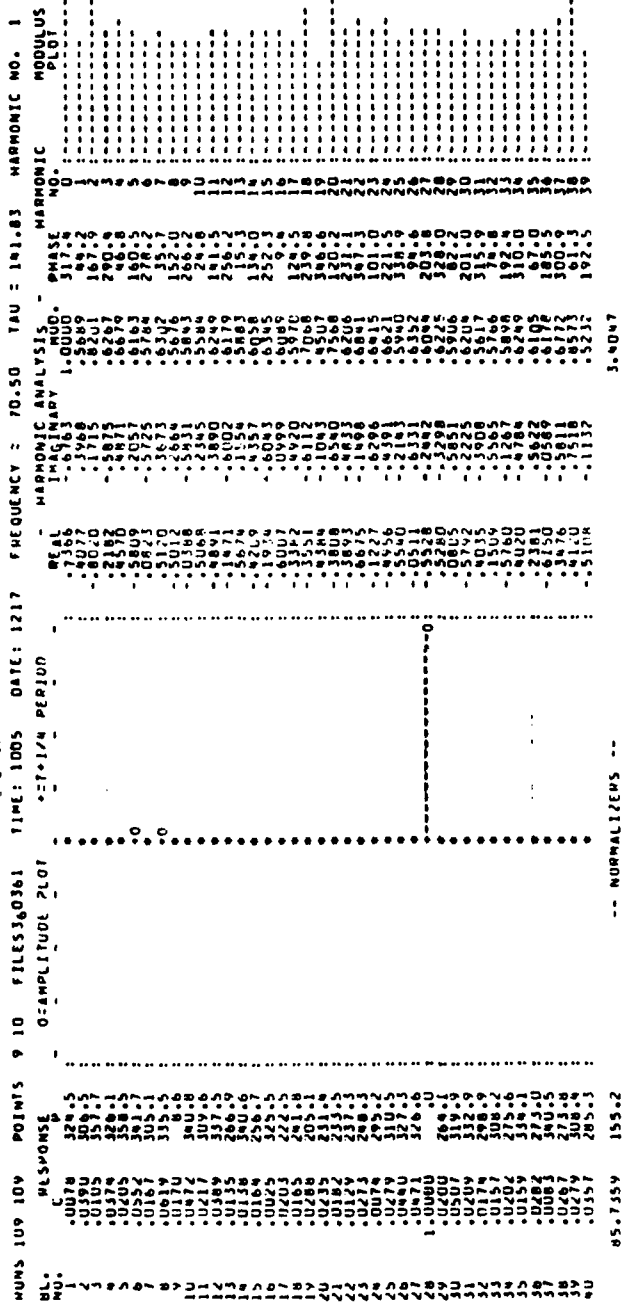


Figure 53 Assembly Response to Excitation of Blade #28 at 70.50 Hz in Evacuated Conditions at 1200 rpm

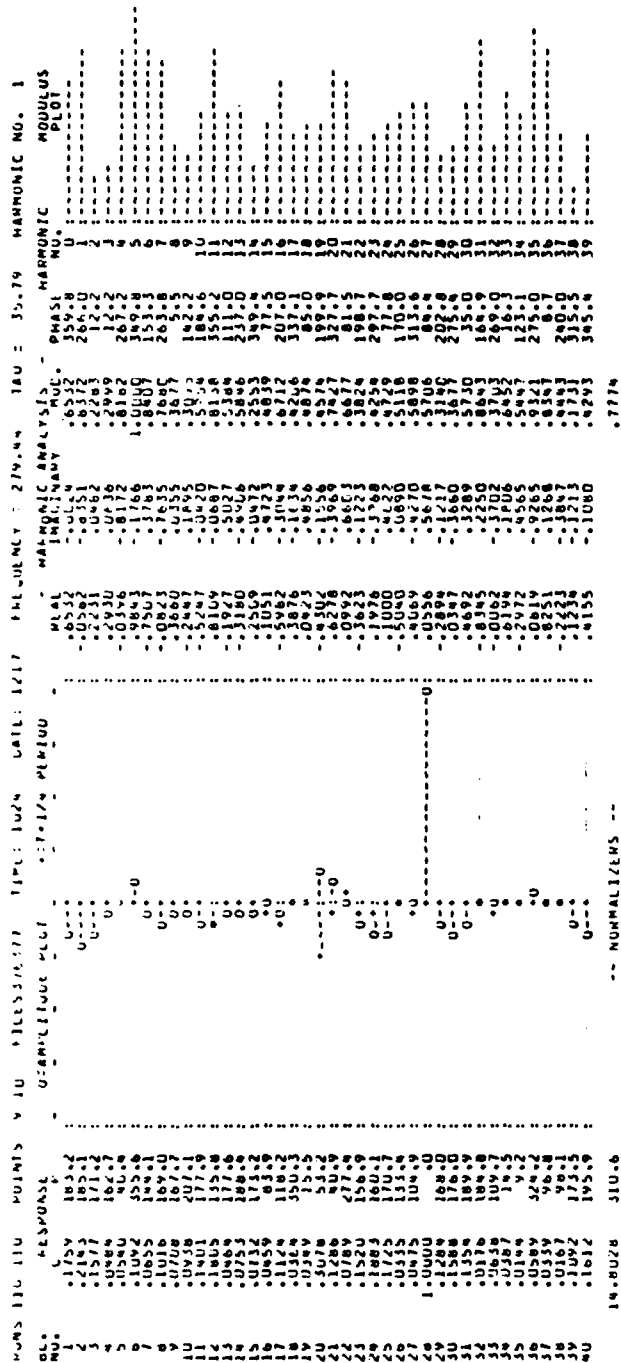
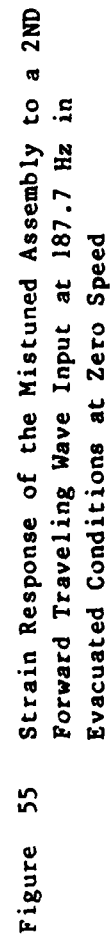


Figure 54 Assembly Response to Excitation of Blade #28 at 279.44 Hz in Evacuated Conditions at 1200 rpm



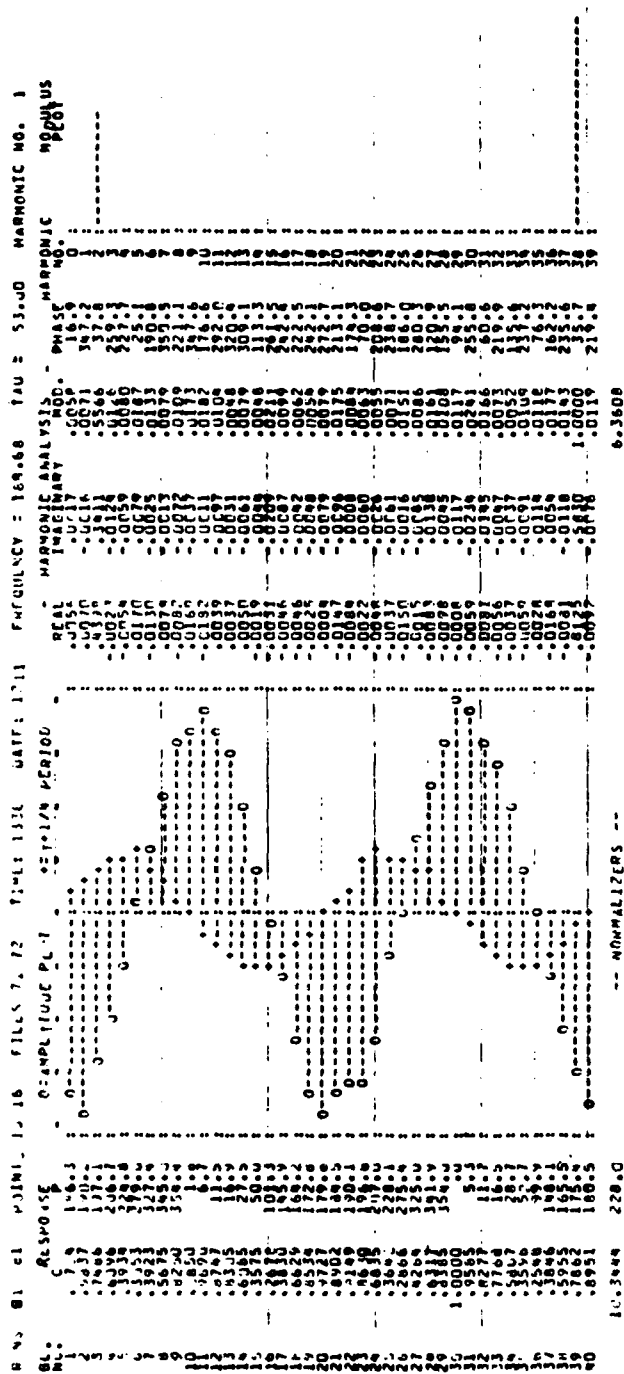


Figure 56 Strain Response of the Mistuned Assembly to a 2ND Forward Traveling Wave Input at 188.68 Hz in Evacuated Conditions at Zero Speed



waves proceed in opposite directions. However, this sum will not represent responses of a "rogue" blade which may experience a much larger strain than indicated by the strain distribution with an  $n$  nodal diameter pattern.

$A_2 + A_{-2}$  is plotted in Fig. 57 as a function of the frequency from the response of the fan to a two nodal diameter forward traveling wave. For the mistuned system, this response pattern has two peaks because of the twin modes occurring at two different frequencies. Thus, the contribution to the "system total" response will have unequal contributions from each of the twins reaching peaks at frequencies corresponding to the degenerate frequencies. Therefore, for the tuned system, the response  $A_2 + A_{-2}$  must have a single peak as is evident from Fig. 57.

This variation in the strengths of contributing harmonics  $A_2$  and  $A_{38}$  (or  $A_{-2}$ ) with input frequency is shown in Fig. 57. The harmonics can be seen to have two peaks each. The two peaks for each of the components  $A_2$  and  $A_{-2}$  are explainable for the mistuned system if the fundamental characteristic of a mistuned assembly is kept in mind, i.e., that it can exhibit two standing wave vibration modes of slightly differing frequencies but with similar patterns. Since each standing wave mode can be looked upon as a combination of two traveling waves, it then becomes clear that there are two frequencies at which each wave can reach its peak. For a perfectly tuned system subjected to a forward traveling wave, the response would be a forward traveling wave, the amplitude of which is controlled entirely by damping at the resonant frequency. With the assumptions of no aerodynamic damping and no uncertainties such as nonuniform rubbing, the mechanical system responds identically to forward and backward travelling waves. Therefore, for a perfectly tuned system, the harmonic  $A_2$  would peak at one frequency and the other harmonic  $A_{38}$  would be zero if the imposed excitation was a forward traveling wave and vice versa if the imposed excitation was a backward traveling wave. A useful parameter, therefore, for comparing the responses of different mistuned systems is  $A_{-n}/A_{+n}$ , the ratio of the strengths of the contributing harmonics i.e.,  $A_{-n}$  traveling in the opposite direction to that of the input and  $A_{+n}$  the harmonic traveling in the same direction. This ratio will be referred to below as the response wave ratio. In the case of a tuned system, the value of this ratio will be zero. For a system with twin modes, a plot of the variation of this parameter with frequency will show a single peak whose amplitude and bandwidth is observed to be inversely proportional to the frequency separation of the twin modes.

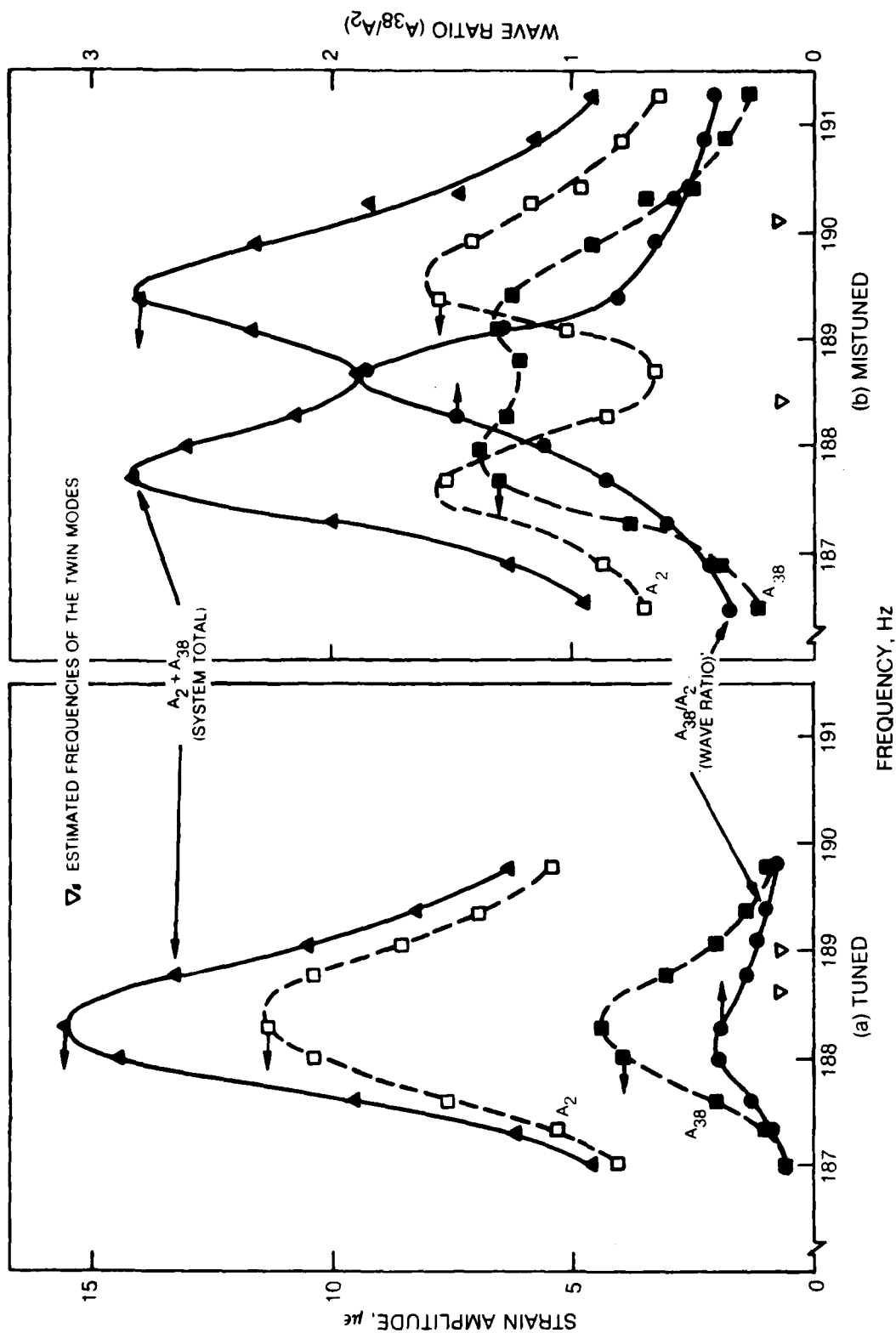


Figure 57. Variation of Response Wave Ratio, "System Total" Response, and Amplitudes of Contributing Harmonics with Frequency for Tuned and Mistuned Assemblies with Excitation Frequency (2ND Forward Traveling Wave Excitation in Evacuated Conditions at Zero Speed).

The single peak at 188.6 Hz with a peak level of 1.87, indicates that for frequencies between 187.9 and 189.2 Hz the strength of the backward traveling component is greater than that of the forward traveling component. The frequencies at which  $A_{38}/A_2$  reaches unity represent standing wave responses.

The same parameter calculated from the corresponding run (Run 11) for the "initially tuned" system is also shown in Fig. 57. Since this system is still mistuned, but to a lesser degree, its characteristic is similar, with a single peak in the plot of  $A_{38}/A_2$ . For reference, the estimated frequencies of the twin modes for each system are included in Fig. 57. They occur at frequencies which are higher than either of the corresponding peaks in the contributing harmonics.

The results for the case with a backward traveling wave excitation (Run 82) were plotted and the same peak frequencies were obtained but with the contributing harmonics interchanged.

The maximum values of the response wave ratio were determined for all tests for which traveling wave excitation was used. Results obtained from the initially tuned and mistuned system were analyzed. These values, obtained directly from the data point results with no interpolation between the points, are tabulated in Table 10. Examination of Table 10 indicates that more uniform values of the wave ratio were obtained for the "tuned" assembly, possibly because of the irregularity (single blade response, etc.) of the higher modes in the mistuned assembly. In general, it was found that the wider spaced twin modes resulted in the highest values for the response wave ratio.

Loss factors were determined from polar plots of individual blade responses for 2ND and 4ND traveling wave excitation, and are given in Table 11 together with their associated frequencies. Comparing the values with those obtained from standing wave excitation (See Table 9) indicates that in general there is close agreement.

TABLE 10. MAXIMUM VALUES OF RESPONSE WAVE RATIO AND CORRESPONDING FREQUENCIES FOR ALL TEST CONDITIONS FOR TUNED AND MISTUNED ASSEMBLY EXCITED WITH TRAVELING WAVES.

EXCITATION		SPEED/PRESSURE RPM/Torr	"TUNED" ASSEMBLY"		MISTUNED ASSEMBLY	
ND	DIRECTION		FREQUENCY	WAVE*	FREQUENCY	WAVE*
			Hz	RATIO	Hz	RATIO
2	FWD	0/760	187.7	0.43	188.5	1.49
2	BWD	0/760			188.3	1.52
2	FWD	0/22	188.0	0.40	188.7	1.85
2	BWD	0/22			188.7	1.50
2	FWD	570(560)/22	189.0	0.35	189.5	1.61
2	BWD	570(560)/22			189.7	1.58
2	FWD	1050/22	191.6	0.38	192.3	1.77
2	BWD	1050/22	191.8	0.40	193.5	1.51
2	FWD	1200/22	193.1	0.46	193.4	1.60
2	BWD	1200/22			194.6	1.59
3	FWD	0/760	265.0	0.55		
3	FWD	0/22	265.3	0.49	264.8	0.64
3	BWD	0/22			264.5	0.33
3	FWD	570(560)/22	265.3	0.59	265.3	0.68
3	BWD	570(560)/22			265.3	0.68
3	FWD	1050/22	266.7	0.19		
3	FWD	1200/22	268.5	0.29	268.2	1.04
3	BWD	1200/22			268.9	1.16
4	FWD	0/760	278.6	1.80		
4	FWD	0/22	279.4	1.91	278.6	1.24
4	BWD	0/22				
4	FWD	570(560)/22	280.8	1.82	281.1	0.31
4	BWD	570(560)/22	280.8	2.88		
4	FWD	1050/22	282.1	1.86		
4	FWD	1200/22	283.3	2.65	283.8	0.56
4	BWD	1200/22			283.8	1.29

Note: Wave ratio is the ratio of contributing harmonics

TABLE 11. LOSS FACTORS AND FREQUENCIES OF MAXIMUM INDIVIDUAL BLADE RESPONSE FOR THE MISTUNED SYSTEM WITH 2ND AND 4ND TRAVELING WAVE EXCITATION.

EXCITATION		SPEED/PRESSURE RPM/Torr	RESPONSE FREQUENCY Hz	LOSS FACTOR $\eta$
ND	DIRECTION			
2	FWD	0/22	189.4	0.0042
			187.7	0.0053
2	BWD	0/22	189.0	0.0042
			187.7	0.0053
2	FWD	1200/22	194.9	0.0052
			193.2	0.0052
2	BWD	1200/22	195.2	0.0051
			192.7	0.0057
4	FWD	0/22	280.8	0.0028
			277.5	0.0018
4	FWD	1200/22	285.3	0.0035
4	BWD	1200/22	285.4	0.0035
			284.6	0.0035

## X. MEASUREMENT OF MOTION AT SHROUD INTERFACES

This section describes the results from the phase of the program that was aimed at measurement of steady as well as vibratory motions at ten successive shroud interfaces of the R-80 fan. This project followed a successful development of an instrumentation system which was used to measure shroud motions on a single fan in which the shroud was allowed to rub on a "rigid" interface. The results from that pilot project established that extremely small motions (as small as  $50 \times 10^{-6}$  in.) could be measured. The motion sensor configuration consisted of a gallium arsenide photo-emitting diode and silicon position sensing detector pair mounted side by side on a shroud. A signal processing electronic circuitry was developed to provide the x, y positions of a motion from each detector. The measurement range target was  $\pm 40$  mils with better than 1 mil resolution in the frequency range of dc to 2 kHz. In the current experiment, ten such units were designed and fabricated. The objective was to obtain, in vacuum, measurements of motion at successive shroud interfaces of the R-80 fan at several rotor speeds up to 1200 rpm.

### 1. System Design and Fabrication

As stated above the motion sensor configuration used in this study consisted of a gallium arsenide photo emitting diode (Texas Instruments Type TIL24) and silicon position sensing detector (UDT Type PIN-SC/4D) pair mounted side by side in small aluminum block housings. The installation is shown in Fig. 58. The detectors were located in separate recessed holes machined into a mounting block/housing and held in position with quick drying epoxy. The light emitting diodes were each mounted in a 0.25 inch diameter disk of copper clad circuit board and were then epoxied into recessed holes machined in the diode housing. Great care was taken to maintain the alignment of the diode/detector pairs to give a dc offset of not greater than 10 mils in each axis. This offset was later nulled using the adjusters on the pre-amplifiers. The design of the housing, is shown in Fig. 59. Ten such sensor assemblies were fabricated.

The details of the signal processing circuitry are shown in Fig. 60. The position reference is provided by an infrared light emitting diode (TIL24) requiring approximately 10 mA of current to produce 1 mW of optical output power. The centroid of the emitted light beam is sensed by the UDT two-axes position sensing photo-detector. Each axis of the detector has two outputs which are amplified to provide adequate signal level. The amplified detector outputs were transferred to the signal conditioning circuits via slip rings. Fifteen slip rings were needed for the complete system. The

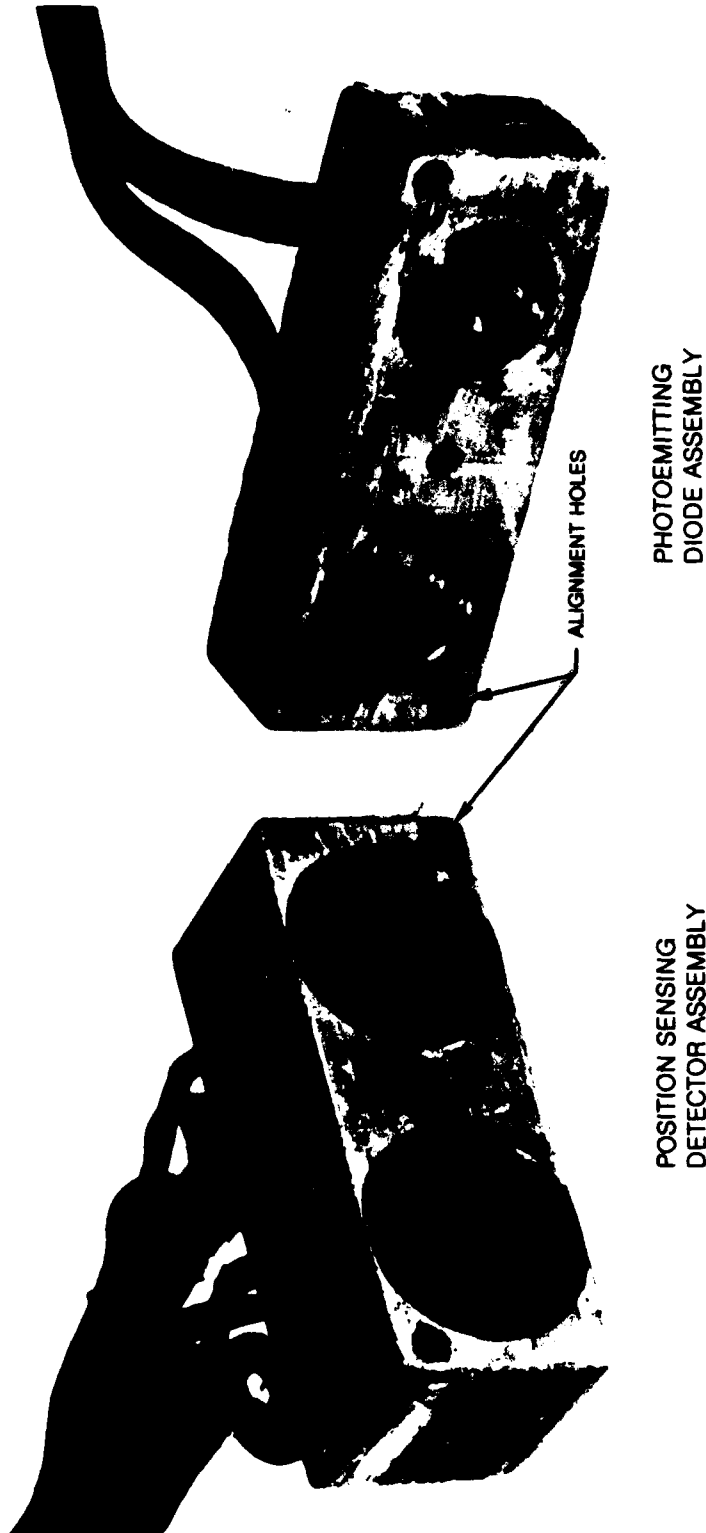
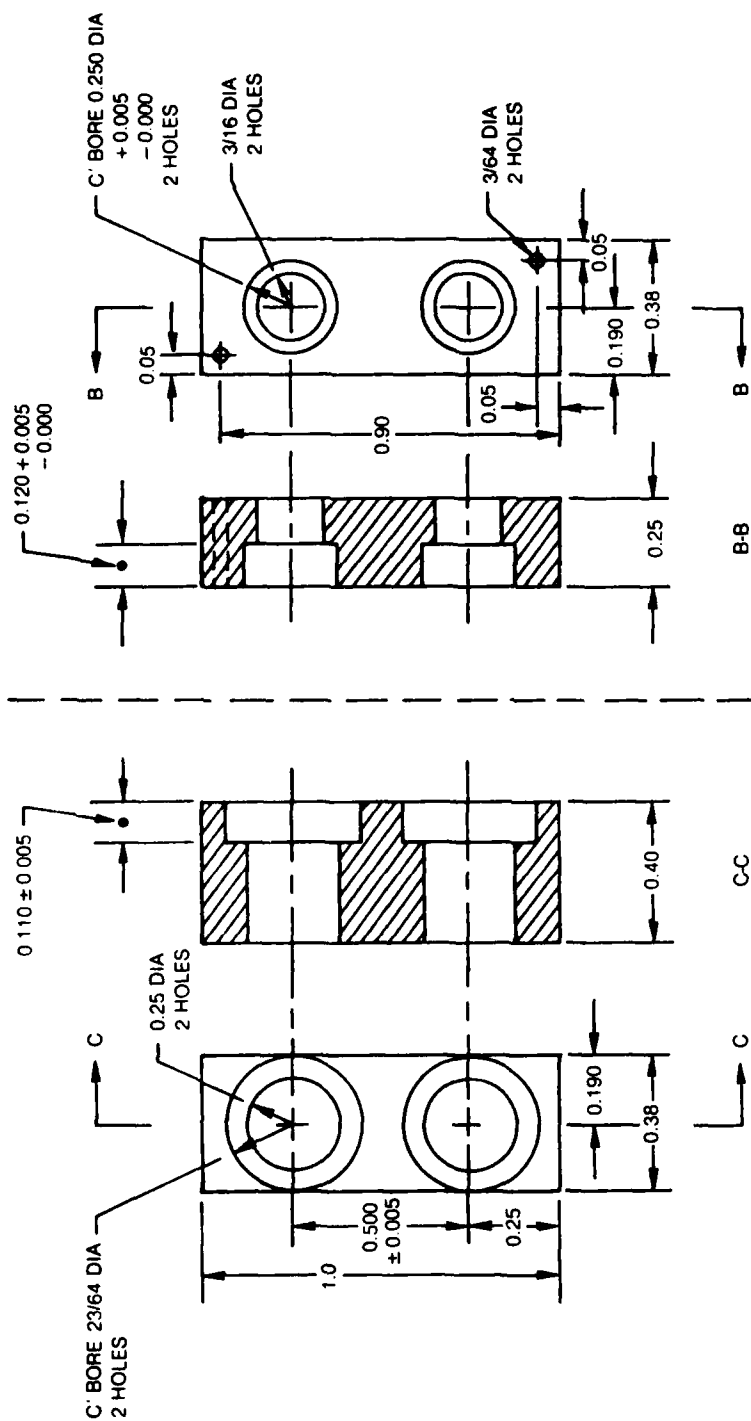


Figure 58 Shroud Motion Measurement Device

MATERIAL: ALUMINUM ALLOY  
DIMENSIONS: INCHES



b) LED HOUSING

a) DETECTOR HOUSING

Figure 59 Motion Sensor Housing Design



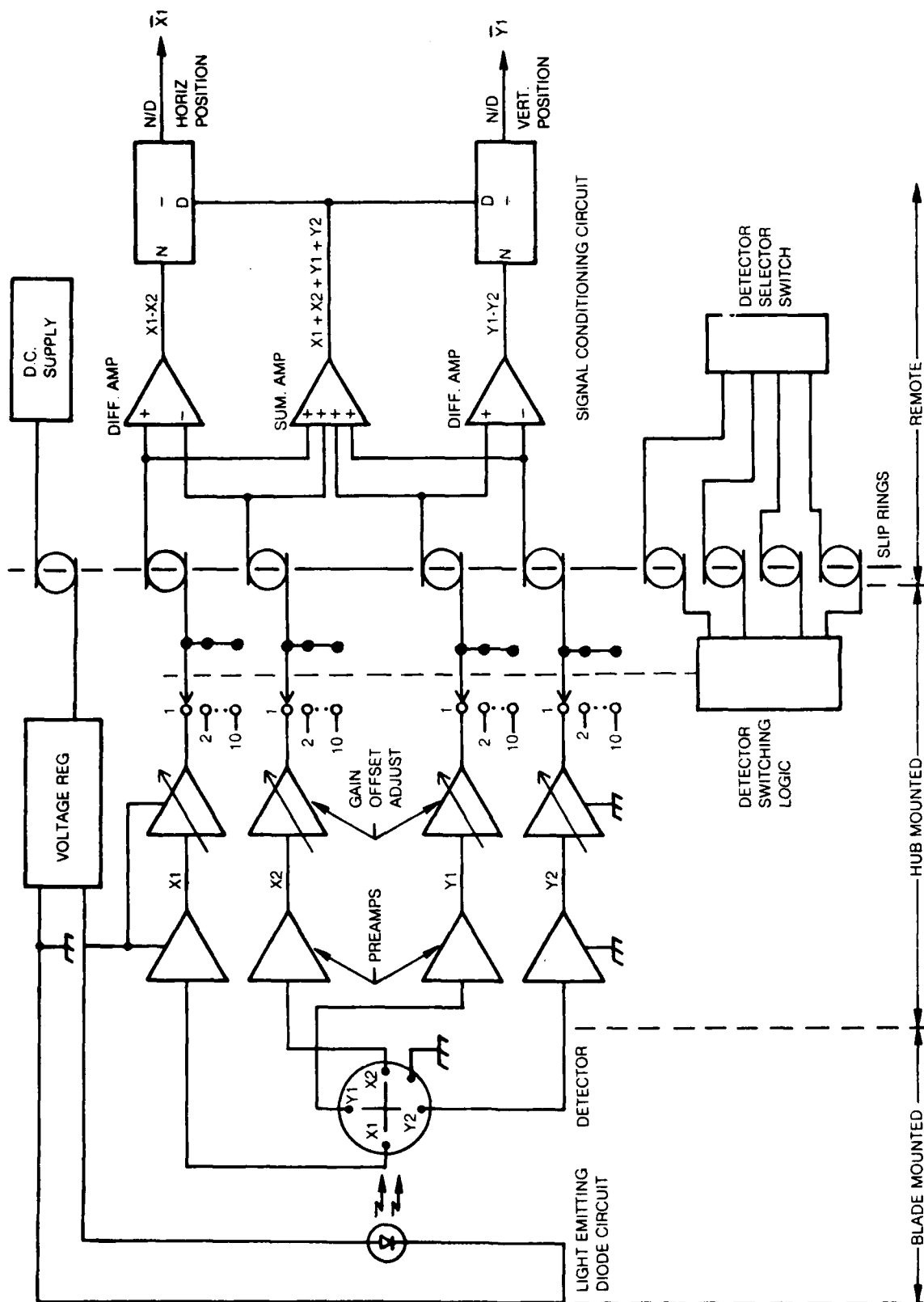


Figure 60 Motion Measurement System Block Diagram

voltage difference between the outputs of each axis provides the X and Y position information. Since the detector outputs are directly proportional to both the position and intensity of the incident light beam, the intensity component must be removed to eliminate errors due to emitter degradation, current fluctuations and the gradual accumulation of dust and grease between the emitter and detector. The intensity component is removed by dividing each axis output signal by the sum of the detector outputs. The divider outputs give purely positional information with optical power fluctuations of up to 20 to 1. The sum and difference amplifiers used to perform the above functions were those built during the feasibility study and were located in a remote control console. A remote channel select switch enabled the four response components from any one of the ten sensor assemblies to be output from the control console via a switching circuit mounted on the hub.

The sensor assemblies were connected by means of flat ribbon cables to their pre-amplifiers which were mounted in two tiers on the hub. Separate gain and offset adjustment stages for each detector were incorporated into the preamplifiers. Hub mounted voltage regulators supplied dc power to the light emitting diodes, the pre-amplifiers and switching circuitry.

## 2. System Calibration

Static calibration of the 40 diode/detector pairs was performed with the diode and detector attached to an optical mount fitted with two micrometer screw gages allowing relative motion between the two components in two orthogonal axes. The output voltages were read on a digital voltmeter. A gap of 12 mm was maintained between the diode and detector housing during calibration. The output sensitivity was determined for displacements input along each of the two sensor axes (X and Y). The results are given in Table 12 and show that the sensitivities varied from 117 to 124 millivolts per mil (0.001 in.) between any two sensors axes. The standard deviation of the values about a mean value of 121.6 was 1.76. The maximum linear travel is shown to be at least  $\pm 15$  mils with most sensors capable of  $\pm 20$  mils.

For reduction of dynamic data, a nominal value of 122 mV/mil was used for the sensitivity of each sensor. It will be shown later that during testing at high speeds, the static relative displacement of the shrouds sometimes exceeded the linear range of a particular sensor and hence a post test calibration was performed. The main purpose of this was to determine the effective sensitivities of the sensors over the range of static deflection. This will be discussed in the Test Results Section.

The fully instrumented assembly is shown in Fig. 61. The location of the sensors at the interfaces is shown in Fig. 62.

TABLE 12

SUMMARY OF MEASUREMENT SYSTEM PRE-TEST  
STATIC CALIBRATION RESULTS

O/P CHANNEL No/AXIS	LOCATION - BLADE NOS.	SENSITIVITY mV/mil		LINEAR RANGE mils	
		Sensor #1	Sensor #2	Sensor #1	Sensor #2
0/X 0/Y	25-26	122 122	123 124	± 20 15	± 20 15
1/X 1/Y	24-25	122 124	122 121	20 15	20 20
2/X 2/Y	27-28	120 124	122 124	20 20	20 20
3/X 3/Y	26-27	122 122	122 123	15 20	20 20
4/X 4/Y	29/30	119 120	121 120	20 20	20 20
5/X 5/Y	28/29	117 123	120 124	20 15	15 20
6/X 6/Y	31-32	120 122	120 124	15 20	20 20
7/X 7/Y	30-31	119 123	121 123	20 15	15 15
8/X 8/Y	32-33	119 118	122 120	20 20	15 15
9/X 9/Y	33-34	123 121	122 123	20 20	20 20

AVERAGE SENSITIVITY = 121.6 mV/mil



Figure 61 Fully Instrumented R-80 Fan Assembly

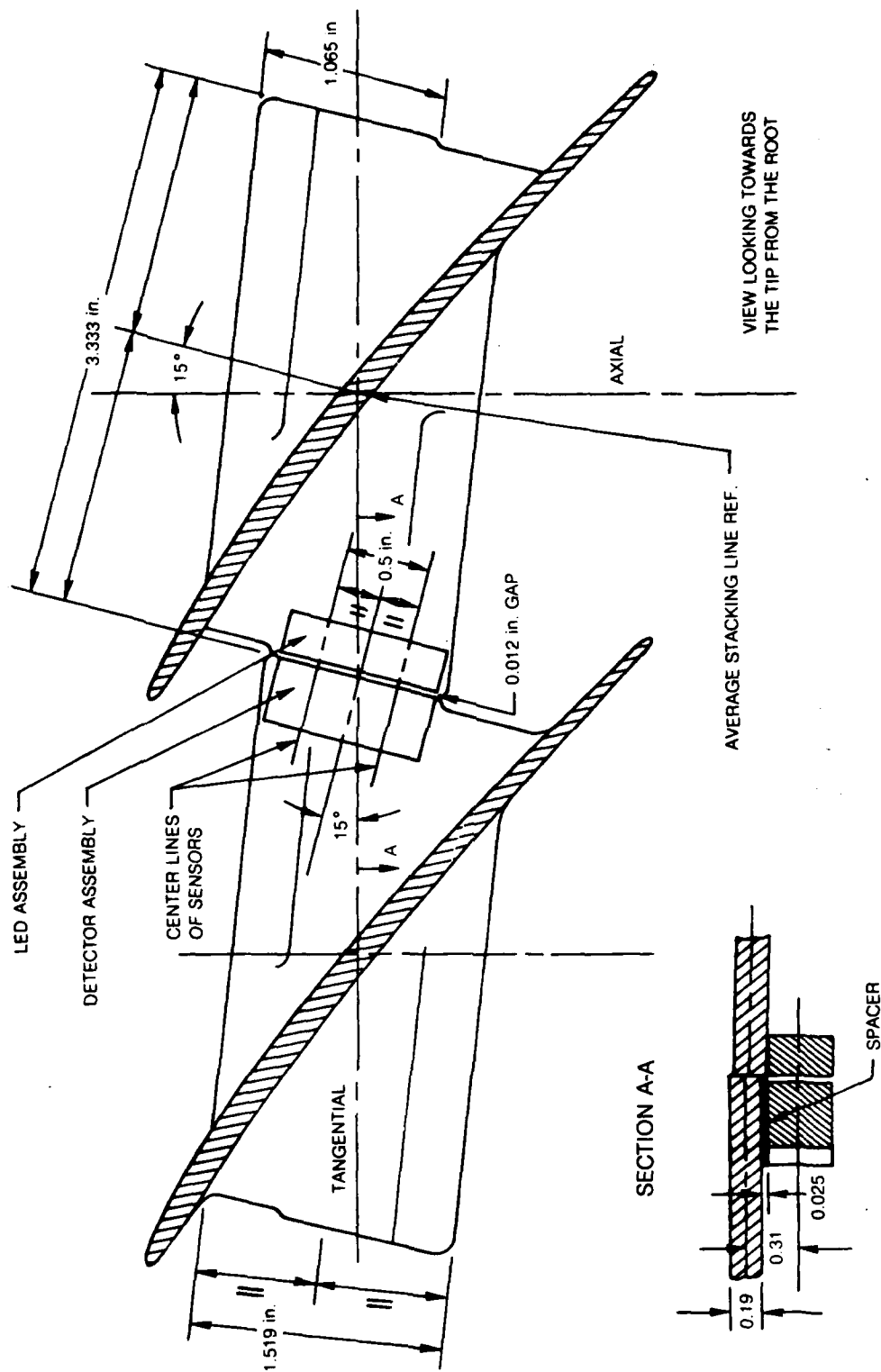


Figure 62 Shroud Geometry and Location of Motion Sensors at Interface

### 3. Data Acquisition and Reduction

Table 13 lists the several test conditions used in the program. Initial testing of the fully instrumented R-80 bladed disk assembly showed that the recording of results using an oscilloscope was completely impractical considering (a) the volume of data in terms of number of channels and number of data points to be output; (b) the need to compare strain distributions at test points corresponding to those recorded during previous mistuned assembly tests. Also, with the emphasis on second family responses, a method of data reduction was required to extract the extremely small shroud motion signals from the recorded signals. The 26 channel transient data system (ATLAS) which was used in the earlier R-80 spin tests was therefore brought on-line and used for recording the steady state strain and shroud motion data. The data recorded at each test point consisted of a pulse corresponding to the zero crossing of the positive going excitation input drive signal, four ac coupled shroud motion signals, seven strain response signals (odd numbered blades), four dc coupled shroud motion signals and the once-per-rev pulse. A second record at the same frequency enabled the strains from the other set of blades (even numbered) and the shroud motion data from all the blades, ten records were required at the same input frequency. A digital record consisted of 1024 samples from each analog signal taken at a rate of 10K samples per second for first family data and 20K samples per second for the second family. The dynamic response data were filtered using the built-in 2 kHz low pass filters.

The data reduction and analysis plan is shown in Table 14. A number of FORTRAN code programs were written for running on the UNIVAC 1100 computer to read the digital data on magnetic tape and perform the various reductions shown in Table 14. The first stage in the reduction process was to perform a Fourier Analysis of each signal and determine coefficients up to the 12th harmonic (0-12). The static deflections of the shrouds were obtained from the output at this stage. The second step was to determine the modulus and phase of each strain response for the first harmonic component and present the spatial distributions in the form of stickplots and in a format similar to that used in the reduction of data from the previous mistuned assembly tests. These results were compared in order to confirm that the desired test points had been recorded. The third step was to plot the shroud motion time history of a sensor assembly over one period of the input signal at any blade location reconstituted from one or more of the Fourier coefficients. Another form of the time history output used was the X-Y plot of displacements at each sensor (two plots per shroud interface). The orientation of the axes is as shown in Fig. 63. These plots show the actual motion of the shroud interface. Finally, the modulus and phase were calculated for each shroud displacement component at each frequency and the spatial distribution

TABLE 13 SUMMARY OF SHROUD MOTION MEASUREMENT TESTS PERFORMED ON MISTUNED FAN ASSEMBLY

FORCING		TESTS PERFORMED				
CONFIGURATION	NODAL DIAM.	TEST CONDITIONS - RPM/PRESSURE (TORR)				
FIRST FAMILY OF MODES	4	0/15	560/13	1050/13	1163 <sup>*</sup> /13	1200/13
		1,2,3,4			1,3	
SECOND FAMILY OF MODES	2	1,2,3,4,5	1,2,3,4	1,3		1,3,5
	3	1,2,3,4	1,3	1,3		1,3
	4	1,2,3,4	1,3			1,3

KEY TO TEST:

- 1 = BACKWARD TRAVELING WAVE - FREQUENCY RESPONSE
- 2 = FORWARD TRAVELING WAVE - FREQUENCY RESPONSE
- 3 = BACKWARD TRAVELING WAVE - VARIATION AROUND QUADRANT
- 4 = FORWARD TRAVELING WAVE - VARIATION AROUND QUADRANT
- 5 = STATIONARY WAVE EXCITATION OF TWIN MODES - VARIATION AROUND QUADRANT

NOTE \* INTEGRAL ORDER SPEED FOR FIRST FAMILY 4ND MODE

TABLE 14

## DATA REDUCTION AND ANALYSIS PLAN

- 2 Types of Test    1. Frequency response ~ phase, amplitude, frequency, damping  
                           2. Resonant condition ~ spatial characteristics

SG = strain data  
 SM = shroud relative displacement data

REDUCTION	PROGRAM NAME	ANALYSIS
1. Compute Fourier coefficients (up to 12 <sup>th</sup> harmonic) of integrated signals from SG and SM data	D2T	Compare relative sizes of coefficients. Examine and tabulate static displacements
2. Produce stick plots of strain responses on the 14 blades for which data are obtained	DTEST	Compare with 40 blade data and assess resonant (or test point) condition
3. Plot reconstituted time histories for one or more coefficients for SM data in form of displacement vs. time and X vs. Y.	DTEST3	Examine time response w.r.t. number of harmonics and noise content. Examine two dimensional shape of shroud slip motion.
4. Calculate modulus and phase of SM (X1, Y1, X2, Y2 and $\theta$ ) for all test points and for 1st harmonic and produce stickplots of each component	DTEST5 DTEST6	Examine slip motion around the fan assembly (10 blades) and compare with strain and relative strain data.



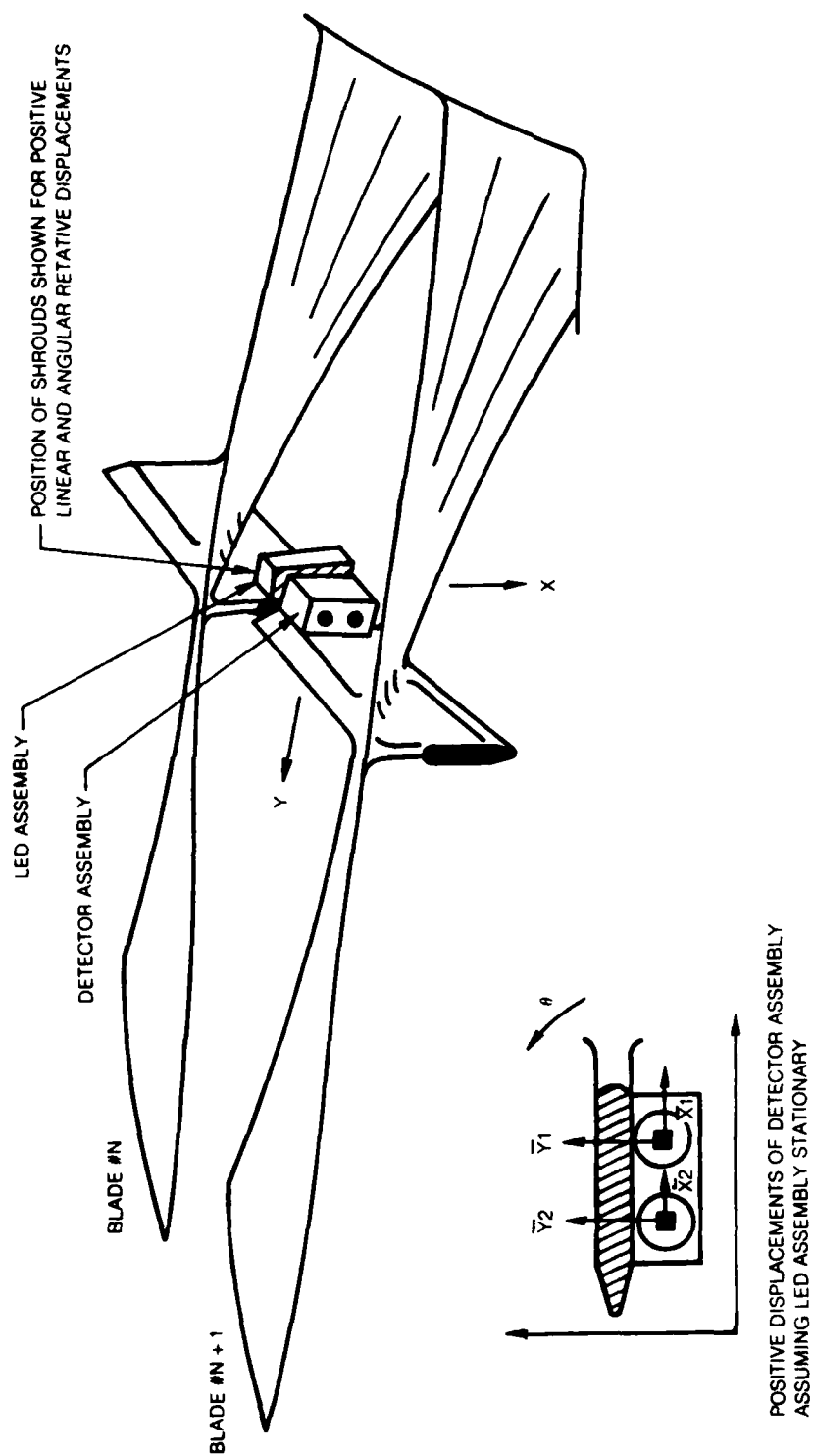


Figure 63 Definition of Shroud Displacement Axis System

presented in stickplot form. It was found, however, that this type of presentation was not as useful in interpreting the response as had first been hoped because of the complex distribution of interblade phase angles. A better means of displaying the response data was in the form of plots of modulus and phase for each blade around the quadrant.

It should be noted that the motions recorded are not the same as those on the shroud rubbing surface. Figure 62 shows that the sensors are located 0.31 in. below the shroud centerline and 0.5 in. apart. Assuming no distortion of the shrouds and/or sensor housings, the linear and angular deflections on the shroud can be expressed in terms of the measured deflections as follows:

$$\theta = \frac{\bar{Y}_1 - \bar{Y}_2}{0.5 + \bar{X}_1 - \bar{X}_2}$$

$$\bar{X}_1 = \bar{X}_1 - 0.31 \sin \theta_s$$

$$\bar{X}_2 = \bar{X}_2 - 0.31 \sin \theta_s$$

$$\bar{Y}_1 = \bar{Y}_1 - 0.31 (1 - \cos \theta_s)$$

$$\bar{Y}_2 = \bar{Y}_2 - 0.31 (1 - \cos \theta_s)$$

Where  $\bar{X}_1$ ,  $\bar{Y}_1$ ,  $\bar{X}_2$ ,  $\bar{Y}_2$  are the components of displacement (inch units) at the shroud centerline.

$\bar{X}_1$ ,  $\bar{Y}_1$ ,  $\bar{X}_2$ ,  $\bar{Y}_2$  are the measured deflections converted to inch units,

$\theta$  is the relative angular displacement of the shrouds in radians.

In the results presented below, only displacements on the shroud rubbing surface are shown, except where specifically noted.

#### 4. Testing

Prior to spinning the assembly, blade alone tests were performed in air at zero speed on selected blades to determine what effect the motion sensors and associated wiring installation had on the first blade bending and first blade torsion modal characteristics. The blades having the highest and lowest modal frequencies and two having intermediate frequencies were selected for investigation. All blades but the one being excited were detuned by placing heavy masses at their tips. The results, as shown in Table 15,

TABLE 15

COMPARISON OF INDIVIDUAL BLADE MODAL FREQUENCIES  
AND DAMPINGS BEFORE AND AFTER SENSOR INSTALLATION

	FIRST BENDING MODE				FIRST TORSION MODE			
BLADE #	FREQUENCY Hz	CHANGE %	DAMPING %	CHANGE %	FREQUENCY Hz	CHANGE %	DAMPING %	CHANGE %
28 B	56.224	+ 0.6	0.012	+42	294.6	- 0.5	0.040	-25
28 A	56.256		0.017		293.1		0.030	
29 B	64.696	+ 0.8	0.005	+20	318.4	+ 1.1	0.025	-8
29 A	65.185		0.006		322.1		0.023	
32 B	67.696	+ 1.2	0.005	0	314.9	- 0.4	ND	ND
32 A	68.503		0.005		313.6		0.010	
33 B	66.883	- 0.2	0.004	+50	315.7	+ 2.5	0.010	+100
33 A	66.742		0.006		322.1		0.020	
B = BEFORE; A = AFTER								

indicated that for the first bending mode, some frequencies apparently increased up to 1.2% with increases in damping ranging from 0 to 50%. For the first torsion mode, some frequencies increased up to 2.5% with variations in damping of -25 to +100%. Because of the considerable scatter in the results, it was concluded that factors other than the presence of sensors and wires were the primary causes of the changes noted and that no changes in the basic response characteristics of the assembly could be expected. The spin test results generally confirmed this conclusion.

Testing of the fan assembly in the mistuned condition with the shroud motion sensors installed on ten blades was accomplished at speeds of 0, 560, 1050, 1163, and 1200 rpm in vacuum conditions of about 13 torr. Modes up to the fourth order in the first and second families were investigated. The input levels used were 20% for first family modes and 60% for second family modes. The above test conditions corresponded to those used in the previous mistuned assembly tests. In all, sixty-four test runs were made, including runs with no input applied in order to assess the overall noise levels. A summary of the tests performed with corresponding test conditions, is given in Table 13.

In general, only backward traveling wave input excitation was used. However, for the second family 2ND mode, a standing wave input excitation was attempted at 0 and 1200 rpm.

Two types of tests were performed. The first was of the frequency response type with the shroud motion (X1, Y1, X2, Y2) at two blade interfaces being recorded as the input frequency was varied in discrete increments ( $\sim 8$ ) over the resonance (twin peaks) being investigated. In the second type of test, the shroud motion components at all the instrumented blades were recorded with the frequency tuned to one or other of the twin resonance peaks as indicated by the results from previous mistuned test runs.

All steady state data from the above tests were digitized and recorded on magnetic tape.

## 5. Noise Levels

The noise levels in the shroud motion measurement system were established by sampling the output from all sensors at all test speeds with no input applied. The data were recorded and reduced using the data reduction programs shown in Table 14. The results indicated that for first family responses, the maximum noise levels occurred at 1163 rpm and reached the equivalent of  $\pm 6$  micro in. (peak) in the first harmonic, however, this may have contained some structural response due to the assembly being run at integral order speed. In the second family responses, the maximum noise level in the first harmonic was about  $\pm 3$  micro in. peak. This obviously compromises the data for the second order response results where the maximum response is 9 micro in. (peak) and explains some of the erratic behavior in the plots. Because of the low signal to noise ratio existing (because of the extremely low response levels), the analysis of harmonics higher than the fundamental was not considered worthwhile. The ripples seen on the displacement time histories shown in Figs. 23, 27, 31, 35, 39 and 45 must be considered as noise and not response.

## 6. Presentation of Results

The amount of data produced by this test program is large and there are many different ways of reducing and presenting the results. The problem arises in choosing from many different response characteristics which manifested themselves. We are dealing with a complicated dynamic system and small changes in input frequency change the nature of the response; backward to forward traveling wave for example. It was determined early in the testing that two of the input parameters, namely input level and speed of rotation, were not significant in determining the nature of response. The basic reason for this is that the system is "tight" and is essentially quite linear within the range of input levels available. No change in the nature of the shroud relative displacement was noted even with the highest input level applied, the motion was essentially microslip and no evidence of stickslip was found. The effect of rotation was to increase the bearing load on the shroud surfaces by approximately 50% to 150 lbs at 1200 rpm and to realign them by less than 0.02 in. The effect of speed is therefore only presented in the static displacement results given in Figs. 64 and 65 and the effect of applied input force level is not considered.

For each shroud interface, the linear ( $\bar{X}$ ,  $\bar{Y}$ ) and angular ( $\theta$ ) relative static displacements at a point on the rubbing surface midway between the sensors are shown plotted against the rotational speed squared in Fig. 64. Since the sensors were not nulled at zero speed, the values shown are differences from the zero speed values.

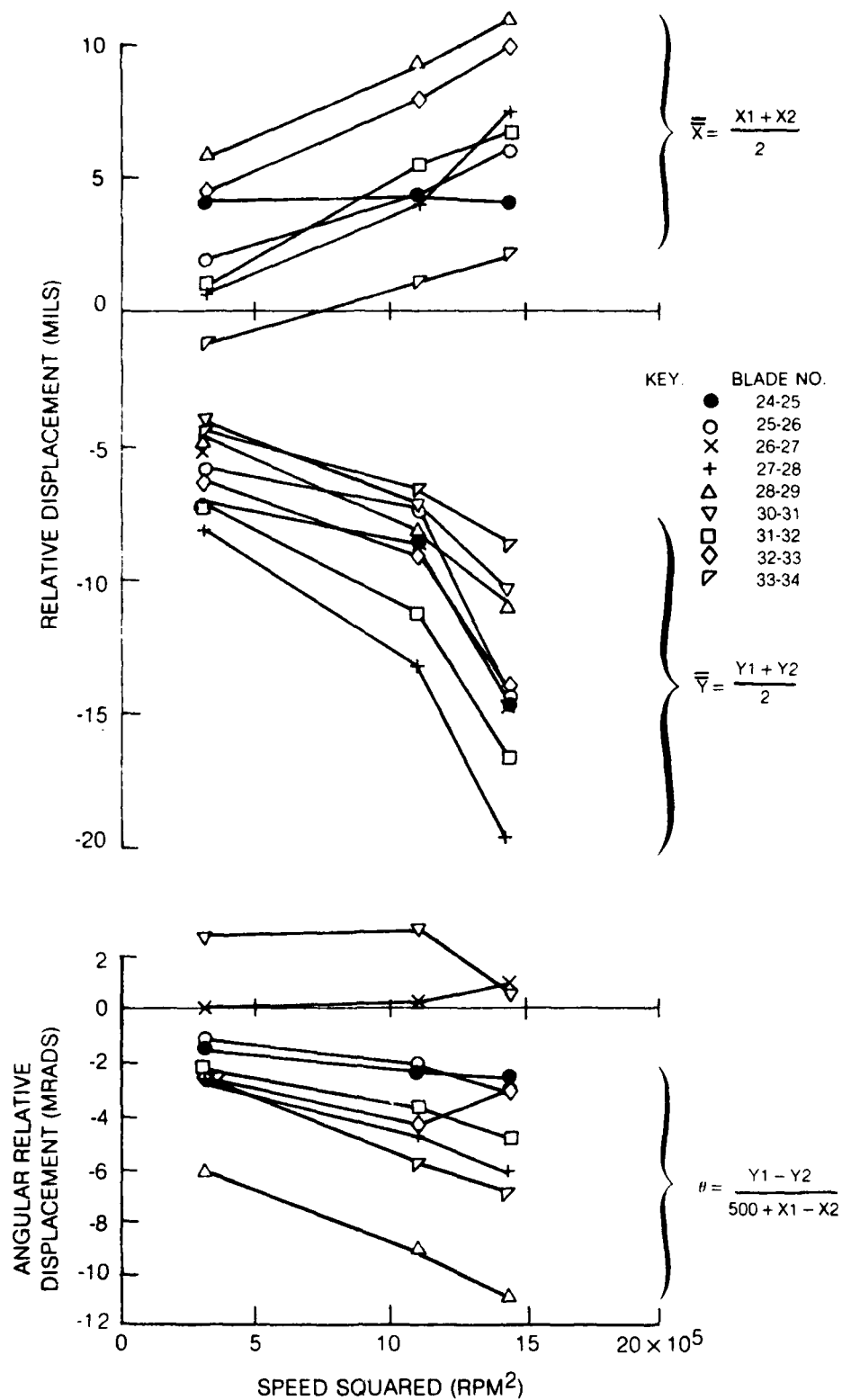


Figure 64 Variation of Averaged Values of Static Shroud Relative Displacements ( $\bar{X}$ ,  $\bar{Y}$  &  $\theta$ ) with Rotational Speed Squared

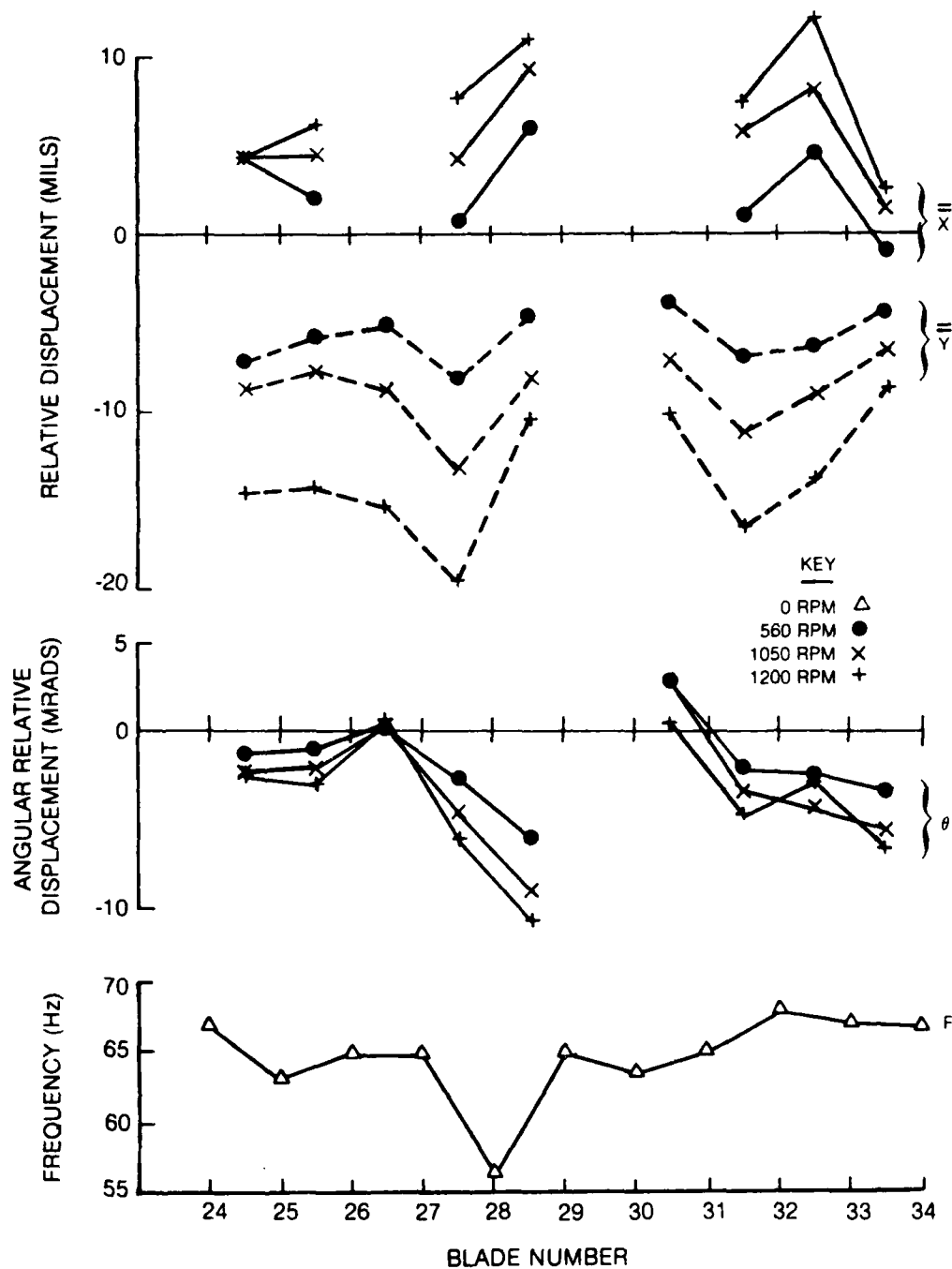


Figure 65 Spatial Variation of Averaged Values of Static Shroud Relative Displacements ( $X$ ,  $Y$  &  $\theta$ ) at Various Speeds and Individual Blade First Bending Modal Frequencies for Blades 24 through 34

Figure 65 shows the above displacements plotted against blade location for various speeds so that the spatial variation can be seen.

Six data samples are presented for the dynamic response. They are chosen on the basis of the nature of the blade response in terms of family, order and wave direction. The data samples are identified in Table 16. The nature of the response was determined indirectly as follows. During the testing, test points were chosen on the basis of tabulated data output from the previous mistuned tests. These reduced data showed the strain responses at all forty blades (modulus, phase and stickplot presentations) and also the results of a spatial harmonic analysis of the strain distribution at each test point (frequency). When the strain data from the present results were reduced in a similar format, the nature of the response in terms of traveling wave components was assumed to be that of the previous analysis where the strain distribution of the fourteen monitored blades most closely matched the previous results. Figures 66 to 77 show the blade strain distributions obtained from previous mistuned tests. It can be seen that the responses include predominantly stationary (with respect to the disk) waves in samples, 1, 3 and 6, and backward traveling waves in samples 2, 4 and 5.

The dynamic response data are presented as a set of four figures for each data sample as described below:

1. Modulus and phase of the X-axis components of shroud displacement of each shroud interface plotted against blade number or location (Figs. 78, 82, 86, 90, 94, 98).
2. Modulus and phase of the Y-axis components plotted against blade number (Figs. 79, 83, 87, 91, 95, 99).
3. The time history reconstituted from all twelve harmonics for the shroud interface having the largest displacement (Figs. 80, 84, 88, 92, 96, 100).
4. An X-Y time history plot of the fundamental response for the same interface (Figs. 81, 85, 89, 93, 97, 101).

In Figures 78, 82 and 86, the modulus and phase information for the X-axis components of displacements as measured at the sensors is superimposed on the shroud motion plots to show the effect of the transformation from sensor to shroud rubbing surface.

For comparison and correlation studies, the modulus and phase information for measured blade strains and the vectorial difference of strains between adjacent blades ( $\epsilon_{N+1} - \epsilon_N$ ) is also superimposed on the modulus and phase plots of shroud motion. The plotted values are connected by straight lines in order to assist in identifying the spatial distribution trends.



TABLE 16

## DATA SAMPLE IDENTIFICATION

DATA SAMPLE	RUN NO.	FAMILY	ORDER	SPEED	NATURE OF RESPONSE
1	156	FIRST	4E	0	STATIONARY WAVE <sup>2</sup>
2	181	FIRST	4E	1163 <sup>1</sup>	BKWD TRAV. WAVE
3	184	SECOND	2E	1200	STATIONARY WAVE
4	196	SECOND	2E	1200	BKWD TRAV. WAVE
5	187	SECOND	3E	1200	BKWD TRAV. WAVE
6	191	SECOND	4E	1200	STATIONARY WAVE

NOTES: 1. INTEGRAL ORDER SPEED  
2. RELATIVE TO DISK

**Figure 66 Strain Response for Instrumented Blades for Data Sample #1**

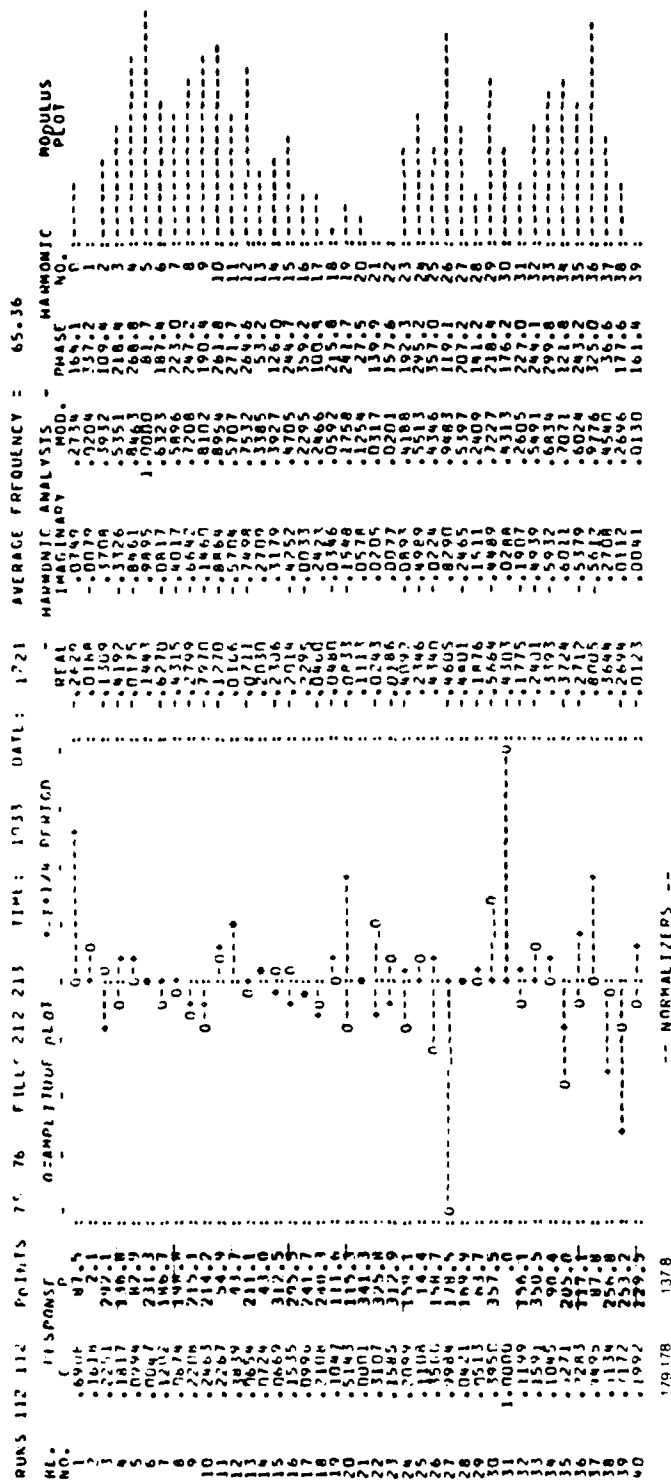
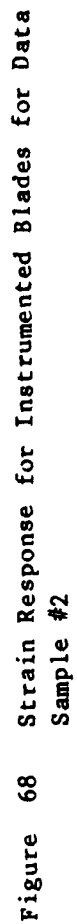


Figure 67 Blade Strain Response and Spatial Harmonic Distribution for Condition Corresponding to Data Sample #1



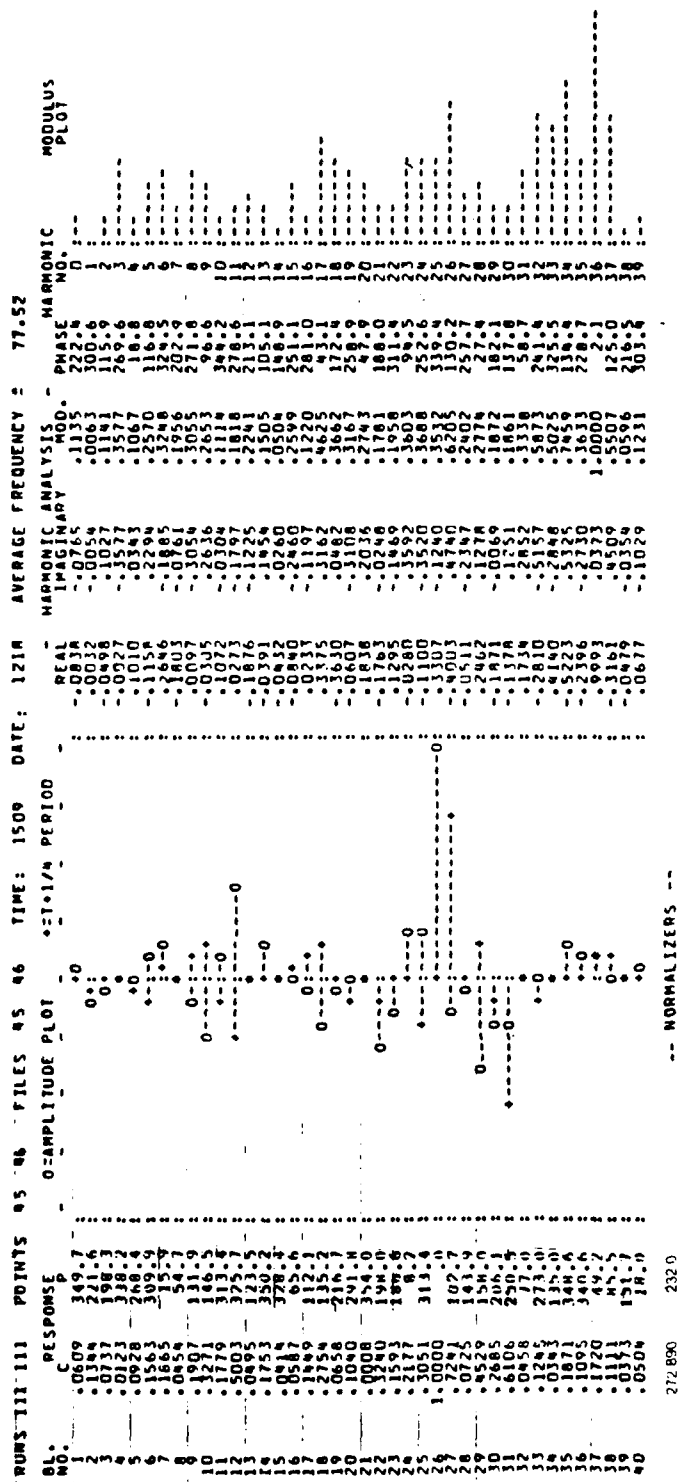


Figure 69 Blade Strain Response and Spatial Harmonic Distribution for Condition Corresponding to Data Sample #2

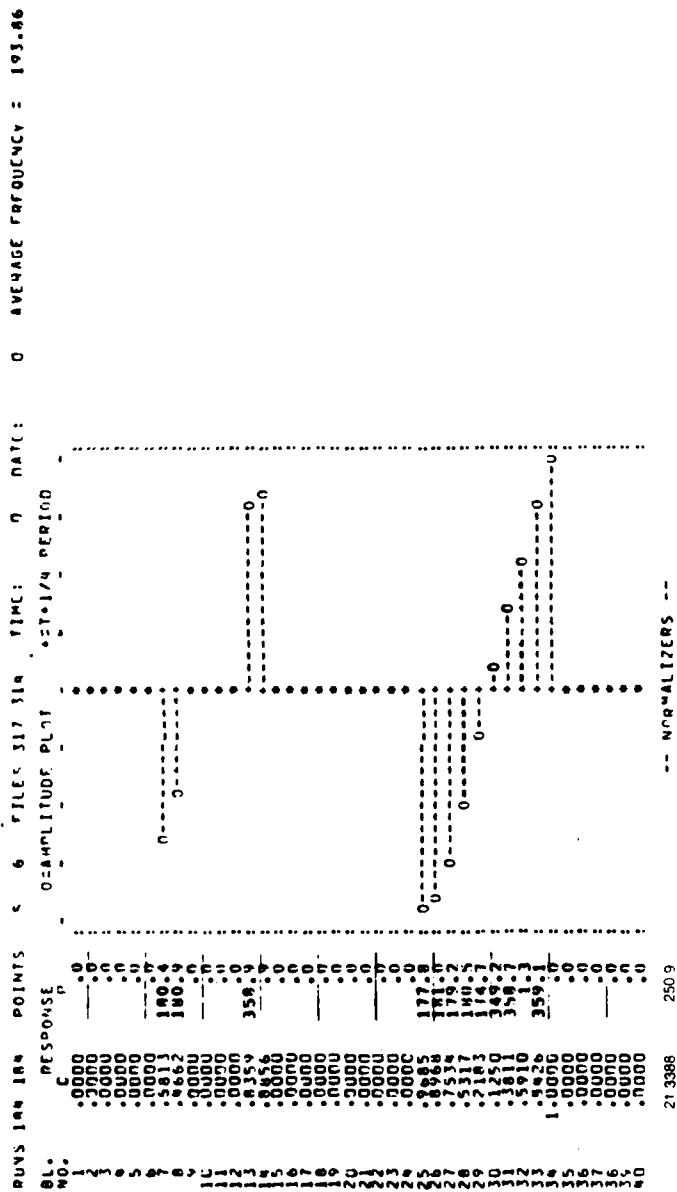
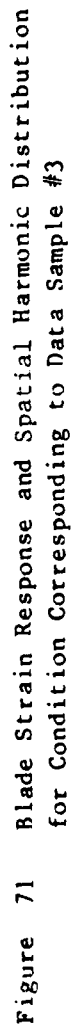


Figure 70 Strain Response for Instrumented Blades for Data Sample #3



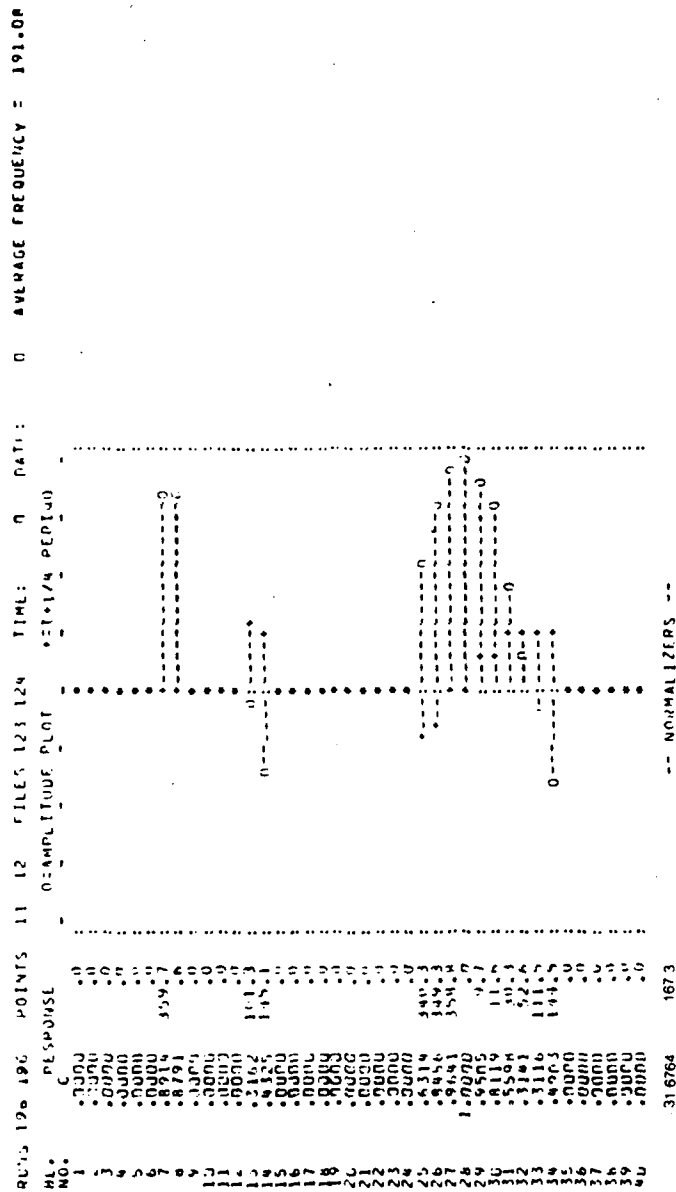


Figure 72 Strain Response for Instrumented Blades for Data Sample #4



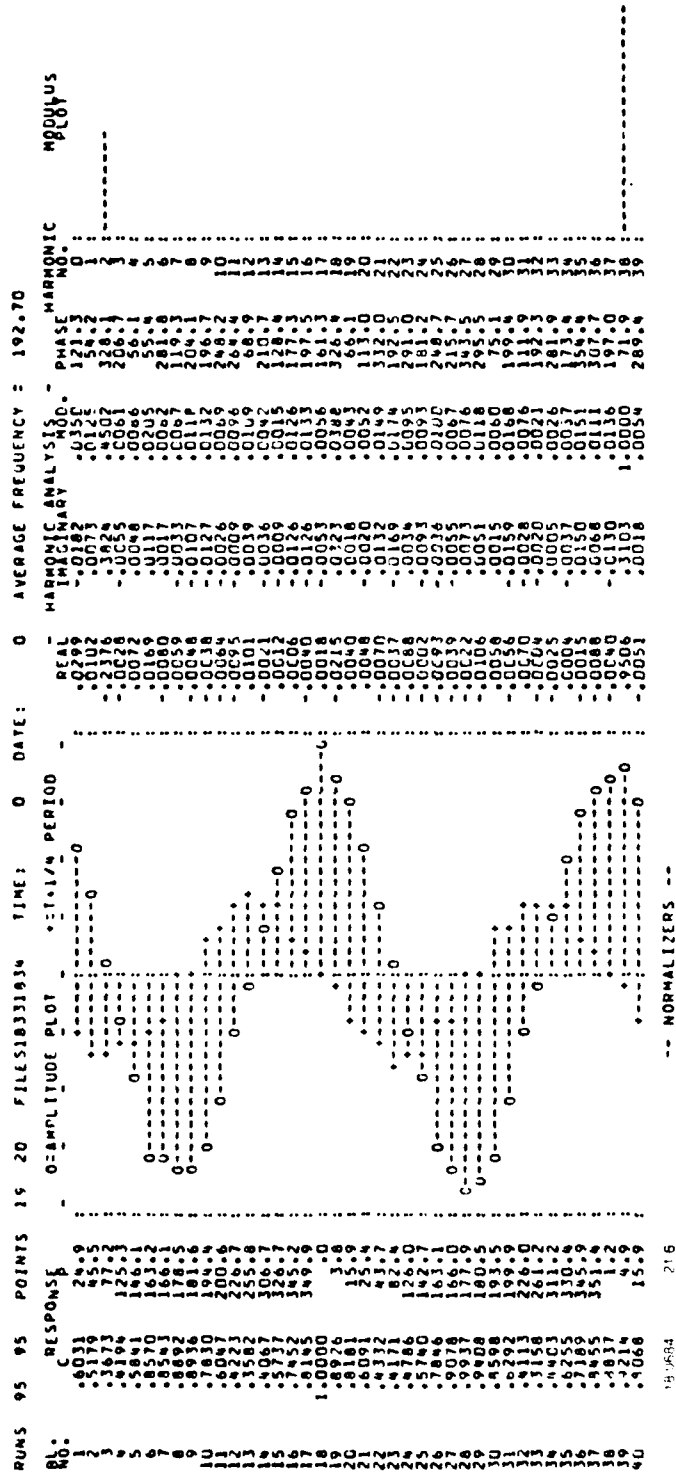


Figure 73 Blade Strain Response and Spatial Harmonic Distribution for Condition Corresponding to Data Sample #4

**Figure 74 Strain Response for Instrumented Blades for Data Sample #5**

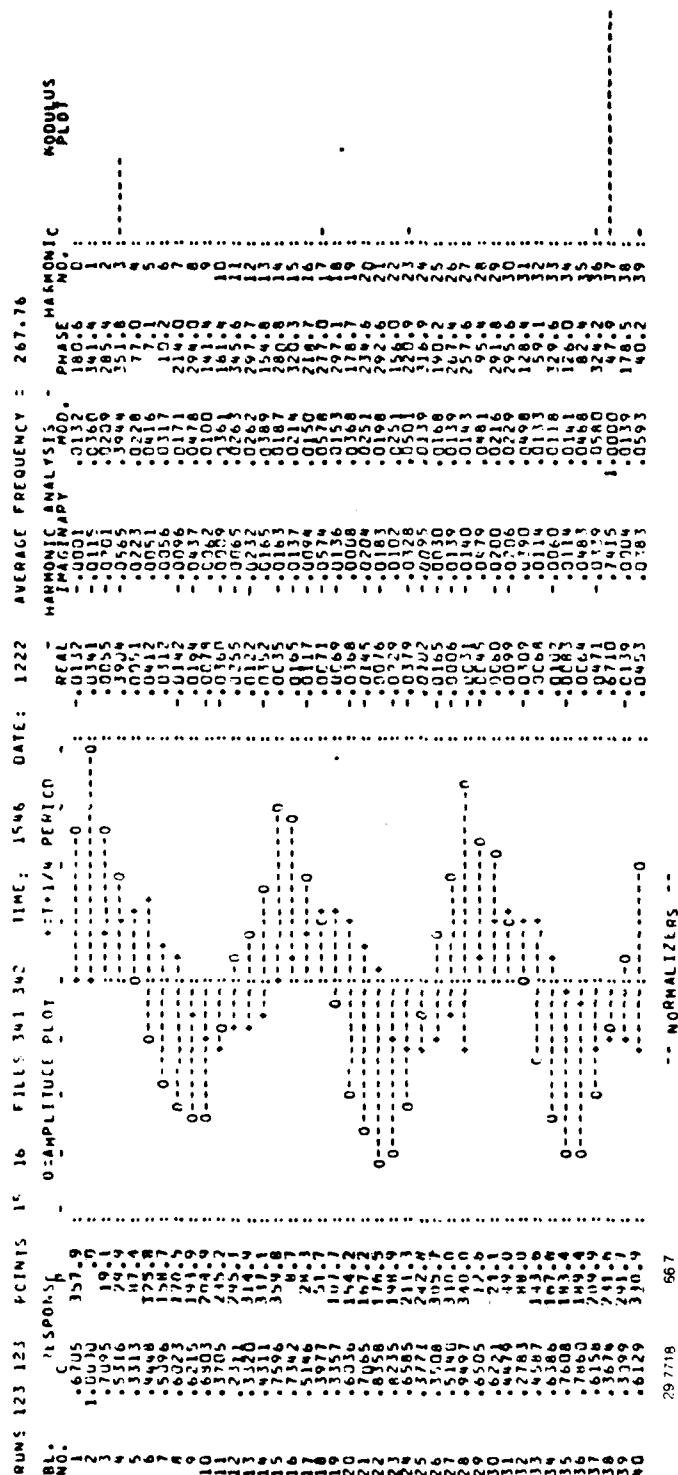


Figure 75 Blade Strain Response and Spatial Harmonic Distribution for Condition Corresponding to Data Sample #5

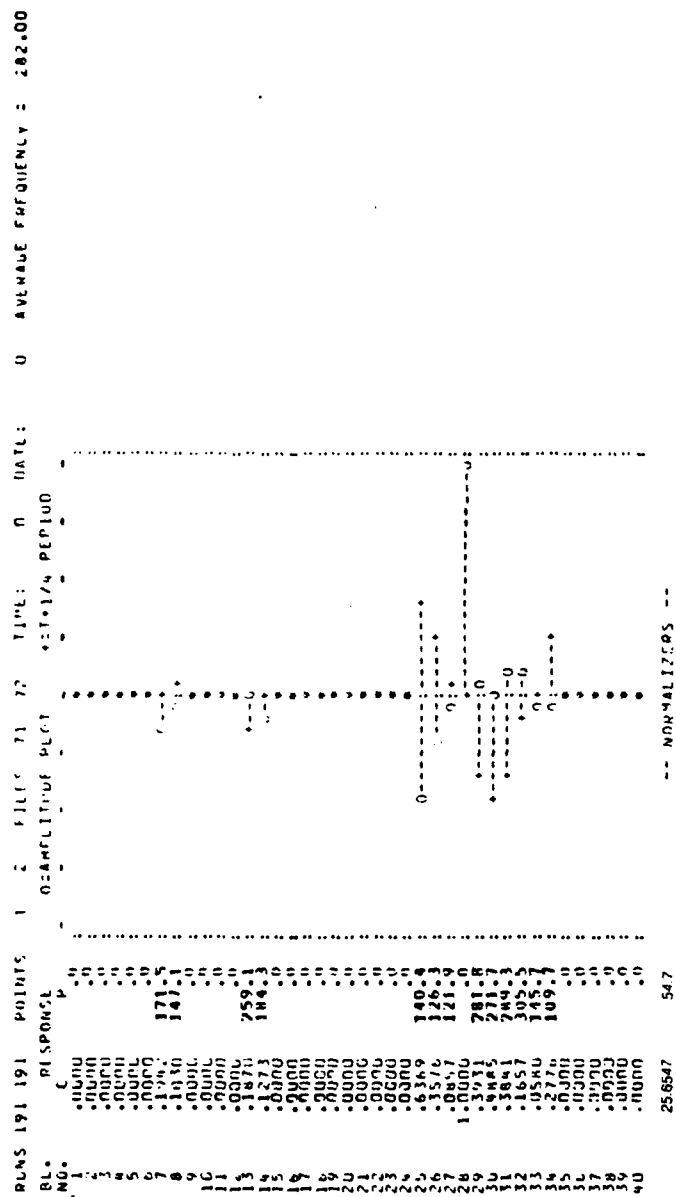


Figure 76 Strain Response for Instrumented Blades for Data Sample #6

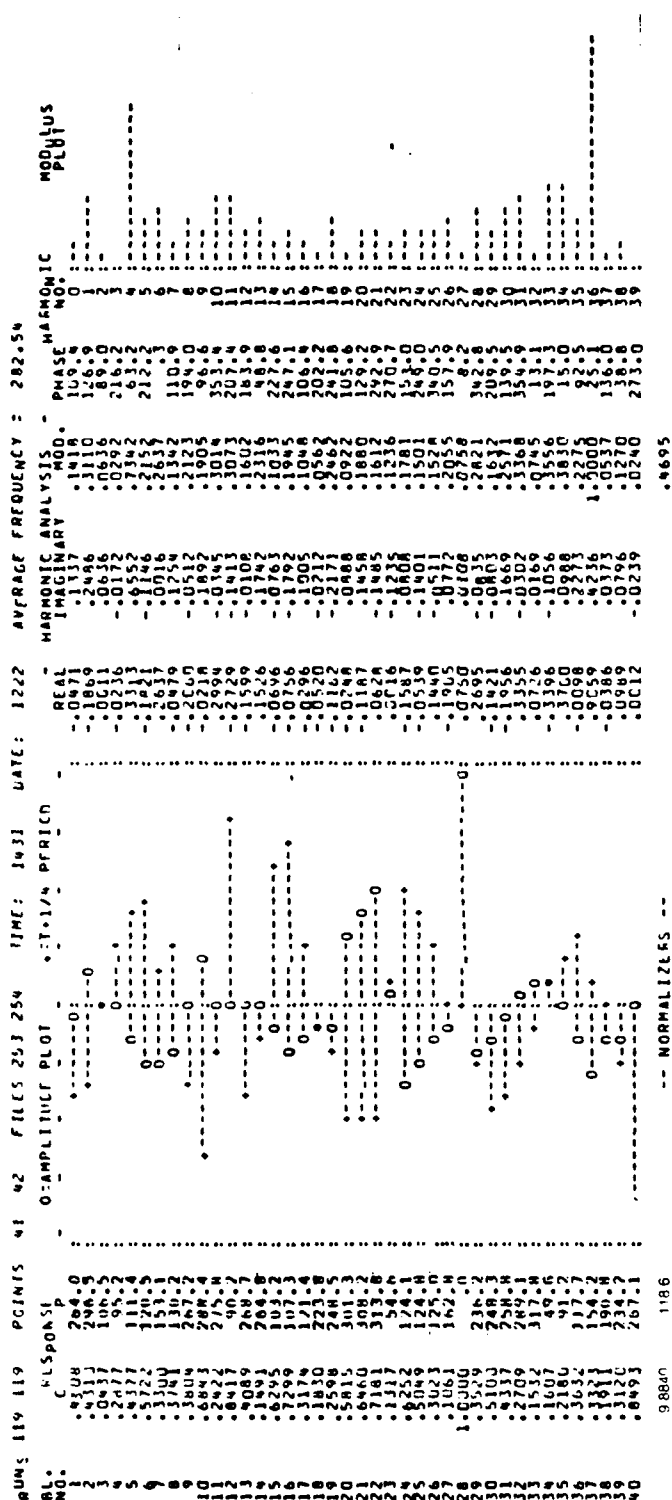


Figure 77 Blade Strain Response and Spatial Harmonic Distribution for Condition Corresponding to Data Sample #6

In the time history plots, it should be noted that the input frequency is given in Hertz and the fundamental period is given in milliseconds.

On the X-Y plots, the time zero and the quarter period points are located to indicate direction of motion.

## 7. Discussion of Results

The principal results from measurements of static relative displacement under centrifugal loading are presented in Figs. 64 and 65. The shroud displacement along the X and Y directions are shown in Fig. 64 as a function of square of the speed. A comparison between X and Y displacements indicates a somewhat predominant Y motion. The implication is that the nature of deformation is one of bending with some torsion in it. The displacement along X, which is indicative of torsion, varies linearly with  $\Omega^2$  whereas the bending motion has a more complicated relationship with speed. The total relative displacement includes both bending and torsional deformation.

Averaged relative displacement at shroud interfaces vary from blade to blade and this variation is attributed to blade to blade differences in mass. The differences in blade mass result in varying normal loads and therefore the friction forces at the interfaces will vary. Further, as the steady state data was obtained subsequent to vibratory tests, and as the extent of rubbing action at interfaces depend on the location of the interface, the coefficient of friction would most likely be different at different interfaces. All these factors could contribute to the considerable changes in measured steady displacements around the rotor.

Figures 66 through 77 represent the blade strain distributions of the six dynamic data samples and the corresponding strain data from previous mistuned tests. The latter were recorded in an earlier phase of the test program before the rotor was instrumented with shroud motion measurement devices. The strain data shown in Figs. 67, 69, 71, 73, 75 and 77 were used as guidelines to define the frequencies at which shroud motion data was to be taken. For example, strain data from Fig. 69 specifies the nature of the spatial response to be expected. Again, a comparison of Figs. 68 and 69 clearly show that the spatial distribution of motion has been duplicated between the two phases of experimentation. It must be noted that the strain data from shroud motion experimental phase were taken for only 14 blades because of available channel limitations. Thus, the similarity between the stickplots from the two phases implies that the contributing harmonics to the total motion are also similar.

Further, these data represent responses to an imposed backward traveling wave excitation. These data samples were chosen to obtain shroud motion corresponding to the assembly response containing both stationary and traveling wave vibration.

In Figs. 78 and 79, modulus and phase of shroud motions, strain gage response and differences in strains of adjacent blades are plotted as a function of blade number, at a frequency (65.28 Hz) that corresponds to the first family 4ND backward traveling wave. Figure 80 represents the time history of shroud motion at the forcing frequency and the vectorial motion is represented in Fig. 81. Figures 78, 79, 80 and 81 form a set with similar sets to follow in this discussion. An examination of these figures leads to the following observations.

In the first set, the results indicate that the strain distribution among the blades in the instrumented quadrant shows two principal, unequal peaks that correspond to the imposed harmonic. However, there appears to be an additional higher harmonic contribution to the total response, as evidenced by the blades #32 and 33 vibrating out of phase with each other. The peak amplitudes of shroud motion occur at interfaces located between two blades exhibiting the largest differences in strain between them.

As expected, X1 and X2 are essentially equal. Y1 and Y2 are out of phase indicating a vibratory motion pivoting about a point on the shroud interface. The pivoting point varies from blade to blade. This implies that the vibratory motion is principally of a bending type, the maximum bending strain occurring at a cross-section close to the shroud. The spatial variation in the phase angle implies contributions to the response from both standing and traveling waves. Shroud motion data appears to correlate both in amplitude and phase with corresponding quantities for strain difference ( $\Delta SG$ ).

Figures 82, 83, 84 and 85 present data similar to Figs. 78, 79, 80 and 81 but at 1163 rpm. A distinct feature of this set of data is that the phase angle variation of the strains show the strong presence of a 4ND travelling wave, in addition to several other spatial harmonics. This is also evident from Fig. 69.

It should be noted from Fig. 82 that the X measurements obtained from the sensors (prior to making corrections to the depth of the interface) correlate with the modulus and phase of the difference in strains. The same applies for Y1 measurements in Fig. 83.

Figures 86 through 101 present data reduced from records obtained from the R-80 fan vibrating in modes that correspond to the second family at 2, 3, and 4 nodal diameter patterns. The strain levels that could be imposed onto

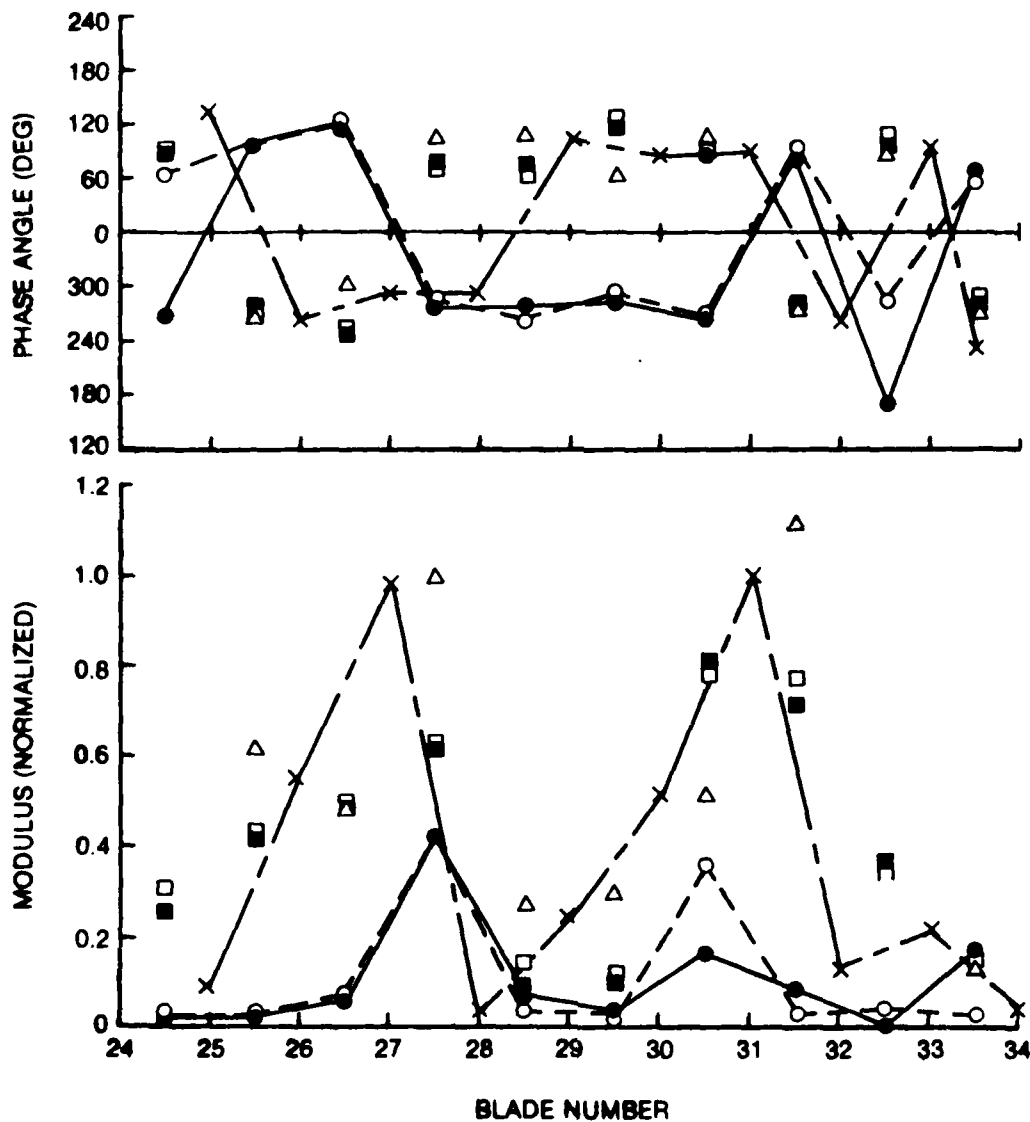
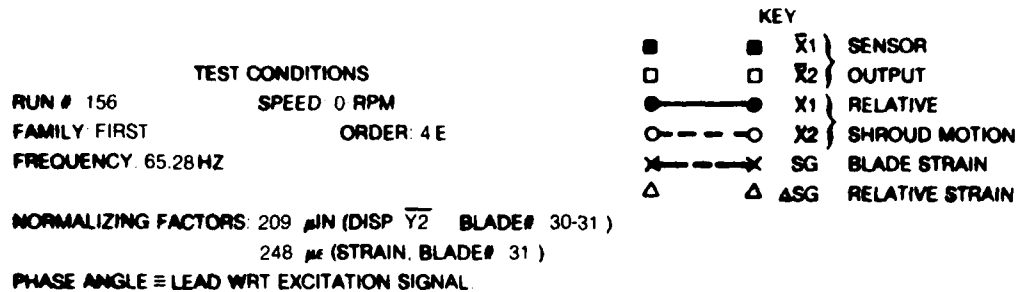


Figure 78 Modulus and Phase Plots of the Measured Response Parameters for Blades #25 through #34 with Backward Traveling Wave Excitation - Data Sample #1 (X - Axis Components of Shroud Motion)



TEST CONDITIONS  
 RUN # 156      SPEED 0 RPM  
 FAMILY FIRST      ORDER: 4 E  
 FREQUENCY: 65.28 HZ

KEY  
 ● ——— ● Y1 } RELATIVE  
 ○ ——— ○ Y2 } SHROUD MOTION  
 x ——— x SG BLADE STRAIN  
 Δ ——— Δ ΔSG RELATIVE STRAIN

NORMALIZING FACTORS 209  $\mu$ IN (DISP Y2 BLADE# 30-31 )  
 248  $\mu$ ε (STRAIN, BLADE# 31 )

PHASE ANGLE  $\equiv$  LEAD WRT EXCITATION SIGNAL

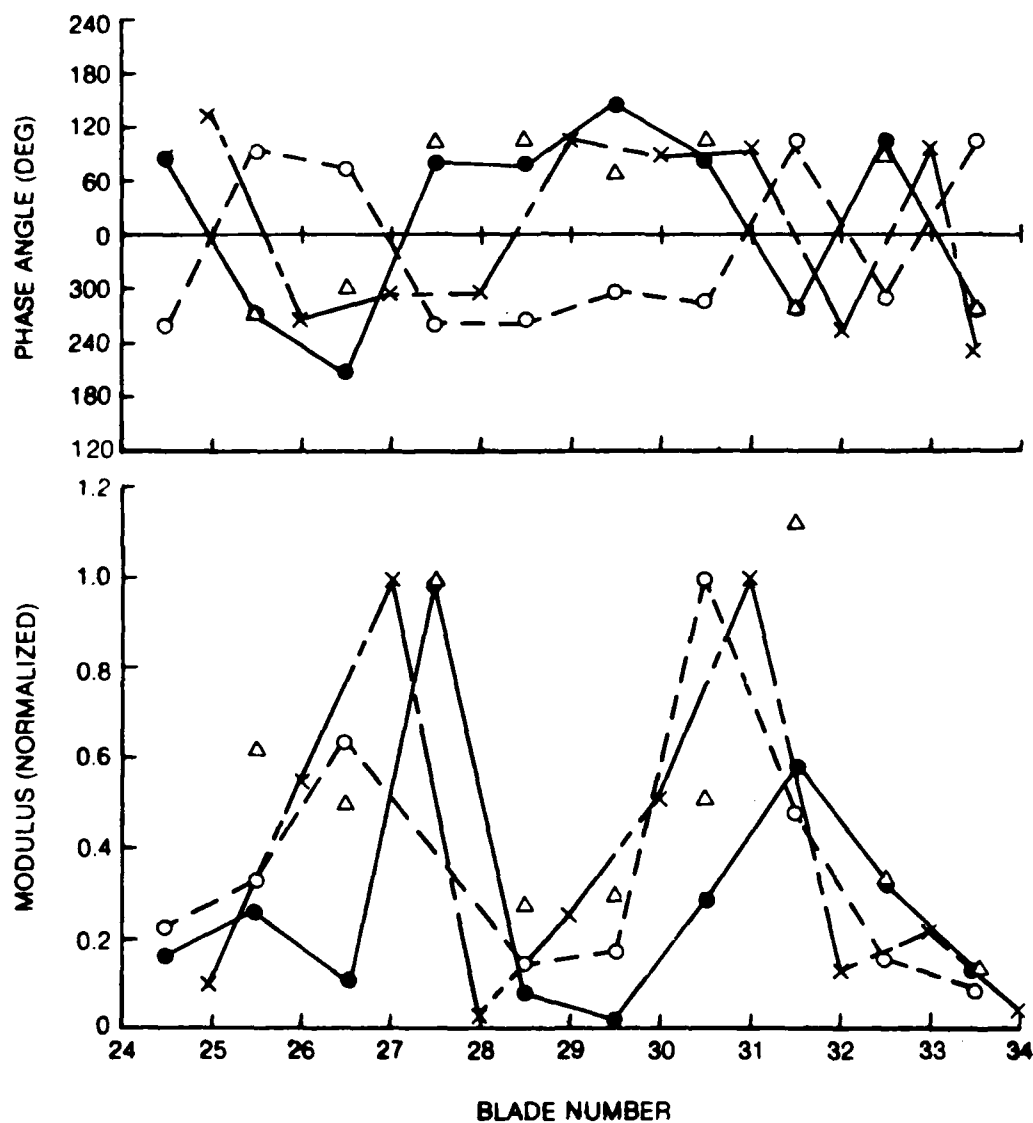


Figure 79 Modulus and Phase Plots of the Measured Response Parameters for Blades #25 through #34 with Backward Traveling Wave Excitation - Data Sample #1 (Y - Axis Components of Shroud Motion)

RUN 156 PT 7 FREQUENCY 65.29 TAU 15.316 HARMONICS 1-12 BLADES 30-31

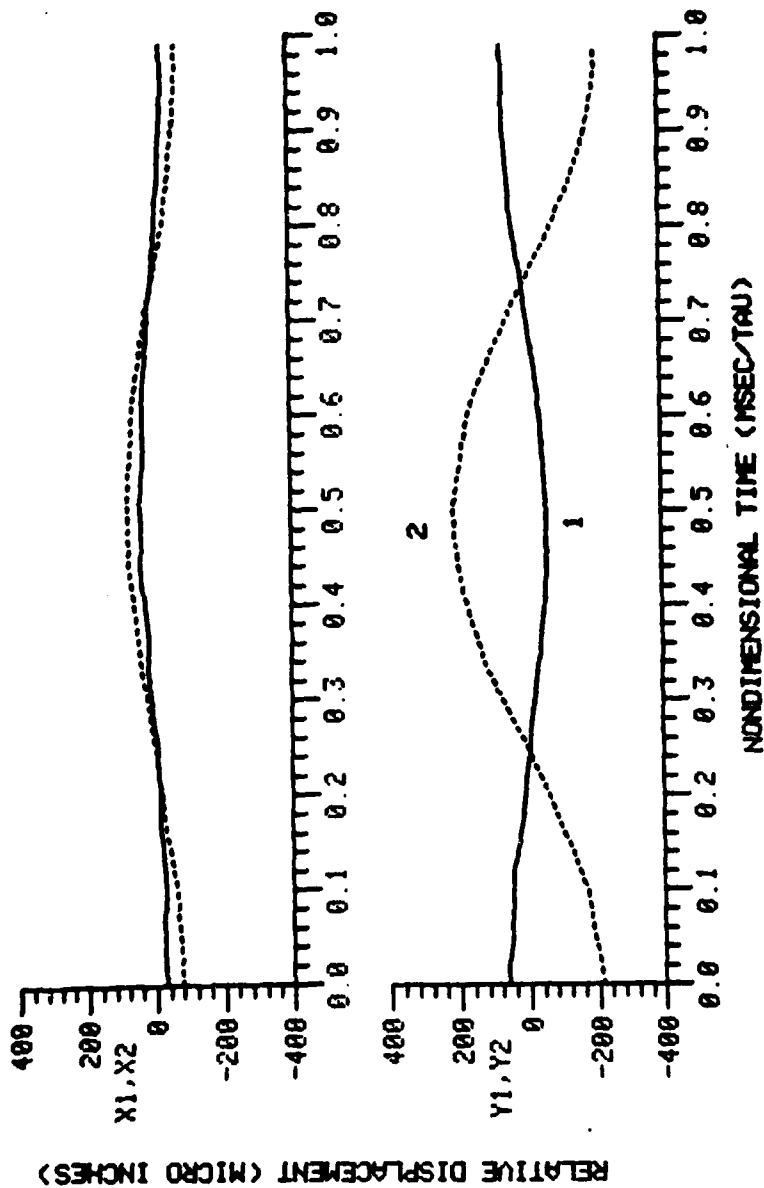


Figure 80 Time History of Relative Displacements at Shroud Interface #30-31 for Data Sample #1

RUN 156 POINT 7 HARMONICS 1- 1 BLADES 30-31 FREQUENCY 65.29

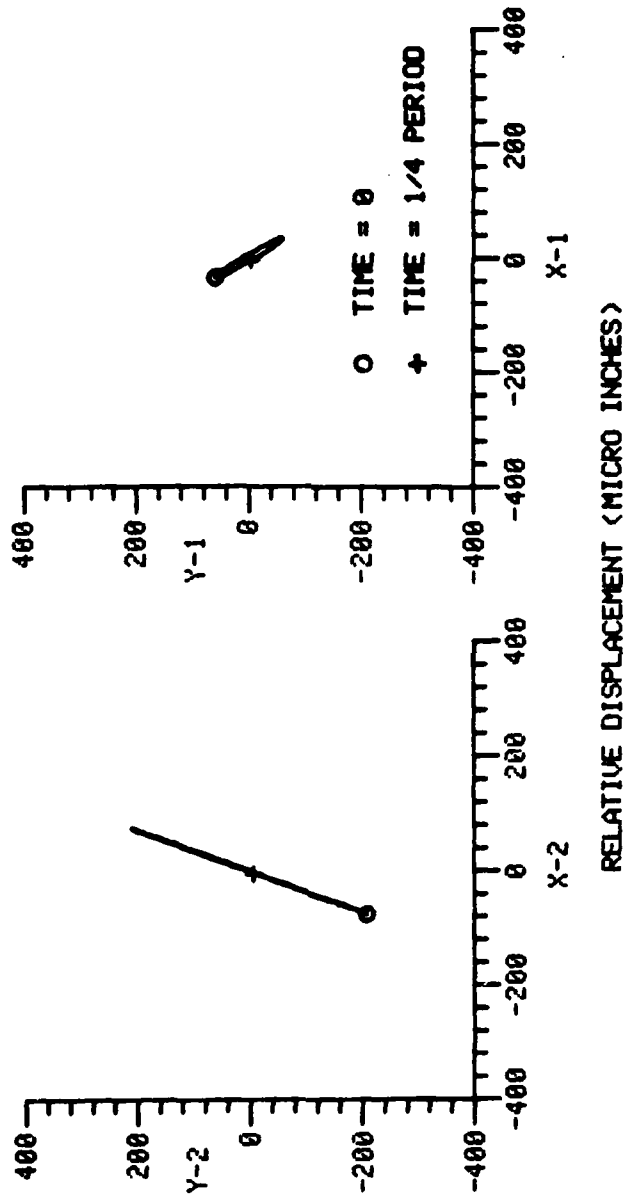


Figure 81 Relative Motion at Two Points on Shroud Interface  
#30-31 for Data Sample #1

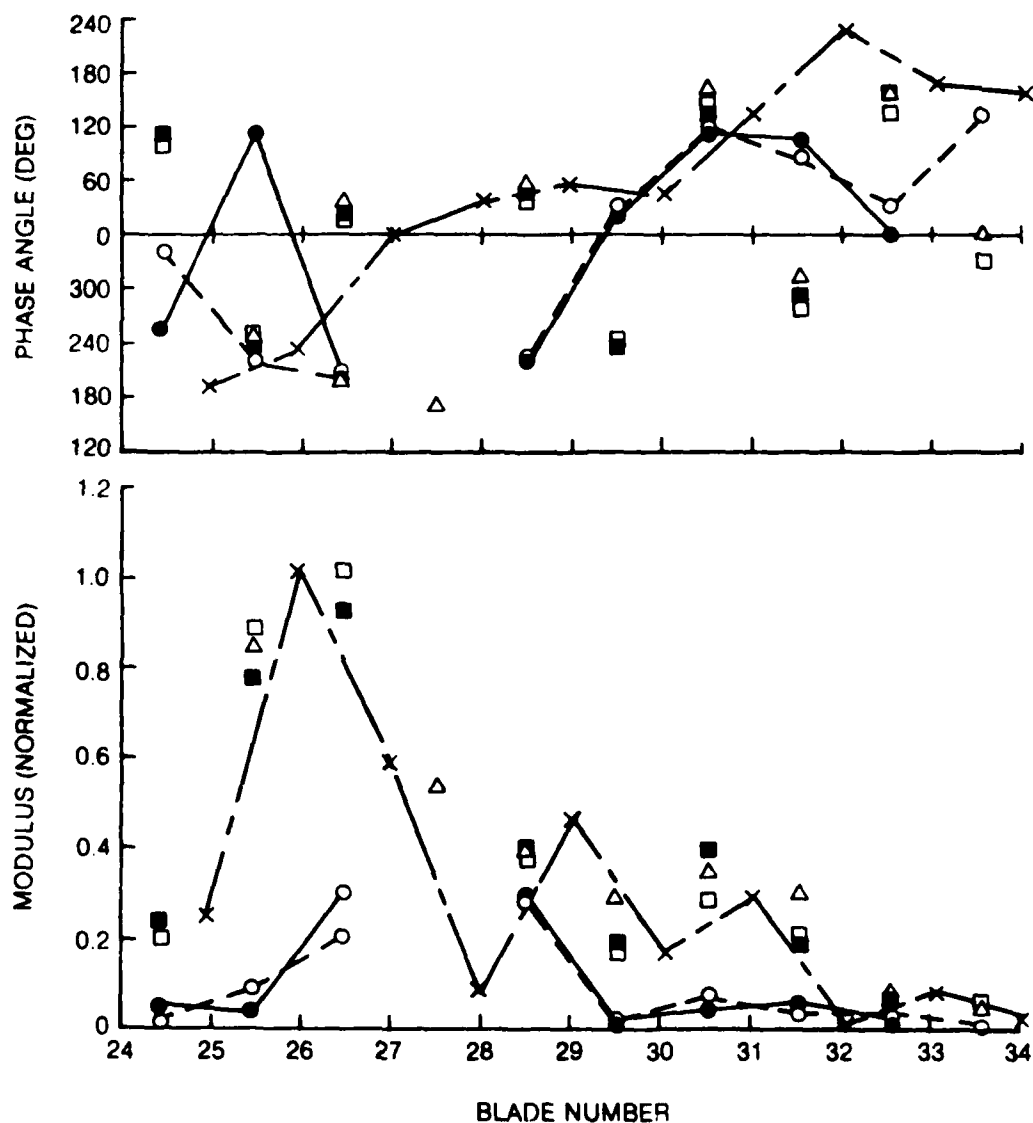
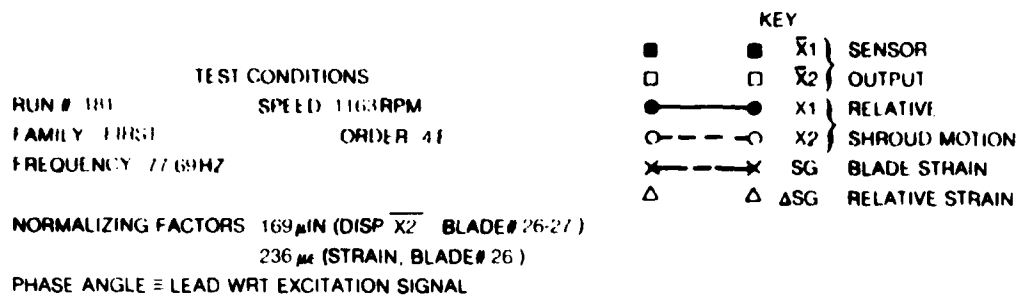


Figure 82 Modulus and Phase Plots of the Measured Response Parameters for Blades #25 through #34 with Backward Traveling Wave Excitation - Data Sample #2 (X - Axis Components of Shroud Motion)

TEST CONDITIONS  
 RUN # 181      SPEED 1163 RPM  
 FAMILY FIRST      ORDER 4 E  
 FREQUENCY 77.69 HZ

KEY  
 ●——● Y1 } RELATIVE  
 ○——○ Y2 } SHROUD MOTION  
 ×——× SG BLADE STRAIN  
 △——△ ΔSG RELATIVE STRAIN

NORMALIZING FACTORS    169 μIN (DISP X2 BLADE# 26-27 )  
                              236 με (STRAIN, BLADE# 26 )

PHASE ANGLE ≡ LEAD WRT EXCITATION SIGNAL

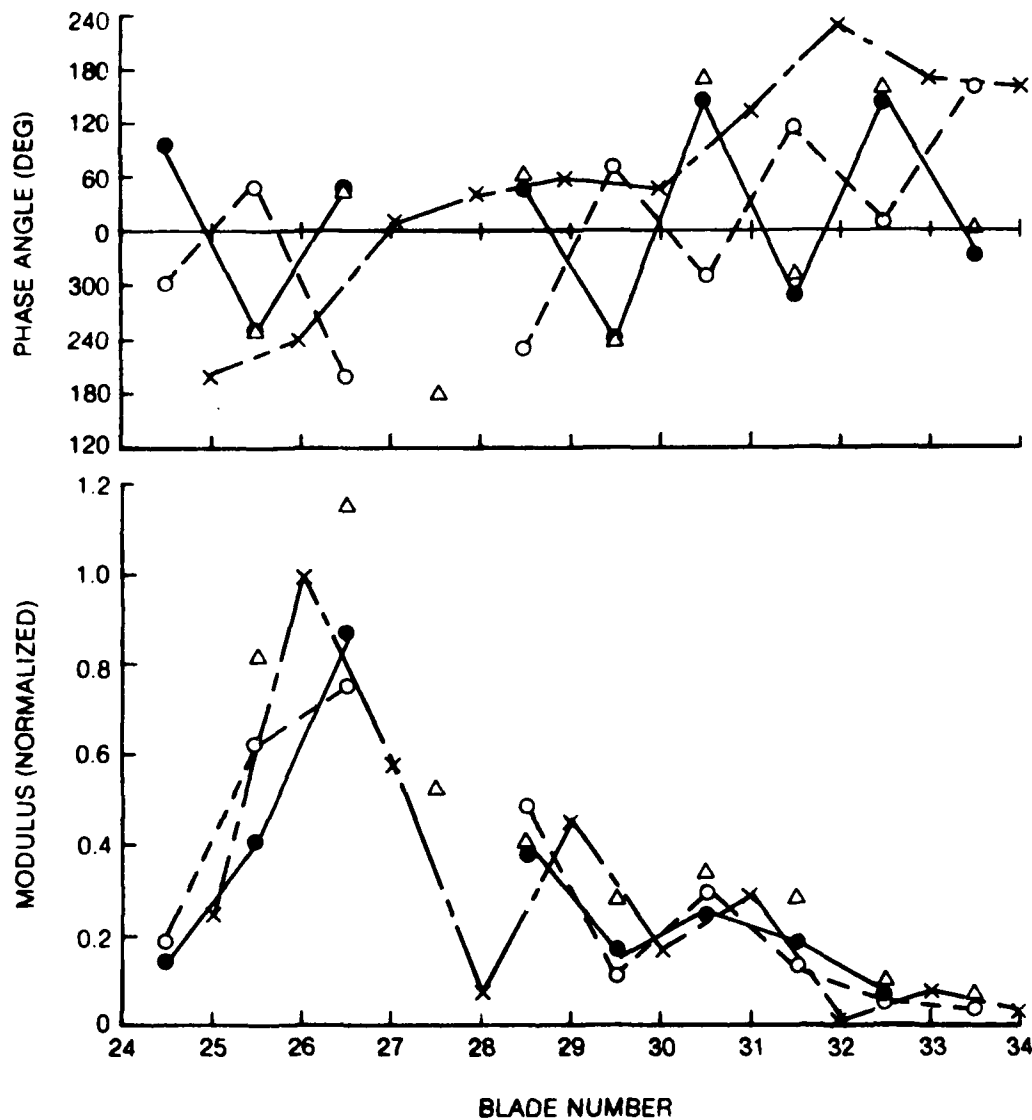


Figure 83 Modulus and Phase Plots of the Measured Response Parameters for Blades #25 through #34 with Backward Traveling Wave Excitation - Data Sample #2 (Y - Axis Components of Shroud Motion)

RUN 181 PT 3 FREQUENCY 77.69 TAU 12.872 HARMONICS 1-12 BLADES 26-27

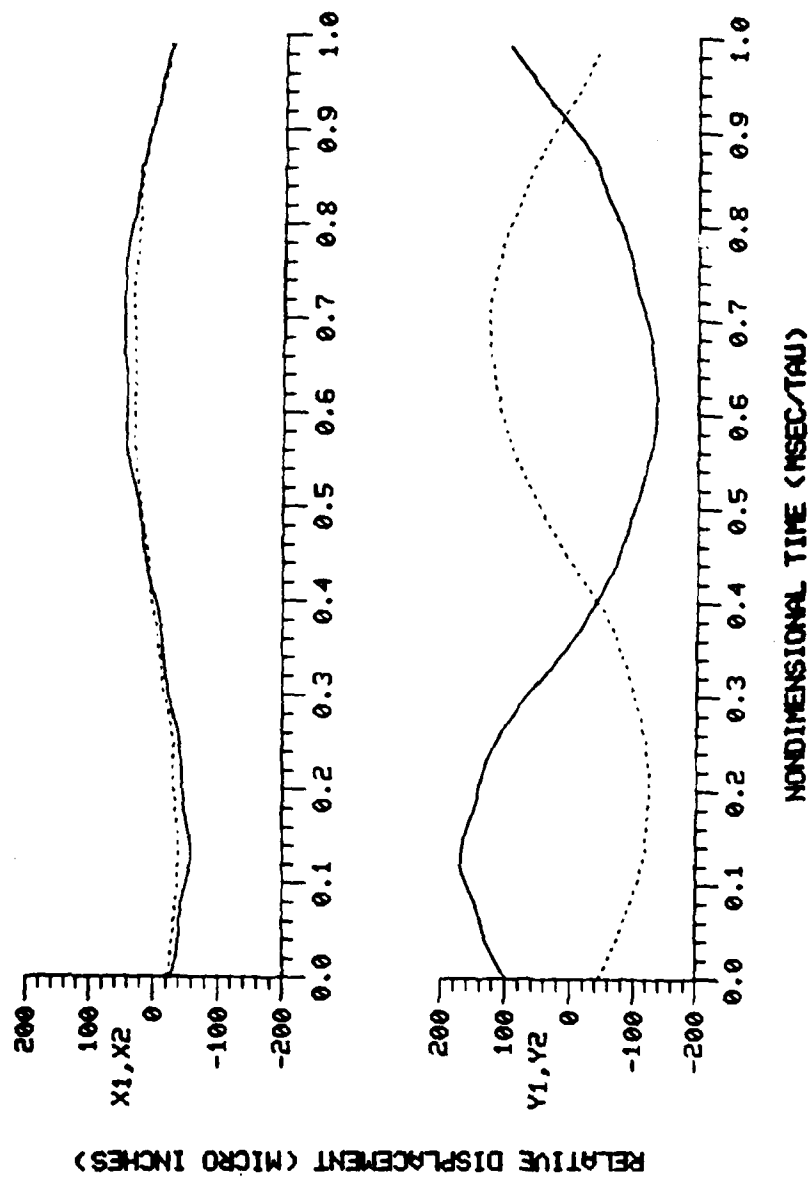


Figure 84 Time History of Relative Displacements at Shroud Interface #26-27 for Data Sample #2

RUN 181 POINT 3 HARMONICS 1- 1 BLADES 26-27 FREQUENCY 77.69

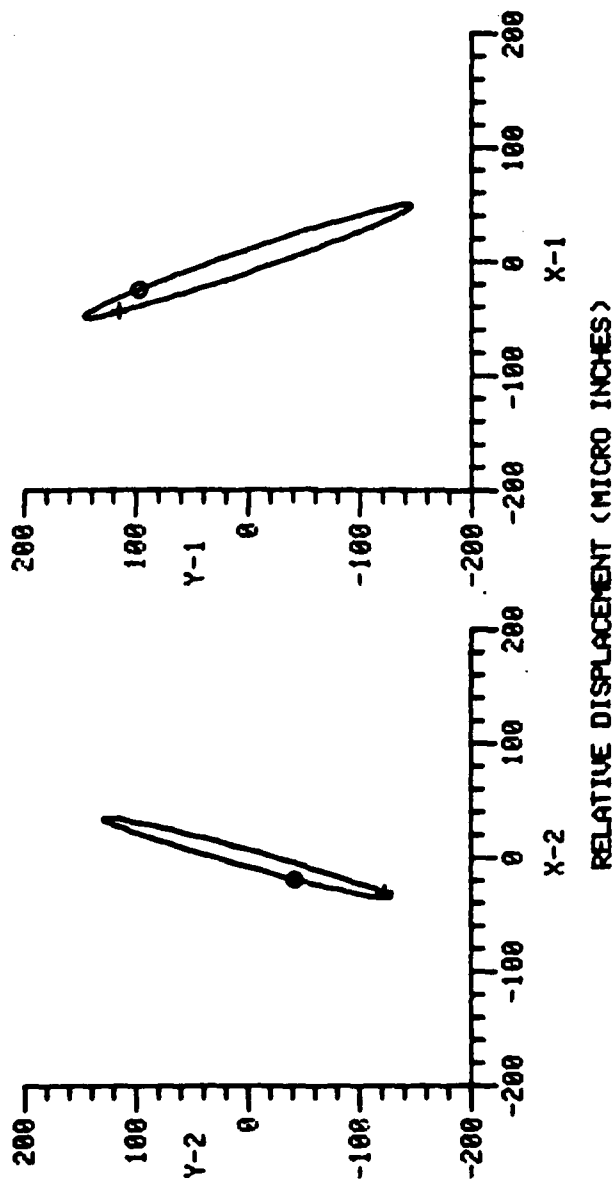


Figure 85 Relative Motion at Two Points on Shroud Interface #26-27 for Data Sample #2

TEST CONDITIONS  
 RUN # 184 SPEED 1200RPM  
 FAMILY SECOND ORDER 2E  
 FREQUENCY 193.9HZ

KEY  
 ■  $\bar{x}_1$  } SENSOR  
 □  $\bar{x}_2$  } OUTPUT  
 ● —●— X1 } RELATIVE  
 ○ —○— X2 } SHROUD MOTION  
 × —×— SG BLADE STRAIN  
 △ —△—  $\Delta SG$  RELATIVE STRAIN

NORMALIZING FACTORS  $9.2 \mu\text{IN (DISP Y1 BLADE# 27-28)}$   
 $21 \mu\text{ (STRAIN, BLADE# 34)}$

PHASE ANGLE  $\equiv$  LEAD WRT EXCITATION SIGNAL

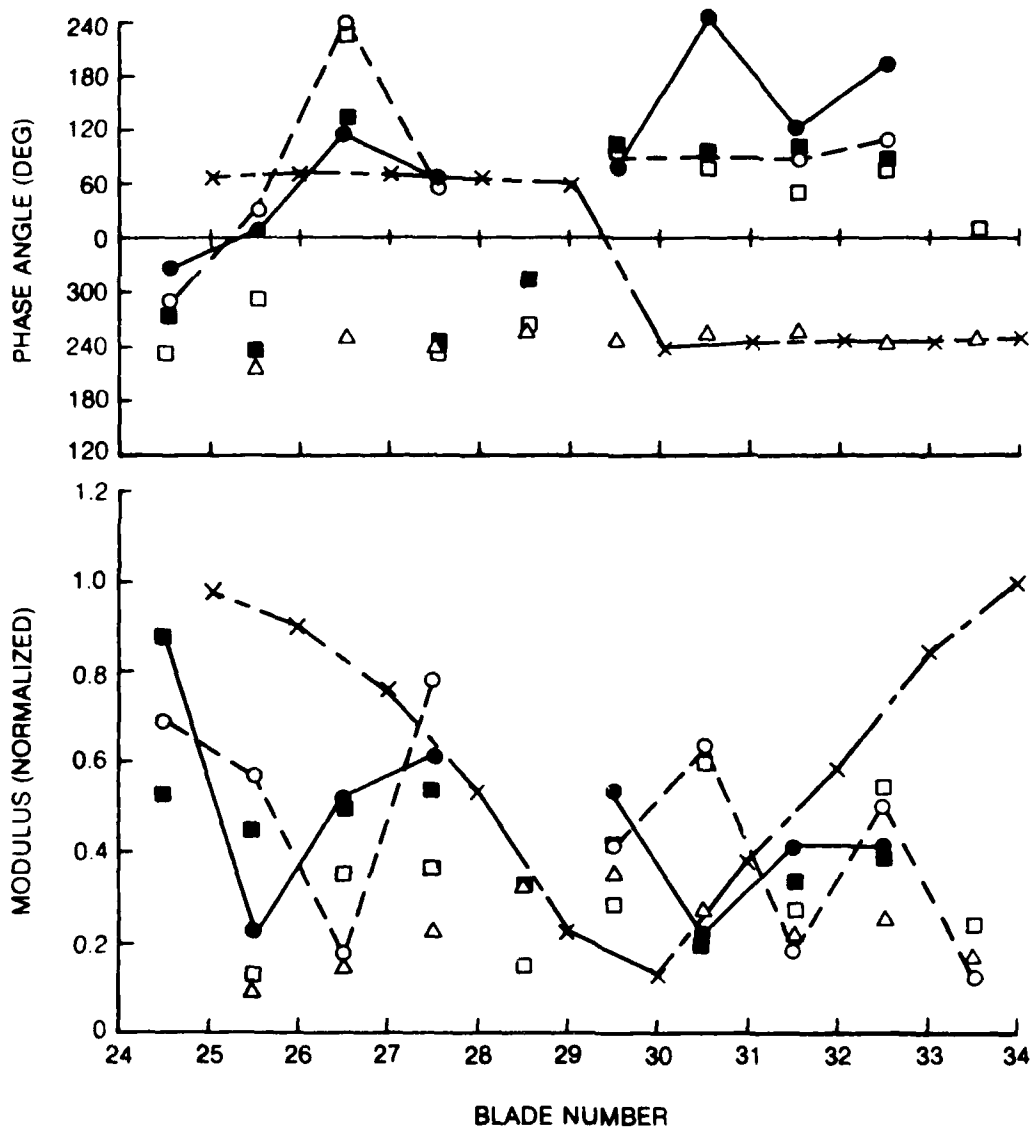


Figure 86 Modulus and Phase Plots of the Measured Response Parameters for Blades #25 through #34 with Backward Traveling Wave Excitation - Data Sample #3 (X - Axis Components of Shroud Motion)



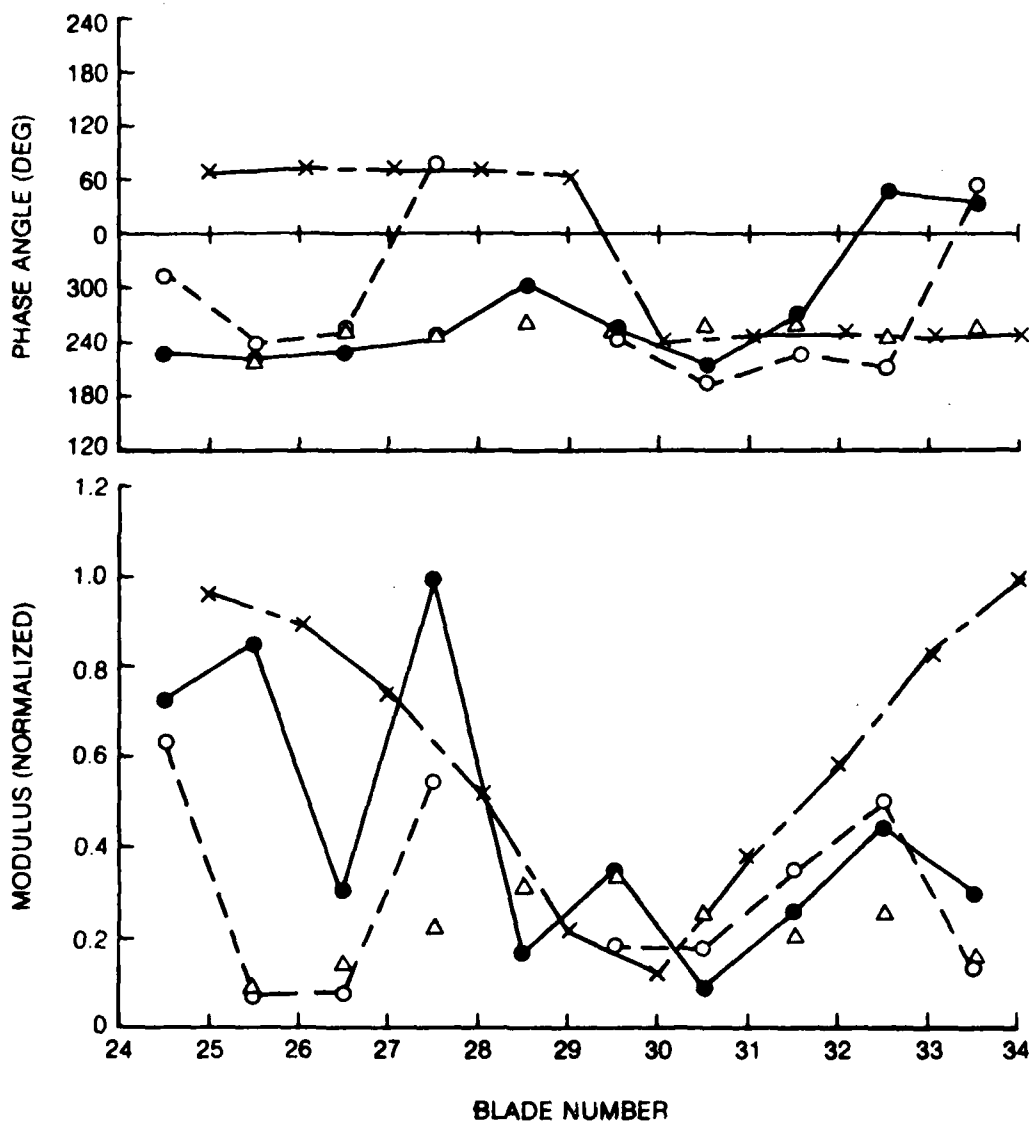
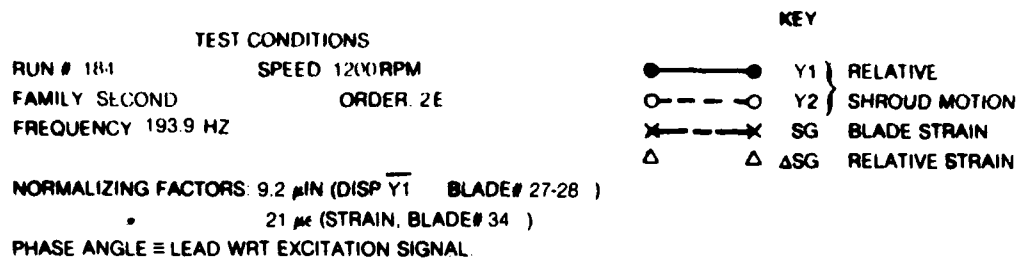


Figure 87 Modulus and Phase Plots of the Measured Response Parameters for Blades #25 through #34 with Backward Traveling Wave Excitation - Data Sample #3 (Y - Axis Components of Shroud Motion)

RUN 184 PT 8 FREQUENCY 193.76 TAU 5.161 HARMONICS 1-12 BLADES 27-28

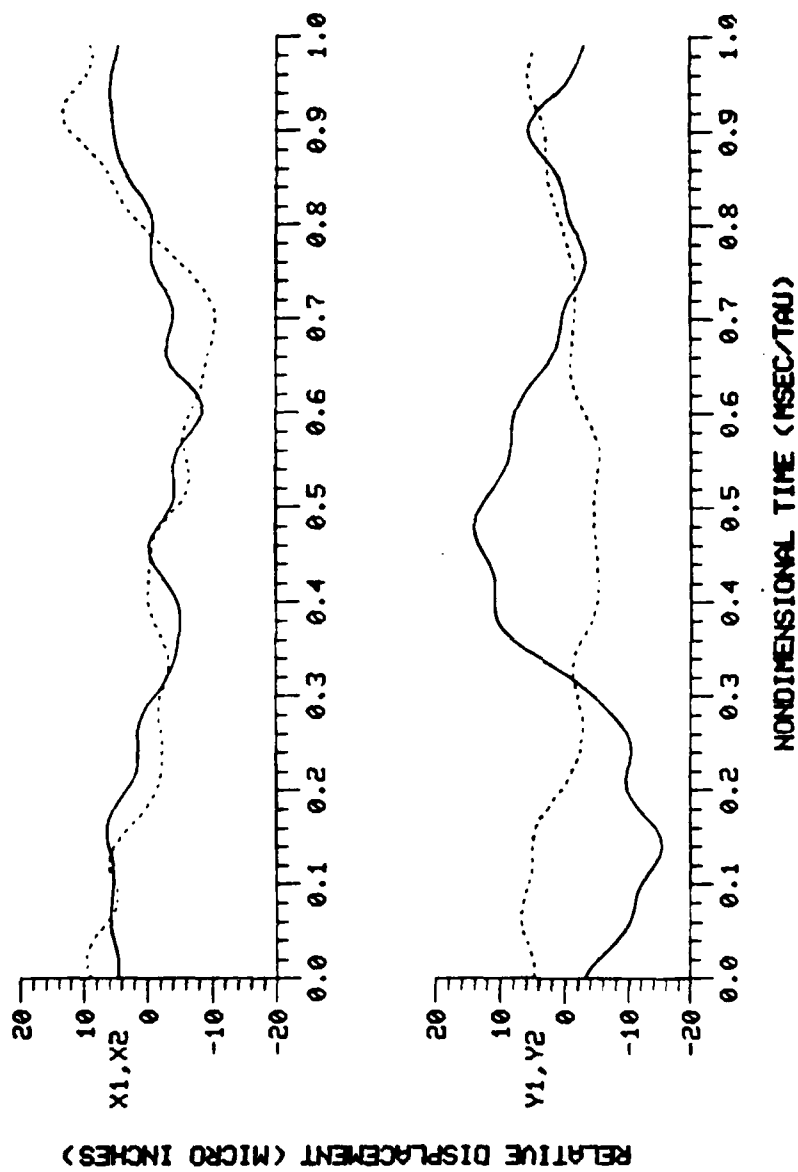


Figure 88 Time History of Relative Displacements at Shroud Interface #27-28 for Data Sample #3

RUN 184 POINT 8 HARMONICS 1- 1 BLADES 27-28 FREQUENCY 193.76

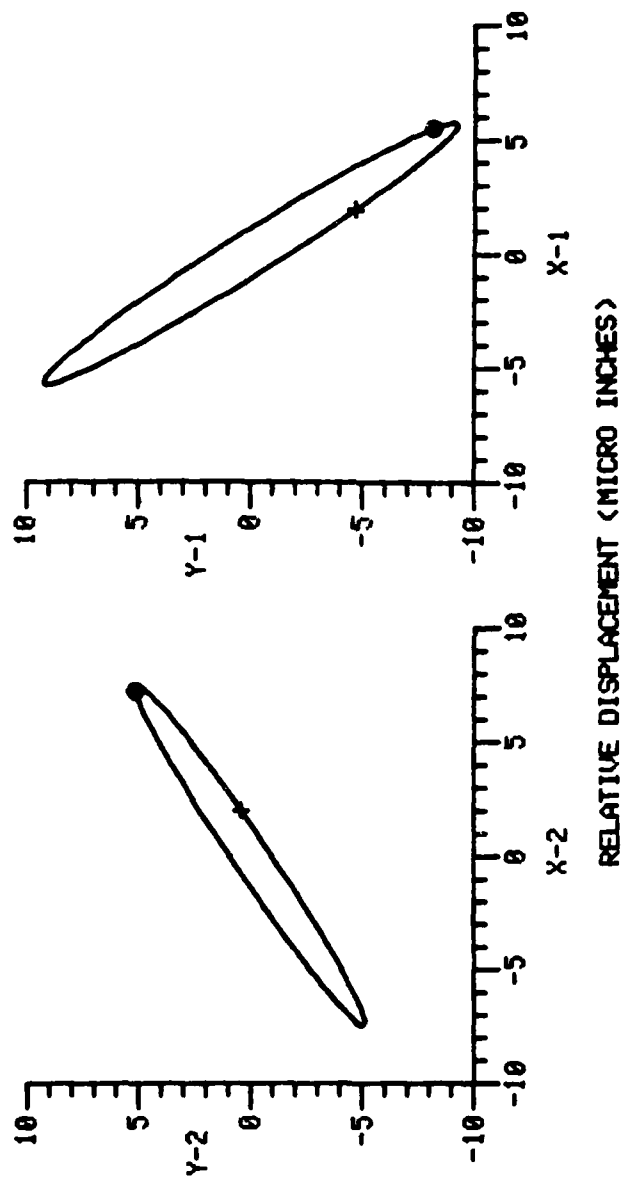


Figure 89 Relative Motion at Two Points on Shroud Interface #27-28 for Data Sample #3

TEST CONDITIONS  
 RUN # 196      SPEED 1200RPM  
 FAMILY SECOND      ORDER 2E  
 FREQUENCY 191.1 HZ

KEY  
 ●——● X1 } RELATIVE  
 ○——○ X2 } SHROUD MOTION  
 ×——× SG BLADE STRAIN  
 △——△ ΔSG RELATIVE STRAIN

NORMALIZING FACTORS 13 μIN (DISP Y1 BLADE # 27-28)

34 με (STRAIN, BLADE # 28)

PHASE ANGLE ≡ LEAD WRT EXCITATION SIGNAL

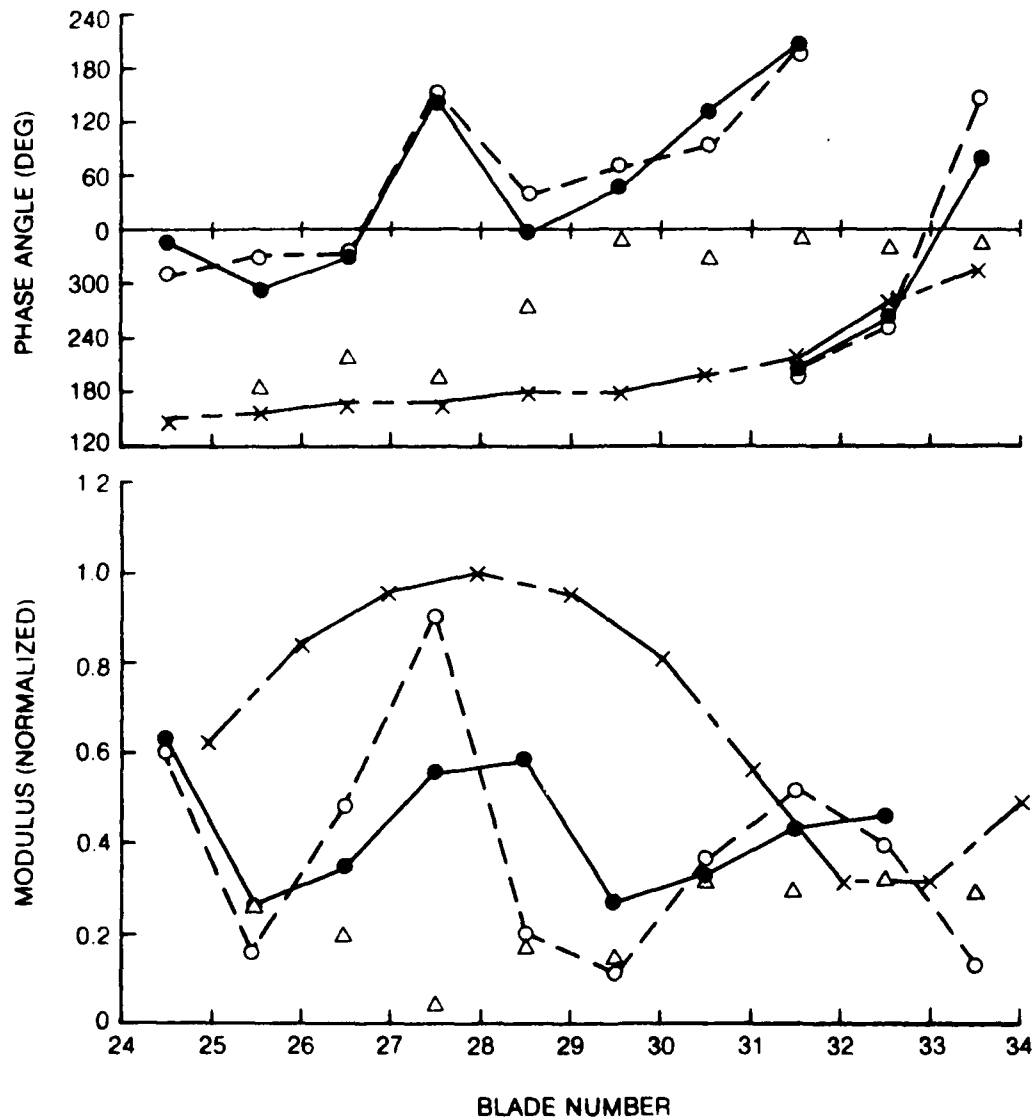


Figure 90 Modulus and Phase Plots of the Measured Response Parameters for Blades #25 through #34 with Backward Traveling Wave Excitation - Data Sample #4 (X - Axis Components of Shroud Motion)

TEST CONDITIONS  
 RUN # 196 SPEED 1200 RPM  
 FAMILY SECOND ORDER 2E  
 FREQUENCY 191.1 HZ

KEY  
 ● Y1 } RELATIVE  
 ○ Y2 } SHROUD MOTION  
 × SG BLADE STRAIN  
 △ ΔSG RELATIVE STRAIN

NORMALIZING FACTORS 13 μIN (DISP Y1 BLADE # 27-28)  
 34 με (STRAIN, BLADE # 28)

PHASE ANGLE ≡ LEAD WRT EXCITATION SIGNAL

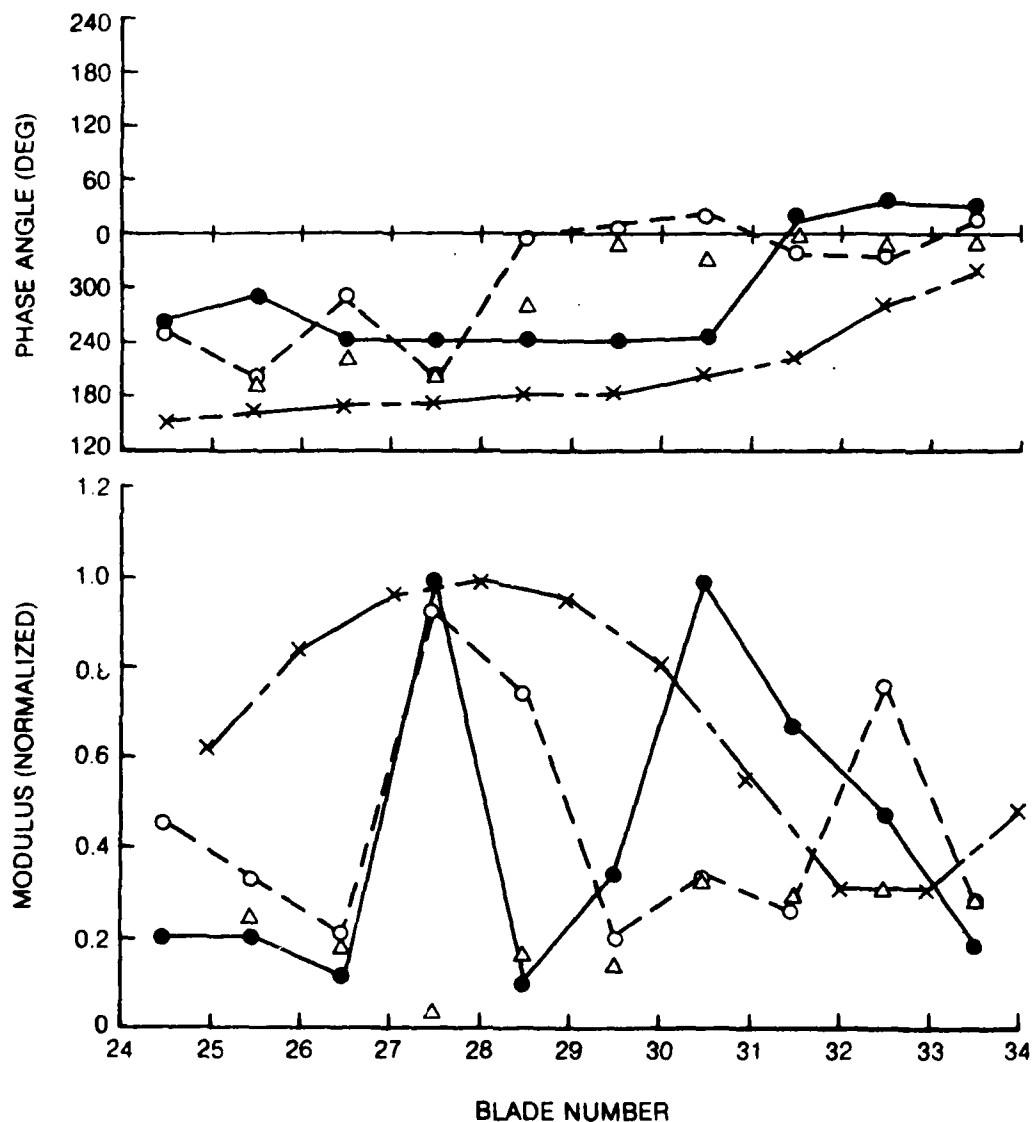


Figure 91 Modulus and Phase Plots of the Measured Response Parameters for Blades #25 through #34 with Backward Traveling Wave Excitation - Data Sample #4 (Y - Axis Components of Shroud Motion)

RUN 196 PT 14 FREQUENCY 191.08 TAU 5.233 HARMONICS 1-12 BLADES 27-28

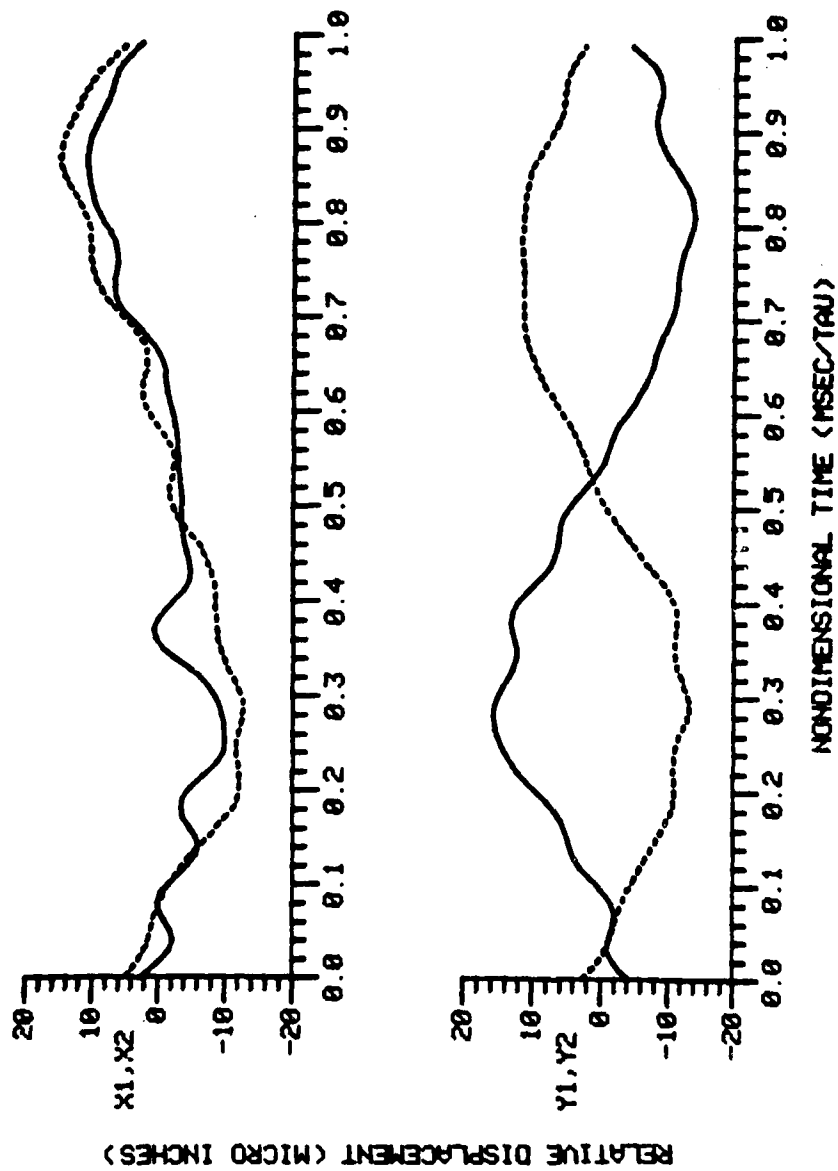


Figure 92 Time History of Relative Displacements at Shroud Interface #27-28 for Data Sample #4

RUN 196 POINT 14 HARMONICS 1- 1 BLADES 27-28 FREQUENCY 191.00

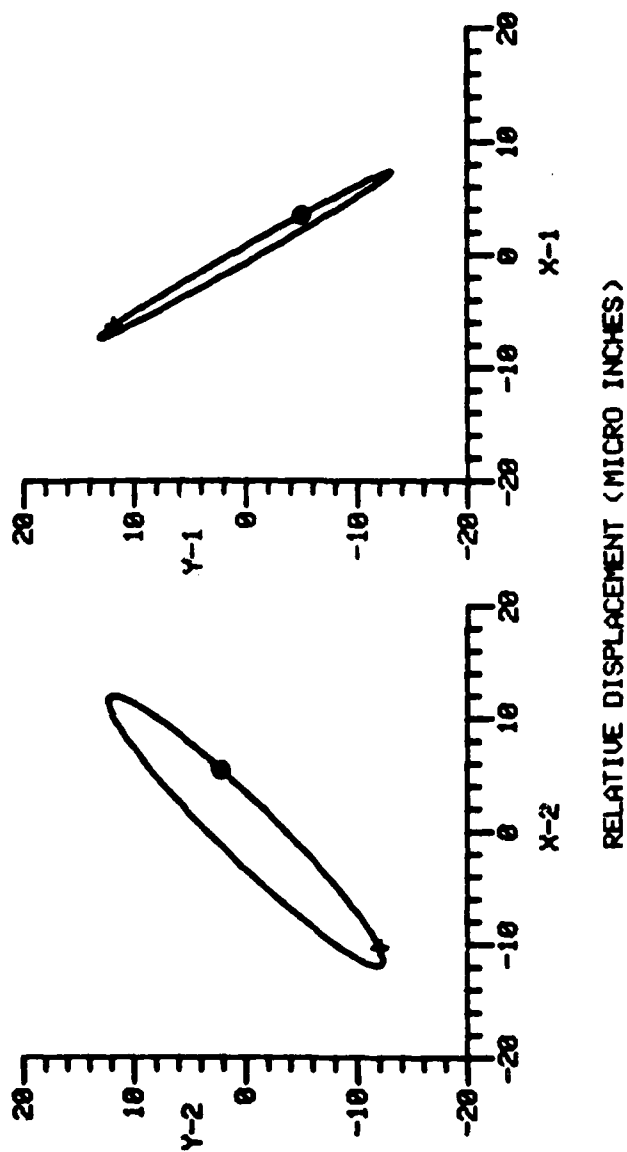


Figure 93 Relative Motion at Two Points on Shroud Interface  
#27-28 for Data Sample #4

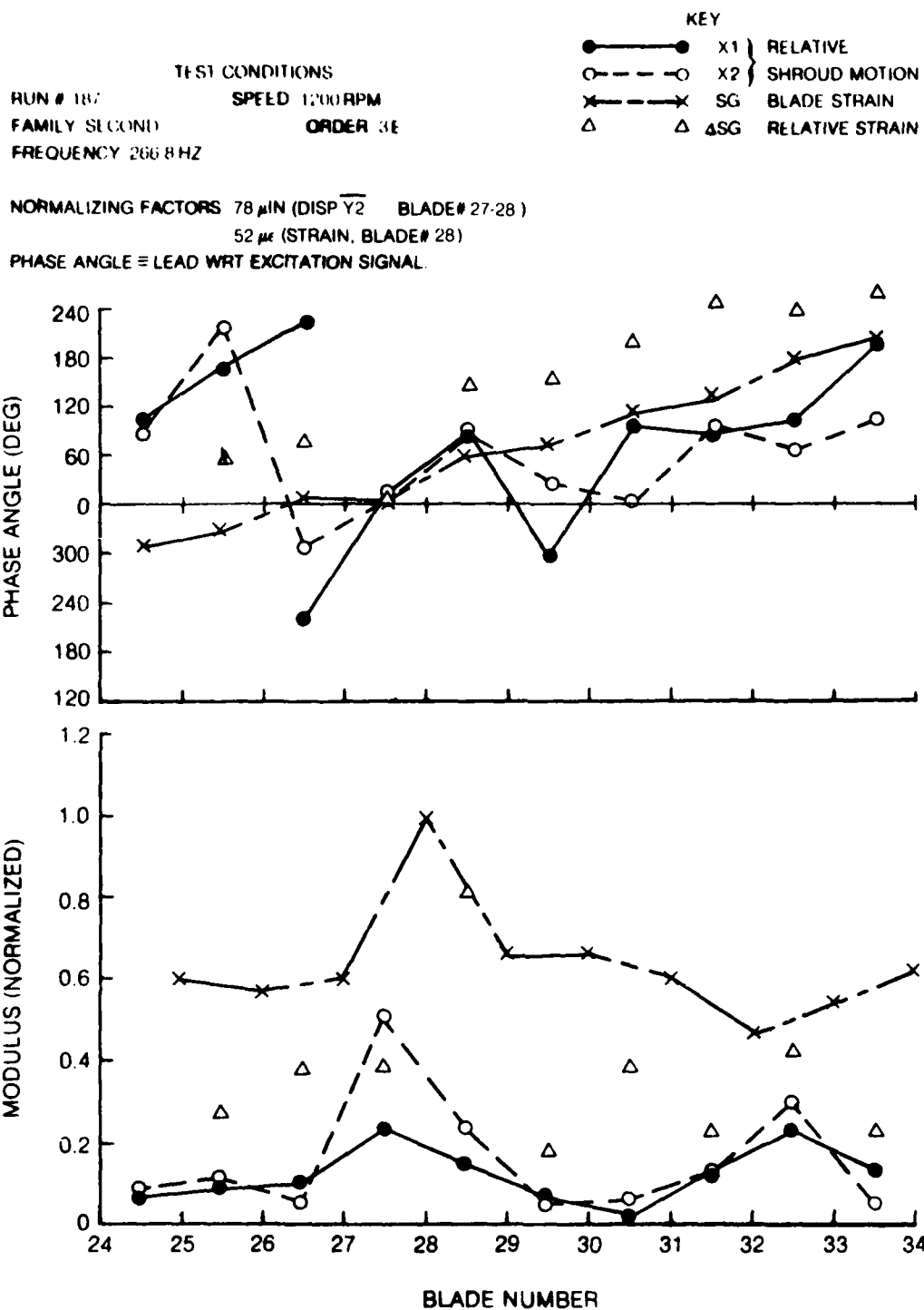


Figure 94 Modulus and Phase Plots of the Measured Response Parameters for Blades #25 through #34 with Backward Traveling Wave Excitation - Data Sample #5 (X - Axis Components of Shroud Motion)



TEST CONDITIONS  
 RUN # 187 SPEED 1200 RPM  
 FAMILY SECOND ORDER 3E  
 FREQUENCY 266.8 HZ

KEY  
 ● Y1 } RELATIVE  
 ○ Y2 } SHROUD MOTION  
 × SG BLADE STRAIN  
 Δ ΔSG RELATIVE STRAIN

NORMALIZING FACTORS 78  $\mu$ IN (DISP Y2 BLADE# 27-28)

52  $\mu$  (STRAIN, BLADE# 28)

PHASE ANGLE  $\equiv$  LEAD WRT EXCITATION SIGNAL

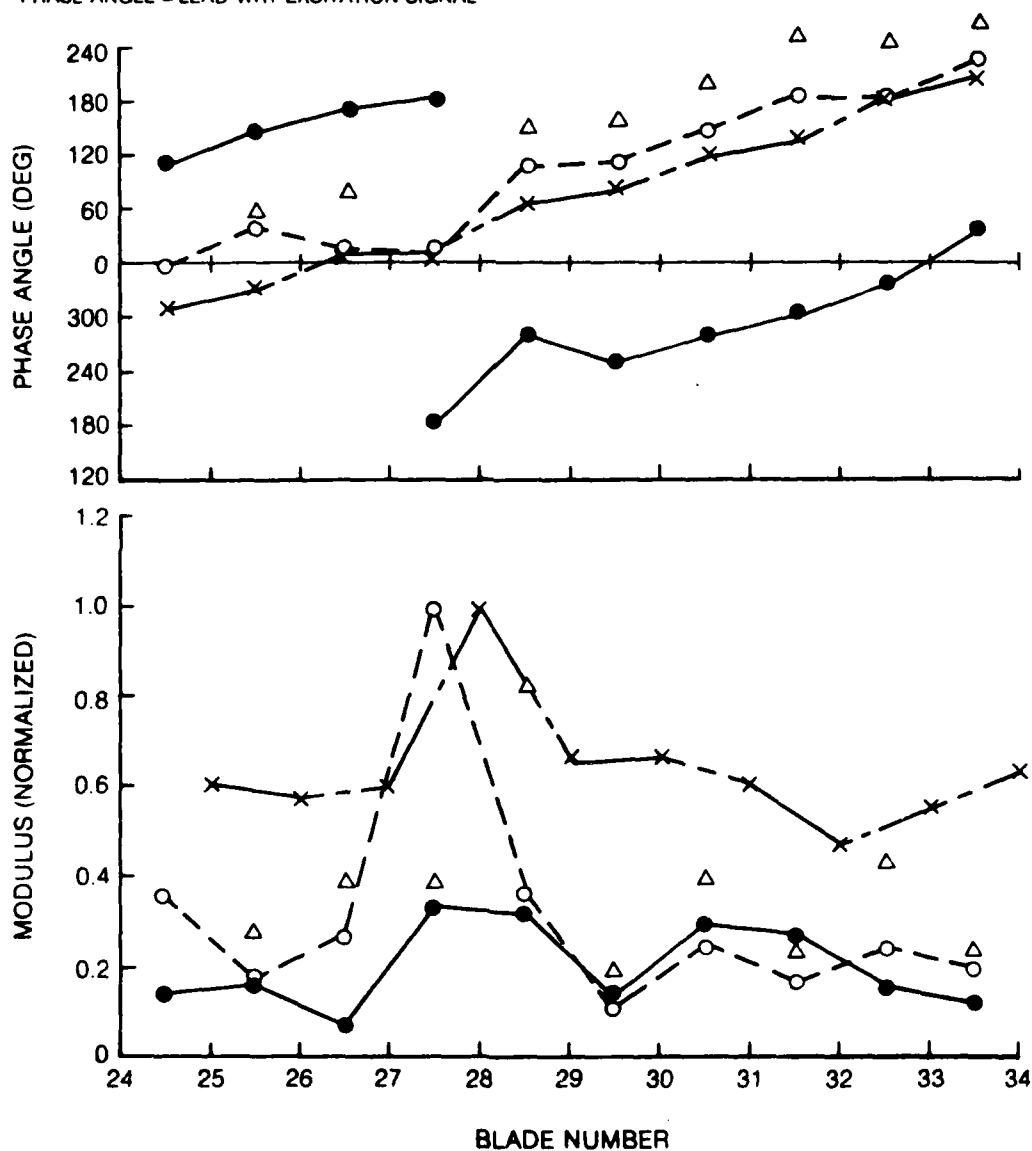


Figure 95 Modulus and Phase Plots of the Measured Response Parameters for Blades #25 through #34 with Backward Traveling Wave Excitation - Data Sample #5 (Y - Axis Components of Shroud Motion)

RUN 187 PT 14 FREQUENCY 266.93 TAU 3.746 HARMONICS 1-12 BLADES 27-28

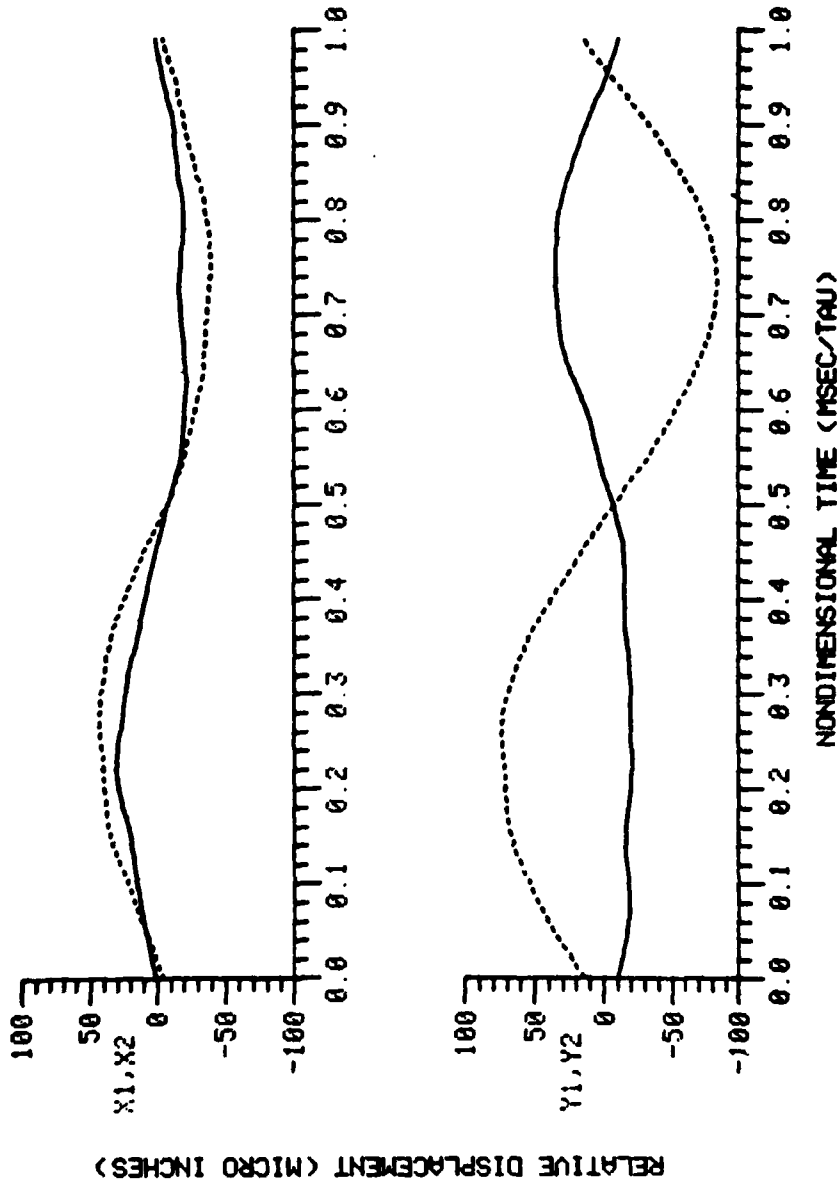
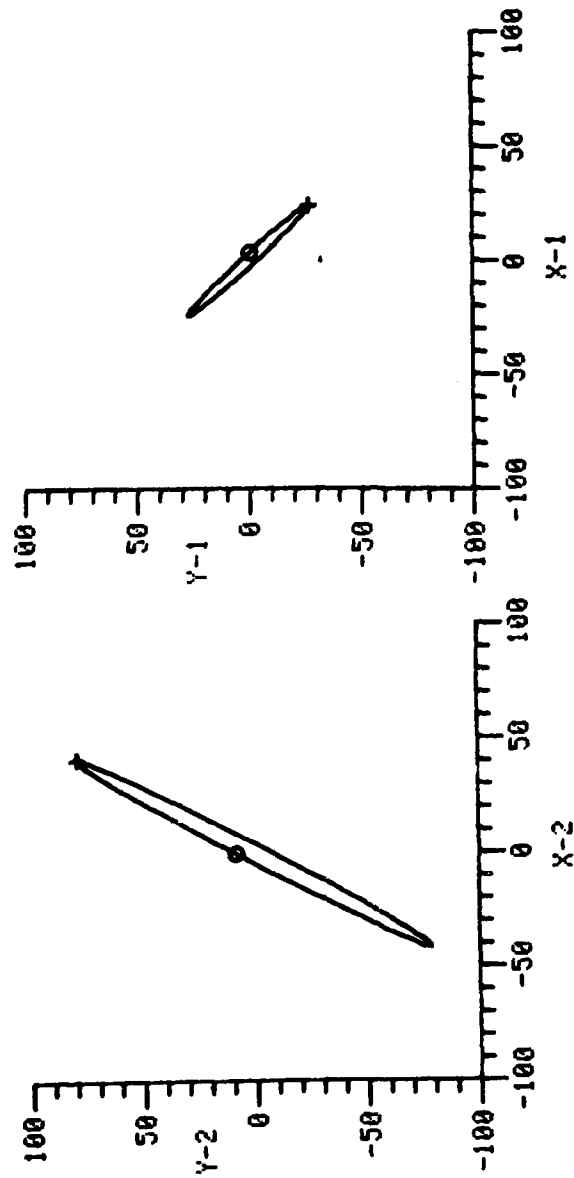


Figure 96 Time History of Relative Displacements at Shroud Interface #27-28 for Data Sample #5

RUN 187 POINT 14 HARMONICS 1- 1 BLADES 27-28 FREQUENCY 266.93



RELATIVE DISPLACEMENT (MICRO INCHES)

Figure 97 Relative Motion at Two Points on Shroud Interface  
#27-28 for Data Sample #5

TEST CONDITIONS  
 RUN # 191 SPEED 1200RPM  
 FAMILY SECOND ORDER 4E  
 FREQUENCY 282.0 HZ

KEY  
 ● X1 } RELATIVE  
 ○ X2 } SHROUD MOTION  
 × SG BLADE STRAIN  
 △ ΔSG RELATIVE STRAIN

NORMALIZING FACTORS 44 μIN (DISP Y2 BLADE # 27-28)  
 26 με (STRAIN, BLADE # 28)

PHASE ANGLE ≡ LEAD WRT EXCITATION SIGNAL

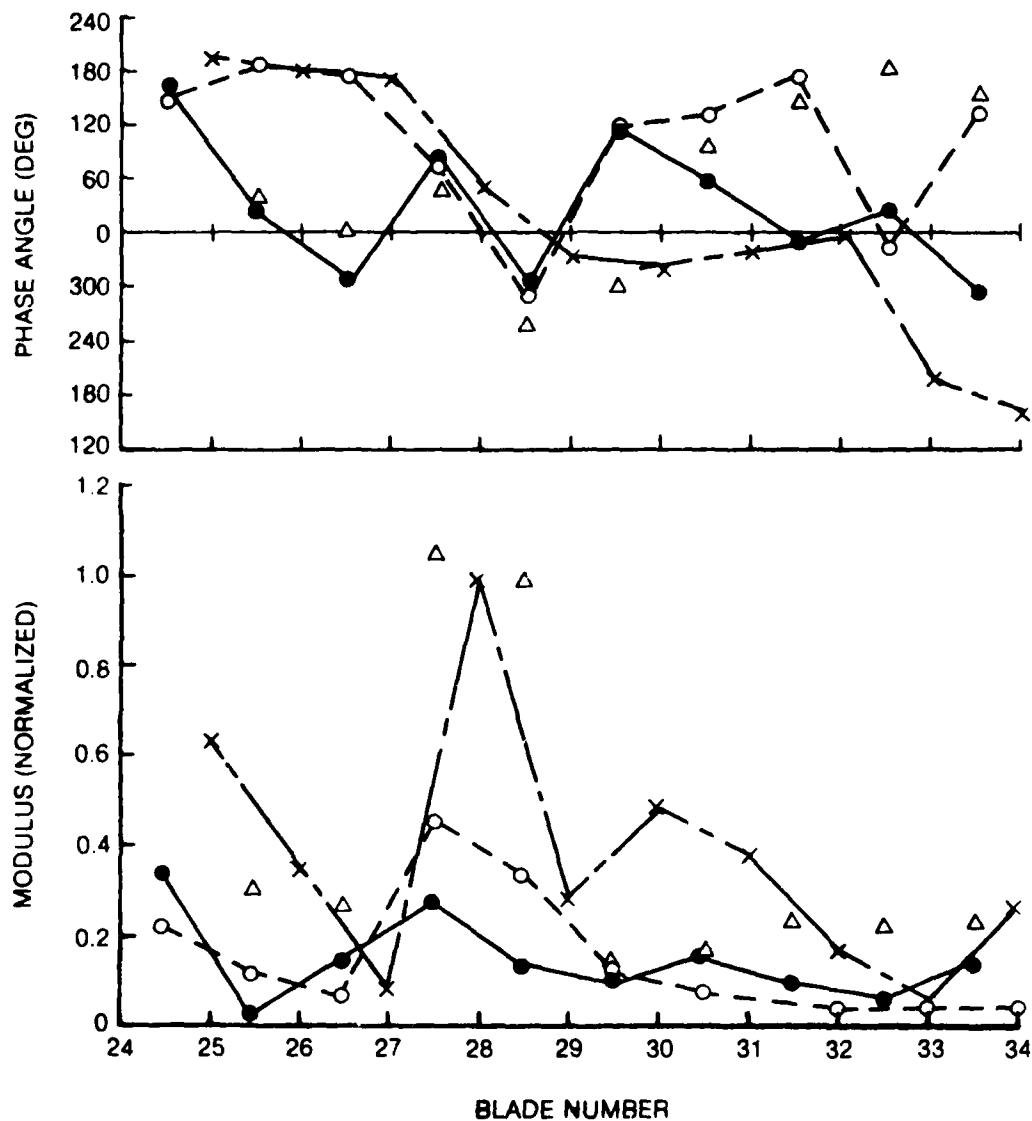


Figure 98 Modulus and Phase Plots of the Measured Response Parameters for Blades #25 through #34 with Backward Traveling Wave Excitation - Data Sample #6 (X - Axis Components of Shroud Motion)

TEST CONDITIONS  
 RUN # 191      SPEED 1200 RPM  
 FAMILY SECOND      ORDER 4E  
 FREQUENCY 282.0 HZ

KEY  
 ●——● Y1 } RELATIVE  
 ○——○ Y2 } SHROUD MOTION  
 ×——× SG } BLADE STRAIN  
 △——△ ΔSG } RELATIVE STRAIN

NORMALIZING FACTORS 44 μIN (DISP Y2 BLADE# 27-28)  
 26 με (STRAIN, BLADE# 28)

PHASE ANGLE ≡ LEAD WRT EXCITATION SIGNAL

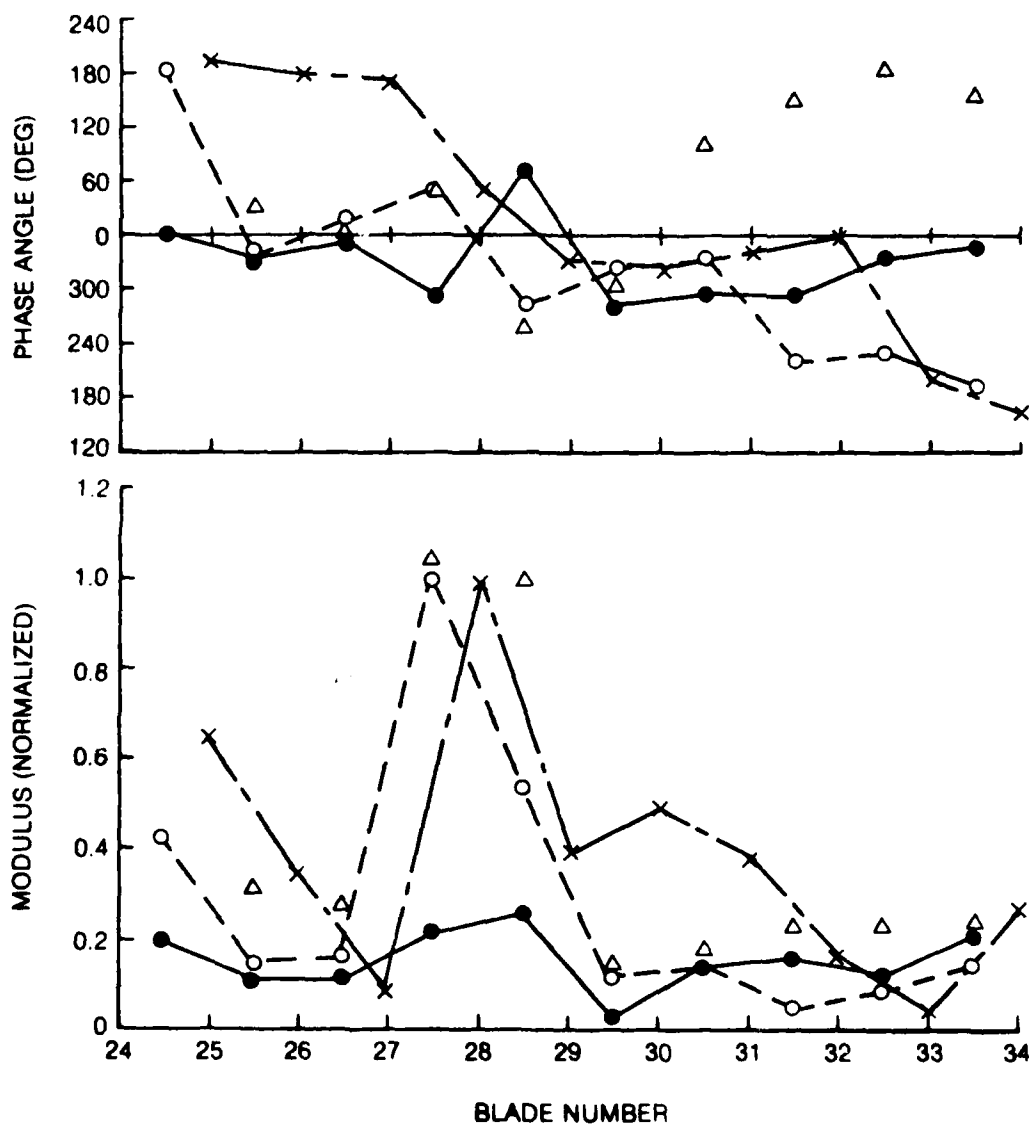


Figure 99 Modulus and Phase Plots of the Measured Response Parameters for Blades #25 through #34 with Backward Traveling Wave Excitation - Data Sample #6 (Y - Axis Components of Shroud Motion)

RUN 191 PT 4 FREQUENCY 281.99 TAU 3.546 HARMONICS 1-12 BLADES 27-28

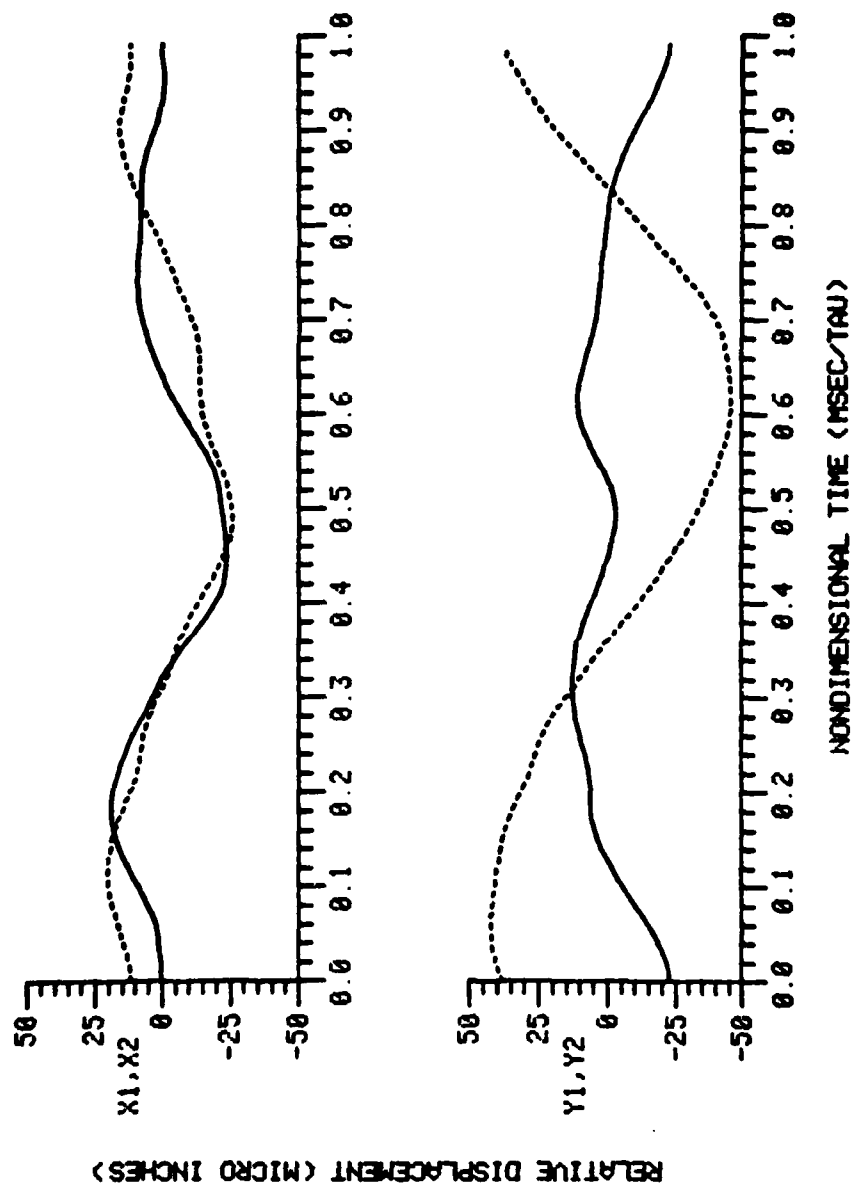


Figure 100 Time History of Relative Displacements at Shroud Interface #27-28 for Data Sample #6

RUN 191 POINT 4 HARMONICS 1- 1 BLADES 27-28 FREQUENCY 281.99

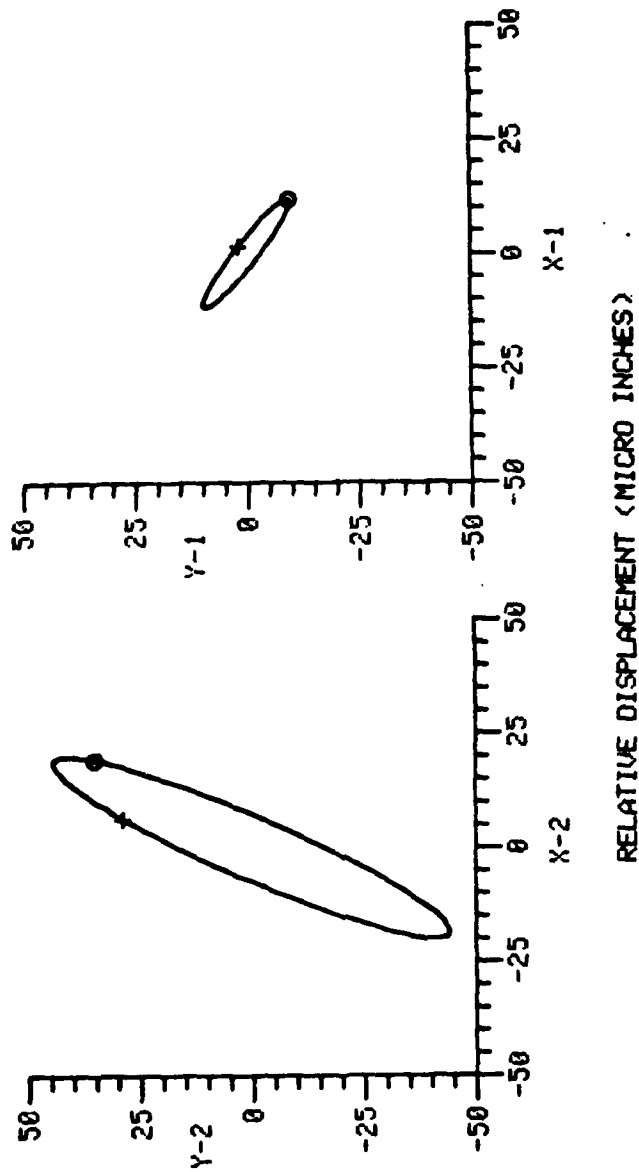


Figure 101 Relative Motion at Two Points on Shroud Interface  
#27-28 for Data Sample #6

the blades at these frequencies were an order of magnitude less (about 20  $\mu\epsilon$ ) than that which could be imposed (about 200  $\mu\epsilon$ ) during experiments involving vibrations in the first family. This may in part be due to higher levels of damping in the second family modes.

An examination of Figs. 86 and 87 and a comparison with Figs. 70, 71 confirm that the nature of vibration is essentially a stationary wave with the nodal line in the vicinity of blade #30. The spatial phase angle distribution (one half of the set of blades within the quadrant in and the rest out of phase) is a clear indication of the stationary vibration characteristics. Y1 and Y2 are essentially in phase with each other indicating a type of vibration which has node lines along the chord, one below the shroud and one above; a feature typical of the second family. Figures 90, 91, 92 and 93 represent data reduced from identical test conditions as those leading to Figs. 86, 87, 88 and 89 except for the slight change in the driving frequency (191.7 Hz instead of 193.9 Hz). Even such a small change has led to a major change in the response content, i.e., the presence of a backward traveling wave component. A reference to Fig. 91 indicates that maximum motion occurs both when the absolute strain is maximum (Y1 and Y2 nearly in phase) as well as as when the strain difference between blades reaches a maximum (Y1 and Y2 nearly out of phase).

A careful examination of the reduced data confirm the sensitivity of response characteristics to the conditions at the shroud in a realistic fan model.



## XI. TWIN MODE ANALYSIS OF MISTUNED SYSTEMS

The most basic modes of a flexible, fan assembly are standing wave vibratory patterns. For an ideal, perfectly symmetric component, the circumferential patterns do not have a bias and therefore the orientation of a mode is arbitrary. However, if there is slight asymmetry, each mode splits into two modes or twins occurring at slightly differing frequencies. These twin modes are identical in all respects except that they are orthogonal to each other in space. They represent the degenerate modes of the system and can be used to develop a simple theoretical model from which forced vibration characteristics of a mistuned system can be predicted. This section discusses the development and application of a theoretical model to the R-80 fan vibration data obtained with traveling wave excitations using the piezo-electric crystal excitation system.

The application of the analysis to an assembly of blades is based on the assumption that the component exhibits measurable split modes, i.e., the frequencies and damping in each twin are available. The shapes are assumed to be simple sines and cosines. Clearly, the response of the assembly to a forcing function over a limited frequency range can then be considered as the sum of contributions from each of the twins. Such an approach is based on an additional important assumption, i.e., that the other modes of the system (and therefore their twins) are sufficiently far away and do not contribute to the response.

The assumptions which form the basis of the analysis of slightly mistuned systems may now be summarized:

1. The structure exhibits measurable, independent twin mode pair at slightly different frequencies.
2. The mode shapes of each twin is a simple cosine or sine wave.

For systems where the coupling among the blades is insignificant or the mistuning is sufficiently large, the definition of twin modes will be severely lacking. The analysis discussed here will therefore not be applicable. The details of the analysis are summarized below. The twin modes of vibration can be described by

$$\left. \begin{aligned} y_I &= A \cos (n\theta - \psi) e^{i\omega t} \\ y_{II} &= B \cos \left( n\theta - \psi - \frac{\pi}{2} \right) e^{i\omega t} \end{aligned} \right\} \quad (i)$$

where  $n$  represents the harmonic number,  $\theta$  represents the position of a blade on the assembly,  $\psi$  provides the reference blade and  $\omega$  is the frequency of excitation.

For a single force  $\hat{F}$  acting on the system, the generalized forces corresponding to each twin are

$$\left. \begin{aligned} F_I &= \hat{F} \cos (n\theta - \psi) e^{i\omega t} \\ F_{II} &= \hat{F} \cos \left( n\theta - \psi - \frac{\pi}{2} \right) e^{i\omega t} \end{aligned} \right\} \quad (ii)$$

$$\text{Response in mode alone due to } F_I \text{ alone} = \frac{x_1}{F_I} \omega_1^2 m_1 = \frac{(1-r_1^2) - i\eta_1}{(1-r_1^2)^2 + \eta_1^2} \quad (iii)$$

Similarly,

$$\text{Response in mode 2 alone due to } F_{II} \text{ alone} = \frac{x_2}{F_{II}} \omega_2^2 m_2 = \frac{(1-r_2^2) - i\eta_2}{(1-r_2^2)^2 + \eta_2^2} \quad (iv)$$

where  $r_1 = \omega/\omega_1$ ,  $r_2 = \omega/\omega_2$ ,  $m_1$ ,  $m_2$  are generalized masses,  $\eta_1$ ,  $\eta_2$  are loss factors. Thus, the total response is a sum of the above contributions. The same analysis can be used to obtain the response to a traveling wave, if we recognize that a traveling wave can be represented in terms of two properly phased (in space and time) standing waves.

$F_I$  and  $F_{II}$  are spatially phased by  $\frac{\pi}{2}$ . A temporal phase also is necessary because a mere addition of  $F_I$  and  $F_{II}$  will not yield a traveling wave.

$$\text{i.e.} \quad F_I + F_{II} = \hat{F} e^{i\omega t} \left\{ \cos(n\theta - \psi) + \sin(n\theta - \psi) \right\} \quad (\text{v})$$

However, if  $F_{II}$  is in temporal phase with  $F_I$  i.e.  $F_{II}$  is written as  $\pm iF_{II}$ , then

$$\begin{aligned} F_I \pm iF_{II} &= \hat{F} e^{i\omega t} \left\{ \cos(n\theta - \psi) + i \sin(n\theta - \psi) \right\} \\ &= \hat{F} e^{i\omega t} \left\{ e^{\pm i(n\theta - \psi)} \right\} \\ &= \hat{F} e^{i(\omega t \pm i(n\theta - \psi))} \quad \text{which is a traveling wave.} \end{aligned} \quad (\text{vii})$$

Therefore, the stationary waves whose combination produces a traveling forcing function are

$$\begin{aligned} F_I &= \hat{F} e^{i\omega t} \cos(n\theta - \psi) \\ F_{II} &= \pm i \hat{F} e^{i\omega t} \cos\left(n\theta - \psi - \frac{\pi}{2}\right) \end{aligned} \quad (\text{viii})$$

Since the responses were derived above for standing waves, the response to traveling waves can be obtained by replacing  $F_{II}$  in Eq. (iv) by  $F_{II}$  in Eq. (viii).

The application of this analysis to the R-80 fan was restricted to tests in Rig A and to the second family of modes both in the initially "tuned" and the mistuned conditions. The steps in the application of the analysis are:

1. The modal properties of each of the twins are specified, i.e. the frequencies and damping of each mode.
2. The generalized force in each mode is calculated.
3. The response in each mode to the generalized force in each mode is calculated.
4. For a specified blade (i.e., specified  $\theta$ ) on the assembly the responses in each mode at the forcing frequency are calculated and added vectorially to obtain the total response of the blade.

In order to illustrate the application of the twin mode analysis two runs from the R-80 tests have been chosen. They are runs #11 and 81 at zero speed in which the fan was subjected to a 2ND forward traveling wave excitation. For the nominally tuned assembly, the ratio of the lower frequency of the twin ( $\omega_1$ ) to the other frequency was measured to be .9976. The corresponding ratio for the mistuned assembly was .9911. The differences in measured damping in each of the twins were such that a loss factor of .005 was used in the calculation for both modes.

Figures 102 through 104 display the polar plots for the nominally tuned assembly and Figs. 105 through 107 display similar plots for the mistuned assembly. In each plot a comparison with corresponding theoretical prediction is shown and in general, the agreement is good to excellent. A perfectly tuned system would show a single circular loop and have displayed identical characteristics for all the blades except for an increment in phase. Some blades in the nominally tuned system ( $\omega_1/\omega_2 = .9976$ ) display the influence of the twins as is evident from the loci. The corresponding figures for the mistuned system ( $\omega_1/\omega_2 = .9911$ ) show the contributions from the two modes with very distinct twin loops in the polar plots.

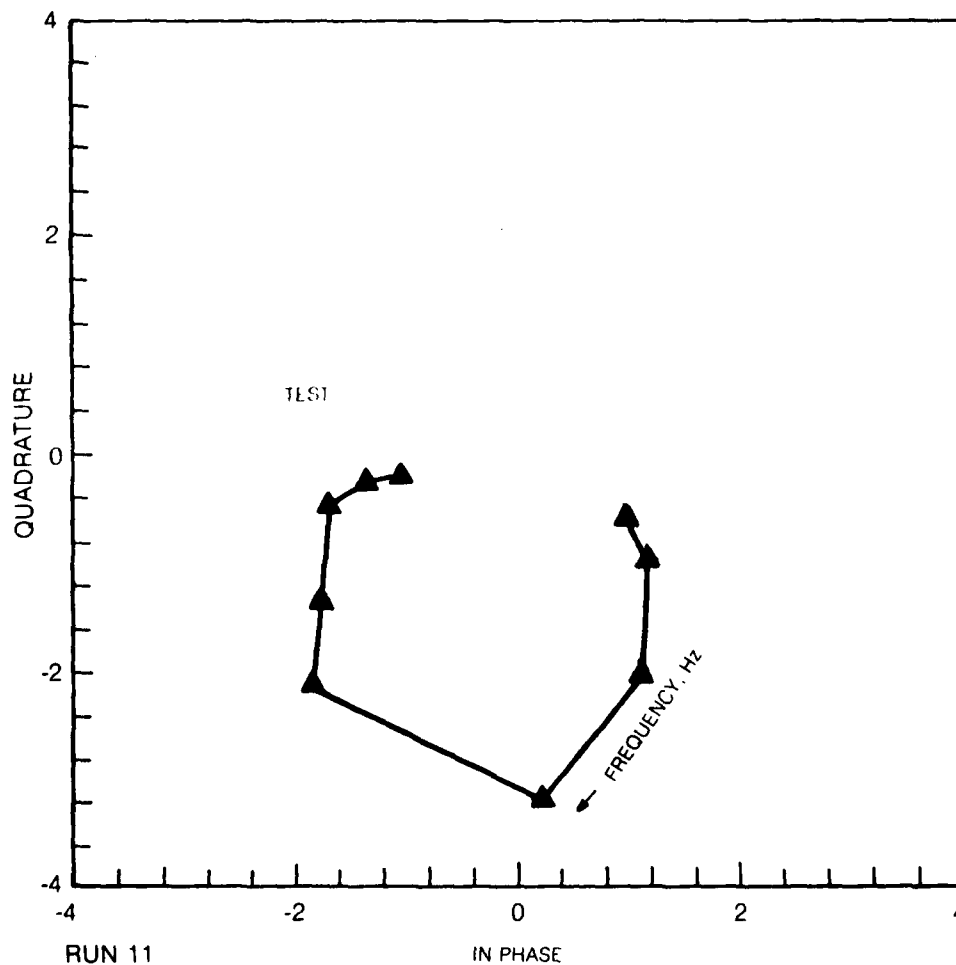
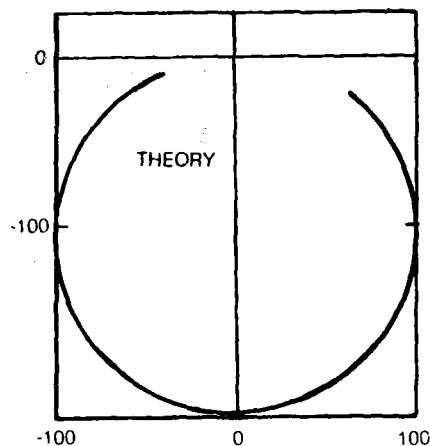


Figure 102 Polar Plots of Response of Blade #29 (Tuned Assembly) to a Forward Traveling Wave Excitation; Comparison of Theory With Test

83-8-36-48

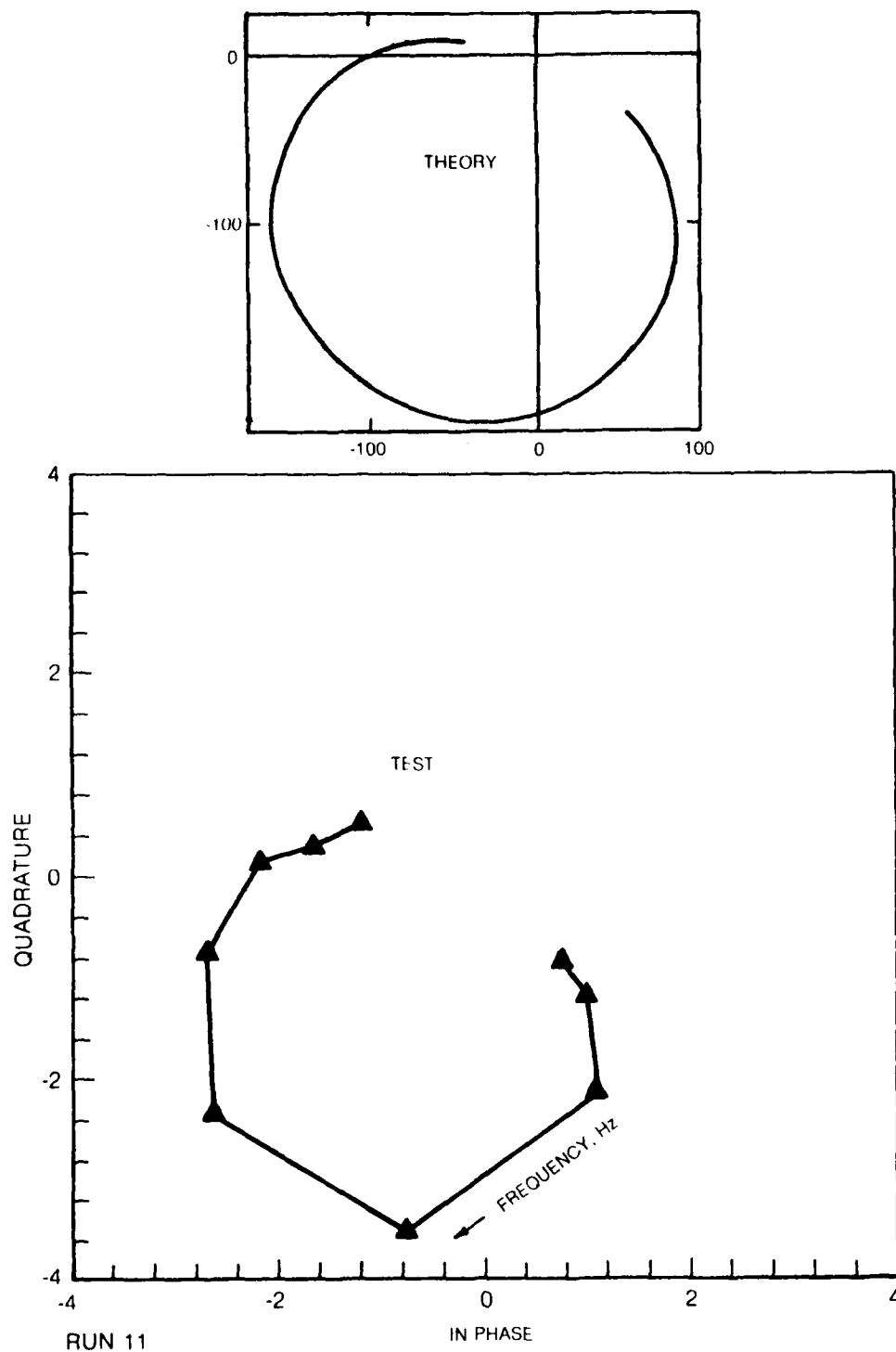


Figure 103 Polar Plots of Response of Blade #30 (Tuned Assembly) to a Forward Traveling Wave Excitation; Comparison of Theory With Test

83-8-36-46

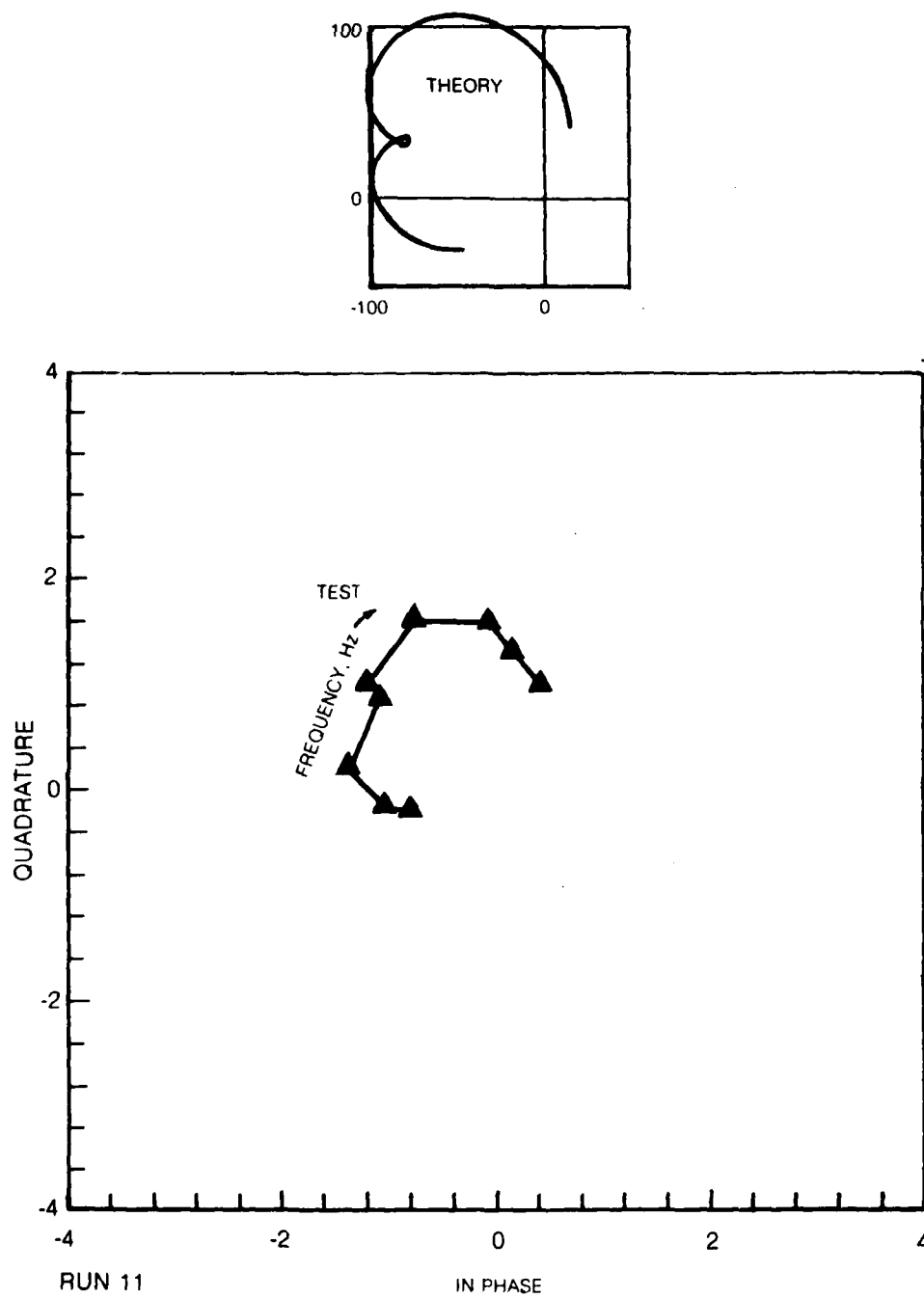


Figure 104 Polar Plots of Response of Blade #36 (Tuned Assembly) to a Forward Traveling Wave Excitation; Comparison of Theory With Test

83-8-36-44

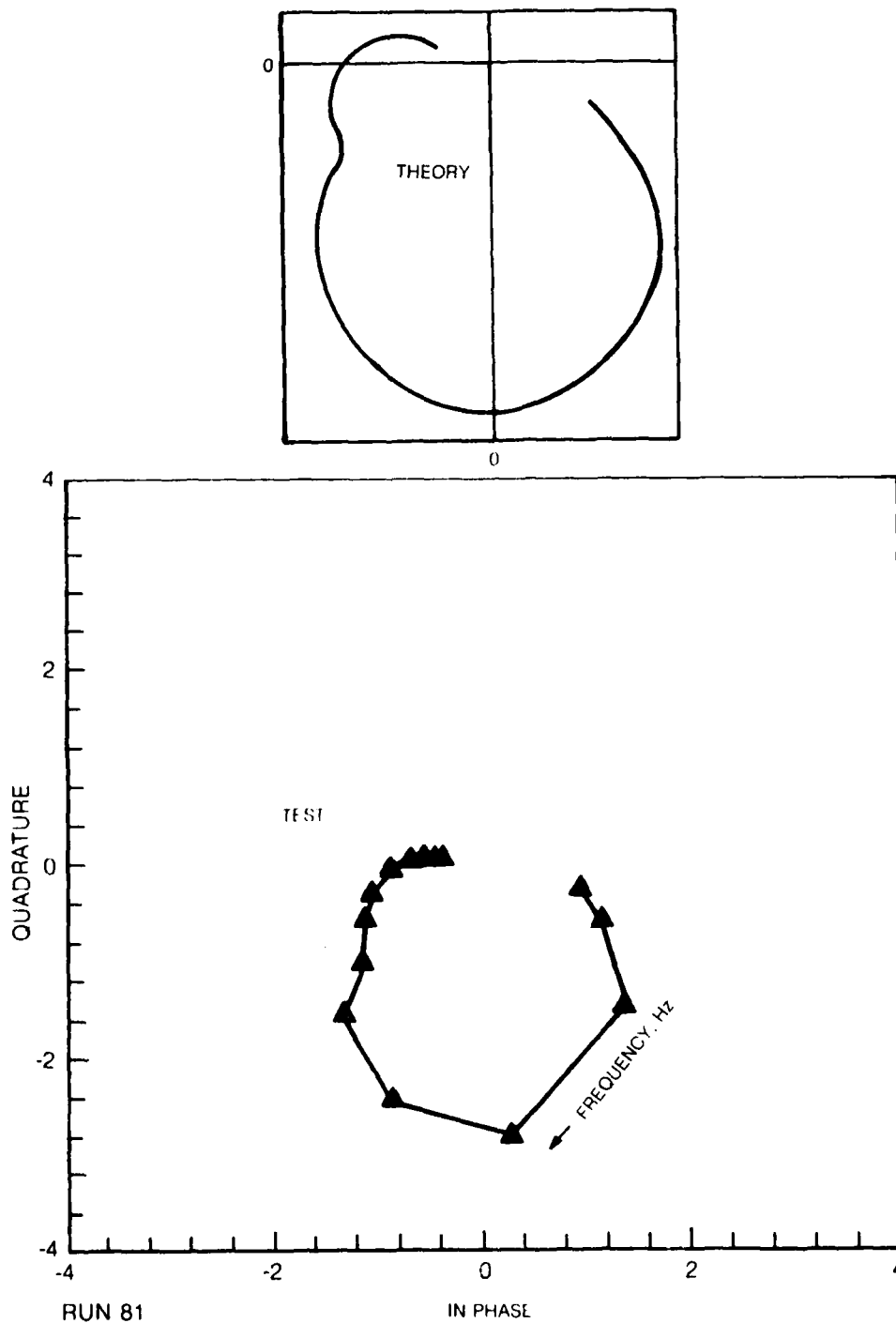


Figure 105 Polar Plots of Response of Blade #29 (Mistuned Assembly) to a Forward Traveling Wave Excitation; Comparison of Theory With Test

3-8-36-47



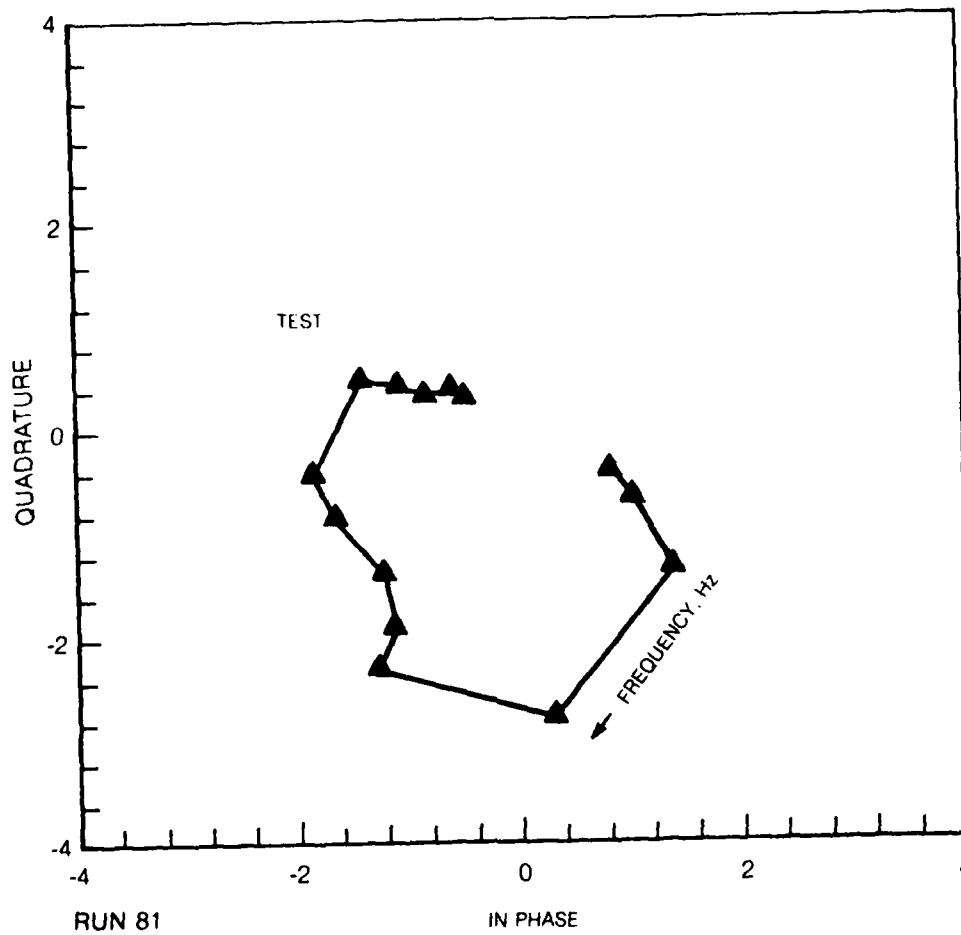
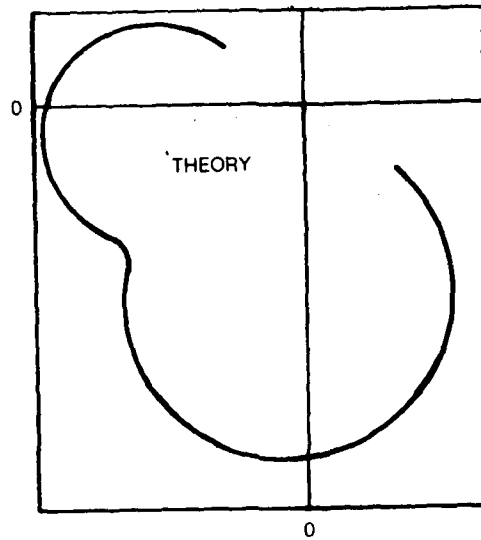


Figure 106 Polar Plots of Response of Blade #30 (Mistuned Assembly) to a Forward Traveling Wave Excitation; Comparison of Theory With Test

83-8-36-45

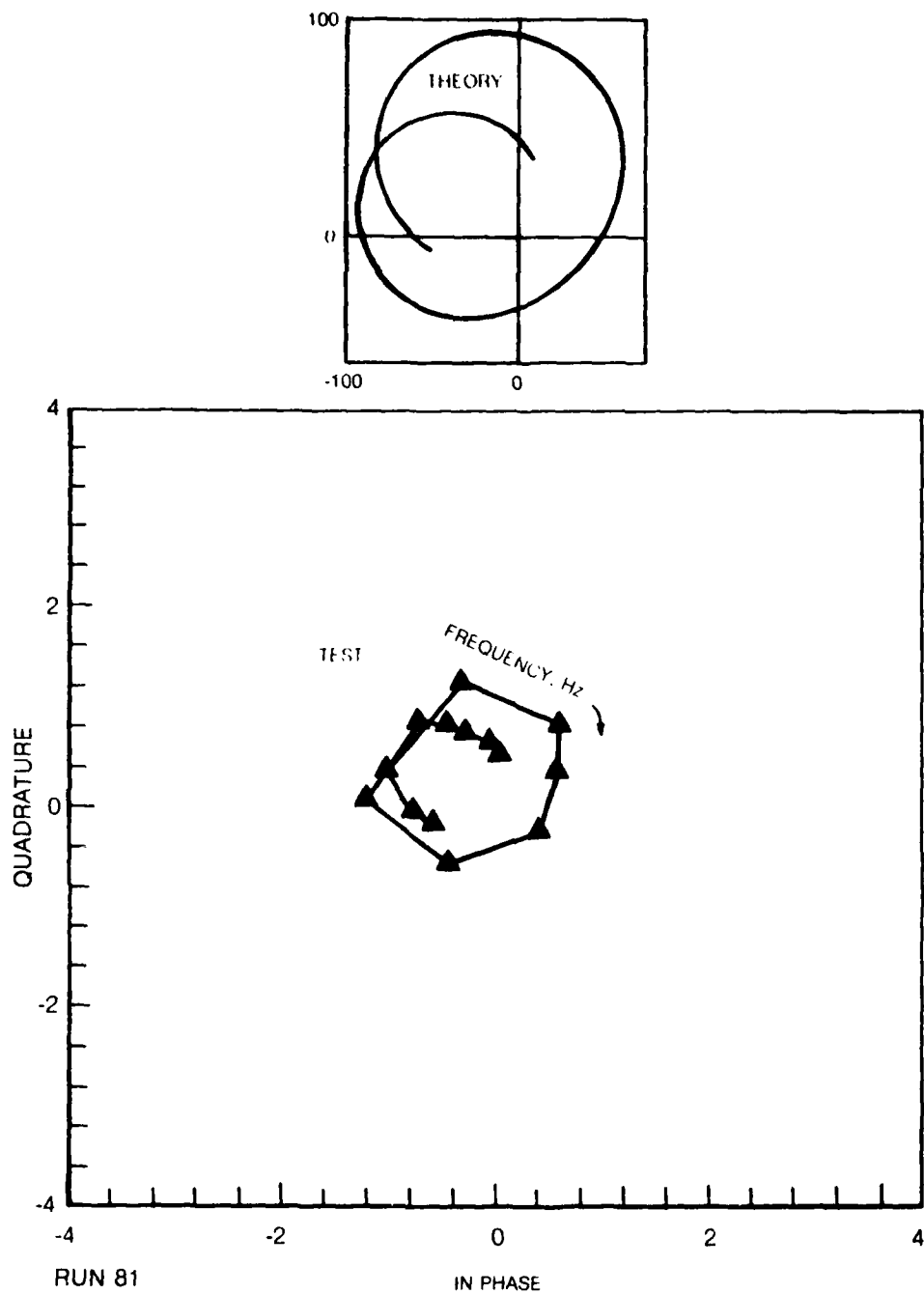


Figure 107 Polar Plots of Response of Blade 36 (Mistuned Assembly) to a Forward Traveling Wave Excitation; Comparison of Theory With Test

## XII. AEROMECHANICAL CHARACTERIZATION OF THE R-80 FAN ASSEMBLY

This phase of the program followed the tests of the mistuned assembly in the spin rig and therefore the assembly in its mistuned condition was tested first before being restored to its "tuned" condition.

The overall objectives of this phase of research was to measure vibratory strains in the fan blade due to forced vibration induced by (a) distortions in the flow field, (b) the piezoelectric crystal excitation system, and (c) exit guide vanes. A distortion screen with four lobes was designed, fabricated and installed in the flow field so that an integral order forced vibration corresponding to a fourth "engine order" (4E) could be induced. Velocity defects in the flow field due to the presence of the distortion screen were measured and correlated with blade strains. The assembly was subjected to traveling wave forced vibration via the piezoelectric crystal excitation system in 2, 3 and 4 nodal diameter patterns corresponding to the second family of modes. Finally, the influence of the exit guide vanes in inducing vibrations in the rotor blades was examined.

Tables 17 and 18 list the entire series of experiments conducted in this phase, and give the corresponding run numbers for reference. Table 19 presents the list of individual blade frequencies in the 1B and 1T modes measured in Rig B for the mistuned and tuned conditions. Figure 108 presents these frequencies in the form of a histogram.

### 1. Instrumentation and Calibration in Rig B

The pneumatic instrumentation in the fixed frame of reference is concentrated at two stations upstream of the fan stage and at one downstream station as shown in Fig. 109. Eight equally spaced static pressure taps were located circumferentially in the outer casing and hub at the upstream stations and in the outer casing at the downstream station. At station 0, closest to the screen, detailed pressure measurements were made using a combination of five pitot-static and three kiel probes placed at various radial positions at eight equally spaced circumferential locations. These measurements were used for rig calibration and also for screen documentation. At station 1, closest to the fan, the radial distribution of pressure was measured using a five element (with Gaussian spacing) total pressure rake. Measurements at this station were used to determine the inflow distortion due to the screen.

TABLE 17. SUMMARY OF TESTS PERFORMED ON FAN ASSEMBLY (MISTUNED CONDITION) IN RIG 3

FORCING		TESTS PERFORMED RUN NUMBERS											
CONFIGURATION	MODAL DIAM.	SPEED (RPM)											
		1	2	3	4	5	6	7	8	9	10	11	12
BLADE ALONE** (All others detuned)	-	x	x				-						-
SINGLE BLADE EXCITATION	-	3	4	3	4	3	4	3	4	3	4	3	4
FIRST FAMILY OF MODES	4	210-216	253-261	-	581-588	-	580	-	673-709	-	510-533	477-499	431-435
SECOND FAMILY OF MODES	2	217-226	667-8	608-626	589-607	670	540-559	-	-	-	510-533	477-499	431-435
	3	655-667		627-636	607	670	540-559	-	-	-	510-533	477-499	431-435
	4	262-275		637	637	654	540-559	-	-	-	510-533	477-499	431-435
	6												

NOTE: FLOW COEFFICIENT (C<sub>x</sub>/U) = 0.6 FOR ALL TESTS

KEY TO TEST:

- 1 = INDIVIDUAL BLADE EXCITATION. 1st BENDING MODE FREQUENCY (40 BLADES)  
 2 = INDIVIDUAL BLADE EXCITATION. 1st BENDING MODE FREQUENCY (40 BLADES)  
 3 = SINGLE BLADE FREQUENCY RESPONSE, 1st BENDING MODE (BLADE #28)  
 4 = SINGLE BLADE FREQUENCY RESPONSE, 1st TORSION MODE (BLADE #28)  
 5 = FORWARD TRAVELING WAVE - FREQUENCY RESPONSE (CRYSTAL EXCITATION)  
 6 = BACKWARD TRAVELING WAVE - FREQUENCY RESPONSE (CRYSTAL EXCITATION)  
 9 = BACKWARD TRAVELING WAVE - FREQUENCY RESPONSE ~ (4ND SCREEN EXCITATION)  
 10 = DECAY - FWD AND BKWD TRAVELING WAVE (CRYSTAL EXCITATION)

NOTES: \* INTEGRAL ORDER SPEED FOR FIRST FAMILY 4ND MODE

\*\* NOT RECORDED ON TAPE.

TABLE 18 SUMMARY OF TESTS PERFORMED ON FAN ASSEMBLY ("TUNED" CONDITION) IN RIG B.

FORCING		TESTS PERFORMED RUN NUMBERS							
CONFIGURATION	NODAL DIAM.	SPEED (RPM)				370/400	560	1050	1150-1200*
		0	1	2					
BLADE ALONE** (All others detuned)	-	x	x	x					1200
FIRST FAMILY OF MODES	4								9 710-734
SECOND FAMILY OF MODES	2								
	3								
	4								
	6								
			11	6	10	6	894	805-824	825-845 846-858 859-873
			913-924						

NOTE: FLOW COEFFICIENT ( $C_x/U$ ) = 0.6 FOR ALL TESTS

KEY TO TEST:

- 1 = INDIVIDUAL BLADE EXCITATION. 1st BENDING MODE FREQUENCY (9 BLADES)
- 2 = INDIVIDUAL BLADE EXCITATION. 1st TORSION MODE FREQUENCY (9 BLADES)
- 6 = BACKWARD TRAVELING WAVE - FREQUENCY RESPONSE (CRYSTAL EXCITATION)
- 9 = BACKWARD TRAVELING WAVE - FREQUENCY RESPONSE (4ND SCREEN EXCITATION)
- 10 = DECAY - FWD AND BKWD TRAVELING WAVE (CRYSTAL EXCITATION)
- 11 = BACKWARD TRAVELING WAVE - FREQUENCY RESPONSE (EGV EXCITATION)

NOTES: \*INTEGRAL ORDER SPEED FOR FIRST FAMILY 4ND MODE

\*\*NOT RECORDED ON TAPE

TABLE 10 RESONANT FREQUENCIES FOR INDIVIDUAL BLADES IN UNCOUPLED  
CONFIGURATION AS MEASURED IN RIG B.

BLADE NUMBER	1B MODE		1T MODE	
	MISTUNED	"TUNED"*	MISTUNED	"TUNED"*
	FREQUENCY-HZ	FREQUENCY-HZ	FREQUENCY-HZ	FREQUENCY-HZ
1	64.78		321.1	
2	63.53		304.7	
3	63.51		305.6	
4	65.88	63.30	322.1	311.5
5	64.09		314.9	
6	64.01		311.5	
7	64.52		315.9	
8	62.12	63.96	306.9	304.3
9	62.92		315.2	
10	64.14		303.6	
11	64.88		320.1	
12	65.29		311.4	
13	67.76	64.55	322.2	317.7
14	65.92	64.60	316.4	314.2
15	64.64		320.5	
16	65.66		315.1	
17	64.27		314.1	
18	64.88		322.2	
19	63.89		316.3	
20	64.83		309.8	
21	63.66		313.8	
22	63.48		303.8	
23	63.61		310.6	
24	67.39	63.57	320.6	315.2
25	63.21		316.1	
26	64.86		320.0	
27	64.85		318.5	
28	55.78	63.17	289.7	297.5
29	64.69		314.6	
30	63.69		319.5	
31	64.74		323.9	
32	67.74	64.50	319.6	314.7
33	66.66	63.40	318.1	315.9
34	66.28	62.90	315.5	312.0
35	64.62		318.1	
36	63.51		312.3	
37	64.59		306.4	
38	64.52		324.3	
39	64.31		318.9	
40	63.72		309.6	

\*Results shown for modified blades only

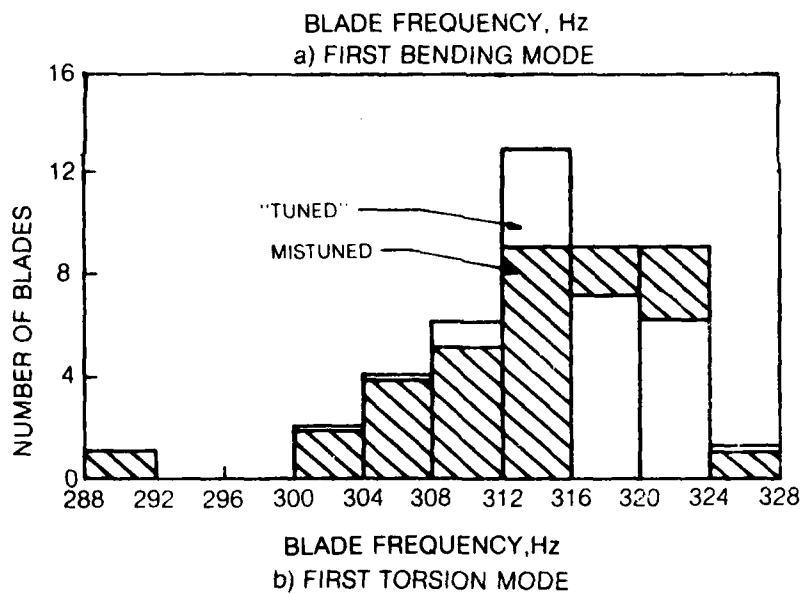
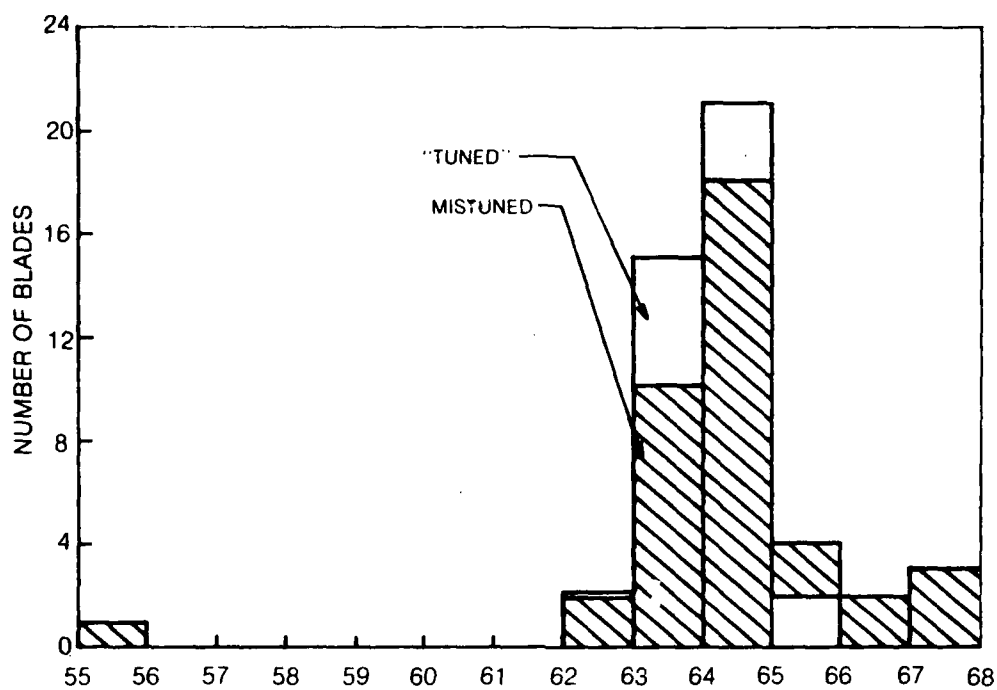


Figure 108 Histograms of "Blade Alone" Modal Frequencies for the "Tuned" and Mistuned Assembly

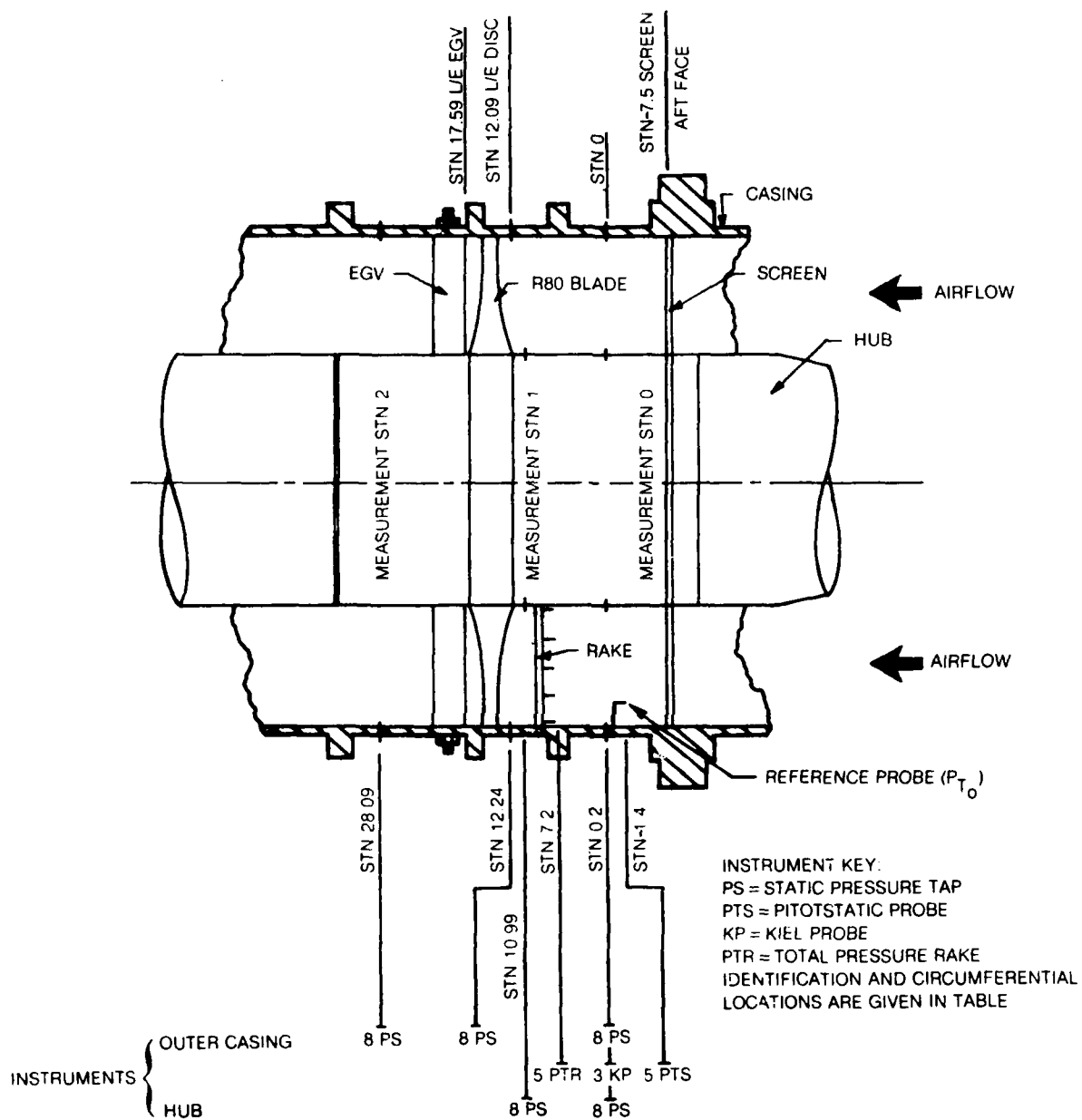


Figure 109 Pressure Instrumentation in Test Section



AD-A146 226

BASIC STUDY OF BLADED DISK STRUCTURAL RESPONSE(U)  
UNITED TECHNOLOGIES RESEARCH CENTER EAST HARTFORD CT  
A V SRINIVASAN ET AL. NOV 83 R83-914806-48

3/3

UNCLASSIFIED

AFWAL-TR-83-2075 F33615-79-C-2054

F/G 1/3

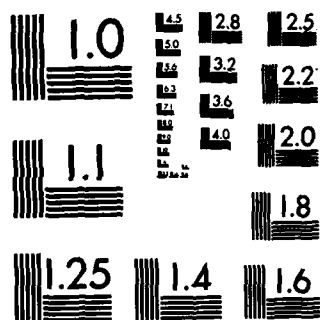
NL



END

FILMED

DTIC



MICROCOPY RESOLUTION TEST CHART  
NATIONAL BUREAU OF STANDARDS-1963-A

Assessment of the static pressure rise across the stage for fan performance and speed line determination utilized the pressure measurements at station 2. The axial and circumferential locations of the taps and probes are detailed in Table 20 along with instrument I/D, scanivalve number and port number for reference.

With the R-80 fan installed in Rig B (see Fig. 110) and with clean inlet conditions, initial runs were made at 810 rpm to calibrate the reference total pressure probe which was used subsequently for the control of tunnel flow conditions. Runs were also made to check for inlet distortion; no significant distortion was found.

The clean inlet speedline characteristic was determined at 1050 rpm with some checkpoints also being made at 810 rpm. Results of these measurements in terms of fan static pressure rise coefficient  $\Delta P/Q_{umid}$ , and axial flow velocity ratio  $C_x/U$  are presented in Fig. 111. The static pressure rise was determined from outer casing wall taps at measuring stations 0 and 2, while the dynamic pressure, and hence the axial velocity  $C_x$ , were determined from a kiel probe and casing pressure tap at measuring station 0. The reference velocity is the rotor tangential velocity at blade midspan (22.5 inches).

Also shown in Fig. 111 are the mass averaged values from design computations. As can be seen, there is good agreement between the design and measured values except near stall. 0.525 was set as the low safe limit for axial flow coefficient. At 1200 rpm the maximum value of flow coefficient attainable was 0.7. All tests except for vibration decay tests reported in a subsequent section, were performed at and near a flow coefficient of 0.6.

## 2. Aerodynamic Distortion Screen Design

During the mechanical characterization testing phase it was shown that in the first family of modes, only a four nodal diameter mode could be excited. A four lobed distortion screen was therefore selected so that this mode could be studied in an aerodynamic environment.

The objective was to design and build a screen which would produce a spatially fixed fan inflow with its axial component varying sinusoidally in the circumferential direction. In this way, only low order (preferably the first family) modes would be excited.

TABLE 20

## IDENTIFICATION AND LOCATION OF PRESSURE INSTRUMENTATION

INST. I/D	TYPE (1)	MEAS. STN	LOCATION			SCAN/VALVE	PORT #
			R (IN)	C (2)	STN (IN)		
C001	PS	0	30.00	67.18	0.2	1	2
C002	PS	0	30.00	20.82	0.2	1	3
C003	PS	0	30.00	338.12	0.2	1	4
C004	PS	0	30.00	292.00	0.2	1	5
C005	PS	0	30.00	247.25	0.2	1	6
C006	PS	0	30.00	204.50	0.2	1	7
C007	PS	0	30.00	157.63	0.2	1	8
C008	PS	0	30.00	112.55	0.2	1	9
H001	PS	0	15.00	38.00	0.2	1	12
H002	PS	0	15.00	353.00	0.2	1	13
H003	PS	0	15.00	308.33	0.2	1	14
H004	PS	0	15.00	363.80	0.2	1	15
H005	PS	0	15.00	218.00	0.2	1	16
H006	PS	0	15.00	187.00	0.2	1	17
H007	PS	0	15.00	127.00	0.2	1	18
H008	PS	0	15.00	82.00	0.2	1	19
PS001	PTS(S)	0	15.70	290.78	-1.4	1	20
PS002	PTS(S)	0	18.47	245.33	-1.4	1	21
PS003	PTS(S)	0	22.50	205.67	-1.4	1	22
PS004	PTS(S)	0	26.54	155.60	-1.4	1	23
PS005	PTS(S)	0	29.30	110.68	-1.4	1	24
K001	KP	0	22.50	65.70	0.2	1	25
K002	KP	0	22.50	20.48	0.2	1	26
K003	KP	0	22.50	336.60	0.2	1	27
PT001	PS(T)	0	15.70	290.18	-1.4	1	28
PT002	PS(T)	0	18.47	245.33	-1.4	1	29
PT003	PS(T)	0	22.50	205.67	-1.4	1	30
PT004	PS(T)	0	26.54	155.60	-1.4	1	31
PT005	PS(T)	0	29.30	110.68	-1.4	1	32
H101	PS	1	15.00	45.00	10.99	1	35
H102	PS	1	15.00	0.00	10.99	1	36
H103	PS	1	15.00	315.00	10.99	1	37
H104	PS	1	15.00	270.00	10.99	1	38
H105	PS	1	15.00	224.00	10.99	1	39
H106	PS	1	15.00	180.00	10.99	1	40
H107	PS	1	15.00	135.00	10.99	1	41
H108	PS	1	15.00	91.00	10.99	1	42
C101	PS	1	30.00	67.00	12.24	2	2
C102	PS	1	30.00	22.00	12.24	2	3
C103	PS	1	30.00	336.00	12.24	2	4
C104	PS	1	30.00	293.00	12.24	2	5
C105	PS	1	30.00	246.00	12.24	2	6
C106	PS	1	30.00	202.00	12.24	2	7
C107	PS	1	30.00	157.00	12.24	2	8
C108	PS	1	30.00	112.00	12.24	2	9
C201	PS	2	30.00	34.00	28.09	2	10
C202	PS	2	30.00	348.00	28.09	2	11
C203	PS	2	30.00	304.00	28.09	2	12
C204	PS	2	30.00	258.00	28.09	2	13
C205	PS	2	30.00	214.00	28.09	2	14
C206	PS	2	30.00	168.00	28.09	2	15
C207	PS	2	30.00	123.00	28.09	2	16
C208	PS	2	30.00	78.00	28.09	2	17
PR1	PTR	1	15.70	112.00	7.2	2	24
PR2	PTR	1	18.47	112.00	7.2	2	25
PR3	PTR	1	22.50	112.00	7.2	2	26
PR4	PTR	1	26.54	112.00	7.2	2	27
PR5	PTR	1	29.30	112.00	7.2	2	28

NOTES: (1) TYPE NOTATION KEY  
 PS = STATIC PRESSURE TAP  
 KP = KIEL TOTAL PRESSURE PROBE  
 PTS = PITOT STATIC PROBE (S) STATIC, (T) TOTAL  
 PTR = TOTAL PRESSURE RAKE (5 PROBES)

(2) ANGLE  $\theta$  MEASURED CLOCKWISE WHEN VIEWED LOOKING UPSTREAM.

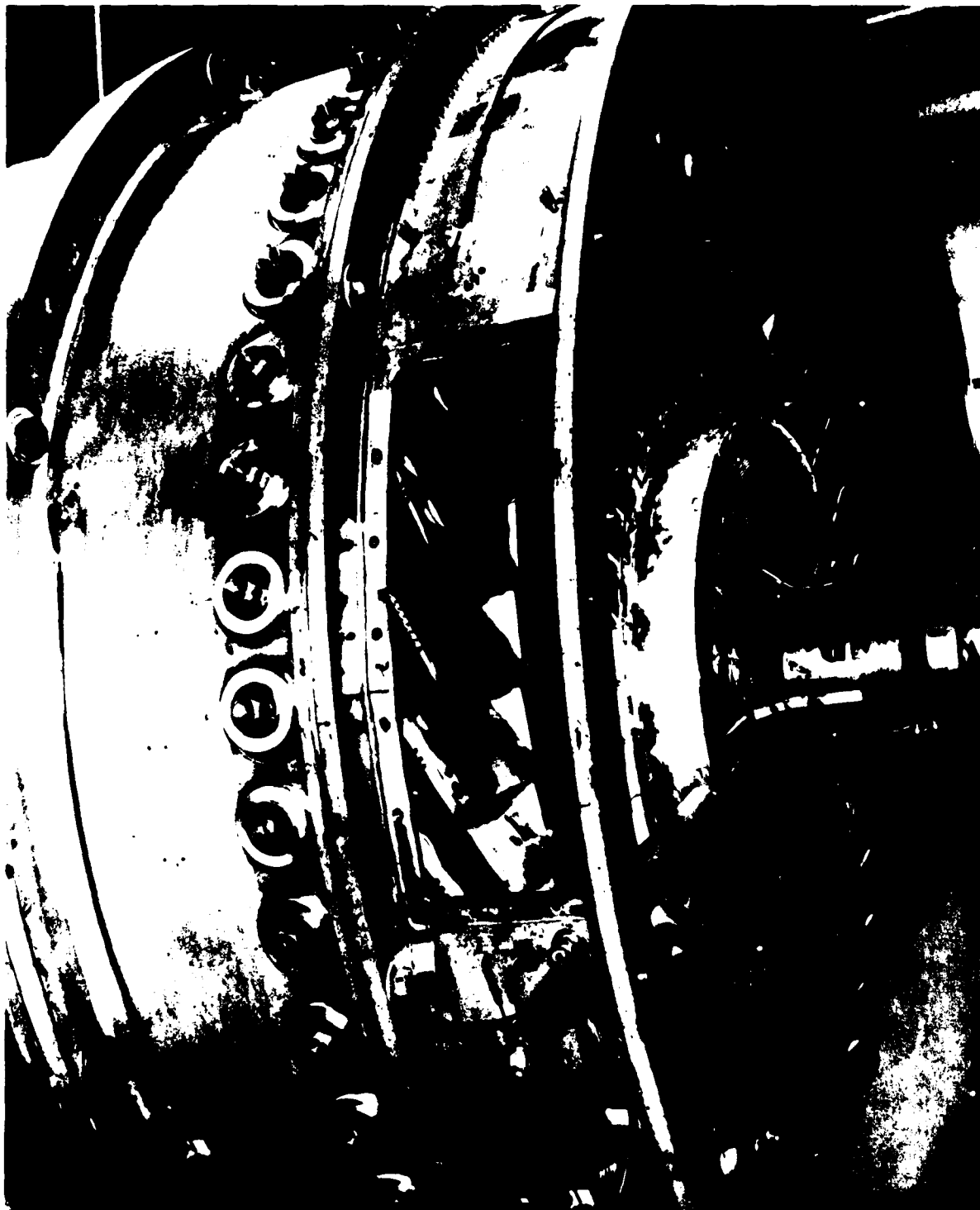


Figure 110 Setup for Measuring "Blade Alone" Modal Frequencies in Rig B

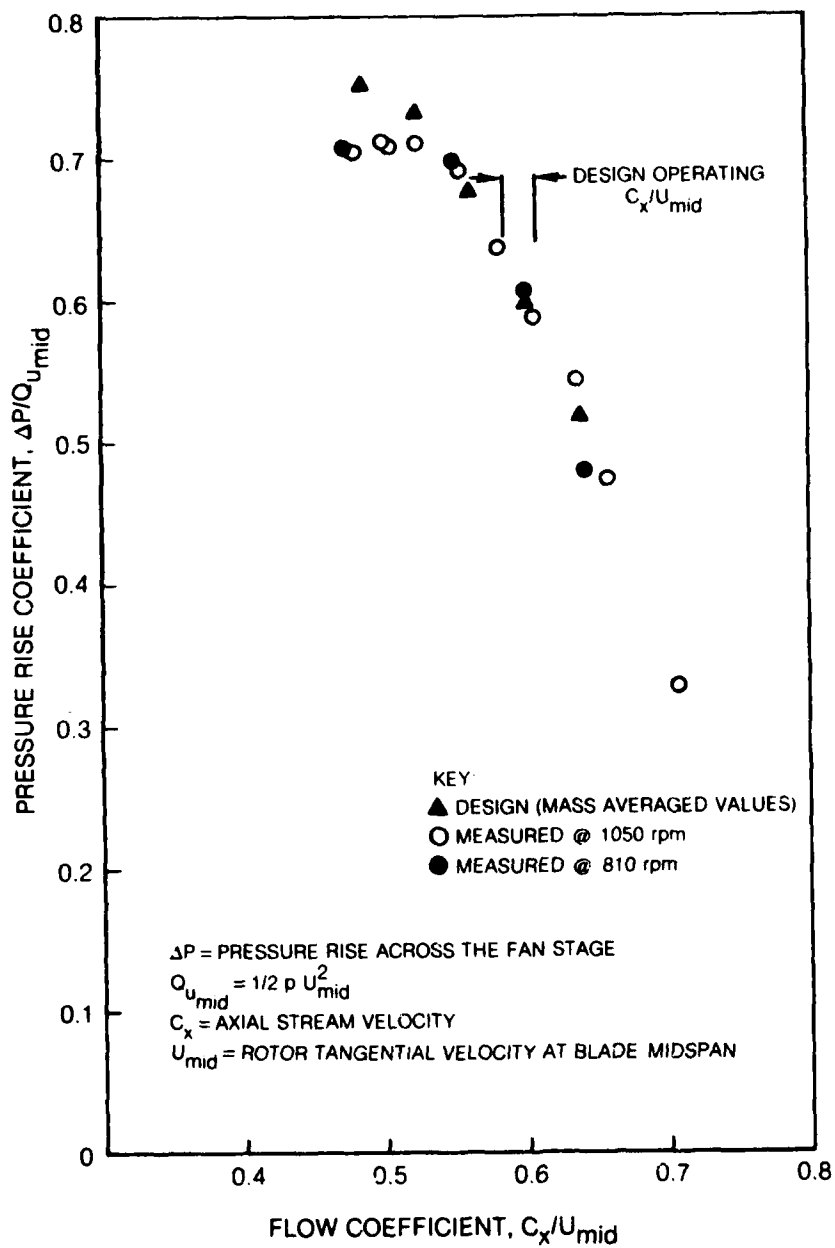


Figure 111 R80 Fan Clean Inlet Speed Line: Comparison of Measured Values with Design Points

The method used to design the screen is given in Refs. 3 and 4 and employed overlays of wire screens which cause a loss in total pressure in the airstream passing through the screen. The overlay method of Ref. 4 allows a variation of total pressure to be calculated using the combined resistance coefficient of the screen. The latter is accurately predicted by summing the individual resistance coefficients of the support, or base screen, and overlay screens for a given value of loss coefficient based on Reynolds number. The design equations of Ref. 3 were programmed to allow various designs to be easily examined.

Theoretical calculations indicated that an axial flow variation of  $\pm 3$  percent would produce a blade vibratory stress (at the above-shroud-maximum-thickness location) of  $\pm 5000$  psi. However, this was based on the assumptions of a low aerodynamic damping (0.00124) and the location of distortion at the fan station. To test the influence of these assumptions, it was decided to build a trial screen and obtain data early in the test program. The distortion chosen for this screen was a 10 percent distortion four lobed square wave with each high resistance region extending over a range of  $45^\circ$ . The trial screen was a temporary modification of the partially built test screen and was made by wiring onto the base screen ( $2 \times 0.035$  i.e. 2 wires per inch, 0.035 inch diameter square mesh) four segments of  $18 \times 0.009$  square mesh screen. The results obtained from this screen at rotor speeds near the integral (4E) order speed confirmed that a distortion of only 3 percent was needed to produce adequate strain in the blades. However, without going to specially made screens or varying the wire size in other ways, spray painting for instance, a design having a reasonably smooth distortion variation using available materials resulted in a calculated distortion of 6.4 percent. This design is shown in Fig. 112. The figure shows the calculated variation of resistance coefficient together with the screen mesh specifications (shown crosshatched) required to approximate the curve with eight resistance steps per lobe. A screen having this design was built and was found to have a distortion of approximately 5 percent at a measuring station close to the fan. However, the strain induced in the blades at the integral order speed was excessive and the screen was subsequently modified by increasing the resistance in the low resistance regions. This caused a distortion of the sinusoidal distribution but reduced the maximum distortion to useable levels. A photograph of the final screen used in this program is shown in Fig. 113. A low-melting-point alloy (Cerrobend) was used to "anchor" the stainless steel screening in the outer rim and hub. This proved to be very satisfactory and convenient. Figure 114 shows the screen mounted in Rig B and the pneumatic instrumentation at measuring station 0.

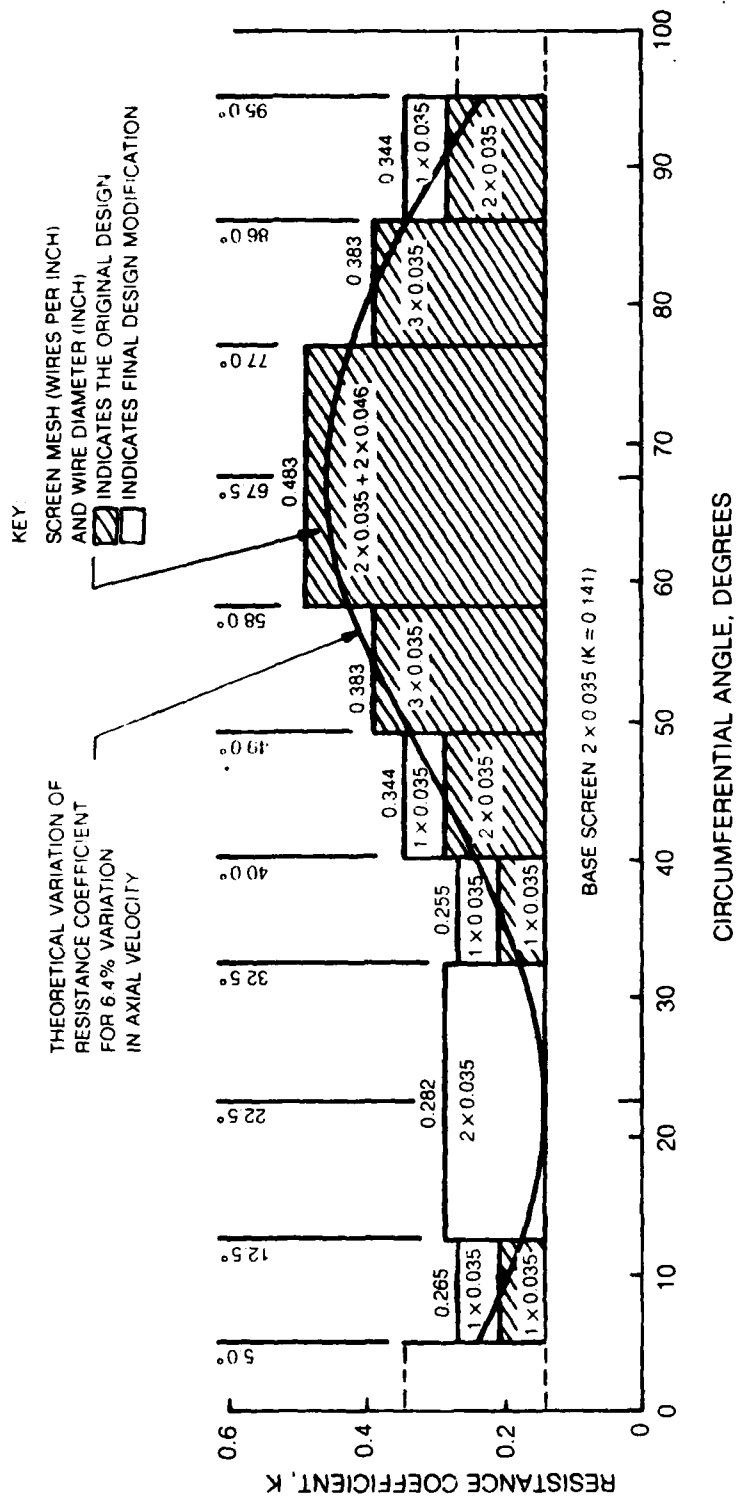


Figure 112 Theoretical Variation of Resistance Coefficient and  
Corresponding Overlay Segment Characteristics for a  
Quadrant of the Four Cycle Distortion Screen



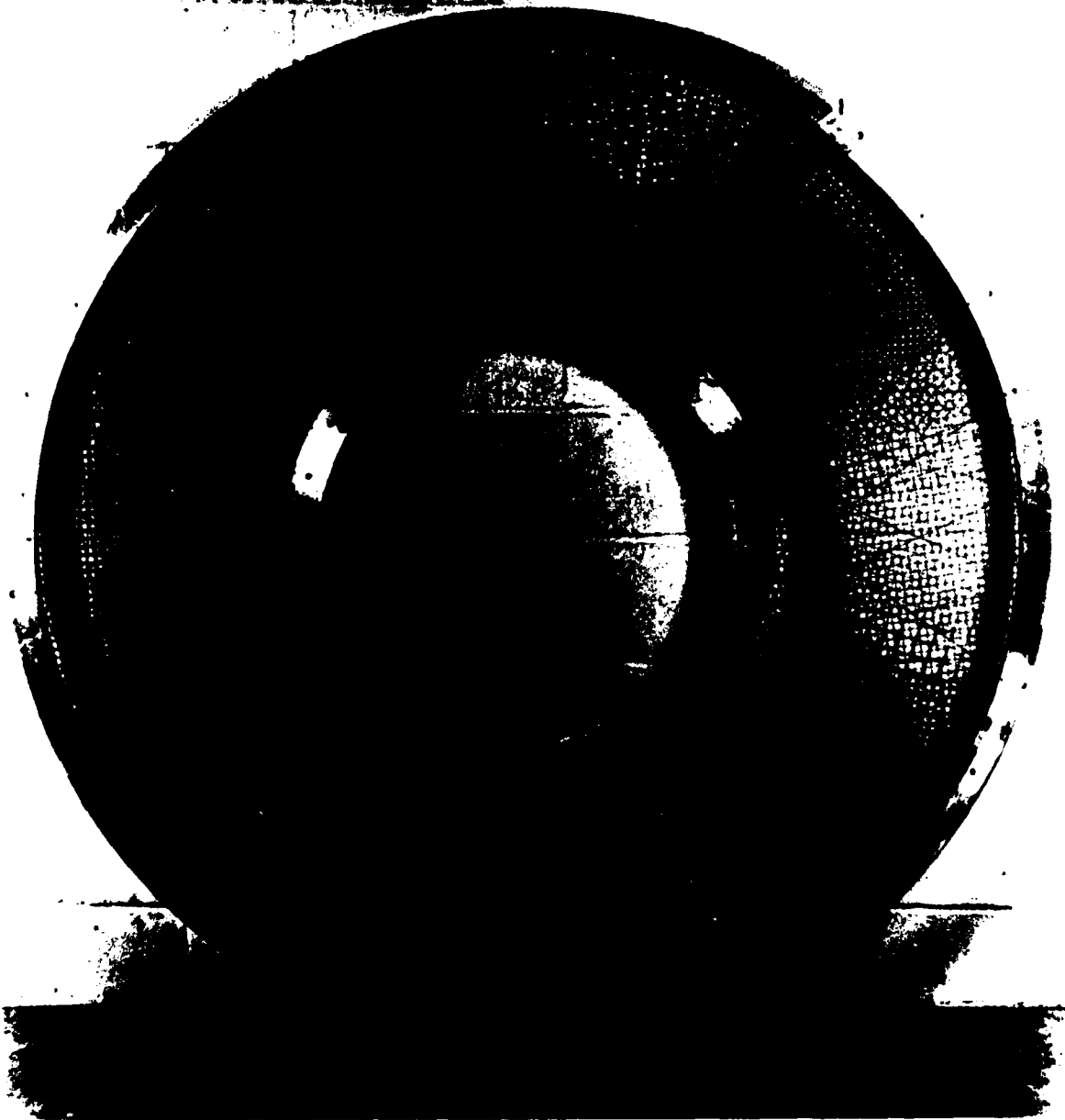


Figure 113 The Four Lobe Aerodynamic Distortion Screen



Figure 114 Distortion Screen Mounted in Rig B

83-194-B

83-8-36-37

### 3. Screen Evaluation and Distortion Measurement

The screen was evaluated at a rotor speed of 1056 rpm and an average flow coefficient ( $C_x/U$ ) of 0.62. The procedure used was to rotate the screen incrementally in front of the fixed frame pneumatic instrumentation described earlier. The pressure readings were digitized and stored on tape in the form of pressure coefficients, i.e.,  $(P_{T0}-P)/1/2\rho U^2$ , where  $P$  is the pressure reading,  $P_{T0}$  is the pressure at a reference probe at measuring station 0 (see Fig. 109),  $\rho$  is air density and  $U$  is the tangential wheel speed at mid blade span. Subsequent data reduction was performed to obtain the Fourier components of the variation in average axial flow coefficient ( $C_x/U$ ) at each increment of angle around a quadrant of the screen. The computation flow chart is given in Fig. 115. The screen is assumed to be cyclic symmetrical and hence the results for a quadrant were applied to the whole screen.

Figure 116 shows the resulting variation of axial coefficient for one quadrant around the screen at the two measuring stations 0 and 1.  $0^\circ$  is at top dead center of the rig. The strength and phase of each Fourier component at the two stations are given below.

#### HARMONIC CONTENT OF $C_x/U$ VARIATION

Harmonic	Station 0		Station 1	
	Amplitude	Phase (Lead)	Amplitude	Phase (Lead)
0	1.2195		1.1986	
4	0.0283	38.6	0.0225	37.2
8	0.0043	67.2	0.0066	26.8
12	0.0056	53.7	0.0042	10.1
Average $C_x/U$	0.610		0.599	
4th Order Distortion	4.64%		3.75%	

$C_x$  = Axial flow velocity  
 $P$  = Measured pressure  
 $P_{ref}$  = Average of the 8 casing static pressures at station 0  
 $P_{T_o}$  = Reference port pressure  
 $\theta$  = Circumferential angle  
 $Q_{u_{mid}} = 1/2 \rho U_{mid}^2$   
 $U_{mid}$  = Tangential velocity at blade mid span

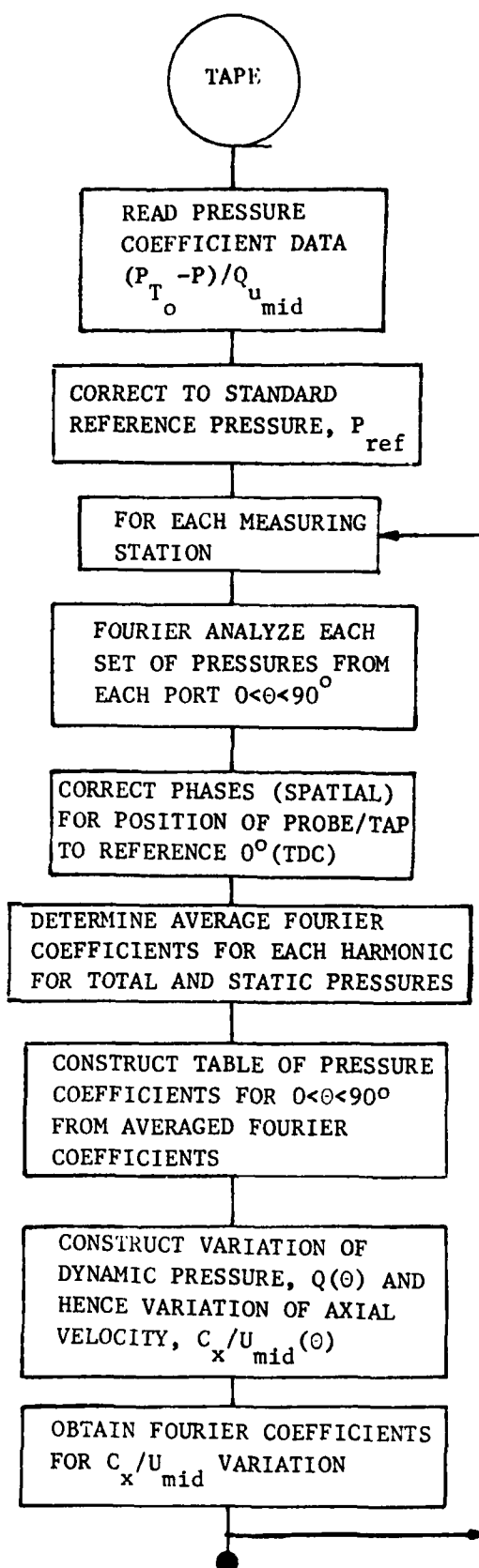


Figure 115 Computational Flow Chart to Obtain the Harmonic Content of the Circumferential Variation of Flow Coefficient.

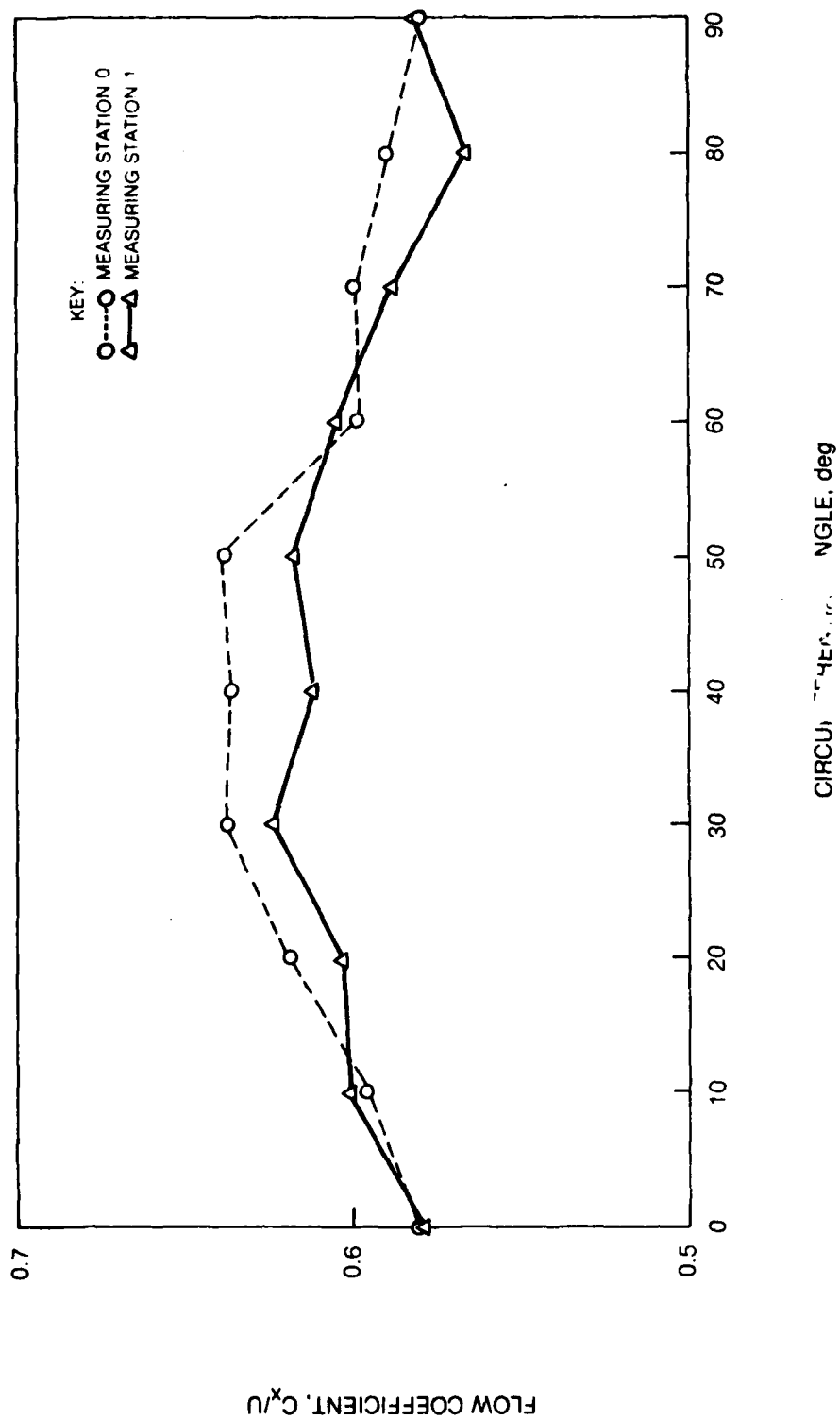


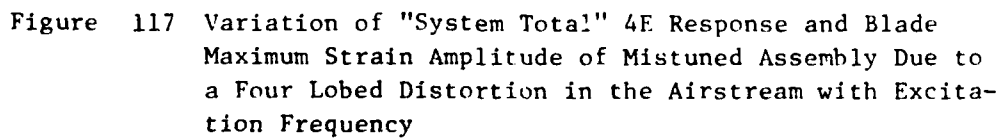
Figure 116 Variation of Average Flow Coefficient with Circumferential Angle at the Two Measuring Stations Downstream of the Distortion Screen

#### 4. Integral Order Resonance

The fan assembly was subjected to forced vibration through aerodynamic excitation provided by a 4 lobed distortion screen that could, according to calculations, cause a predominantly 4E resonant vibration around 1100 rpm. The aerodynamic conditions of flow were set at the design point (i.e.  $C_x/U=0.6$ ) and the blades were surveyed to determine the extent of vibratory strain levels experienced. The observations clearly confirmed that the assembly responded with stress levels of over  $\pm 10,000$  psi even before the integral order speed could be reached. It was evident that the assembly whose modal characteristics in the first family modes in vacuum were irregular, was responding quite actively under the influence of strong aerodynamic excitations provided by the distortion screen. However, the strain levels were unacceptably large and the risks of high frequency fatigue failures were not minimal. Therefore, it was decided to redesign the screen in order to reduce the level of distortion. The redesigned screen, as discussed earlier, was found to be adequate and resulted in stress levels of around  $\pm 10,000$  psi at integral order speed. The latter was determined experimentally to be 1149 rpm.

A plot of maximum strain measured, in the mistuned assembly, in the region of the integral order speed is shown in Fig. 117. The different blade numbers shown indicate that the maximum strain experienced by different blades at different speeds reached a peak with blade #11 as the integral order speed is reached. The stick plots shown in Figs. 118 and 119 confirm that the general nature of the response mode is a 4 nodal diameter backward traveling wave, although blades #28 and #11 record a much larger strain at 66.36 Hz and 77.04 Hz respectively. Thus, the response of the assembly as a whole is essentially characterized by the backward traveling wave whose behavior over the frequency range around the integral order is also shown in Fig. 117 as the system "total" response. This (and similar responses to follow) should be viewed as the response of the assembly in a "regular system mode" and is obtained from stickplots by summing the contributions of the fundamental harmonics ( $A_4 + A_{-4}$ ) in the present example.

From Fig. 117, it is clear that blades #11, #30, and #32 are the most responsive blades near the integral order speed. The in-phase and out-of-phase components of their response over a frequency range spanning the system resonance in a four nodal diameter mode are plotted in Fig. 120. These plots were used to obtain an "integral order resonant frequency" of 77.1 Hz with a loss factor of 0.034.



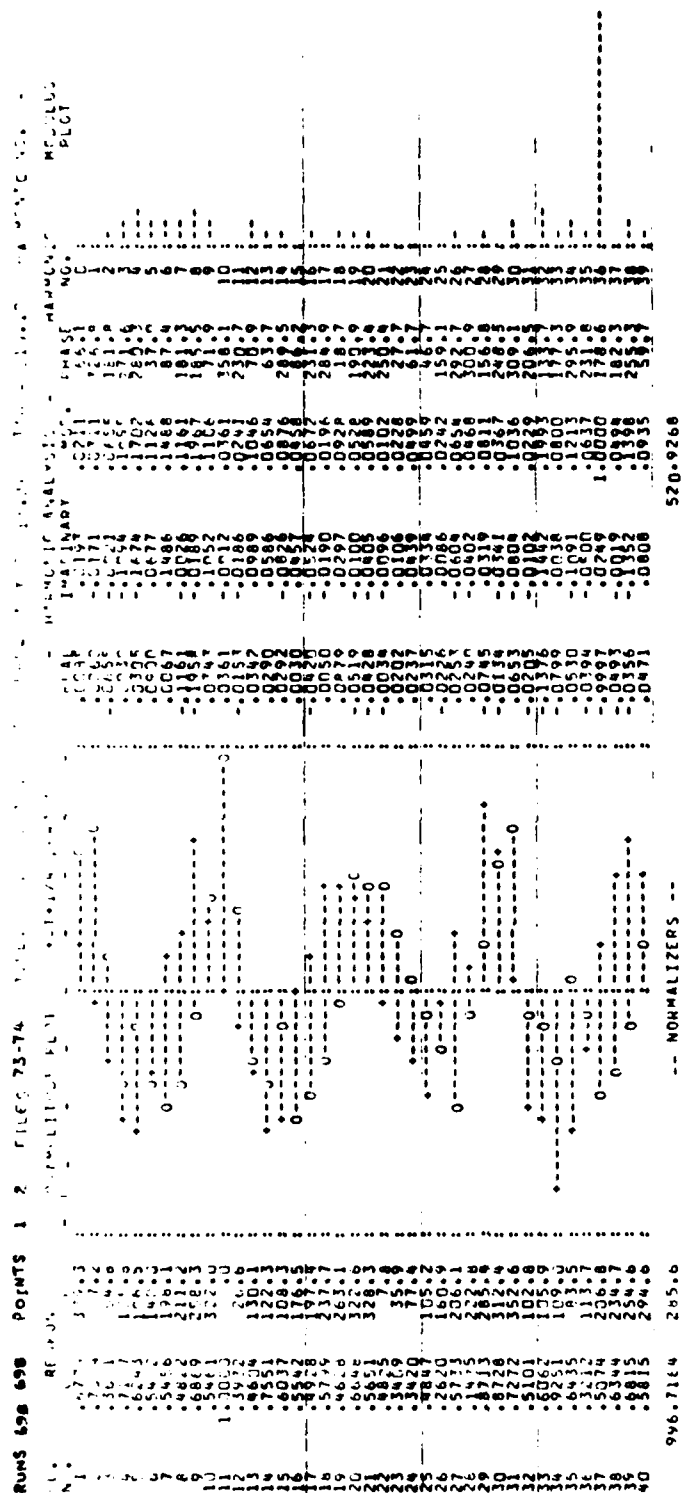


Figure 11.3 Response of the Mistuned Assembly to the Four Lobed Distortion in the Airstream at an Excitation Frequency of 77.04 Hz (1156 RPM): Peak "System Total" Response and Maximum Blade Strain



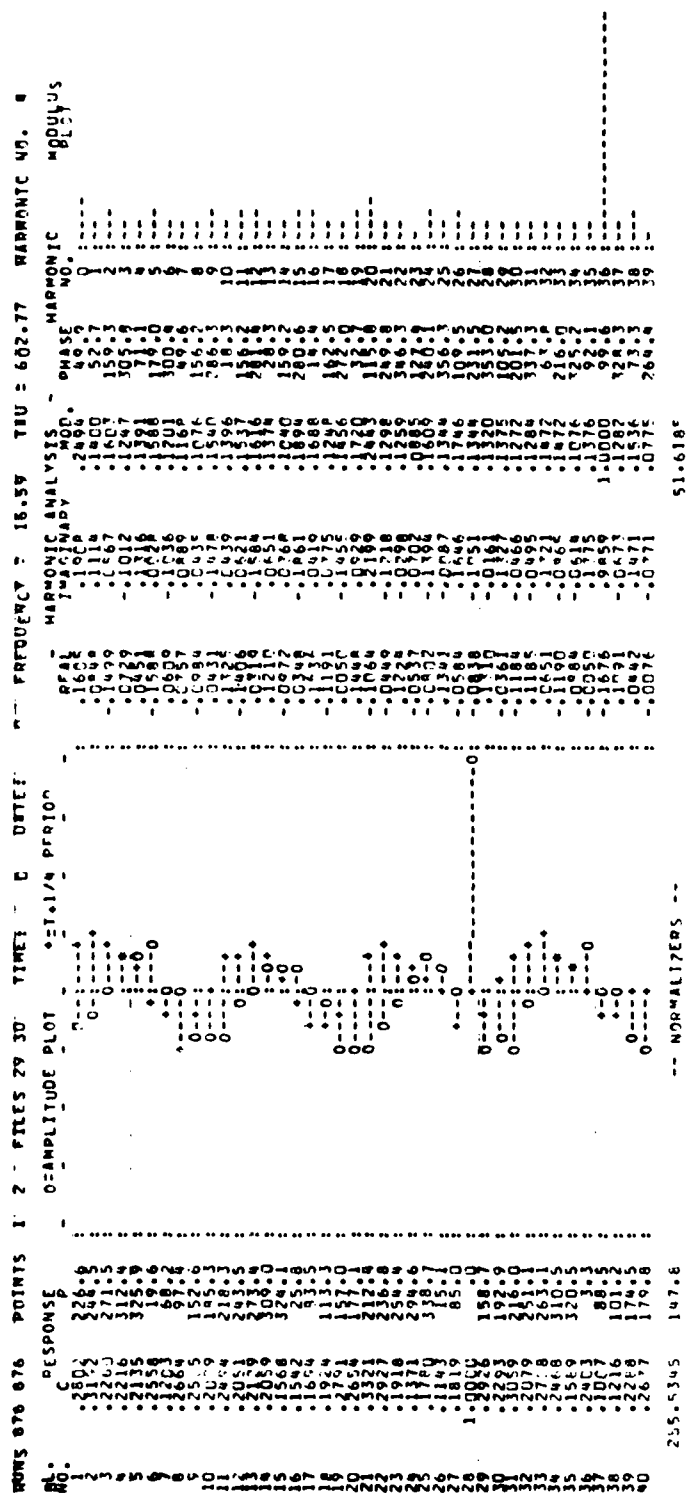
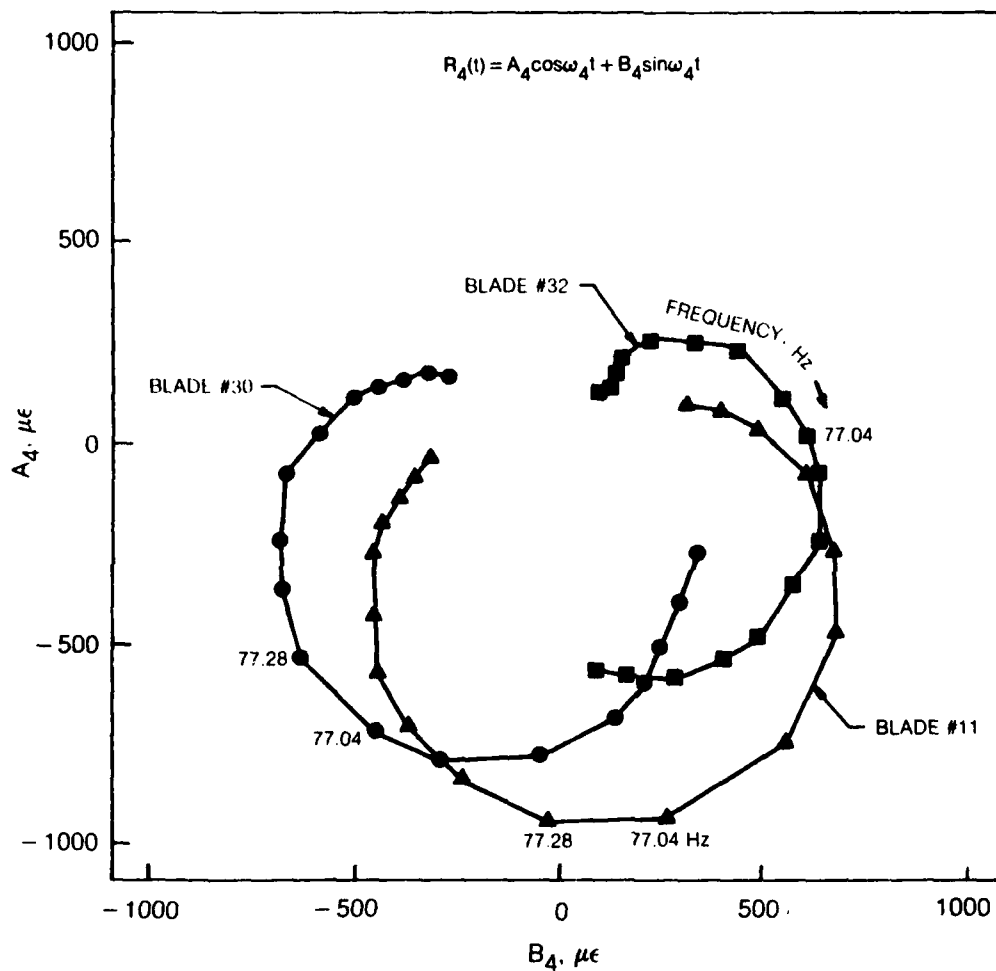


Figure 119 Response of the Mistuned Assembly to the Four Lobed Distortion in the Airstream at an Excitation Frequency of 66.36 Hz (995.4 RPM). Peak Response of Blade #28.



FILES 59 TO 94, RUNS 691-708  
 FREQUENCIES 74.68 — 80.32 Hz

Figure 120 Polar Plots of Fourth Harmonic of Blade Response  $R_4(t)$  in Mistuned Assembly with 4ND Aerodynamic Excitation. Responses shown for Blades #11, #30, and #32.

Similar results were obtained for the "tuned" assembly. The assembly is somewhat "better behaved" as can be observed by examination of Figs. 121 through 123. In this case, the resonant frequency was found to be 76.6 Hz with a loss factor of 0.026. Comparison of the responses of the tuned and mistuned assemblies shows that the blades in the mistuned assembly do not experience strains larger than those in the tuned system.

#### 5. Nonintegral Order Vibration through the Piezoelectric Crystals

Within the speed capability of the aerodynamic rig, the only modes that could be induced at integral order belonged to the first family in a 4 nodal diameter pattern. However, the piezoelectric crystal excitation system that was used in the earlier phase of testing could be used in an attempt to excite modes in the second family at nonintegral order speeds. The objective was to induce traveling wave forcing functions in 2, 3 and 4 nodal diameter patterns at frequencies corresponding to the second family of modes. The responses from this phase of testing could then be compared with corresponding results from the spin rig in order to compare modal characteristics. All the results were obtained in a "clean inlet" configuration with the aerodynamic operating conditions set at design point.

Both forward and backward traveling wave forcing functions were applied to the tuned and mistuned assembly operating at 0, 560, 1050 and 1200 rpm. Blade strain responses to these forcing functions were recorded as before over a range of excitation frequencies. These responses were reduced to display the pattern of vibration around the rotor at time  $T$  and a quarter period later in the form of stick plots. Figures 124 through 131 show such stick plots for data points close to peak "system total response" for certain selected test runs as shown. On these figures, the results of a harmonic analysis of the vibratory pattern are also shown so that the strength of the contributing harmonics can be readily seen. For example, in Fig. 128, the response to a backward traveling forcing function acting on the assembly rotating at 1200 rpm is a predominant backward traveling wave, 84% larger than the stationary wave component.

Harmonic analysis of this type performed for all the test runs in this series were used to represent the overall behavior of the assembly as shown in Figs. 132 through 135. This overall behavior pattern presents the dynamic characteristics of the assembly in terms of the "system total" amplitude as a function of frequency. It may be recalled that the "system total" amplitude is obtained by summing the components of the fundamental in the harmonic analysis. For example  $A_2$  and  $A_{-2}$  are added from a stick plot that represents the response due to an impressed 2ND forcing pattern.

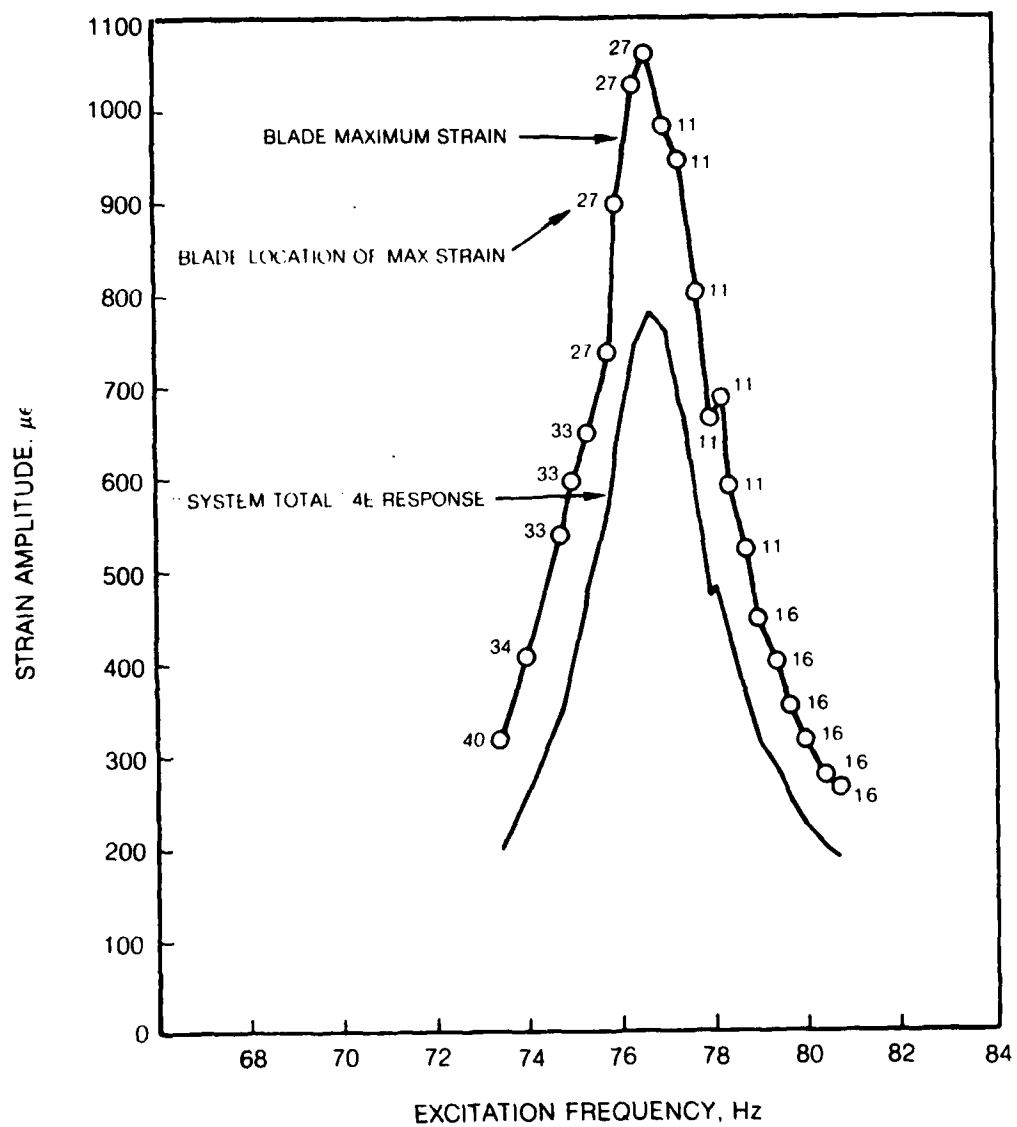


Figure 121 Variation of "System Total" 4E Response and Blade Maximum Strain Amplitude of Tuned System due to a Four Lobed Distortion in the Airstream with Excitation Frequency

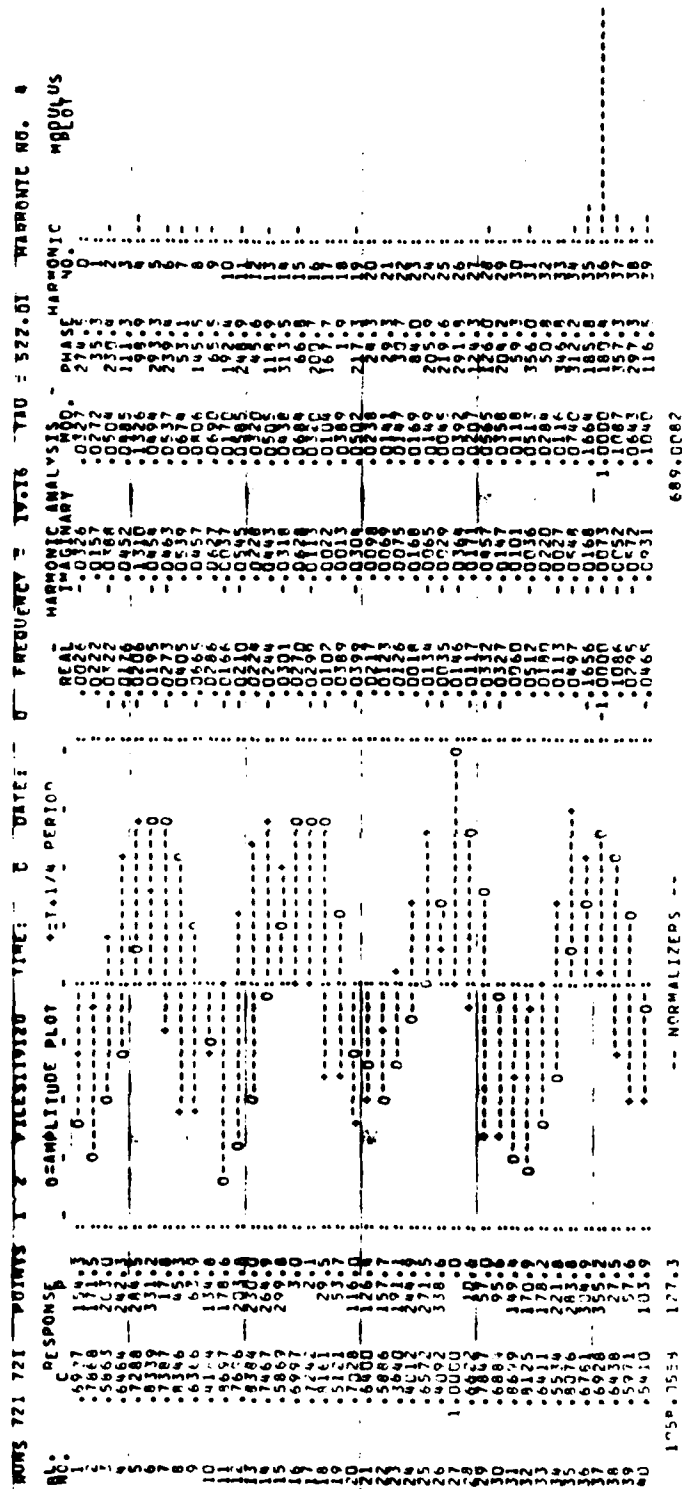
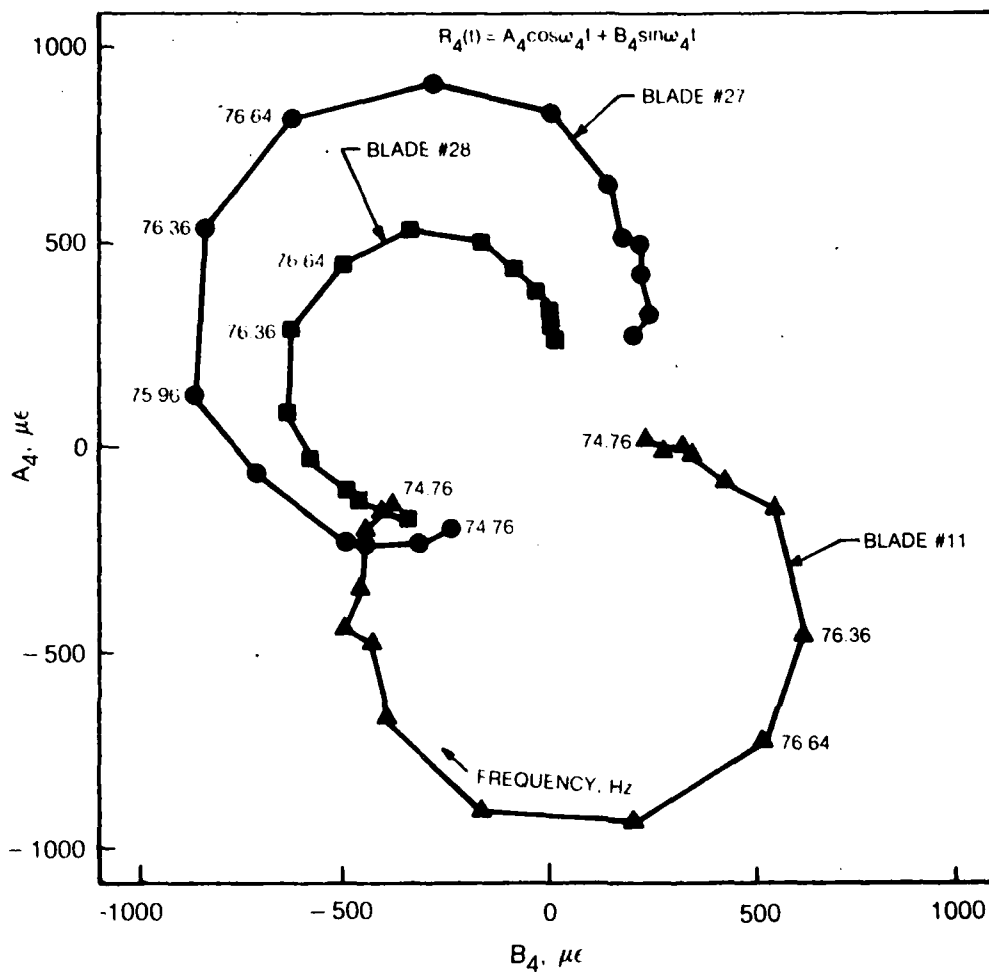


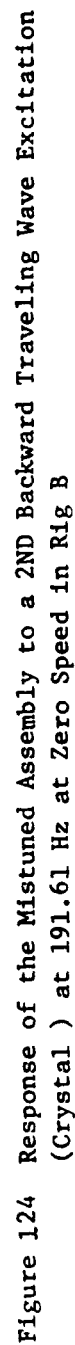
Figure 122 Response of Tuned Assembly to the Four Lobed Distortion in the Airstream at an  
 Excitation Frequency of 76.64 Hz (1150 RPM); Peak "System Total" Response and  
 Maximum Blade Strain

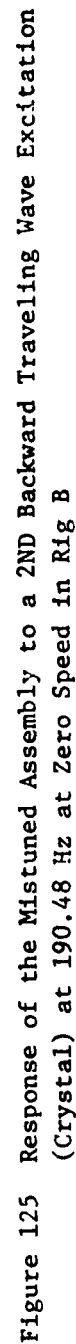


FILES 105 TO 136, RUNS 714-729

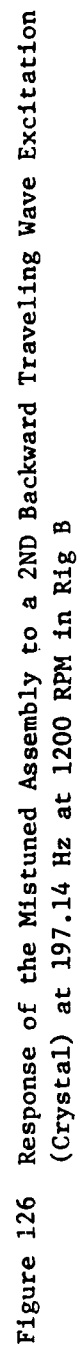
FREQUENCIES 74.76 — 79.04 Hz

Figure 123 Polar Plots of Fourth Harmonic of Blade Response  
 $R_4(t)$  in Tuned Assembly With 4ND Aerodynamic  
 Excitation Responses Shown for Blades #11, #27, and #28.









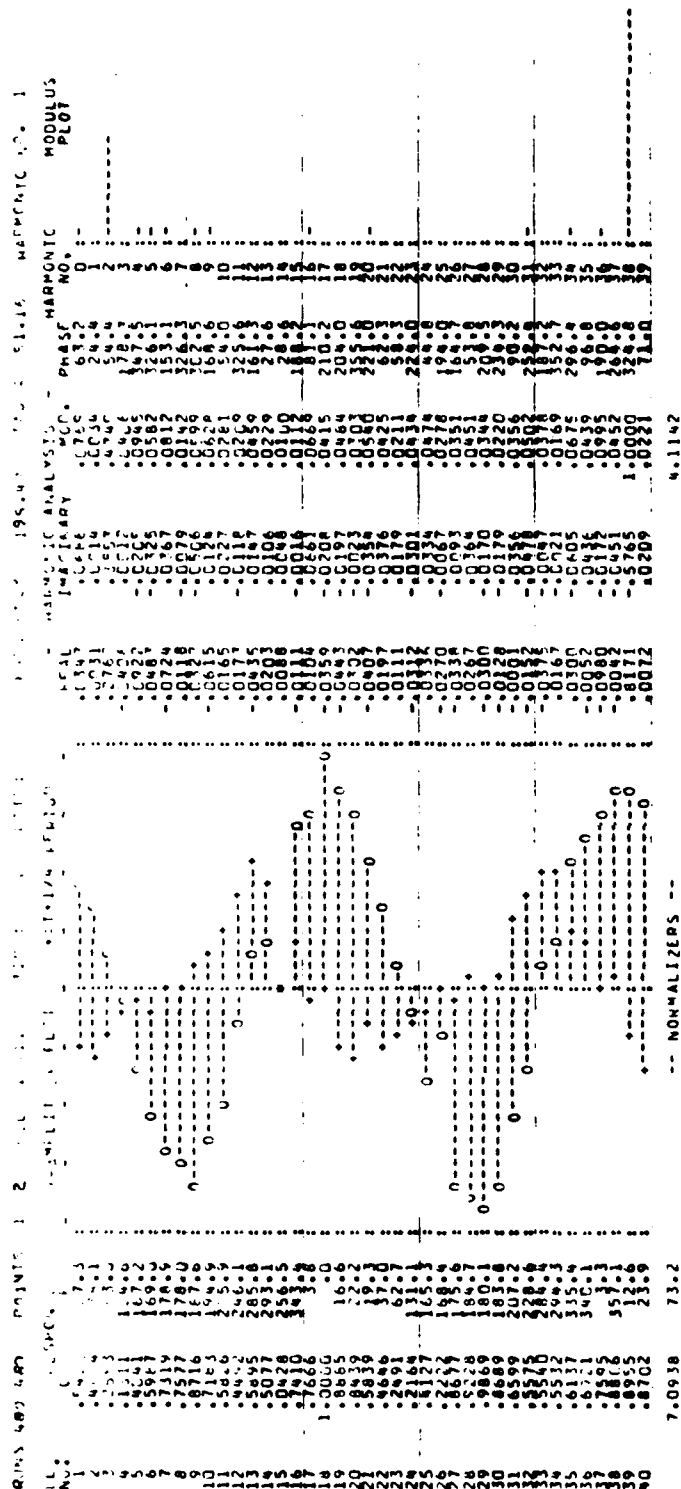


Figure 127 Response of the Mistuned Assembly to a 2ND Backward Traveling Wave Excitation (Crystal) at 195.47 Hz at 1200 RPM in Rig B

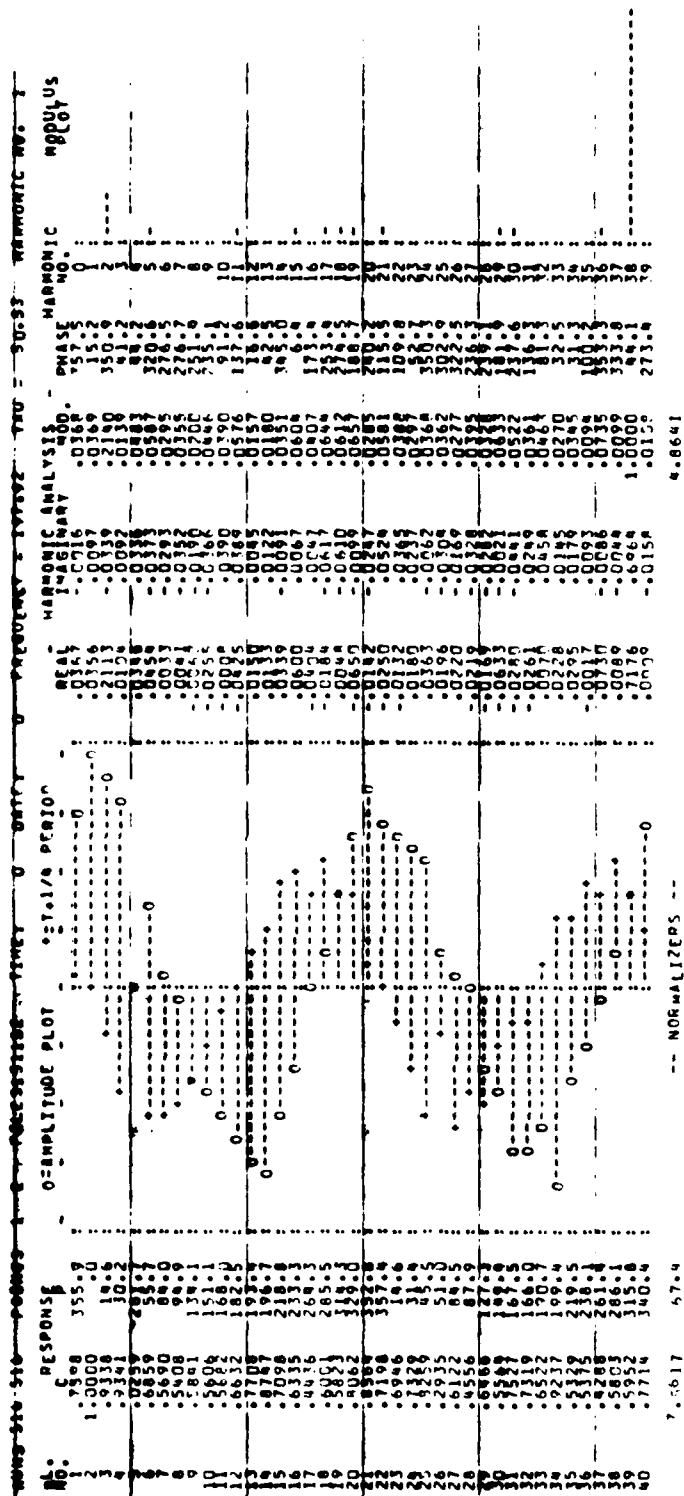


Figure 128 Response of Mistuned Assembly to a 2ND Forward Traveling Wave Excitation (Crystal) at 197.92Hz at 1200 RPM in Rig B

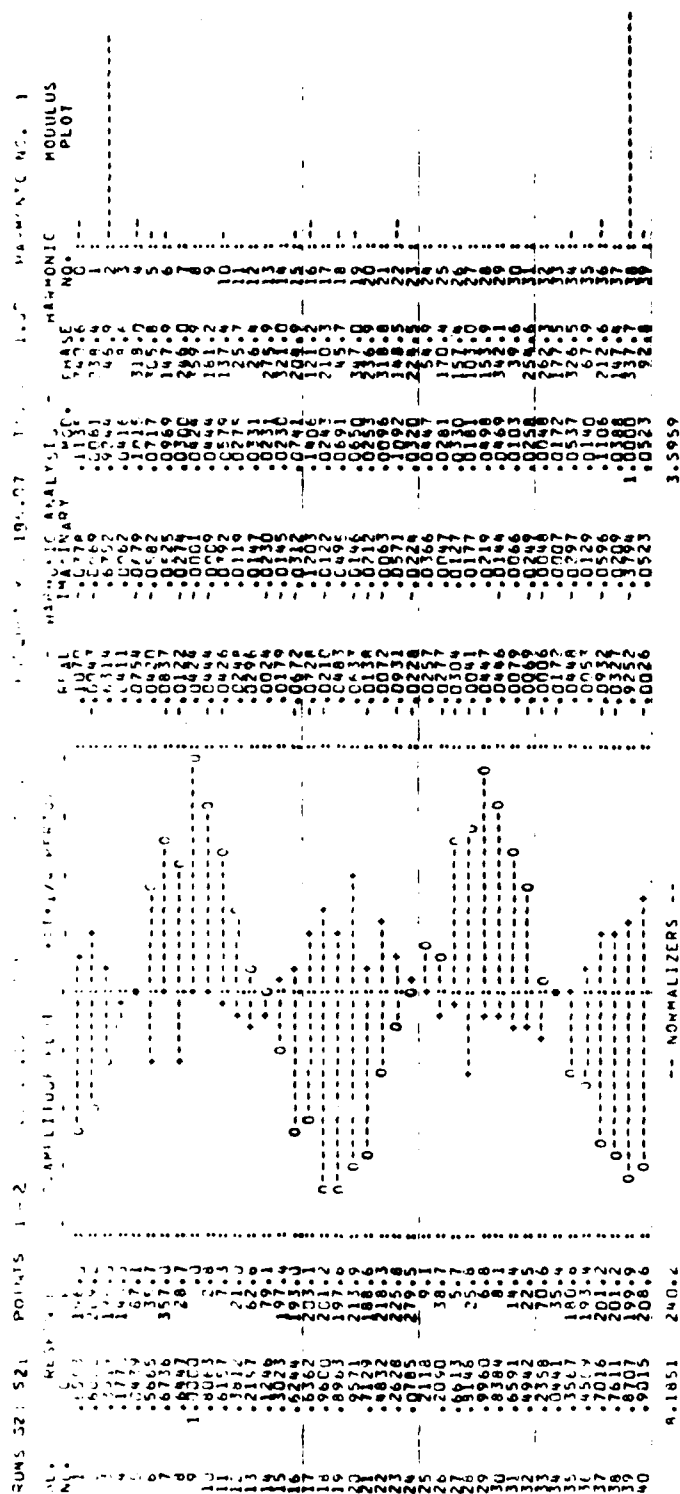


Figure 129 Response of the Mistuned Assembly to a 2ND Forward Traveling Wave Excitation (Crystal) at 196.07 Hz at 1200 RPM in Rig B

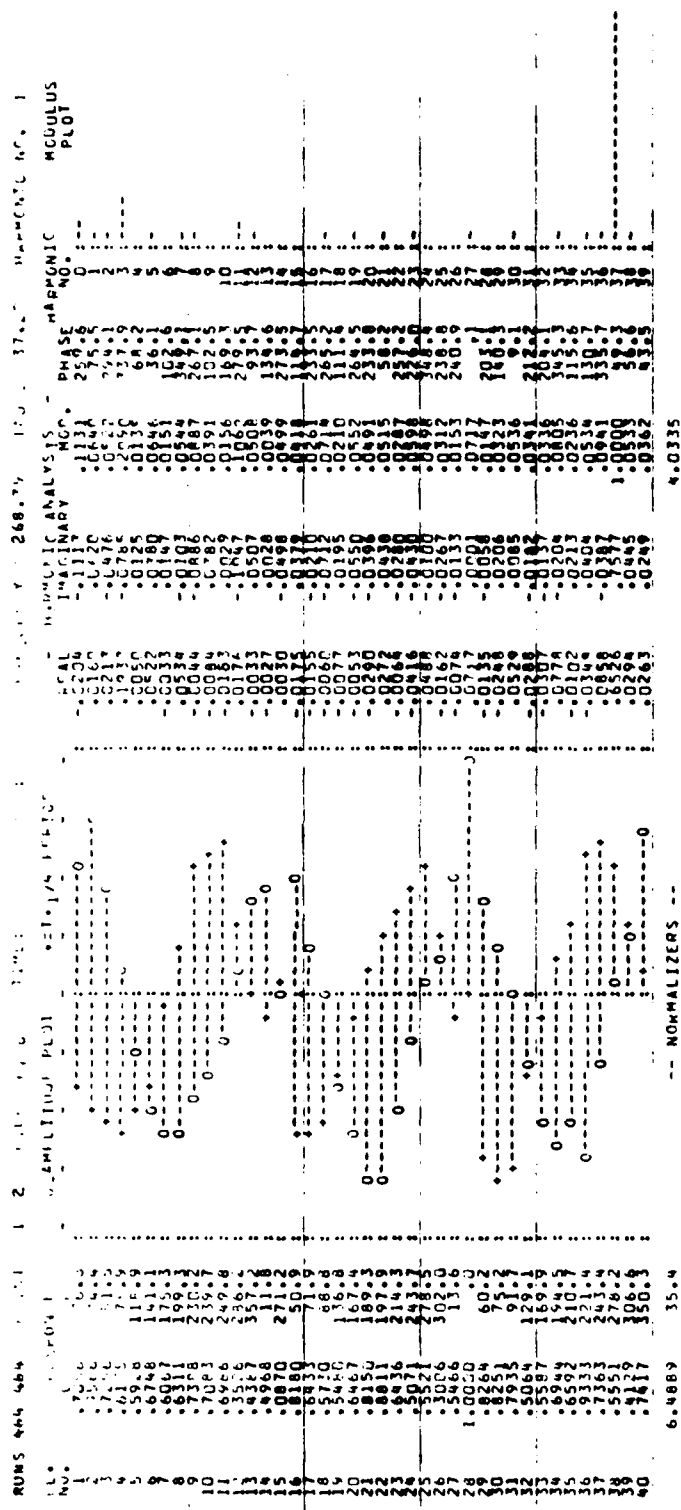
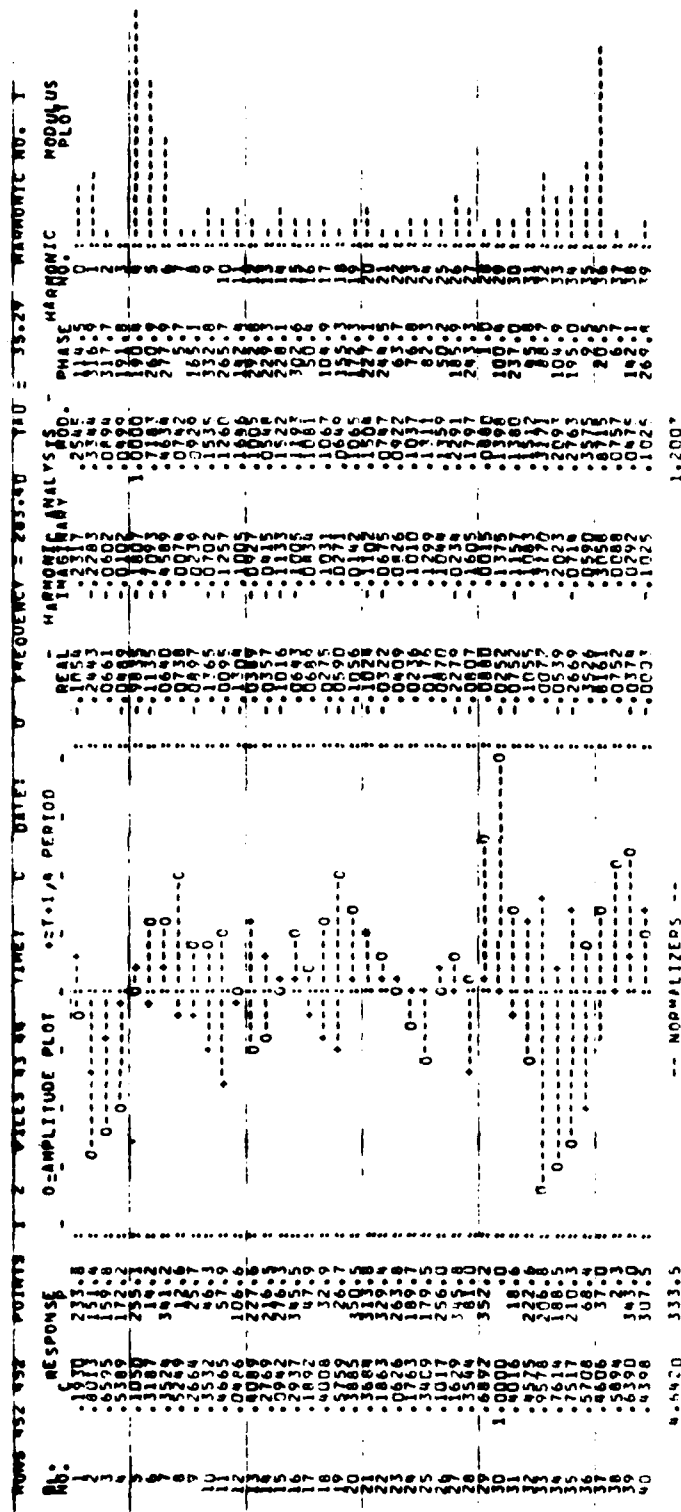


Figure 130 Response of the Mistuned Assembly to a 3ND Backward Traveling Wave Excitation  
(Crystal) at 268.79 Hz at 1200 RPM in Rig B



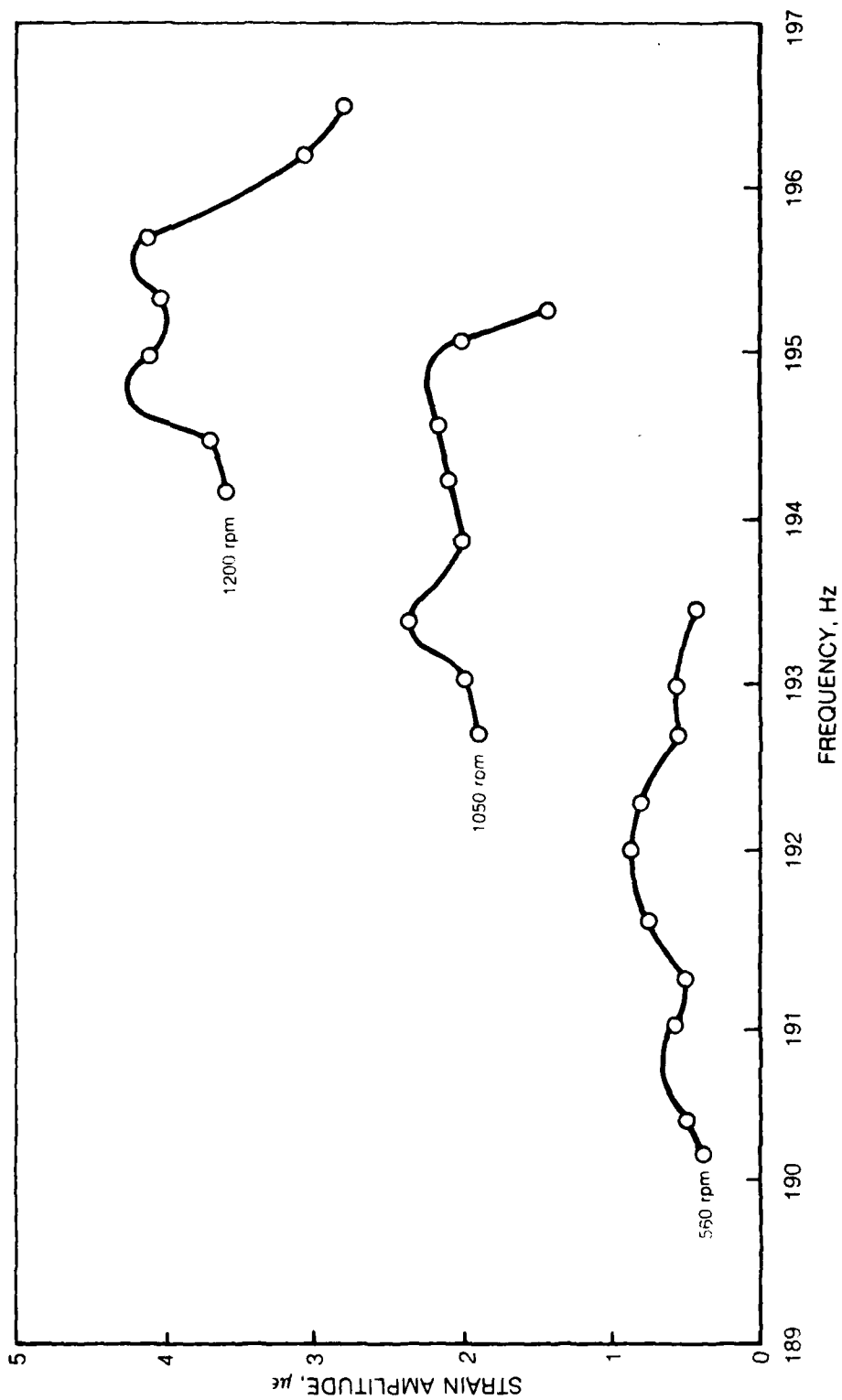


Figure 132 Tuned Assembly "System Total" Response Variation with Frequency for  
2ND Backward Traveling Wave Excitation at Speed in Rig B

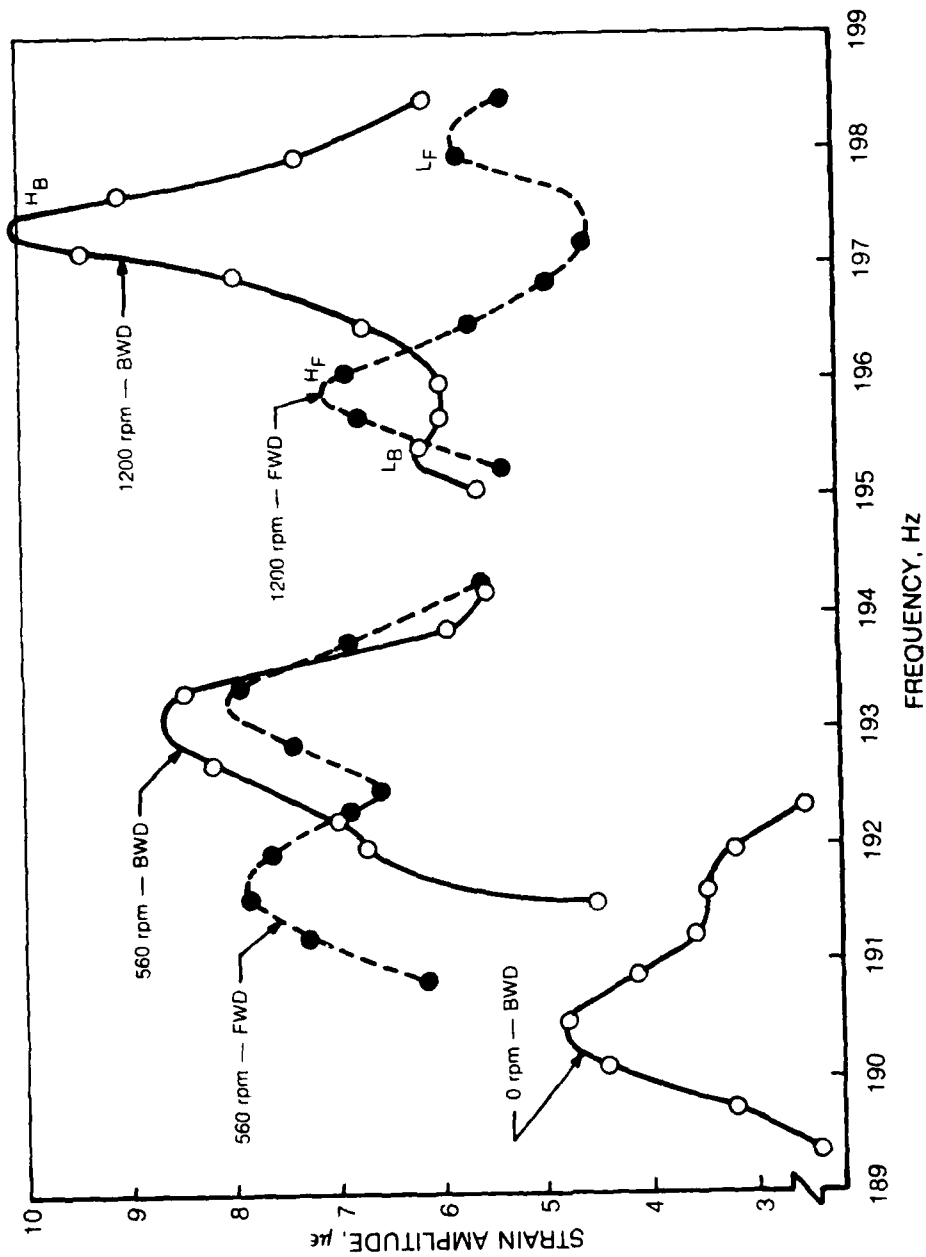


Figure 133 Mistuned Assembly "System Total" Response Variation with Frequency for 2ND Backward and Forward Traveling Wave Excitation at Speed in Fig B



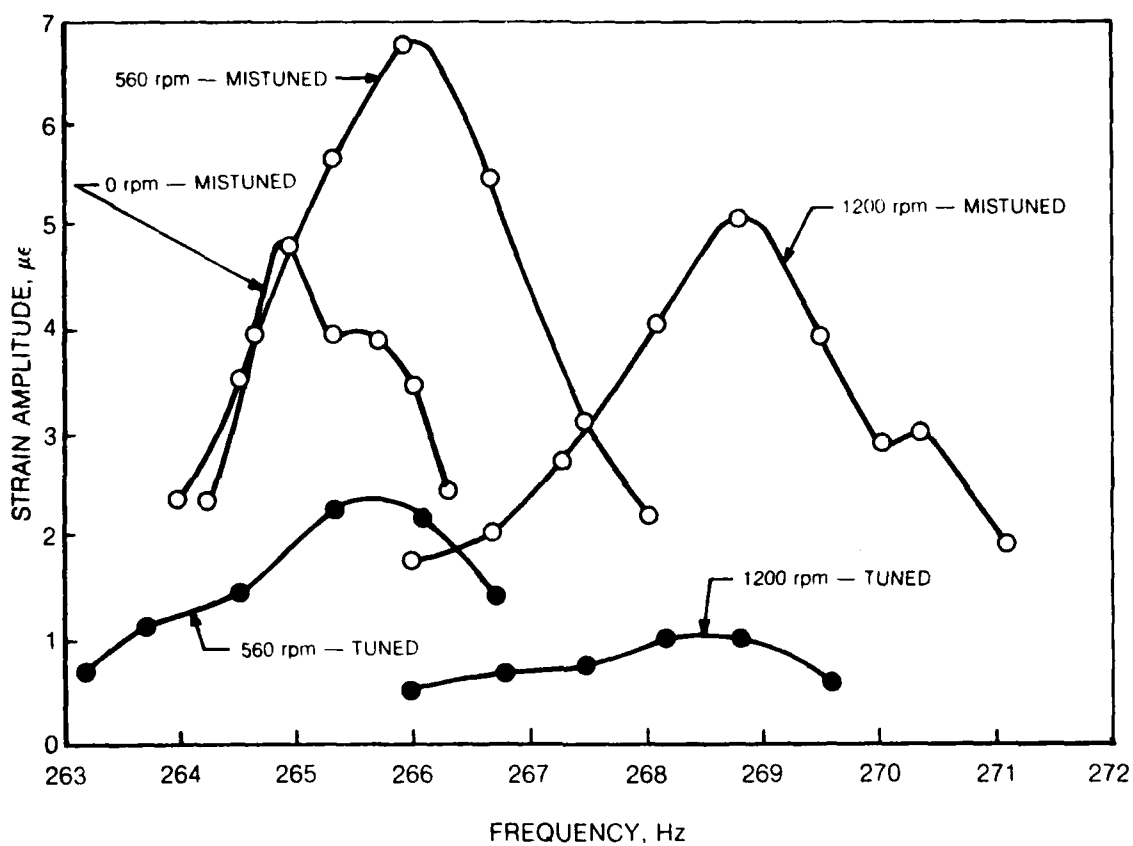


Figure 134 Tuned and Mistuned Assembly "System Total" Response Variation with Frequency for 3ND Backward Traveling Wave Excitation at Speed in Rig B

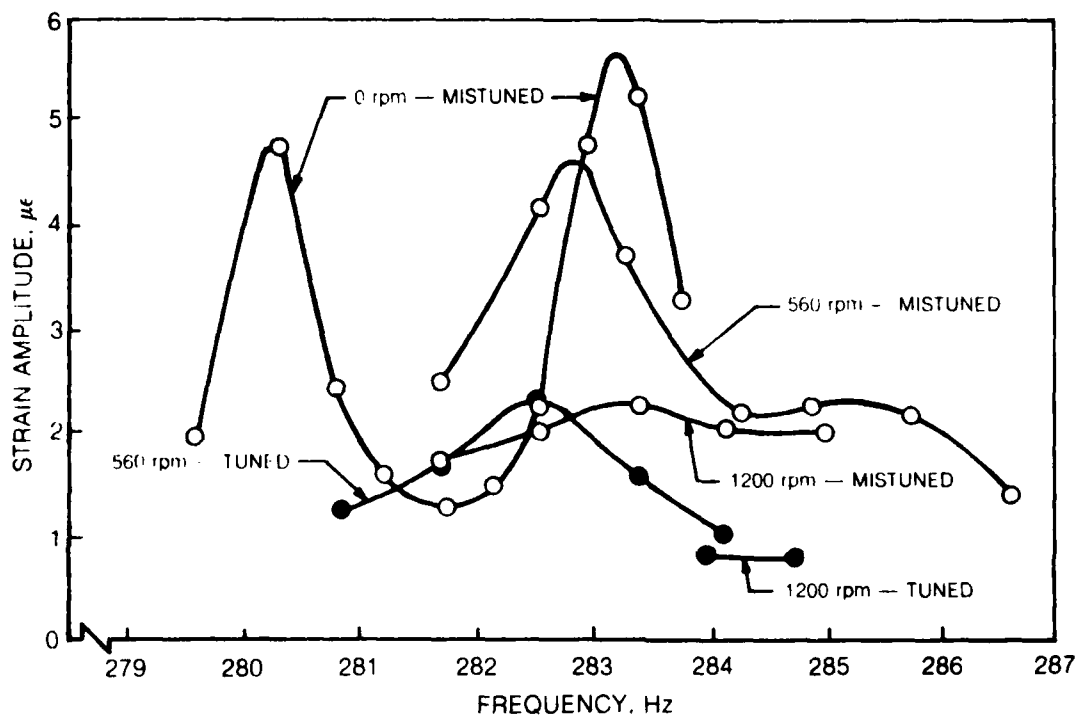


Figure 135 Tuned and Mistuned Assembly "System Total" Response Variation with Frequency for 4ND Backward Traveling Wave Excitation at Speed in Rig B

Figure 132 represents the behavior of the tuned assembly at 560, 1050 and 1200 rpm, when the assembly is subjected to a 2ND backward traveling wave forcing function. The response of the mistuned system when subjected to backward and forward traveling wave forcing functions at 0, 560 and 1200 rpm is shown in Fig. 133. Figures 134 and 135 show tuned and mistuned assembly response to 3ND and 4ND backward traveling wave forcing functions, respectively. Tables 21, 22 and 23 provide a complete summary of these results for all test conditions. In these tables, the frequency and strain amplitude of the response at the data point closest to each peak in the "system total" frequency response function are given. The traveling wave component magnitude in the assembly response at each given data point is also shown as a percentage of the standing wave component magnitude. The loss factors were obtained from the polar plots of response for individual blades. The ranges of values stem from the values obtained from different blades at peak blade responses close to that of the data point. Finally, the maximum strain in the assembly and the blade location for the data point are listed.

## 6. Discussion of Results

An examination of Figs. 132 through 135 indicates that the overall behavior of the assembly is characterized by two peaks, one of which is higher than the other. In Fig. 132 for the tuned system 2ND response, the lower peak occurs at a lower frequency for 560 rpm only. For 1050 and 1200 rpm, the trend is reversed. Increase in frequencies at these peaks as well as increased response amplitudes are attributed to centrifugal effects on stiffness as well as added tightness at shroud interfaces.

The 2ND response of the mistuned system, as shown in Fig. 133, is characterized by the enhancement of the unequal peaks especially at 1200 rpm. The trend at 1200 rpm is particularly interesting in that the peaks are not only unequal but the higher of the two peaks ( $H_B$ ) occurs at the higher of the two frequencies for a backward traveling wave excitation whereas it occurs at the lower of the two frequencies ( $H_F$ ) for a forward traveling wave excitation. The stick plots shown in Figs. 128 and 129 (Runs 516 and 521) show that close to the lower peak  $L_F$ , the response is a predominately backward traveling wave whereas at  $H_F$  it is essentially a stationary wave. At the peaks designated  $H_B$  and  $L_B$  the response is a predominately backward wave. Thus, these features depend not only on the speed but also on the impressed harmonic. A partial explanation of these interesting and complex features must lie in the nature of aeroelastic coefficients. It is known that these coefficients are strong functions of reduced frequency and inter-blade phase angles (magnitude and sign), among other parameters and therefore lead to wider variation in the aerodynamic forces.

TABLE 21

SUMMARY OF PEAK RESPONSE CHARACTERISTICS FOR THE MISTUNED ASSEMBLY IN RIG B.

EXCITATION		RESPONSE CHARACTERISTICS				
		SPEED RPM	0	560	1050	1200
2ND B-T-W	Response #1	Frequency (Hz)	191.6	193.4	196.1	197.1
		Strain ( $\mu\epsilon$ )	3.5	8.5	6.3	9.5
		TW Comp (%)	30.8	58.6	112.0	124.0
		Damping ( $\eta$ )	.004-.010	.003-.004	.006-.007	.007
		Bld#/Strain( $\mu\epsilon$ )	6/4.28	4/10.02	25/10.79	34/11.01
2ND F-T-W	Response #2	Frequency (Hz)	190.5	192.0	194.2	195.5
		Strain ( $\mu\epsilon$ )	4.8	6.7	6.7	6.1
		TW Comp (%)	18.1	43.9	22.2	55.7
		Damping ( $\eta$ )	.004-.005	.004-.005	.004	.006
		Bld#/Strain( $\mu\epsilon$ )	18/5.414	18/8.10	28/7.55	18/7.09
3ND B-T-W	Response #1	Frequency (Hz)	ND	193.4	196.1	197.9
		Strain ( $\mu\epsilon$ )	ND	7.9	6.3	5.8
		TW Comp (%)	ND	13.8	112.0	192.0
		Damping ( $\eta$ )	ND	.008-.011	.004	.004
		Bld#/Strain( $\mu\epsilon$ )	ND	2/8.85	13/7.88	2/7.56
3ND F-T-W	Response #2	Frequency (Hz)	ND	191.6	194.3	196.1
		Strain ( $\mu\epsilon$ )	ND	7.8	4.5	6.9
		TW Comp (%)	ND	1.5	42.9	4.5
		Damping ( $\eta$ )	ND	.005-.009	.01	.004
		Bld#/Strain( $\mu\epsilon$ )	ND	39/8.57	29/10.11	9/8.18
4ND B-T-W	Response #1	Frequency (Hz)	265.3	265.9	ND	270.4
		Strain ( $\mu\epsilon$ )	3.9	6.7	ND	3.0
		TW Comp (%)	11.5	68.5	ND	141.0
		Damping ( $\eta$ )	.002-.004	.005	ND	-
		Bld#/Strain( $\mu\epsilon$ )	6/5.01	28/8.94	ND	28/5.11
4ND F-T-W	Response #2	Frequency (Hz)	264.9	No Peak	ND	268.8
		Strain ( $\mu\epsilon$ )	4.8		ND	5.1
		TW Comp (%)	17.3		ND	164.0
		Damping ( $\eta$ )	.002-.004		ND	.008
		Bld#/Strain( $\mu\epsilon$ )	28/7.14		ND	28/6.49
Single Blade #28	IB	Frequency (Hz)	283.3	284.9	ND	283.4
		Strain ( $\mu\epsilon$ )	5.4	2.3	ND	2.3
		TW Comp (%)	5.2	50.8	ND	7.9
		Damping ( $\eta$ )	.003	.008	ND	.007
		Bld#/Strain( $\mu\epsilon$ )	40/6.10	28/10.93	ND	30/4.64
Single Blade #29	IT	Frequency (Hz)	280.3	282.5	ND	NO PEAK
		Strain ( $\mu\epsilon$ )	4.8	4.2	ND	
		TW Comp (%)	2.3	12.6	ND	
		Damping ( $\eta$ )	.002	.006	ND	
		Bld#/Strain( $\mu\epsilon$ )	28/24.6	40/5.72	ND	
Single Blade #30	IT	Frequency (Hz)	55.7	ND	ND	ND
		Strain ( $\mu\epsilon$ )	24.0	ND	ND	ND
		Damping ( $\eta$ )	.007	ND	ND	ND
		Frequency (Hz)	ND	279.0	ND	279.4
Single Blade #31	IT	Strain ( $\mu\epsilon$ )	ND	4.8	ND	5.8
		Damping ( $\eta$ )	ND	.004	ND	.006

ND = No Data

TABLE 22

SUMMARY OF PEAK RESPONSE CHARACTERISTICS FOR TUNED ASSEMBLY IN RIG B.

EXCITATION		RESPONSE CHARACTERISTICS			
		SPEED RPM	560	1050	1200
2ND B-T-W	Response #1	Frequency (Hz)	192.0	194.6	195.7
		Strain ( $\mu\epsilon$ )	.9	2.2	4.2
		TW Comp (%)	5.2	249.0	542.0
		Damping ( $\eta$ )	.004	?	0.010
		Bld#/Strain( $\mu\epsilon$ )	36/1.57	34/3.27	15/6.46
	Response #2	Frequency (Hz)	191.0	193.4	195.0
		Strain ( $\mu\epsilon$ )	.7	2.4	4.1
		TW Comp (%)	12.3	75.8	259.0
		Damping ( $\eta$ )	.004	?	.006
		Bld#/Strain( $\mu\epsilon$ )	8/1.21	9/3.73	19/6.41
3ND B-T-W	Response #1	Frequency (Hz)	265.3	ND	268.8
		Strain ( $\mu\epsilon$ )	2.3	ND	1.0
		TW Comp (%)	59.5	ND	146.0
		Damping ( $\eta$ )	0.004	ND	0.004
		Bld#/Strain( $\mu\epsilon$ )	37/2.79	ND	11/2.92
4ND B-T-W	Response #1	Frequency (Hz)	282.5	ND	ND
		Strain ( $\mu\epsilon$ )	2.3	ND	ND
		TW Comp (%)	20.6	ND	ND
		Damping ( $\eta$ )	0.006	ND	ND
		Bld#/Strain( $\mu\epsilon$ )	40/3.52	ND	ND

ND = No Data

TABLE 23

MAXIMUM VALUES OF RESPONSE WAVE RATIO AND CORRESPONDING FREQUENCIES  
FOR ALL TEST CONDITIONS FOR TUNED AND MISTUNED ASSEMBLY. EXCITED  
WITH TRAVELING WAVES IN RIG B.

Excitation		Speed	"Tuned" Assembly		Mistuned Assembly	
ND	Direction	RPM	Frequency Hz	Wave* Ratio	Frequency Hz	Wave* Ratio
2	FWD	0			190.9	0.81
2	BWD	560	190.4	1.27	191.5	0.75
2	FWD	560			192.5	2.18
2	BWD	1050	190.9	1.55	193.8	0.65
2	FWD	1050			195.7	2.47
2	BWD	1200	193.3	0.75	193.5	0.55
2	FWD	1200			197.6	47.40
3	BWD	0			265.3	0.81
3	BWD	560	265.3	0.46	265.3	0.67
3	BWD	1200	266.8	0.81	261.2	0.50
4	BWD	0			281.8	4.10
4	BWD	560	284.9	1.38	284.3	3.84
4	BWD	1200			280.8	2.67

\* Wave Ratio is the ratio of contributing harmonics

A comparison between these dynamic characteristics in vacuum (Rig A) and in air (Rig B) was made and is shown in Fig. 136. At zero rpm, the forced response characteristic measured in Rig B shows frequencies at the twin peaks that are different from those measured in Rig A. The assembly configuration is essentially the same but the support structural systems are obviously different as the nonaerodynamic tests were conducted in a spin rig (Rig A) and the aerodynamic tests were conducted in an aerodynamic rig (Rig B). In the former, the assembly mounts in a horizontal plane whereas in the latter the assembly is in a vertical plane with obvious differences in the supporting structure. This may, in part, explain the differences in frequencies. However, damping measured in both the rigs at zero speed (in air) remains the same.

The feature of unequal peaks is enhanced in vacuum and demonstrates a clear antisymmetry between responses to forward and backward traveling forcing waves. With an aerodynamic environment, these characteristics are influenced unequally leading to responses discussed earlier with references to Figs. 132 through 135.

Figures 137A and B illustrate the Campbell diagram for the bladed disk assembly on which the forced vibration responses under aerodynamic excitations are also shown. It may be recalled that the Campbell diagram is a representation of the in-vacuo natural vibration frequencies of an assembly of blades over a speed range and is normally used to locate the red-line speed such that the low integral order resonances are sufficiently far from the safe operating range of a fan. The natural response frequencies measured when individual blades were excited on the assembly are also shown for comparison. Also the results of calculations made during the design of the fan are also indicated on the diagram.

That the response characteristics in the first family 4ND pattern were irregular (containing contributions from nearby modes) and occurred over a range of frequencies is clear from Fig. 137A. The lack of agreement between the calculated 4E speed and the measured speed is indicative of the difficulties reported earlier (Ref. 5) in modeling shrouded blades.

The frequencies representing the aerodynamic response under the influence of distortion "rides" the engine order line as has been observed in very many engine and rig tests.

The second family resonances are somewhat better behaved and the measured frequencies fall in a narrow band as can be expected from a mistuned assembly.

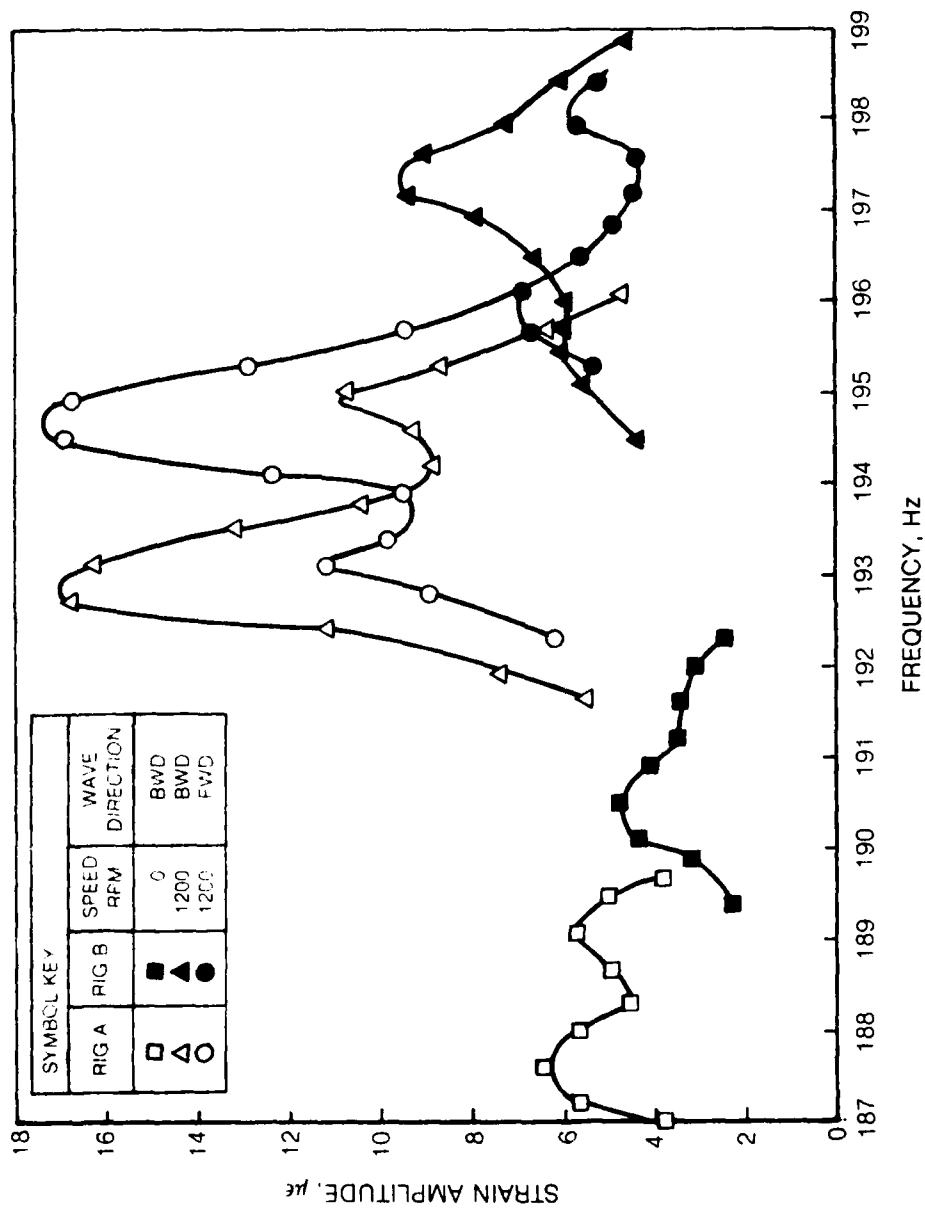


Figure 136 Comparison of Mistuned Assembly System "Total" 2ND Response in Rig A and Rig B



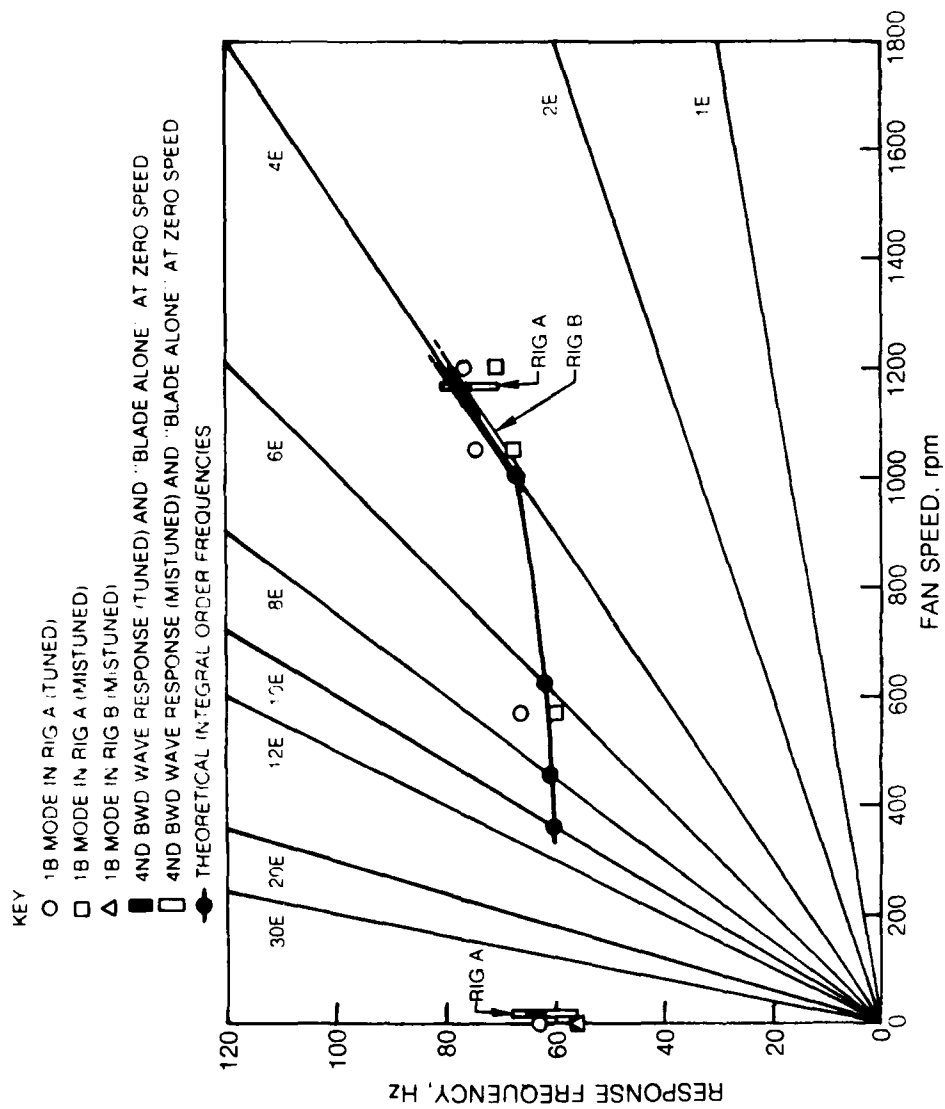


Figure 137A Campbell Diagram showing First Family Response Frequencies from Theoretical Calculations and Test

83-8-36-84

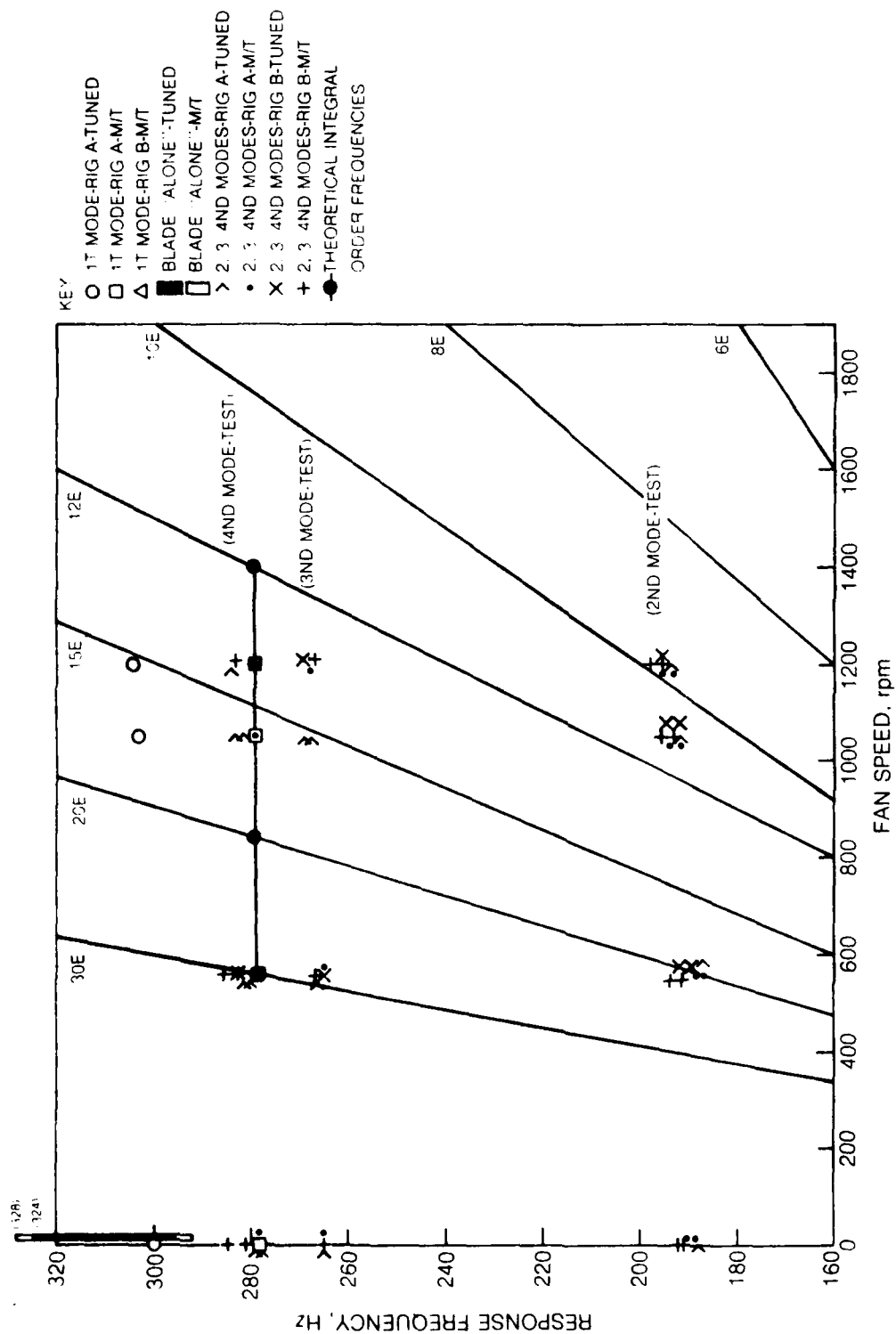


Figure 137B Campbell Diagram Showing Second Family Response Frequencies from the Theoretical and Test

## 7. Correlation Between Measured Strain and Aerodynamic Stimulus

To correlate the distortion pattern with the strain response, it appears desirable to use an indirect method based on the Fourier series (spatial) of the distortions and the corresponding spatial harmonic analysis of the single-frequency Fourier analysis of the time series from strain gages. The amplitude of the distortion/strain correlation can then be derived from the normalization coefficients of the various harmonic analyses. The phase can be derived from the relative orientations of the spatial patterns of the distortion and strain. As an example, consider the data at 1150 rpm (Run 721) where the system response is a maximum for the tuned assembly.

With reference to Fig. 138, the 4ND component of the inlet distortion provides four maxima of  $C_p/U$  at .0225 above its average value of .599, at angular positions of  $37.2^\circ$ ,  $127.2^\circ$ ,  $217.2^\circ$  and  $307.2^\circ$  from TDC in the direction of rotation. Each blade will encounter a varying incidence angle reaching a minimum at these locations. The response to this gust was measured and is typified by the 4ND strain response, a backward-traveling wave with an amplitude of  $689 \mu\epsilon$  and time phase of  $180.4^\circ$  relative to blade #1 at the moment of the timing pulse. This pulse is triggered when blade #24 passes the vertical at TDC. The maximum strain therefore occurs when any given blade is phased at  $153^\circ - 180.4/4$  or  $107.9^\circ$  past the vertical (also at  $197.9^\circ$ ,  $287.9^\circ$  and  $17.9^\circ$ ).

In order to compare the phase lag in this response with the unsteady aerodynamic gust functions, the lag due to the dynamics of the blades must be subtracted (the blades are being driven at resonance, hence lag the gust force by a quarter cycle,  $22.5^\circ$ ). The location of maximum incidence angle just before TDC is  $7.8^\circ$ , or  $25.7^\circ$  ( $17.9 + 7.8$ ) before the closest location of maximum strain. The equivalent time lag of  $102.8^\circ$  ( $4 \times 25.7$ ) is reduced by ninety degrees to  $12.8^\circ$ ; this is the phase angle between the force and response due to aerodynamics alone.

The amplitude of the unsteady aerodynamic gust function requires knowledge of the blade force to strain response relationship. This is not yet available, but some comparisons of relative gust function amplitudes for 4ND and 8ND responses can be made if theoretical corrections are made for amplification factors resulting from resonances.

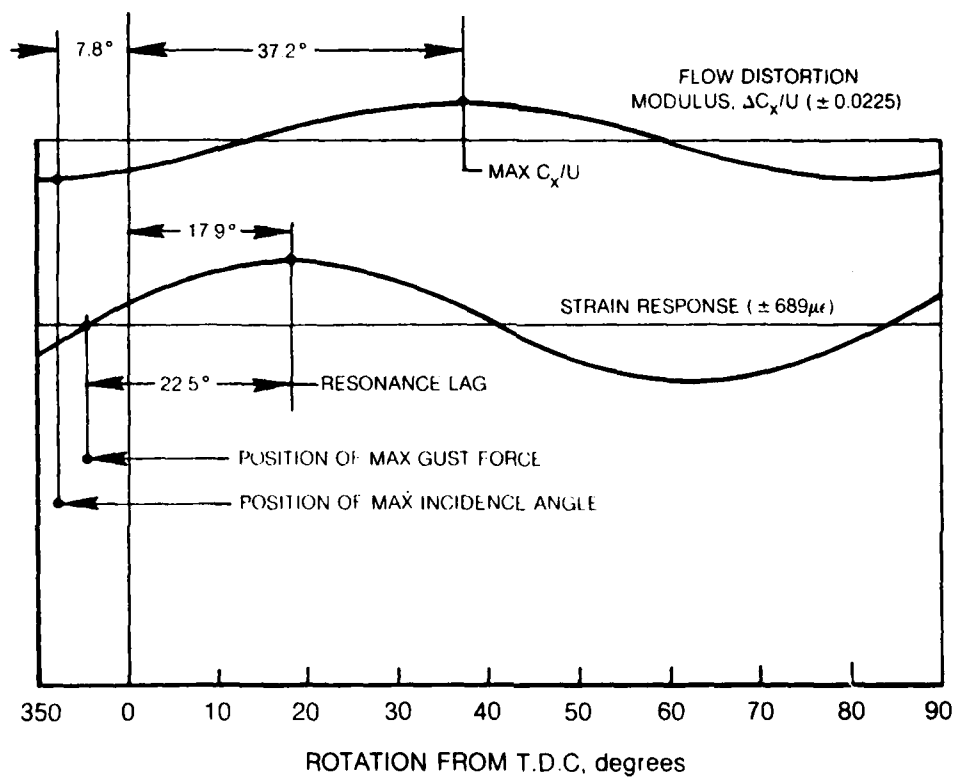


Figure 19. Spatial Positions of 4ND Flow Coefficient and Tuned Assembly Strain Response Distributions (One Quadrant)

The .013 of critical damping measured for the 4ND mode corresponds to a theoretical displacement magnification factor of 38.5 (i.e.,  $1/2 \zeta$  calculated on a single-degree-of-freedom basis). The strain amplitude of 689  $\mu\epsilon$  may therefore be reduced to 17.9  $\mu\epsilon$  (i.e.,  $689/38.5$ ) which would have resulted at a frequency far below resonance. The ratio of this strain to the distortion of 0.0225 is 796, which is therefore proportional to the aerodynamic gust function.

The 8ND component of  $C_x/U$  distortion was measured as .0066 with a phase of  $26.8^\circ$  resulting in an 8ND strain pattern of 2.4  $\mu\epsilon$  amplitude at  $357.4^\circ$  phase from blade #1. The 8ND component of the strain response therefore has a maximum at  $44.7^\circ$  ( $357.4/8$ ) from blade #1, or  $108.3^\circ$  ( $153-44.7$ ) from the vertical (also  $18.3^\circ$ ,  $198.3^\circ$ ,  $288.3^\circ$ ). The lobe at  $18.3^\circ$  therefore lags a region of maximum resistance at  $4.3^\circ$  ( $26.8-22.5$ ) by  $14.0^\circ$ . This mode excites blade vibrations at 153.28 Hz ( $19.16 \times 8$ ), probably in the second modal family where frequencies are about 190 Hz. A phase correction of about  $5^\circ$  may be applied. Therefore, the phase lag (spatial) of  $14.0^\circ$  is equivalent (at the 8ND frequency) to a temporal phase of  $107^\circ$  as an aerodynamic gust function phase. The damping in this mode is not known, but the magnification factor will be about 3 regardless of the exact value of damping so that 0.713 ( $2.14/3$ ) equivalent units of strain vibration in 8ND result from .0066 units of distortion. The relative gust function amplitude is 108 ( $0.713/0.0066$ ).

A similar calculation for the mistuned assembly may be made. Using the results from Run 698 at 1156 rpm, the backward-traveling 4ND response component was 520  $\mu\epsilon$  at  $178.6^\circ$  phase. The 4ND maximum strain response is now at  $108.4^\circ$  ( $153 - \frac{178.6}{4}$ ) from the vertical, and the maximum incidence angle occurred at  $7.8^\circ$  before TDC. Hence the maximum strain at  $18.4^\circ$  ( $108.4-90$ ) lags the maximum incidence angle by  $26.2^\circ$  and the temporal (gust function) phase lag is therefore  $14.8^\circ$  ( $4 \times 26.2 - 90$ ). The relative gust function amplitude is 786 based on 0.017 of critical damping, which is essentially the same as for the tuned case.

To compare these phase lags with that predicted by the aerodynamic gust response function for an isolated airfoil in translation, the reduced frequency is required. The reduced frequency is given by  $\lambda = \omega b / (U^2 + C_x^2)^{1/2}$ , where  $\omega$  is the frequency,  $b$  is the semichord at midspan,  $U$  is the tangential velocity at midspan and  $C_x$  is the axial velocity. Inserting appropriate values for the variables, the reduced frequency is found to have a value of 0.36 for the first family response. Assuming a Sears sinusoidal gust function, a lag angle of  $8^\circ$  can be expected (see Fig. 13.4 of Ref. 6) to compare with the  $12.8^\circ$  and  $14.8^\circ$  determined above.

The correlation of distortion and strain may be considered in terms of the harmonics of their respective circumferential distributions around the fan. The aerodynamic distortion was described earlier in terms of multiples

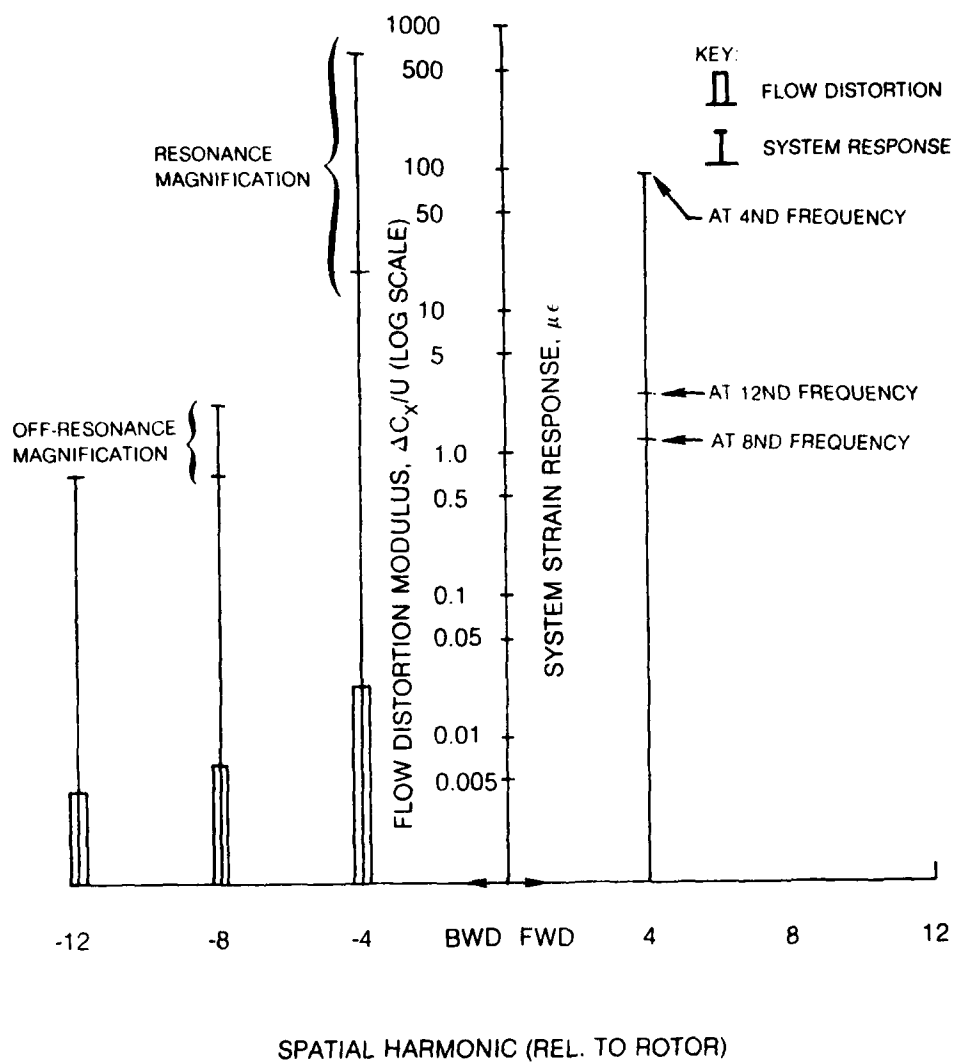


Figure 139 Correlation Between Principal Components of Flow Distortion and Tuned Assembly System Strain Response

of 4ND harmonics and it was assumed to have cyclic symmetry. The magnitudes of the three major harmonics of the distortion are shown plotted on Fig. 139 along with the resulting harmonics of the strain response for the tuned system. For complete correlation, the strain response should be entirely in the backward traveling ND patterns, but as can be seen, the response includes forward traveling components (i.e., 4ND from 4ND, 8ND and 12ND excitation). In particular, the response to the 12ND excitation is mostly a forward traveling 4ND wave. This presumably is the principal feature of a mistuned second family 4ND mode whose resonance is about 280 Hz but which has significant 12ND content. It should be noted that although a similar response for the first family 4ND resonance was obtained for the mistuned assembly as for the "tuned", no significant higher order (8 and 12ND) harmonics were excited.

#### 8. Dynamic Response Due To Blade/Vane Interaction

During this phase of testing, the influence of exit guide vanes on the rotating blades was examined from the point of view of identifying the excitation source called the (M-K) type (see Ref. 7). This type of excitation can be present when flow distortions due to K vanes interact with wakes from M blades. Such an interaction between wakes having M lobes and pressure fields having K lobes can lead to forcing functions of (M+K) and (M-K) lobes. One of the important requirements of blade design is that the frequency of excitation i.e. K/Rev of the (M-K) or (M+K) lobes, not match the frequency of a natural mode of the rotating system within the operating range. The R-80 fan assembly has 40 blades and the exit guide vane assembly has 46 blades and therefore the objective was to determine if a 6 nodal diameter pattern vibration could result at speed under "clean" inlet flow condition in the rig operating at design point.

The plan was to vary the speed of the fan in a region where the 6ND modes can be expected with an excitation frequency =  $(46 \times \text{rpm})/60 \text{ Hz}$  and record strain responses from all blades. In addition, a once per rev timing signal was to be recorded. Fourier analysis (with respect to time) of the signals (fundamental @ excitation frequency) along with a corresponding spatial analysis of blade strain around the assembly was to be used to determine amplitudes of components.

The 46 vanes were cantilevered from bosses bolted in the outer casing of the rig (see Fig. 109). The inner hub rotated beneath them. The bosses were designed to slide (0.75 inch, 1.9 cm) in slotted holes machined in the outer casing. Large washers with O-rings outside the casing and thin spring steel cover plates on the inside provided the sealing and smooth contouring required. Flats on the outer threaded portion of the bosses enabled a special tool to be attached for adjusting the vane angle from outside of the rig.

The testing was performed on the tuned assembly with the rotor and stator configured as they had been for all previous testing, i.e. vane stagger angle ( $\alpha_{\text{chord}}$  at root) set to  $12^\circ$  and the gap between vane leading edge and rotor blade trailing edge of 0.5 inch (1.27 cm) at the blade root.

The 6ND mode of the second family was found to occur, using crystal excitation, between 290 and 293 Hz at zero speed. Assuming no change due to speed effects, this corresponds to a speed range of  $\left(\frac{290}{46} \times 60\right) = 378$ , and  $\left(\frac{293}{46} \times 60\right) = 382$  rpm.

With the flow conditions maintained at the design point, (i.e.  $C_x/U=0.6$ ), the speed was increased in increments of 2 rpm from 370 to 400 rpm and the strain responses were recorded at each speed. At each data point the response signal from each blade was Fourier analyzed with respect to time based on a fundamental frequency of  $46 \times$  rotational speed.

The fundamental blade response was spatially, harmonically analyzed and the results expressed in terms of traveling wave components.

Figure 140(a) shows the variation of the "system total" 6ND response (which is the sum of the 6ND backward and forward components) with rotational speed. The excitation frequency is also indicated. Figure 140(b) shows the variation of the ratio of standing to traveling wave components of the response with rotational speed.



Figure 141 shows the stick plot of the fundamental response of the assembly and the harmonic content of the data point having the maximum response (i.e. at 379.7 rpm).

Figure 142 shows the polar plots of the responses of blades #28 and #36 as the speed is varied.

## 9. Discussion of Results

The tests established that (M-K) type excitations can occur as a result of an aerodynamic interaction between blade wakes and pressure fields from vanes downstream of the rotor. The measured strain amplitudes were less than those obtained when the assembly was subjected to an upstream distortion in flow. The response to the upstream flow distortion was in the first family 4ND mode whereas the response to the (M-K) type excitation was in the second family 6ND mode. The measured strains in the second family were generally smaller in all the tests. The reduced data clearly show that the expected mode was excited as can be seen from the response and stick plots.

The response at maximum amplitude (see Fig. 141) has a strong 6ND standing wave component (S/T, the ratio of standing wave to traveling wave being 2.5) oriented at  $4.8^\circ$  from blade slot #1. Clearly other harmonics are also present as can be seen from Fig. 141. Blades 28 and 40 respond nearly 2 to 3 times the "system total" response and therefore the harmonic analysis shows the additional components. A resonance circle fit was attempted on the polar plots (see Fig. 142) with only three points leading to a calculated value of about .006 for loss factor. This value of damping is consistent with values calculated in earlier tests with the second family modes.

## 10. System Damping Variation on the Constant Speed Line

The fan map shown in Fig. 111 clearly illustrates the well known characteristic of operating fans, i.e., the tendency towards increasing  $\Delta p/Q_u$  at low  $C_x/U$  as the conditions approach stall. In order to examine the influence, if any, on the vibratory characteristics of the fan, as the fan approaches the stall boundary, tests were performed to measure system damping as a function of  $C_x/U$ . The method used was to induce a two modal diameter second family mode at 1200 rpm using the Piezoelectric Crystal Excitation System and then abruptly cut off the input simultaneously recording the decay of vibratory signatures from all the blades. These decay signals were analyzed using a time domain analysis based on Ref. 8. Tests were conducted for both the tuned and mistuned conditions of the R-80 fan.

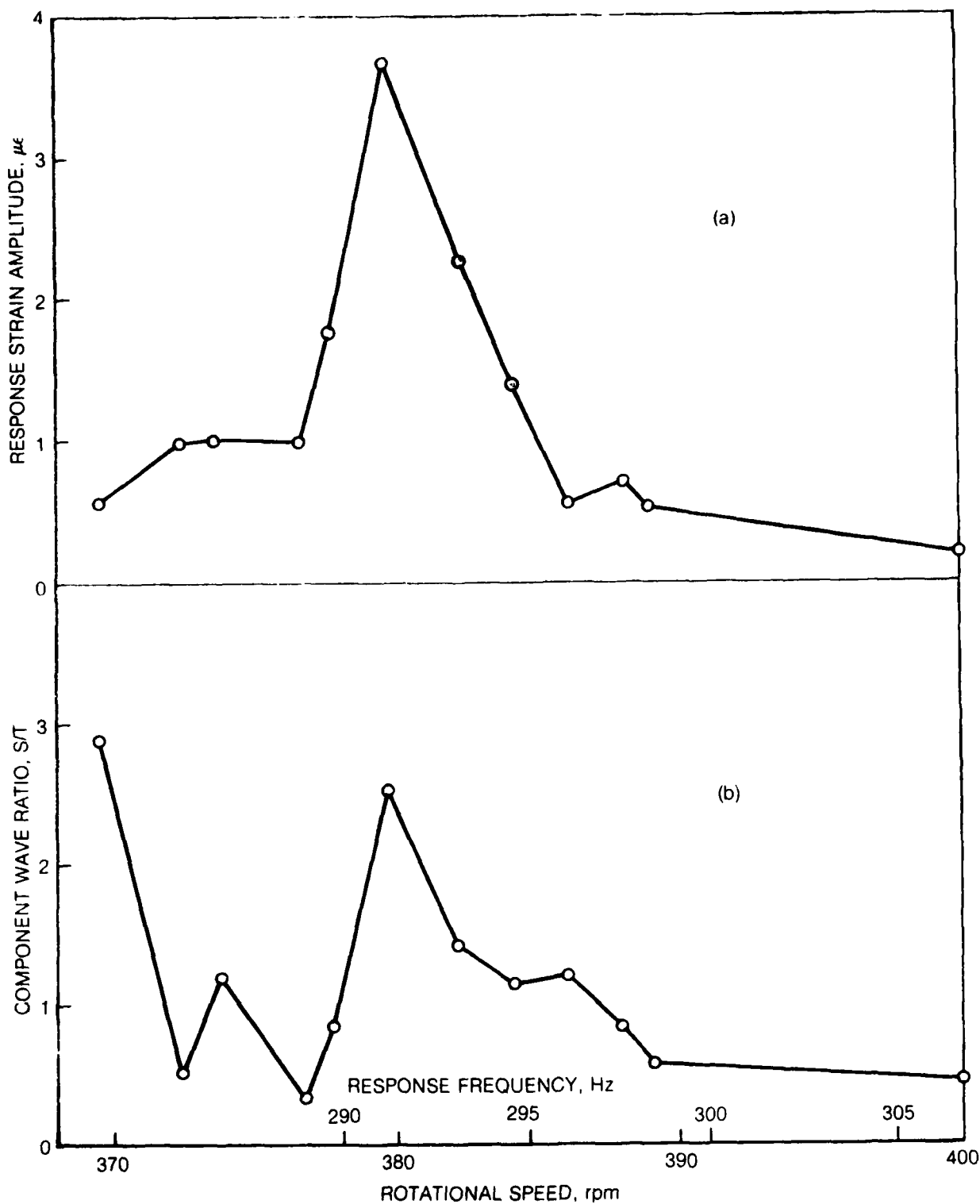


Figure 140 Variation of Blade Strain Amplitude and Component Wave Ratio (Stationary/Traveling) in the 6ND Modal Response due to Exit Guide Vane Excitation with Rotational Speed

83-8-36-51

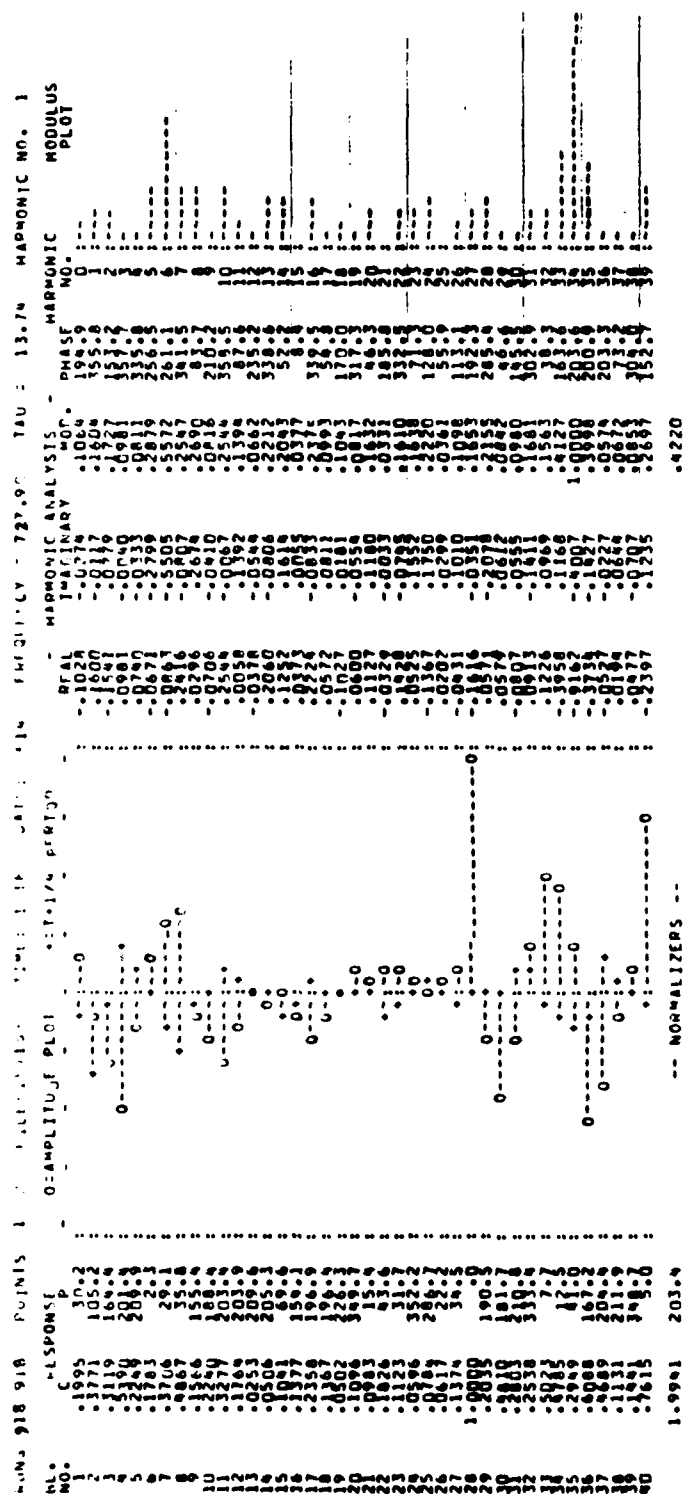
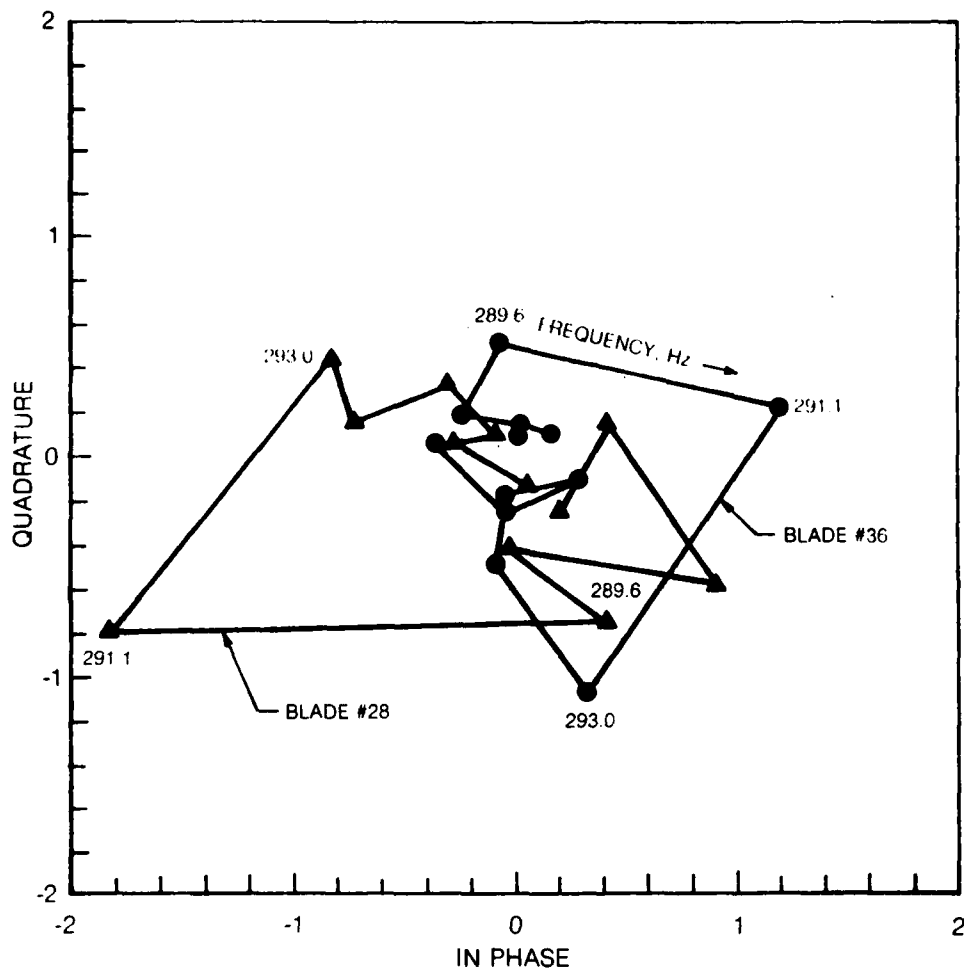


Figure 141 Response of the Tuned Assembly to Exit Guide Vane Excitation at 379.7 RPM in Rig B



FILES 1 TO 24 RUNS 913-924  
 FREQUENCIES 283.3-306.8 Hz

Figure 142 Polar Plots of Blade Strain Response in the 6ND Mode due to Exit Guide Vane Excitation for Blades #28 and #36

Considerable care was necessary in reducing this data and only a judicious choice of channels based on several trials led to meaningful results. First of all, it was found that elimination of noise at 60 Hz and its harmonics (particularly at 300 Hz) was essential. Secondly, different choices of blade data channels were made to accentuate a particular orientation of a stationary 2ND mode. These choices are designated as "spatial filters" and in each of the choices, those channels close to a nodal line are discarded.

This series of tests was aimed at establishing any trend system damping may have as the fan approaches the stall boundary. With the care needed and exercised in the choice of data and elimination of noise, the reduced data indicates a trend only for the mistuned assembly as can be observed from Fig. 143. A band of "probable variation" in damping is indicated to reflect data interpretations having high confidence factors in the time domain analysis. The dip in damping at the low end of  $C_x/U$  is consistent with the concept of a tendency towards stall flutter at high  $\Delta P/Q_u$ . This trend could be established only for the mistuned fan at 1200 rpm. It could not be established either for the mistuned assembly at 560 rpm or for the tuned assembly as can be seen from Figs. 144 and 145. No firm conclusions can therefore be drawn without additional data.

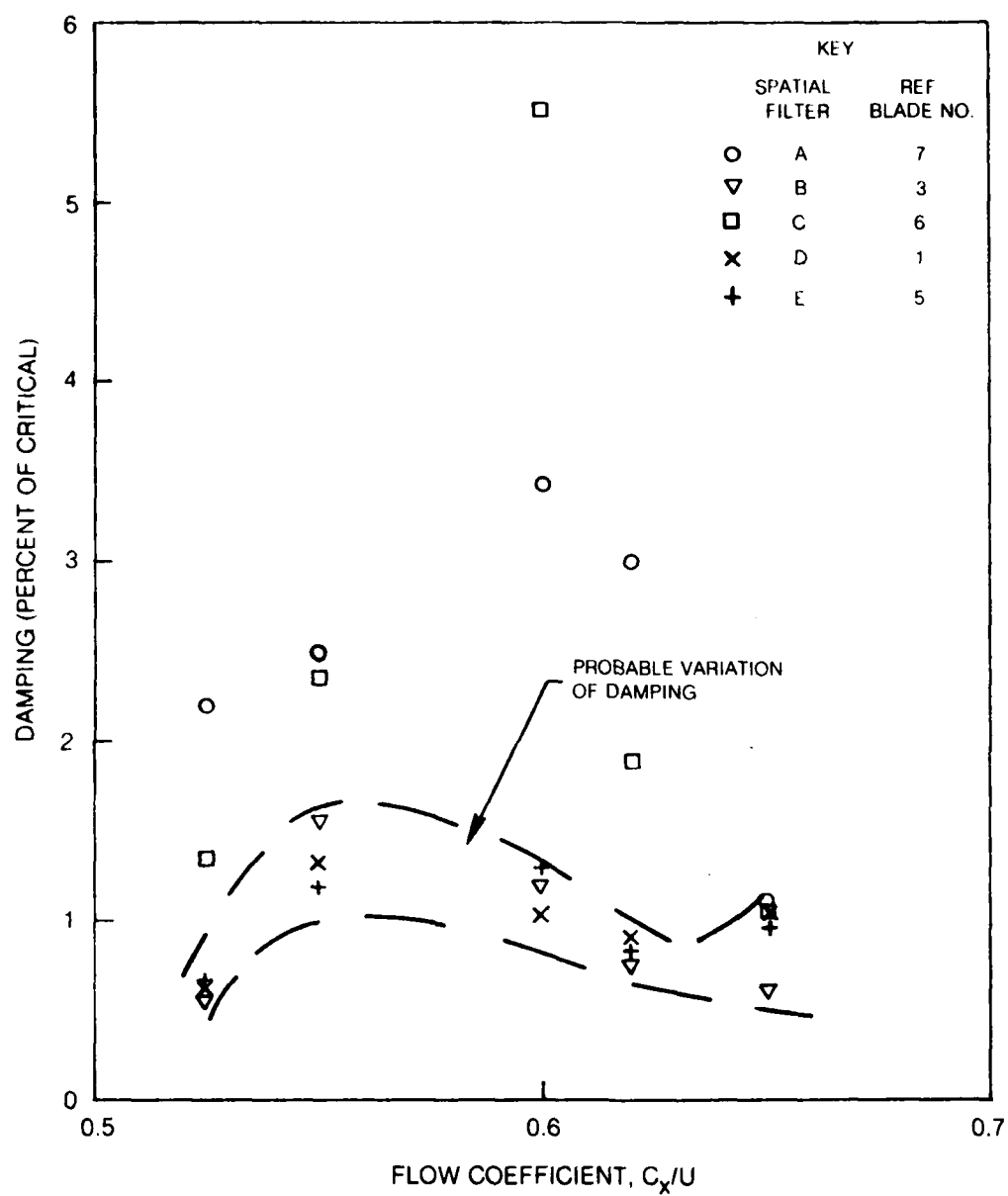


Figure 143 Time Domain Analysis of 2ND Mode Decay at 1200 RPM of the Mistuned Fan

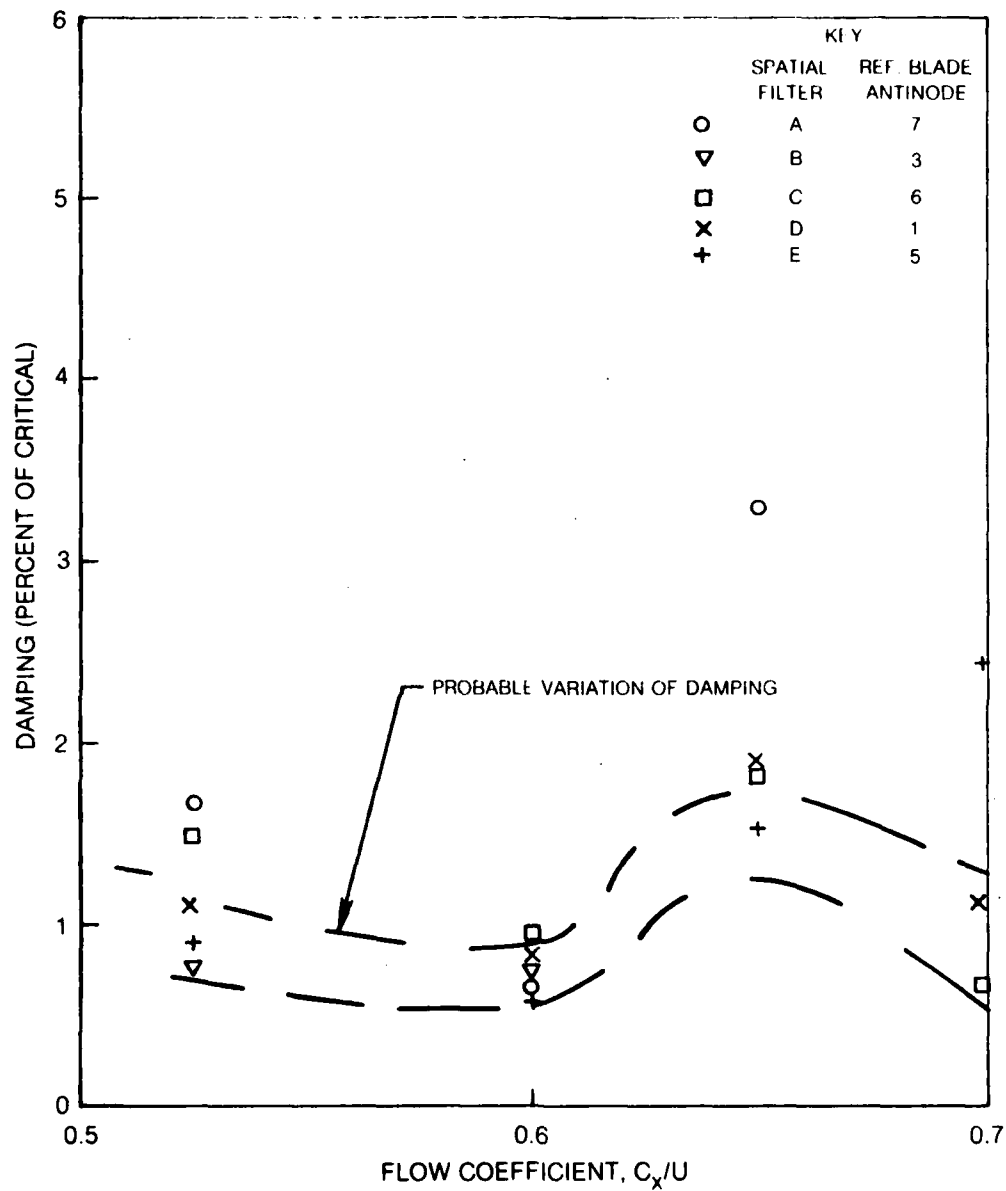


Figure 144 Time Domain Analysis of 2ND Mode Decay at 560 RPM of the Mistuned Fan

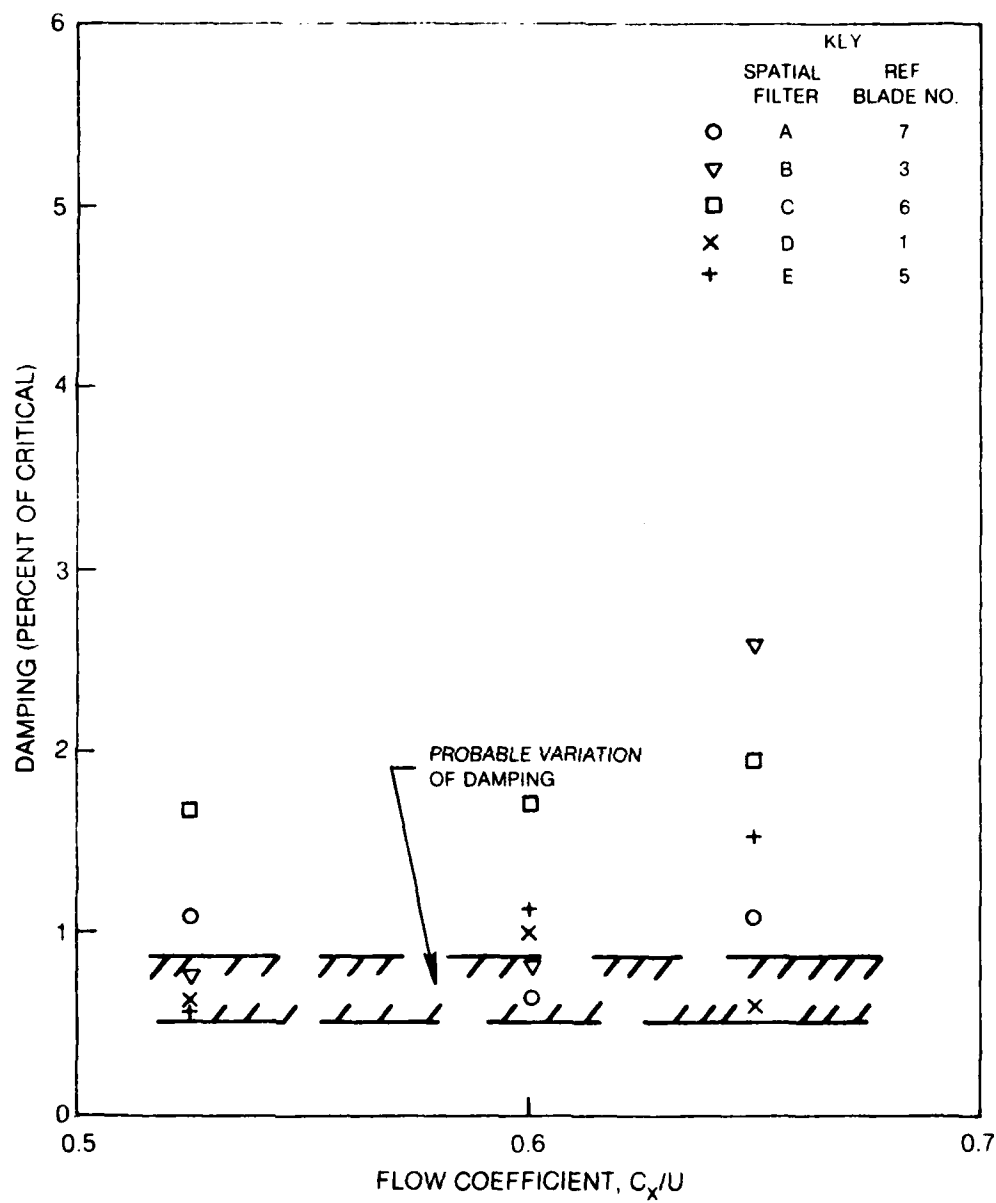


Figure 145 Time Domain Analysis of 2ND Mode Decay at 560 RPM of The Tuned Fan



### XIII. GENERAL SUMMARY AND CONCLUSIONS

A part-span shrouded experimental fan 60 inches in diameter was subjected to forced vibration in vacuum as well as in an aerodynamic environment. The bladed disk assembly consisted of 40 blades made of aluminum. The blades were 15 inches long and of aspect ratio varying from 2.5 (tip) to 3.0 (root). Tests were conducted at speeds not exceeding 1200 rpm. In the spin rig, the assembly was subjected to vibration via piezoelectric crystals mounted on each blade. In the aerodynamic rig, the uniform flow field was interrupted by a distortion screen so that the cascade of blades experienced a forcing function of a four nodal diameter pattern in the fixed system. Responses at both integral and nonintegral order were measured on all blades.

It has been shown that the piezoelectric crystal excitation system of the type used in this program is a convenient, reliable and accurate way of imposing vibration in a rotor to study its dynamic behavior. The system was developed over a period of nearly two years and served well throughout the program, including in the aerodynamic testing phase. It was only at the very end of the program some channels appeared to be ineffective. It is concluded that a system such as the one used in this program is feasible in both non-aerodynamic and aerodynamic environments.

The rotor had been designed such that the four nodal diameter mode in the first family would be integral with a rotor speed below the maximum speed of 1200 RPM. However, because of the mistuned conditions, the nonuniform shroud coupling among blades and the close proximity of other circumferential modes, the low levels of forcing imposed through the crystals resulted in irregular modal patterns. In contrast to this, under the influence of flow distortion, the rotor response at integral order was strong and unambiguous because of the higher excitation forces and the interblade aerodynamic coupling.

Responses in the second family were satisfactory and twin modes could be measured with acceptable accuracy. It has been shown that each of the twin modes can have different and measurable damping factors and that a simple analysis using these modes can be formulated to calculate the response of the rotors provided the other circumferential modes are not too closely spaced.

One of the important findings from this program is that the maximum strain levels measured in the deliberately mistuned shrouded rotor are lower than those measured in the "tuned" rotor. However, the level of tuning in the "tuned" assembly was such that the comparison is actually between two mistuned rotors.

The effort to correlate measured strains with the aerodynamic stimulus has shown an excellent correlation between the principal component of the distortion pattern and the corresponding strain pattern. In addition multiples of the principal harmonic are present in the distortion which correlate with corresponding strain patterns measured in the assembly. However, an interesting feature of this correlation is that, in addition to backward traveling waves, forward traveling waves are also present so that the response pattern in the fixed system will not appear as a standing wave at integral order speed. Again this feature is attributed to the influence of mistuning present in the rotor.

That the response patterns of a mistuned assembly do not always follow the imposed excitation was abundantly clear in all data analyzed (see for example, Figs. 56 and 57). Therefore one should not be surprised if a backward traveling wave forcing function resulted in a response pattern containing a predominant forward traveling wave. It all depends on the degenerate modes of the system, their phasing and the manner in which they combine. A knowledge of the modal characteristics of the assembly is essential in order to be able to interpret data from forced vibration responses.

Although these tests were conducted in two rigs (the spin rig and the aerodynamic rig with different support systems) a comparison between the values of damping in the second family of modes measured in the aerodynamic environment can be made with those measured in vacuum in the spin rig. The overall range of damping (loss factor) measured in the aerodynamic tests was from 0.002 to 0.011 depending on the system configuration (tuned or mistuned) and on the mode. Comparing these values with those from tests in vacuum for similar configurations and modes, the maximum contribution from aerodynamic damping for the test flow conditions (low Mach number, reduced frequency of about 0.4 on a semichord basis) was 0.007 as measured in the 3ND mode for the mistuned assembly at 1200 rpm.

For the first family 4ND response, the comparison between the damping values obtained in the vacuum and aerodynamic tests is complicated by the

fact that the strain response caused by the aerodynamic distortion was about six times that obtained using the crystal excitation. However, in the aerodynamic tests, the loss factor was estimated as 0.026 for the tuned system and 0.034 for the mistuned system. These values are just double that estimated from the in-vacuum tests (0.013-0.015). The in-vacuum estimates were obtained from the "system total" response variation with frequency. Individual blade responses show much lower levels of damping ( $\sim 0.005$ ).

Response patterns measured in the vicinity of a natural mode over a range of frequencies can be quite similar leading to difficulties in identifying twin modes. Care should be exercised in using the criterion of maximum strain because in a mistuned system a rogue blade could experience a considerably larger strain than the strain due to a weak system mode. This feature is evident in several of the stickplots in this report. An examination of the ratio of standing to traveling waves and orthogonality of the modes can serve as an important criterion.

Tests conducted to examine the influence of exit guide vanes have established the presence of modes of patterns equal to the difference between the number of blades and vanes. An attempt was made to establish the variation, if any, of damping as the fan is subjected to vibration when the pressure on it changes along a constant speed line. The results for the mistuned assembly appears to indicate a tendency toward a dramatic drop close to the stall boundary. This merits further study.

Shroud vibratory and steady motions were measured in the spin rig and contribute the first-ever data of this type. These motions are undoubtedly small, the steady motions being of the order of 10 to 20 mils at 1200 rpm. The vibratory motions were of a microslip type with no evidence of stick-slip type of motion. A thorough examination of the data indicates that the nature of boundary conditions at the interfaces in the first family vibratory modes is different from that observed in the second family of modes. This implies that in an analytical model of a shrouded fan, a single representation of the shroud boundary may not be adequate to represent all families of modes.

The data generated has proven that extremely small motions can be measured using the LED technique developed at the Research Center. Measurements in an aerodynamic environment would require additional development leading the miniaturized LED units. However, the data, in its present form, can be used to calculate contributions to damping from rubbing motion at shroud interfaces.

#### XIV. REFERENCES

1. Srinivasan, A. V., D. G. Cutts and S. Sridhar: Turbojet Engine Blade Damping. NASA CR 165406, July 1981.
2. Fabunmi, J. C.: Forced Vibrations of a Single Axial Compressor Rotor. Ph.D Thesis, MIT, 1978.
3. Bruce, E. P.: Design and Evaluation of Screens to Produce Multi-Cycle  $\pm 20\%$  Amplitude Sinusoidal Velocity Profiles. AIAA Paper No. 74-623.
4. McCarthy, J. H.: Steady Flow Past Non-Uniform Line Grids. Journal of Fluid Mechanics, Vol. 19, pp. 491-512, 1964.
5. Srinivasan, A. V., S. R. Lionberger and K. W. Brown: Dynamic Analysis of an Assembly of Shrouded Blades Using Component Modes. Paper presented at the Design Engineering Technical Conference, Chicago, Ill. September 26-30, 1977. Journal of Mechanical Design, Vol. 100, No. 3, July 1978.
6. Fung, Y. C.: An Introduction to the Theory of Aeroelasticity. Dover Publications, Inc., New York, 1969.
7. Jay, R. L., J. C. MacBain and D. W. Burnes: Structural Response Due to Blade Vane Interaction. Paper presented at the 28th International Gas Turbine Conference, Phoenix, Arizona, March 27-31, 1983. ASME Paper No. 82-GT-133.
8. Ibrahim, S. R. and E. C. Mikulcik: A Method for the Direct Identification of Vibration Parameters from the Free Response. Shock and Vibration Bulletin, No. 47, Part 4, pp. 183-198, September 1977.

**END**

**FILMED**

**10-84**

**DTIC**